Exact Conditions in Density Functional Theory and their application to Hubbard type Corrective Functionals

Andrew C. Burgess

A thesis presented for the degree of
Doctor of Philosophy

School of Physics,
Trinity College Dublin,
the University of Dublin
3 March, 2025

Declaration

I declare that this thesis has not been submitted as an exercise for a degree at this or any other university and it is entirely my own work. I agree to deposit this thesis in the University's open access institutional repository or allow the Library to do so on my behalf, subject to Irish Copyright Legislation and Trinity College Library conditions of use and acknowledgement. I consent to the examiner retaining a copy of the thesis beyond the examining period, should they so wish (EU GDPR May 2018). Except where otherwise stated, the contents of this thesis are the product of my own work carried out in the Quantum Theory of Materials group at the School of Physics, Trinity College Dublin, supervised by Professor David D. O'Regan.

This dissertation does not exceed 100,000 words in length.

Andrew C. Burgess
Trinity College Dublin
30 September 2024

Acknowledgements

There are a great many people who I have the joy of sharing my life with and without whom the work of this thesis could ever have been completed. In no particular order, I would like to explicitly mention quite a number of these people.

In my early schooling I was a less than exemplary student, in part due to my astonishingly poor reading skills but also thanks to a boyish level of hyperactivity. I would like to thank Mr. Morton and Roda Dover for their boundless patience and for seeing potential in me. A special thanks must also go to the teaching staff at Wesley College, in particular Mrs. Lewis, Mr. Hosford, Mr. Fox and Ms. Wallace. Their passion, enthusiasm and patience is truly exemplary and I am extremely grateful to have had them as my science and maths teachers. On the topic of inspiring teachers, I of course must express enormous gratitude to my PhD supervisor David O'Regan. Despite the arduous burdens of undergraduate teaching and university administration, David dedicates an enormous amount of time to one-on-one guidance with his PhD and postdoctoral researchers. I am forever indebted to David for this generosity. I would also like to emphasise David's kindness and consideration for others, traits that unfortunately often go undervalued in the field of physics research. As a supervisor David always remained conscious and respectful of people's personal lives and offered bountiful guidance and advice for future career progression. To any new PhD student who might be reading this thesis, you are very lucky to have David as your supervisor.

I am grateful for the support provided by the Trinity Centre for High Performance Computing, without whom none of the DFT calculations in this thesis could have been completed. This research work would also never have been completed without the financial support of the Irish Research Council provided through the Government of Ireland Postgraduate Scholarship (grant number

GOIPG/2020/1454). I am very grateful for the Irish taxpayers, who through funding this scholarship have supported basic science research. I would also like to thank my collaborator Edward Linscott, who it has been a great pleasure to work with and David Gavin, who in many ways helped me find my feet as a new PhD researcher, particularly in using Trinity's High Performance Computing Cluster. The research work in chapters 5,6 and 7, where a new family of DFT+U-type functionals has been derived and tested, would also not have been possible without earlier research work completed by Glenn Moynihan, whose sample ONETEP input files and method of evaluating the Hubbard U parameter, I have made great use of.

Outside of my academic life, a pair of miscreants who are both deserving but also expecting a "shout out," are my fantastic sisters Aoife and Emma. I would like to thank the gruesome twosome for always being their to "put me back in my box." I am also extremely grateful for my beloved parents Órla and Michael. The love, care and devotion they have shown both me and my two sisters is beyond measure. I know that I will never be able to truly repay them for their herculean efforts but I simply hope that one day I can behave likewise as a parent myself. I am also forever grateful for my Grandparents Gráinne, Dorothy and Paddy; my Godparents Sinéad and Edward and to the wider Burgess family.

For the last six and a half years, I have been blessed to have Claire by my side. She has been a bedrock of support to me through out my university studies and I have particularly enjoyed travelling and eating with her. It has also been a particular pleasure to be welcomed in to her circle of friends and family- my life is much richer as a result of it. I hope to be fortunate enough to continue to have her as my companion as we navigate our adventure through life together. I am an extremely lucky man.

Finally, life would be a lot duller if it wasn't for the friends I have made along the way. In particular I would like to thank David, Rob, Dáire, Owen, Robin, Maggie, Ryan, Chans, Emily, Conor, Jason, Oisín, Liam, Ciarán, Eoin, Luke, Elle, Beth and Dawn.

Associated Publications

Chapters of this dissertation, or parts thereof, which have been previously published or which are intended for publication are as follows:

Chapter 3: *Andrew C. Burgess, Edward Linscott, and David D. O'Regan*, "The convexity condition of density-functional theory" J. Chem. Phys. **159**, 211102 (2023).

Chapter 4: *Andrew C. Burgess, Edward Linscott, and David D. O'Regan*, "Tilted-Plane Structure of the Energy of Finite Quantum Systems" Phys. Rev. Lett. **133**, 026404 (2024).

Chapter 5: *Andrew C. Burgess, Edward Linscott, and David D. O'Regan*, "DFT+U-type functional derived to explicitly address the flat plane condition" Phys. Rev. B **107**, L121115 (2023).

Chapter 6: *Andrew C. Burgess, and David D. O'Regan*, "Flat plane based double-counting free and parameter free many-body DFT+U" Phys. Rev. B **110**, 205150 (2024). An "Editor's Suggestion".

Presentations

Contributed Talks:

- *"Capturing static correlation using a new DFT+U-type functional"*, 3rd Quantum International Frontiers (2023), Łódź.
- *"A first-principles DFT+U functional for the flat-plane condition robust against stringent test cases"*, American Physical Society March Meeting (2024), Minneapolis.
- *"Exact Conditions in Density Functional Theory"*, Trinity College Dublin, School of Physics Postgraduate Seminar (2024), Dublin.

Posters:

- *"Comparison of Hubbard Functionals for Strongly Correlated Systems"*, Psi-k Conference (2022), Lausanne.
- *"A DFT+U-type functional to correct both self interaction error and static correlation error"*, 17th International Congress of Quantum Chemistry (2023), Bratislava.
- *"Exact double counting correction schemes from the flat plane condition"*, American Physical Society March Meeting (2024), Minneapolis.
- *"Error Correction Methods for Local & Semi-Local DFT"*, International HPC Summer School (2024), Kobe.
- *"The Tilted Plane Condition"*, DFT2024 (2024), Paris.
- *"In situ correction of self-interaction & static correlation errors"* DFT2024 (2024), Paris.

Academic Duties

Over the course of the PhD I fulfilled a number of academic duties outside of my core research work, which I list below for posterity, including the academic years over which these duties took place.

1. Teaching Assistant for Senior Fresh Computational Physics Labs (2020-2021, 2021-2022, 2022-2023 & 2023-2024).
2. Teaching Assistant for Senior Fresh Engineering Mathematics (2020-2021 & 2022-2023).
3. Teaching Assistant for Junior Fresh Mathematics for Scientists (2022-2023).
4. Mentor for an Undergraduate Summer Research Project on a novel method for evaluating the Hubbard U parameter (2022-2023).
5. Mentor for a Senior Sophister Research Project on Hubbard U parameters in doped and undoped Lathanum Cuprates (2023-2024).
6. Mentor for a Senior Sophister Research Project on modelling kesterites using the DFT+U+J functional (2023-2024).
7. Secretary to the Scholars (2023-2024).

Contents

Chapter 1

Summary

The work of this thesis falls within the topic of Kohn Sham (KS) and Generalised Kohn Sham (GKS) theory, the practical implementation of which are the most popular tools for predicting the electronic properties of atoms, molecules, materials and nano-structures. The importance of these methods within the fields of physics, chemistry and material science is exemplified by the vast computational resources expended annually running such calculations on High Performance Computing (HPC) systems, approximately 30% of the total core hours, based on Ireland's national HPC system. It is also worth noting that the most cited papers across the disciplines of physics and chemistry pertain to this very topic.

Although a formally exact theory, practical KS and GKS calculations require the use of an approximate Exchange Correlation functional. Over the past sixty years an intense and unbroken effort has been made to both improve the underlying exchange correlation approximations, but also through the development of correction schemes to supplement standard approximations, such as van der Waals, self interaction and Hubbard type corrective functionals.

Of particular interest is the development of improved methods for modeling specific types of materials where conventional exchange correlation approximations qualitatively fail, such as transition metal and lanthanide oxides. This qualitative failure of conventional exchange correlation functionals is best exemplified by their spurious prediction of many of the aforementioned materials as being metallic when they are known experimentally to be insulating. The reliable modeling of transition metal oxides is a matter of particularly pressing concern as they include many materials of technological and scientific interest,

such as cathode materials for lithium ion batteries, heterogeneous catalysts for hydrogen production, high-temperature superconducting oxides and inorganic solid state electrolytes to name but a few.

Hubbard type corrective functionals have shown much promise at correcting for the deficiencies of conventional exchange correlation functionals in the modeling of transition metal and lanthanide oxides. Traditionally these corrective functionals are derived by employing an electron-electron interaction term inspired by the Hubbard model, however this electron-electron interaction is already accounted for to a less favorable extent by the conventional exchange correlation functional which the Hubbard functional is designed to supplement. This necessitates the use of a double counting correction scheme. Over the decades several double counting schemes have been derived but crucially, computed material properties have been shown to depend strongly on the choice of double counting scheme. The aim of this thesis is to dispense with the need to invoke a double counting correction term and instead derive a new Hubbard type corrective functional inspired solely by exact conditions, i.e. known physical properties of the exact exchange correlation functional.

It is with this in mind that, in chapters three and four, new exact conditions of the exchange correlation functional are derived, namely the convexity condition and tilted plane condition. The convexity condition is a long assumed, but until now, unproven exact condition of the exchange correlation functional, which states that the total energy of a finite electronic system should be convex with respect to electron count. Proving this exact condition is an important result not only from a purely academic perspective but also because it lifts a standing assumption in the original proof of the piecewise linearity condition with respect to electron count by Perdew et al. [1]. This piecewise linearity condition is itself widely used to motivate the mathematical form of many Hubbard type corrective functionals and will be invoked in the derivation of our new Hubbard functional in later chapters of the thesis. In passing, we note that the piecewise linearity condition is also employed to justify the use of the KS and GKS gap as a method of evaluating the fundamental bandgap of an electronic system. Thus, proving the convexity condition places the aforesaid on a firmer theoretical footing.

In chapter four, another exact condition of the exchange correlation functional, namely the tilted plane condition is derived. This exact condition defines

the shape of the total electronic energy surface with respect to total electron count N and total magnetization M, including non-integer values of N and M. This exact condition is a generalization of the well known flat plane condition, which defines the total electronic energy surface only for a limited range in values of M. Again, deriving this exact condition is interesting not only from a purely academic standpoint but also because a plethora of density functional approximations and corrective functionals have been designed based on the flat plane condition. Hence, the tilted plane condition could help stimulate the extension and generalization of many of these methods. In particular for our purposes, knowledge of this complete total energy surface will be employed in later chapters of the thesis to derive a new class of Hubbard-type functional.

In chapters five and six, we do exactly that and develop a Hubbard-type functional named BLOR after the authors, and its many body generalisation mBLOR, based on our understanding of the flat and tilted plane conditions. To be more specific, these Hubbard type functionals are solely derived based on the differing behaviours between the exact and approximate exchange correlation functionals at non-integer values of subspace electron count and magnetization. We benchmark our newly derived Hubbard-type functional using stretched homo-nuclear s and p block molecules and find that our corrective functional yields considerable improvements in the total energy compared to standard Hubbard-type functionals. Finally, in chapter seven, we test the mBLOR functional on MnO, an archetypal transition metal oxide system where standard local and semi-local exchange correlation approximations benefit from being supplemented by a Hubbard type corrective functional. With the inclusion of an additional stabilisation term, the mBLOR functional yields an energy of cohesion for MnO in very close agreement with the Diffusion Monte Carlo reference value. Further testing of the mBLOR functional on transition metal oxide systems is needed. Nevertheless, this is a very promising preliminary result.

Chapter 2

Background Theory

2.1 The Electronic Schrodinger Equation

Within electronic structure theory we are primarily interested in predicting the physical and chemical properties of materials. If we ignore special relativistic effects, apply the Born–Oppenheimer approximation [2] and assume there are no time dependent interactions, these properties can be ascertained by solving the time-independent Schrödinger eigenvalue equation [3],

$$\left[-\frac{1}{2}\sum_i \nabla_i^2 - \sum_{i,\alpha}\frac{Z_\alpha}{|\mathbf{R}_\alpha - \mathbf{r}_i|} + \frac{1}{2}\sum_{i,j}\frac{1}{|\mathbf{r}_i - \mathbf{r}_j|}\right]\Psi_k = E_k\Psi_k, \tag{2.1}$$

for our electron system of interest. In Eq. 2.1 atomic units have been used and the first three terms on the left hand side are the electron kinetic energy operator $\hat{T}$, the electron-nuclei interaction operator $\hat{V}_{\text{en}}$ and the electron-electron interaction operator $\hat{V}_{\text{ee}}$, respectively. Together these three operators form the electronic Hamiltonian, named after the Trinity College Dublin mathematician William Rowan Hamilton. The set $\{\Psi_k\}$ and $\{E_k\}$ denote the eigenfunctions and eigenvalues of the equation. The lowest eigenvalue is referred to as the total ground state electronic energy of the system and the corresponding eigenfunction is referred to as the ground state electronic wavefunction of the system.

There exists a suite of quantum chemical methods that are designed to directly solve the time independent electronic Schrödinger equation of Eq. 2.1, either in principle exactly or to some level of approximation. These techniques include coupled cluster [4–6], configuration interaction [7–9] and complete active

space methods [10–12]. These techniques enjoy widespread use in the prediction of molecular properties. However, despite a growing level of interest [13–16], these methods remain largely outside the scope of solid state prediction due to the vast computational resources required. In the solid state, the diffusion quantum Monte Carlo method [17–23] offers an extremely accurate tool for solving the Schrödinger Equation but it too requires vast computational resources and is thus not an appropriate method for large scale screening of materials [24–26] or for the prediction of complex solid state defects [27–29].

2.2 Density Functional Theory

As an alternative, most material scientists and condensed matter physicists invoke Density Functional Theory (DFT) [30], as it sidesteps the need to evaluate the many-body electronic wavefunction $\Psi_0(\mathbf{x}_1, \ldots, \mathbf{x}_N)$, which depends on the combined position and spin co-ordinate $\mathbf{x}_i = (\mathbf{r}_i, s_i)$, of each electron in the N electron system. Instead, the chemical and physical properties of the system are determined solely by the electron density,

$$\begin{aligned}\rho(\mathbf{r}) = \langle\Psi_0|\hat{\rho}|\Psi_0\rangle &= \langle\Psi_0|\sum_i^N \delta(\mathbf{r}-\mathbf{r}_i)|\Psi_0\rangle \\ &= N\sum_{s_1}\cdots\sum_{s_N}\int_{\mathbf{r}_2}\cdots\int_{\mathbf{r}_N}|\Psi_0(\mathbf{x}_1,\ldots,\mathbf{x}_N)|^2, \qquad (2.2)\end{aligned}$$

which is a significantly simpler mathematical object that is a function solely of position $\mathbf{r}$. In practice, most calculations classified as 'DFT' employ a more complex object than simply the electron density, but this will be discussed at a later stage.

The first DFT calculations were performed independently in 1927 by Thomas [31] and Fermi [32]. However, a firm theoretical justification for this method through two theorems, was published much later in 1964 by Hohenberg and Kohn (HK) [33], the latter of which was awarded half of the Nobel prize in chemistry in 1998 for his development of DFT. The first HK theorem states that:

There exists a one-to-one mapping between the ground-state density $\rho_0(\mathbf{r})$ of an N-electron system and the external potential $v(\mathbf{r})$ acting upon it,

the simple proof by contradiction of which can be found in the original paper or the several hundred other PhD theses on DFT produced annually. For a

chemical system without any external electric or magnetic fields, the external potential is simply the Coulombic potential due to the clamped nuclei. Across all N electron systems, the electron-nuclei interaction operator is the only term in the electronic Hamiltonian which varies. From the first HK theorem, it follows that the electronic Hamiltonian $\hat{H}_{\text{ele}}$ is uniquely determined by the ground-state density, and by extension, all ground and excited state wavefunctions of the system are also uniquely determined by the ground-state density. It follows that all chemical and physical properties of the system are determined by the ground state density alone,

$$\rho_0(\mathbf{r}) \rightarrow v(\mathbf{r}) \rightarrow \hat{H}_{\text{ele}} \rightarrow \{\Psi_k\}. \tag{2.3}$$

In particular, the total ground state electronic energy is therefore a unique functional of the ground state density. The second HK theorem states that:

For all pure-state v-representable densities $\rho_v(\mathbf{r})$, $E_0 \leq E_v[\rho_v]$, where $E_0 = E_v[\rho_0]$, is the ground-state energy for N electrons in the external potential $v(\mathbf{r})$ with corresponding ground-state density $\rho_0(\mathbf{r})$,

which follows from the variational principle. A pure-state v-representable density $\rho_v(\mathbf{r})$ [34–36], is defined as any density associated with the ground-state wavefunction of some Hamiltonian. The total electronic energy functional

$$E_v[\rho_v] = \int d\mathbf{r}\rho_v(\mathbf{r})v(\mathbf{r}) + F_{\text{HK}}[\rho_v], \tag{2.4}$$

where $F_{\text{HK}}[\rho_v]$ is the HK universal functional (the sum of kinetic and electron-electron interaction energies), so-called due to its independence from the system under consideration. From the second HK theorem we know that the ground state density of a given system with external potential $v(\mathbf{r})$ can be found by minimising the energy functional of Eq. 2.4. However, this minimisation procedure should be carried out solely over v-representable densities — a serious limitation when searching for the ground-state [34–39]. It is also worth noting that the HK theorems apply only to systems with non-degenerate ground states. The HK formulation of DFT was also extended to non-zero temperature by Mermin [40]. Since the development of the HK formulation of DFT, a variety of other formulations have been devised.

Levy [41] offered an alternative formulation (see also Lieb [42]), which is defined for all N-representable densities, i.e., the density associated with some

antisymmetric wavefunction Ψ, such that

$$E_{\text{Levy}}[\rho] = \int d\mathbf{r}\ \ \rho(\mathbf{r})v(\mathbf{r}) + \min_{\Psi\to\rho} \langle \hat{T} + \hat{V}_{\text{ee}} \rangle_{\Psi}\,, \tag{2.5}$$

where $\hat{T}$ and $\hat{V}_{\text{ee}}$ are the kinetic energy and electron-electron interaction operators. Valone [43] extended the Levy constrained search formulation to all N-particle density operators,

$$E_{\text{Valone}}[\rho] = \int d\mathbf{r}\ \ \rho(\mathbf{r})v(\mathbf{r}) + \min_{\hat{\Gamma}_N\to\rho} \langle \hat{T} + \hat{V}_{\text{ee}} \rangle_{\hat{\Gamma}_N}\,, \tag{2.6}$$

where the N-particle density operator is

$$\hat{\Gamma}_N = \sum_i p_i \left|\Psi_{Ni}\right\rangle \left\langle\Psi_{Ni}\right|. \tag{2.7}$$

This was later extended by Perdew et al. [1] to a constrained search over mixed-states, including non-integer particle counts, in which case $\hat{\Gamma}_N$ in Eq. 2.6 is replaced by the ensemble density operator

$$\hat{\Gamma} = \sum_N \sum_i p_{Ni} \left|\Psi_{Ni}\right\rangle \left\langle\Psi_{Ni}\right|. \tag{2.8}$$

This formulation of DFT is referred to as the zero-temperature grand canonical ensemble formulation. Ayers et al. [44] extended the Levy constrained-search formulation to all wavefunctions in Fock space

$$\left|\Psi\right\rangle = \sum_N c_N \left|\Psi_N\right\rangle. \tag{2.9}$$

By construction, this yields the same ground-state total energies as the zero-temperature grand canonical ensemble formulation.

2.3 The Thomas Fermi Method

These formulations of DFT provide a rigorous theoretical underpinning for the method but do not provide a practical computational scheme. A practical DFT computational scheme was first devised in 1927 independently by Thomas and Fermi [31, 32], predating the Hohenberg Kohn theorems [33] by thirty-

seven years. In the Thomas Fermi model the total electronic energy $E[\rho]$ is decomposed into three terms, a kinetic energy term $T[\rho]$ taken from the uniform non-interacting electron gas,

$$T[\rho] = \frac{3}{10}(3\pi^2)^{2/3} \int d\mathbf{r}\, \rho(\mathbf{r})^{5/3}, \tag{2.10}$$

a Hartree term that accounts for the classical electrostatic repulsion between the electrons,

$$E_{\mathrm{H}}[\rho] = \frac{1}{2} \iint d\mathbf{r}\, d\mathbf{r}' \frac{\rho(\mathbf{r})\rho(\mathbf{r}')}{|\mathbf{r} - \mathbf{r}'|}, \tag{2.11}$$

and the electron-nuclei interaction energy,

$$E_{\mathrm{ext}}[\rho] = \int d\mathbf{r}\, v(\mathbf{r})\rho(\mathbf{r}). \tag{2.12}$$

This method was further improved by Dirac, who devised an approximate expression for the exchange energy [45] and von Weizsäcker [46] who supplemented the kinetic energy expression with a correction term,

$$T_{\mathrm{W}}[\rho] = \frac{1}{8} \int d\mathbf{r}\, \frac{|\nabla\rho(\mathbf{r})|^2}{\rho(\mathbf{r})}. \tag{2.13}$$

However, the Thomas Fermi model, in its simplest form predicts molecules as being physically unstable. Within the field of orbital-free DFT [47–50], progress continues on developing improved approximations for the kinetic energy term [51, 52], including via machine learning based techniques [53, 54]. However, in practice, most calculations instead resort to the Kohn Sham method instead.

2.4 The Kohn Sham Method

As an alternative, Kohn and Sham proposed [55] evaluating the kinetic energy of a system of N non-interacting electrons,

$$T_{\mathrm{s}}[\rho] = -\frac{1}{2} \sum_i^N \sum_s \int d\mathbf{r}\, \psi_i^*(\mathbf{x}) \nabla^2 \psi_i(\mathbf{x}), \tag{2.14}$$

whose density is equal to the true electron density of the system,

$$\rho(\mathbf{r}) = \sum_{i}^{N} \sum_{s} |\psi_i(\mathbf{x})|^2. \tag{2.15}$$

In doing so, their total electronic energy functional $E[\rho]$ is no longer an explicit functional of the electron density alone. Kohn and Sham also invoked an exchange correlation energy functional $E_{\mathrm{xc}}[\rho]$ to account for the difference between the Hartree energy and the true electron-electron interaction energy $V_{\mathrm{ee}}[\rho]$ of the system, as well as for the difference between the non-interacting kinetic energy $T_{\mathrm{s}}[\rho]$ and the true kinetic energy $T[\rho]$,

$$E_{\mathrm{xc}}[\rho] = T[\rho] - T_{\mathrm{s}}[\rho] + V_{\mathrm{ee}}[\rho] - E_{\mathrm{H}}[\rho]. \tag{2.16}$$

Therefore, unlike the Thomas Fermi model, the Kohn Sham total electronic energy functional

$$E[\rho] = T_{\mathrm{s}}[\rho] + E_{\mathrm{H}}[\rho] + E_{\mathrm{ext}}[\rho] + E_{\mathrm{xc}}[\rho], \tag{2.17}$$

is formally exact, but in practical calculations an approximate expression for $E_{\mathrm{xc}}[\rho]$ must be employed. The minimisation of $E[\rho]$ can be conducted in the space of continuous, square integrable KS orbitals $\{\psi_i\}$ so long as the variational search is constrained so that the set $\{\psi_i\}$ remain ortho-normal,

$$\Omega[\{\psi_i\}] = E[\rho] - \sum_{i}^{N} \sum_{j}^{N} \epsilon_{ij} \int d\mathbf{x} \psi_i^*(\mathbf{x}) \psi_j(\mathbf{x}). \tag{2.18}$$

Minimising the functional of Eq. 2.18 results in the equations

$$\left[-\frac{1}{2}\nabla^2 + v_{\mathrm{eff}} \right] \psi_i = \sum_{j}^{N} \epsilon_{ij} \psi_j. \tag{2.19}$$

The local KS effective potential is equal to the sum of the external, Hartree and exchange correlation potentials,

$$v_{\mathrm{eff}}(\mathbf{r}) = v(\mathbf{r}) + \int d\mathbf{r}' \frac{\rho(\mathbf{r}')}{|\mathbf{r} - \mathbf{r}'|} + \frac{\delta E_{\mathrm{xc}}[\rho]}{\delta \rho(\mathbf{r})}. \tag{2.20}$$

The standard Kohn Sham equations can finally be ascertained by diagonalising the ϵ_{ij} matrix via a unitary transformation of the orbitals,

$$\left[-\frac{1}{2}\nabla^2 + v_{\text{eff}}\right]\psi_i = \epsilon_i\psi_i. \tag{2.21}$$

Therefore, in practice the Kohn Sham scheme necessitates solving a set of N, one-electron Schrödinger-like equations to determine $\{\psi_i\}$, which can then be substituted into Eq. 2.15 to determine the ground-state density of the system and finally the total ground-state energy of the system can be ascertained from Eq. 2.17. This is of course significantly more computationally demanding than the Thomas-Fermi method.

2.5 Exchange-Correlation Functionals

In practical KS DFT calculations, an approximate exchange-correlation functional must be employed [56–59]. Some of the most widely used exchange-correlation approximations [60, 61] have been designed to satisfy certain exact conditions [62–64] and fitted to appropriate norms. In this context exact conditions are known physical properties of the exact exchange correlation functional and appropriate norms are properties of specific reference systems, such as the hydrogen atom, noble gas atoms [65] or the homogeneous electron gas [66, 67], that are known to a high degree of accuracy. The simplest such functional is the Local Density Approximation,

$$E_{\text{LDA}}[\rho] = \int d\mathbf{r}\, \rho(\mathbf{r})\epsilon_{\text{xc}}(\rho(\mathbf{r})), \tag{2.22}$$

where $\epsilon_{\text{xc}}(\rho(\mathbf{r}))$ is the exchange correlation energy density of the homogeneous electron gas of density ρ. Highly accurate Quantum Monte Carlo calculations of the homogeneous electron gas were first produced by Ceperley and Alder in 1980 [68], which provided the necessary numerical data for $\epsilon_{\text{xc}}(\rho(\mathbf{r}))$. By virtue of the LDA employing the homogeneous electron gas as an appropriate norm, it satisfies certain exact conditions [39], such as the sum rule,

$$\int d\mathbf{r}'\bar{\rho}_{\text{xc}}(\mathbf{r}, \mathbf{r}') = -1, \tag{2.23}$$

where $\bar{\rho}_{\mathrm{xc}}(\mathbf{r}, \mathbf{r}')$ is the average exchange-correlation hole, which can be used to define the exchange correlation functional,

$$E_{\mathrm{xc}}[\rho] = \frac{1}{2} \int \int d\mathbf{r}\, d\mathbf{r}' \frac{\rho(\mathbf{r}) \bar{\rho}_{\mathrm{xc}}(\mathbf{r}, \mathbf{r}')}{|\mathbf{r} - \mathbf{r}'|}. \tag{2.24}$$

For spin polarised systems, in the absence of spin-orbit coupling, a separate set of KS orbitals can be solved for each spin channel [69, 70], resulting in spin-resolved densities $\rho^{\sigma}(\mathbf{r})$. In such cases the LDA can be readily extended to yield the Local Spin Density Approximation,

$$E_{\mathrm{LSDA}}[\{\rho^{\sigma}\}] = \sum_{\sigma} \int d\mathbf{r}\, \rho^{\sigma}(\mathbf{r}) \epsilon_{\mathrm{xc}}^{\sigma}(\rho(\mathbf{r})). \tag{2.25}$$

Several LSDAs have been devised [69, 71–74], each employing different homogeneous electron gas reference data or fitting procedures. More advanced exchange correlation approximations incorporate increasingly complex ingredients into the functional such as Generalised Gradient Approximations [60, 65, 75–77], which depend not only on the spin-resolved density at each point in space but also the gradient of $\rho^{\sigma}(\mathbf{r})$,

$$E_{\mathrm{GGA}}[\{\rho^{\sigma}\}] = \int d\mathbf{r}\, f(\rho^{\uparrow}, \rho^{\downarrow}, \nabla\rho^{\uparrow}, \nabla\rho^{\downarrow}). \tag{2.26}$$

The Perdew-Burke-Ernzerhof (PBE) functional [60] is the most widely used Generalised Gradient Approximation and the one employed in all practical DFT calculations within this thesis. The PBE functional is designed to satisfy a number of exact conditions including the Lieb-Oxford bound [62, 78, 79], the spin-scaling relation for exchange [80] and the exact slow and rapidly varying limits for correlation. Its functional form is less aethetically pleasing than the LDA,

$$\begin{aligned} E_{\mathrm{PBE}}[\{\rho^{\sigma}\}] = & \sum_{\sigma} \int d\mathbf{r}\, \rho^{\sigma} \epsilon_{\mathrm{x}}^{\mathrm{LSDA}} \left(1 + \kappa - \frac{\kappa}{1 + 4\mu|\nabla\rho^{\sigma}|^2/\pi^2 k_{\mathrm{s}}^4 \kappa(\rho^{\sigma})^2}\right) \\ & + \int d\mathbf{r}\, \rho \left(\epsilon_{\mathrm{c}}^{\mathrm{LSDA}} + \gamma\phi^3 \ln\left(1 + \frac{\beta t^2}{\gamma} \frac{1 + At^2}{1 + At^2 + A^2 t^4}\right)\right), \end{aligned} \tag{2.27}$$

where κ, μ, γ and β are constants and $\epsilon_{\mathrm{x}}^{\mathrm{LSDA}}$, $\epsilon_{\mathrm{c}}^{\mathrm{LSDA}}$ are the exchange and correlation energy densities of the homogeneous electron gas, while k_{s} is the Thomas-Fermi screening wavenumber, ϕ is a spin scaling factor and t is a di-

mensionless density gradient,

$$k_{\mathrm{s}} = \sqrt{\frac{4\left(3\pi^2\rho\right)^{1/3}}{\pi}}, \quad \phi = \frac{1}{2}\left(1+\frac{\rho^{\uparrow}-\rho^{\downarrow}}{\rho}\right)^{2/3} + \frac{1}{2}\left(1-\frac{\rho^{\uparrow}-\rho^{\downarrow}}{\rho}\right)^{2/3},$$
$$\& \quad t = \frac{|\nabla\rho|}{2\phi k_{\mathrm{s}}\rho}. \tag{2.28}$$

Finally, please note that the $\epsilon_{\mathrm{x}}^{\mathrm{LSDA}}$ and k_{s} terms on the first line of Eq. 2.27 depend on the non-spin polarized density $\rho(\mathbf{r}) = 2\rho^{\sigma}(\mathbf{r})$, where $\rho^{\sigma}(\mathbf{r})$ is the spin-σ density of the system of interest and

$$A = \frac{\beta}{\gamma}\left(\exp\left(-\epsilon_{\mathrm{c}}^{\mathrm{LSDA}}/\gamma\phi^3\right)-1\right)^{-1}. \tag{2.29}$$

More complex functional forms have also been devised [61, 81–86], many of which are not explicit functionals of the spin-resolved electron density but rather the first-order non-interacting spin reduced density matrix,

$$\rho_{\mathrm{s}}^{\sigma}(\mathbf{r}',\mathbf{r}) = \sum_i f_i^{\sigma}\phi_{i\sigma}(\mathbf{r}')\phi_{i\sigma}^{*}(\mathbf{r}), \tag{2.30}$$

where f_i^{σ} is the occupancy of the KS orbital $\phi_{i\sigma}$. Such exchange correlation approximations result in a non-local effective potential,

$$v_{\mathrm{eff}}(\mathbf{r}',\mathbf{r}) = v_{\mathrm{xc}}(\mathbf{r}',\mathbf{r}) + v(\mathbf{r})\delta(\mathbf{r}',\mathbf{r}) + v_{\mathrm{H}}(\mathbf{r})\delta(\mathbf{r}',\mathbf{r}). \tag{2.31}$$

Use of a non-local effective potential is referred to as the Generalised Kohn Sham scheme. This category includes hybrid [87] and DFT+U-type functionals [88], the later of which will be discussed at length in a later section. There exists a wide variety of subcategories within the hybrid functional group, including global [86], range-separated [89], double [90] and optimally-tuned range separated hybrid functionals [91]. Global hybrids have arguably the simplest functional form, incorporating a GGA type correlation energy term in addition to both a Hartee-Fock type exchange term using the Kohn Sham orbitals,

$$E_{\mathrm{X}}^{\mathrm{HF}} = -\frac{1}{2}\sum_{ij}\iint d\mathbf{r}\, d\mathbf{r}'\, \frac{\psi_i^{*}(\mathbf{r})\psi_j^{*}(\mathbf{r}')\psi_j(\mathbf{r})\psi_i(\mathbf{r}')}{|\mathbf{r}-\mathbf{r}'|}. \tag{2.32}$$

and a GGA type exchange term in some specified ratio, such as 1:3 in the case

of PBE0 [86].

2.6 The Piecewise Linearity Condition

The piecewise linearity condiiton with respect to electron count N [1, 92, 93], is an example of exact condition not satisfied by any conventional LSDA or GGA functional. It specifies that the total electronic energy of a system with non-integer electron count $N = N_0 + \omega$, where $N_0 \in \mathbb{N}^0$ and $0 \leq \omega \leq 1$, is equal to a linear interpolation of the energies of the same system with N_0 and $N_0 + 1$ electrons,

$$E_v[N_0 + \omega] = (1 - \omega)E_v[N_0] + \omega E_v[N_0 + 1]. \tag{2.33}$$

This condition was originally derived by Perdew et al. [1] for the zero temperature grand canonical ensemble formation of DFT, assuming the convexity condition is satisfied,

$$2E_v[N_0] < E_v[N_0 - 1] + E_v[N_0 + 1]. \tag{2.34}$$

Using the infinite separation limit technique, Ayers et al. [92] later extended the proof of the piecewise linearity condition with respect to electron count to all formulations of DFT that are (1) exact for all v- representable densities, (2) size-consistent and (3) translationally-invariant. Later, Ayers further extended this proof to the domain of real numbers $\mathbb{R}$ [93].

Analogously, there exists the constancy condition with respect to magnetization M [92, 94], which states that the total electronic energy remains constant as one varies the system's magnetization over some limited interval,

$$E_v(N_0, M) = E_v(N_0, M_0) = E_v(N_0, -M_0). \tag{2.35}$$

Here, $M_0 \in \mathbb{N}^0$ is the maximum magnetization of the lowest-energy state for a given integer electron count $N_0 \in \mathbb{N}^0$. These two exact conditions are special cases of the more general flat plane condition [92, 95–106], which states that the total electronic energy

$$E_v(N, M) = (1 - \omega)E_v(N_0, M_0) + \omega E_v(N_0 + 1, M_1) \tag{2.36}$$

for $|M| \leq M_0 + \omega(M_1 - M_0)$, where $N = N_0 + \omega$ and $M_1 \in \mathbb{N}^0$ is the maximum magnetization of the lowest-energy state for the $N_0 + 1$ electron system. As mentioned earlier, conventional XC approximations violate these exact conditions. The deviation in the total energy of the system from the piecewise linearity condition with respect to N is referred to as many-electron self interaction error [107, 108] and the corresponding energetic error for the constancy condition is referred to as static correlation error [94]. The flat-plane condition has motivated the development of a number of functionals [102, 109–118] that either fully or partially satisfy this exact condition.

2.7 Many Electron Self-Interaction Error

Many electron electron self-interaction error (MSIE) is defined as the energetic deviation of approximate functionals from the piecewise linearity condition with respect to electron count [107, 108, 119–121],

$$\begin{aligned} &E^{\mathrm{MSIE}}(N) = E_v^{\mathrm{approx}}(N) - \left[(1-\omega)E_v^{\mathrm{approx}}(N_0) + \omega E_v^{\mathrm{approx}}(N_0+1)\right], \\ &\text{where} \quad N = N_0 + \omega, \quad 0 \leq \omega \leq 1 \quad \& \quad N_0 \in \mathbb{N}^0. \end{aligned} \tag{2.37}$$

MISE is therefore an intrinsic error associated with an approximate XC functional. By definition, $E^{\mathrm{MSIE}}(N)$ is zero at integer values of electron count, this differs from one-electron self-interaction error which is explicitly defined for systems where $N = 1$. In one-electron systems the XC energy should cancel the Hartree energy,

$$E_{\mathrm{H}}[\rho] = -E_{\mathrm{xc}}[\rho], \tag{2.38}$$

to ensure the electron-electron interaction energy is equal to zero. The energetic deviation from this exact condition is referred to as one-electron self-interaction error (SIE). Unlike MSIE, SIE is an energetic error that occurs at integer ($N = 1$) values of electron count, so MSIE and SIE are certainly not equivalent. There exists a suite of self-interaction correction methods to treat this error in approximate XC functionals [73, 122–124].

MSIE has been shown to be almost quadratic in character between consecutive integer values of electron count across a wide range of chemical systems and approximate XC functionals [125]. Thus, this error could be largely treated by mitigating the curvature in the total energy with respect to electron count.

Static correlation error, can analogously be defined as the energetic deviation of approximate XC functionals from the constancy condition with respect to magnetization M [92, 94],

$$E^{\mathrm{SCE}}(N_0, M) = E_v^{\mathrm{approx}}(N_0, M) - E_v^{\mathrm{approx}}(N_0, M_0),$$
$$\text{where} \quad M \in (-M_0, M_0) \quad \& \quad M_0, N_0 \in \mathbb{Z}. \tag{2.39}$$

Here, $M_0 \in \mathbb{N}^0$ is the maximum magnetization of the lowest-energy state for a given integer electron count $N_0 \in \mathbb{N}^0$. Similarly, Cohen et al. [94] have shown that static correlation error is also highly quadratic in character for values of magnetization in the interval $(-M_0, M_0)$.

In this thesis, static correlation error is solely considered as an energetic error between different magnetization states which would be degenerate if the exact XC functional was applied. However, static correlation error can more generally be defined as the difference in energy between any two nominally degenerate states due to use of an approximate XC functional. The energy difference between the symmetry broken and spherically averaged charge densities of open-shell atoms is an example of static correlation error involving electronic states of the same magnetization.

It is worth noting that for the majority of chemical systems investigated, the spurious curvature in the total energy with respect to M is negative while the spurious curvature with respect to N is positive. Therefore, error cancellation can occur in systems with fractional values of both N and M. The total energy of such a system is defined by the flat plane condition of Eq. 2.36. The failure of a functional to comply with the flat plane condition can also result in errors in the total energy of systems with integer values of N and M. This is explicated in full by Mori-Sánchez et al. [126], using a closed shell H_8 cube at large internuclear separation lengths. Approximate functionals such as PBE [60] and B3LYP [75, 85] yield large energetic errors for any integer value of electron count N that yields an electron count per atomic site, $N/N_{\mathrm{site}} \neq 0, 2$. Such energetic errors are expected to occur in any chemical system with highly localized atomic states, including 3d transition metal oxides.

Finally, for finite systems, the decay of the total electron density as $r \to \infty$

is typically governed by the highest occupied KS orbital, which decays as

$$\lim_{r\to\infty} \psi_{\mathrm{HOKS}}(r) \propto \exp\left(-\sqrt{-2\epsilon_{\mathrm{HOKS}}}r\right). \tag{2.40}$$

From this exponential decay [127–133], it follows that the exchange-correlation potential must decay as

$$\lim_{r\to\infty} v_{xc}(r) \propto -\frac{1}{r}. \tag{2.41}$$

The failure of approximate functionals to satisfy the piecewise linearity condition and by extension the ionisation potential theorem (which will be discussed in the next section), results in the incorrect exponential decay of both $\psi_{\mathrm{HOKS}}(r)$ and the electron density. Many XC potentials also exhibit incorrect asymptotic behaviour, with the LDA for example decaying exponentially [134]. The failure of approximate XC potentials to exhibit the correct asymptotic behaviour has been linked to poor performance in the prediction of charge transfer and Rydberg excitations as well as the stability of anions [135].

2.8 The Fundamental Bandgap

A proof by Janak [136] that predates the proof of the piecewise linearity condition by Perdew et al. [1], equates the frontier KS eigenvalue to the variation in the total energy with respect to frontier orbital occupancy [135, 137], namely

$$\epsilon_{\mathrm{f}} = \frac{\partial E_v}{\partial f_{\mathrm{f}}}. \tag{2.42}$$

The proof by Janak in 1978 is based on an earlier proof by Slater for the $X\alpha$ method [138], which is itself motivated by the analogous approximate expression in Hartree Fock theory known as Koopmans' condition [139]. By simply combining Janak's theorem and the piecewise linearity condition and assuming Aufbau filling, one can readily show that the highest occupied Kohn Sham eignevalue ϵ_{HOKS} is equal in magnitude to the ionization potential,

$$-I_p = \epsilon_{\mathrm{HOKS}}. \tag{2.43}$$

Analogously, the electron affinity E_A must be equal in magnitude to the lowest unoccupied KS eigenvalue ϵ_{LUKS} plus an additional contribution from the

derivative discontinuity [126, 133, 140–144] of the exact XC functional Δ_{xc}^{N},

$$-E_A = \epsilon_{\mathrm{LUKS}} + \Delta_{\mathrm{xc}}^{N}. \tag{2.44}$$

The derivative discontinuity Δ_{xc}^{N} arises because the exchange correlation potential may shift by a global constant at integer values of electron count,

$$\Delta_{\mathrm{xc}}^{N} = \lim_{\delta \to 0} \left(v_{\mathrm{xc}}^{N+\delta}(\mathbf{r}) - v_{\mathrm{xc}}^{N-\delta}(\mathbf{r}) \right). \tag{2.45}$$

The fundamental bandgap Δ is defined as the difference between the ionisation potential and the electron affinity,

$$\Delta = I_p - E_A = \epsilon_{\mathrm{LUKS}} - \epsilon_{\mathrm{HOKS}} + \Delta_{\mathrm{xc}}^{N}. \tag{2.46}$$

Conventional LSDA and GGA functionals offer no derivative discontinuity Δ_{xc}^{N}. Hence, at this level of approximation, the computed KS gap is the predicted fundamental gap of the system. However, such functionals are known to severely underestimate the bandgap [119, 145, 146], in many cases even predicting insulators as being metallic. This failure motivates many practioners to employ an on-site Hubbard U type correction [88, 147, 148] to supplement the LSDA or GGA functional in the hope of opening the bandgap. This is referred to as the DFT+U method, which we will explore in detail in a later section.

In finite systems, the poor performance of LSDAs and GGAs at bandgap prediction can be attributed to the presence of MSIE. The presence of MSIE will typically reduce or completely eliminate the derivative discontinuity in the total energy at integer values of electron count. With such approximate functionals the ionization potential theorem of Eq. 2.43 is no longer satisfied but Janak's theorem of Eq. 2.42 remains valid [149] and as such, the left and right hand partial derivatives of the total energy remain equal to ϵ_{HOKS} and ϵ_{LUKS} respectively, assuming $\Delta_{\mathrm{xc}}^{N} = 0$ for the approximate XC functional. As discussed, MSIE typically reduces or eliminates the difference between these left and right hand partial derivatives and as such, it reduces the magnitude of

the predicted fundamental bandgap,

$$\Delta^{\text{approx}} = \epsilon^{\text{approx}}_{\text{LUKS}} - \epsilon^{\text{approx}}_{\text{HOKS}} = \left.\frac{\partial E^{\text{approx}}_{\text{tot}}}{\partial N}\right|_{N_0+\delta} - \left.\frac{\partial E^{\text{approx}}_{\text{tot}}}{\partial N}\right|_{N_0-\delta} < \left.\frac{\partial E^{\text{exact}}_{\text{tot}}}{\partial N}\right|_{N_0+\delta} - \left.\frac{\partial E^{\text{exact}}_{\text{tot}}}{\partial N}\right|_{N_0-\delta} = \Delta^{\text{exact}}, \quad (2.47)$$

where by virtue of Eq. 2.43 and Eq. 2.44 the exact left and right hand partial derivatives must be equal in magnitude to the ionisation potential and electron affinity and their difference yields the exact fundamental bandgap, Δ^{exact} of the system.

2.9 The DFT+U Method

With over five thousand peer reviewed publications to date [1], the DFT+U method is an extremely popular tool for modelling systems with localized electronic states, such as 3d-transition metal oxides [150–165] 4f-lanthanide oxides [166–173] and transition metal complexes [174–180]. Applying a Hubbard type functional can help correct for standard (semi-)local exchange correlation functionals preferential treatment of delocalised states [181,182], which is linked to the failure of such functionals to satisfy the piecewise linearity condition with respect to electron count. This spurious preference for delocalised states is best exemplified by the infinitely stretched H_2^+ molecule. In the infinite separation limit, approximate exchange correlation functionals will spuriously predict that the system with half an electron localised on each atomic site is significantly lower in energy than the system where one electron localizes on one of the two atomic sites. These two options would be degenerate with the exact XC functional [2].

For this simple system, the most widely used DFT+U functional by Dudarev et al. [183] will take the form,

$$E_{\text{u}} = \frac{U_{\text{eff}}}{2} \sum_I n^I - n^I n^I, \quad (2.48)$$

[1] Based on a bibliometric search conducted using the Scopus database.

[2] In the case of the non-infintely stretched H_2^+ molecule, these states are no longer degenerate but at large separation lengths the total energy of the delocalised state will also be artificially low.

where n^I is total subspace occupancy at atom site I and U_{eff} is the effective Hubbard U parameter, which is typically greater than zero. The DFT+U functional will yield no energetic correction for the localized state, where the single electron occupies one of the atomic sites, but the functional will contribute an energetic correction of magnitude $U_{\text{eff}}/4$ to the delocalised state. Thus, for a suitable value of the effective Hubbard U parameter, the XC functional's spurious preference for the delocalised state can be ameliorated [184, 185].

DFT+U can also be used to alleviate the bandgap problem [145, 148], i.e., standard (semi-)local XC functionals tendency to vastly underestimate the fundamental bandgap, frequently even predicting insulators as being metallic. By way of example, consider the corrective potential associated with Dudarev's functional,

$$\hat{v}_{\text{u}} = \frac{U_{\text{eff}}}{2} \sum_{\sigma} \left(\hat{P} - 2\hat{P}\hat{\rho}^{\sigma}\hat{P} \right), \tag{2.49}$$

where $\hat{\rho}^{\sigma}$ is the spin-σ Kohn Sham density operator and $\hat{P}$ is the projection operator used to define the subspace to which the Hubbard type corrections are being applied. In the idealised limit where both the highest occupied and lowest unoccupied Kohn Sham orbitals project perfectly onto the subspace projection operator $\hat{P}$, the Hubbard type corrective functional will, to first-order perturbation theory, apply a shift of minus $U_{\text{eff}}/2$ to the highest occupied orbital and plus $U_{\text{eff}}/2$ to the lowest unoccupied orbital, thus increasing the bandgap by an amount equal to the effective Hubbard U parameter. Thus, DFT+U functionals are routinely employed to alleviate the two aforementioned deficiencies in standard (semi-)local XC approximations.

Another benefit of the DFT+U method is that once the effective Hubbard U parameter has been evaluated or selected, the method exhibits a comparable computational cost to a bare DFT calculation employing the same XC functional. This enables the DFT+U method to be employed for large scale material screnning [24–26] and the development of material property databases [186–188] as well as the prediction of complex solid state defects [27–29]. These noble endeavours could not be readily achieved using methods such as coupled cluster [4–6], Diffusion Monte Carlo [17–23] or even hybrid functionals [85, 86] due to their significant computational overhead.

A suite of other methods have been developed, which have shown much success in modelling strongly correlated systems with localised electronic states,

such as Gutzwiller DFT [189–191], Dynamical Mean Field Theory [192–194] and Reduced Density Matrix Functional Theory [195, 196]. However, these methods fall beyond the realm of Kohn Sham and Generalized Kohn Sham theory. Rather than developing an entirely new theoretical framework to treat certain classes of materials, by contrast DFT+U resides within the Generalised Kohn Sham scheme and can simply be viewed as a correction term for standard exchange correlation approximations. This also allows the method to be readily implemented within existing DFT codes.

The Self-Interaction Correction (SIC) method [73, 197] is another commonly used corrective functional that fits within the Generalised Kohn Sham scheme. However, unlike modern DFT+U functionals, the SIC method suffers from the significant drawback that it is not invariant under unitary transformations of the orbitals as the SIC energy functional depends explicitly on the individual orbital densities.

2.10 The Original DFT+U Functionals

The DFT+U method was originally developed by Anisimov et al. [198] to eliviate the shortcomings of the local spin density approximation (LSDA) in describing Mott insulators. In particular, Anisimov et al. noted the LSDA's severe underestimation of the band-gap and local magnetic moments in 3d-transition metal oxides, with the LSDA even predicting CoO and FeO as being metallic [199].

However, these systems are well described by the simple multi-band Hubbard model. Anisimov et al. proposed supplementing the local density approximation (LDA) with an additional interaction energy term to treat the localised 3d states,

$$E_{\text{int}} = \frac{U}{2} \sum_{\sigma m m'} n^{\sigma}_{mm} n^{\bar{\sigma}}_{m'm'} + \frac{U-J}{2} \sum_{\substack{\sigma m m' \\ m \neq m'}} n^{\sigma}_{mm} n^{\sigma}_{m'm'}, \tag{2.50}$$

where U and J are the Hubbard U and Hund's rule exchange parameters and n^{σ}_{mm} is the spin-σ occupancy of orbital m, which can be defined as

$$n^{I\sigma}_{mm'} = \langle \phi^I_m | \hat{\rho}^{\sigma} | \phi^I_{m'} \rangle \,, \tag{2.51}$$

where $\hat{\rho}^{\sigma}$ is the spin-σ Kohn-Sham density operator and $\{\phi^I_m\}$ are the set of

atomically localized orbitals at atom I (the atomic site index is often suppressed for clarity). This interaction term is simply the expectation value of the Hubbard model Hamiltonian,

$$\hat{H}_{\mathrm{mod}} = \frac{U}{2} \sum_{mm'\sigma} \hat{n}_{m\sigma}\hat{n}_{m'\bar{\sigma}} + \frac{U-J}{2} \sum_{\substack{\sigma mm' \\ m\neq m'}} \hat{n}_{m\sigma}\hat{n}_{m'\sigma}, \tag{2.52}$$

where only the on-site interaction term has been considered, i.e., the hopping term has been excluded. However, the inter-electron interactions described by Eq. 2.51 have already been accounted for to a less favourable extent by the LDA functional itself. This necessitates the use of a double counting correction scheme. Anisimov et al. postulated that the on-site inter-electron interactions would be well described by the LDA in the homogeneous limit, i.e., when each of the $2(2l+1)$ orbitals are equally occupied, where l is the orbital angular momentum quantum number. The orbital occupancies in Eq. 2.50 are thus replaced by the deviation from the average occupancy n_0. This is referred to as the Around Mean Field (AMF) double counting correction scheme, where for completeness the average occupancy

$$n_0 = \frac{\sum_{\sigma m} n^{\sigma}_{mm}}{2(2l+1)}. \tag{2.53}$$

Anisimov et al.'s DFT+U-type functional can be written as

$$\begin{aligned} E_{\mathrm{u}}^{\mathrm{Anisimov-AMF}} = \frac{U}{2} \sum_{\sigma mm'} (n^{\sigma}_{mm} - n_0)(n^{\bar{\sigma}}_{m'm'} - n_0) \\ + \frac{U-J}{2} \sum_{\substack{\sigma mm' \\ m\neq m'}} (n^{\sigma}_{mm} - n_0)(n^{\sigma}_{m'm'} - n_0). \end{aligned} \tag{2.54}$$

The newly derived DFT+U-type functional offered a significant improvement in the bandgaps and magnetic moments of transition metal oxide test systems compared to the bare DFT(LSDA) values. However the method still left much to be desired, particularly in the case of the predicted bandgaps. In an attempt to further improve the predicted transition metal oxide bandgaps, Anisimov et al. [200] devised an alternative double counting correction scheme commonly referred to as the Fully Localised Limit (FLL) double counting scheme. Ansimov et al. proposed treating the 3d subspace of the transition metal site as an isolated system that exchanges electrons with the bath (the rest of the electronic

system). In this case, the total subspace energy, which they assume is solely composed of the 3d inter-electron interaction energy, should obey the piecewise linearity condition with respect to electron count, originally developed by Perdew et al. [1].

Anisimov et al. argue that the LDA yields relatively accurate total energies but by virtue of it being an explicit and differentiable functional of the electron density, it is a continuous function of the electron count N. They therefore approximate that the 3d inter-electron interaction energy within the LDA is given as

$$E_{\mathrm{dc}} \approx \frac{U}{2} N(N-1), \tag{2.55}$$

where N is the total subspace occupancy and for now we have ignored the exchange interaction parameter J. Using Eq. 2.55 as our double counting correction term, in combination with a simple Hubbard like interaction term yields

$$E_{\mathrm{u}} = \frac{U}{2} \sum_{\substack{\sigma\sigma' mm' \\ \sigma m \neq \sigma' m'}} n^{\sigma}_{mm} n^{\sigma'}_{m'm'} - \frac{U}{2} N(N-1). \tag{2.56}$$

For systems with integer orbital occupancies ($n^{\sigma}_{mm} = 0$ or 1), whose valence and conduction bands project perfectly onto the 3d subspace, this corrective functional will, to first order perturbation theory, open a gap of magnitude U between the occupied and unoccupied Generalised Kohn Sham states, thus alleviating the LDA's significant underestimation of the quasi-particle bandgap. This corrective functional introduces a derivative discontinuity in the XC potential within the Kohn Sham scheme but does not do so in the Generalised Kohn Sham scheme as it is an explicit functional of the first-order non-interacting reduced spin density matrix.

Anisimov et al. accounted for the non-sphericity of the Coulomb interactions by using an orbitally resolved Coulomb interaction parameters $U_{mm'}$ within the Hubbard like interaction term. Accounting also for the exchange interactions, they arrived at the following final expression for the DFT+U-type functional,

$$\begin{aligned} E_{\mathrm{u}}^{\mathrm{Anisimov-FLL}} = \quad & \frac{1}{2} \sum_{\sigma m m'} U_{mm'} n^{\sigma}_{mm} n^{\bar{\sigma}}_{m'm'} + \frac{1}{2} \sum_{\substack{\sigma m m' \\ m \neq m'}} (U_{mm'} - J_{mm'}) n^{\sigma}_{mm} n^{\sigma}_{m'm'} \\ & - \frac{U}{2} N(N-1) + \frac{J}{4} N(N-2). \end{aligned} \tag{2.57}$$

Motivated by Anisimov et al.'s seminal papers, several groups later developed DFT+U-type functionals using either around mean field or fully localised limit double counting schemes. We will explicate some of these functionals in the following two sections.

2.11 AMF Double Counting Schemes

Czyżyk et al. [201] propose using the same orbitally resolved Hubbard like interaction term

$$E_{\text{int}} = \frac{1}{2}\sum_{\sigma mm'} U_{mm'} n^{\sigma}_{mm} n^{\bar{\sigma}}_{m'm'} + \frac{1}{2}\sum_{\substack{\sigma mm' \\ m\neq m'}} (U_{mm'} - J_{mm'}) n^{\sigma}_{mm} n^{\sigma}_{m'm'} \tag{2.58}$$

used by Anisimov et al. [200] in their DFT+U functional with a Fully Localised Limit Double Counting Scheme, as given by Eq. 2.57. To allow for an improved treatment of magnetic states, Czyżyk et al. propose replacing the average occupancy n_0 in their around mean field double counting scheme with the average spin resolved occupancy n^{σ}_0,

$$\begin{aligned} E_{\text{u}}^{\text{Czyżyk}-\text{AMF}} = \quad & \frac{1}{2}\sum_{\sigma mm'} U_{mm'} (n^{\sigma}_{mm} - n^{\sigma}_0)(n^{\bar{\sigma}}_{m'm'} - n^{\bar{\sigma}}_0) \\ & + \frac{1}{2}\sum_{\substack{\sigma mm' \\ m\neq m'}} (U_{mm'} - J_{mm'})(n^{\sigma}_{mm} - n^{\sigma}_0)(n^{\sigma}_{m'm'} - n^{\sigma}_0). \end{aligned} \tag{2.59}$$

Pickett et al. [202] proposed using the spin and orbital resolved LDA occupancies $n^{\sigma mm}_0$ as the reference occupancies as opposed to the average spin resolved occupancies n^{σ}_0. This ensures that the LDA solution is a stationary solution of the LDA+U functional,

$$\begin{aligned} E_{\text{u}}^{\text{Pickett}} = \quad & \frac{1}{2}\sum_{\sigma mm'} U_{mm'} (n^{\sigma}_{mm} - n^{\sigma mm}_0)(n^{\bar{\sigma}}_{m'm'} - n^{\bar{\sigma} m'm'}_0) \\ & + \frac{1}{2}\sum_{\substack{\sigma mm' \\ m\neq m'}} (U_{mm'} - J_{mm'})(n^{\sigma}_{mm} - n^{\sigma mm}_0)(n^{\sigma}_{m'm'} - n^{\sigma m'm'}_0). \end{aligned} \tag{2.60}$$

Motivated by the failure of Czyżyk et al.'s [201] around mean field type functional of Eq. 2.59 to provide a correction to fully spin polarised systems at half occupancy, Seo developed a new DFT+U-type functional with an around

mean field double counting scheme. Seo [203] rearranged the orbitally resolved Hubbard like interaction term of Eq. 2.58 to give

$$E_{\text{int}} = \frac{1}{2}\sum_{\sigma mm'} U_{mm'}(n^{\sigma}_{mm}n^{\bar{\sigma}}_{m'm'} + n^{\sigma}_{mm}n^{\sigma}_{m'm'}) - \frac{1}{2}\sum_{\sigma mm'} U_{mm'}n^{\sigma}_{mm}n^{\sigma}_{m'm'} + \frac{1}{2}\sum_{\substack{\sigma mm' \\ m\neq m'}} (U_{mm'} - J_{mm'})n^{\sigma}_{mm}n^{\sigma}_{m'm'}. \tag{2.61}$$

Seo identified the first term as the Hartree Energy component E_{H} and proposed using average Hubbard U and Hund's J parameters for the second two terms so that

$$E_{\text{int}} = E_{\text{H}} - \frac{U-J}{2}\sum_{\sigma m} n^{\sigma}_{mm}n^{\sigma}_{mm} - \frac{J}{2}\sum_{\sigma} N^{\sigma}N^{\sigma}, \tag{2.62}$$

where N^{σ} is the total spin-σ subspace occupancy. For the double counting correction Seo proposes replacing the spin resolved orbital occupancies with the average spin resolved occupancy n^{σ}_{0} and argues that $(U + 2lJ)/(2l + 1)$ should be replaced simply by the Hund's J parameter so that the double counting correction,

$$E_{\text{dc}} = E_{\text{H}} - \frac{J}{2}\sum_{\sigma} N^{\sigma}N^{\sigma}. \tag{2.63}$$

Seo's DFT+U-type functional is given by the combination of the interaction term of Eq. 2.62 and the double counting term of Eq. 2.63,

$$E^{\text{Seo}}_{\text{u}} = -\frac{U-J}{2}\sum_{\sigma m} n^{\sigma}_{mm}n^{\sigma}_{mm}. \tag{2.64}$$

Unlike many conventional DFT+U-functionals with fully localised limit double counting schemes, the DFT+U functional of Eq. 2.64 offers a suitable correction to the potential of one-electron systems, which are traditionally plagued from issues related to one-electron self-interaction error. The success of Seo's functional at predicting the band structure of metallic Gd is ascribed to this key feature [203].

2.12 FLL Double Counting Schemes

Czyżyk et al. [201] propose using the same orbitally resolved Hubbard interaction term of Eq. 2.58 that Anisimov et al. [200] used for the original DFT+U functional with a Fully Localised Limit Double Counting Scheme. Czyżyk et

al. correctly pointed out that the interaction term as given by Eq. 2.58 in the fully localised limit (with $n^{\sigma}_{mm} = 0$ or 1) and $U_{mm'}$ and $J_{mm'}$ replaced by the average Coulomb repulsion and exchange parameters U and J, is given by

$$E_{\mathrm{dc}} = \frac{U}{2}N(N-1) - \sum_{\sigma}\frac{J}{2}N^{\sigma}(N^{\sigma}-1), \tag{2.65}$$

which slightly differs from the double counting scheme used by Anisimov et al. [200]. Combining the interaction energy term given by Eq. 2.58 with the double counting term given by Eq. 2.65 yields the DFT+U energy functional

$$\begin{aligned} E_{\mathrm{u}}^{\mathrm{Czyżyk-FLL}} = \quad & \frac{1}{2}\sum_{\sigma mm'} U_{mm'}n^{\sigma}_{mm}n^{\bar{\sigma}}_{m'm'} + \frac{1}{2}\sum_{\substack{\sigma mm' \\ m\neq m'}}(U_{mm'}-J_{mm'})n^{\sigma}_{mm}n^{\sigma}_{m'm'} \\ & -\frac{U}{2}N(N-1) + \sum_{\sigma}\frac{J}{2}N^{\sigma}(N^{\sigma}-1). \end{aligned} \tag{2.66}$$

In Ref. [204] Solovyev et al. claim to propose a DFT+U functional with a fully localised limit double counting scheme, but the proposed functional is equivalent to Anisimov et al.'s DFT+U functional [200] as given by Eq. 2.57. It is worth emphasising that Anisimov and Solovyev are named authors on both papers, the later paper should be regarded as a follow up study rather than the introduction of a novel DFT+U functional.

Due to the neglect of off diagonal terms in the occupancy matrix $n^{\sigma}_{mm'}$, the interaction energy of Eq. 2.58 is not rotationally invariant and by extension, neither are the DFT+U functionals derived from it, i.e., Eqs. 2.57,2.59,2.64,2.66. Liechtenstein et al. [205] proposed using the full Hartree-Fock expression for the interaction energy, without neglecting the off diagonal terms,

$$\begin{aligned} E_{\mathrm{int}} = \frac{1}{2}\sum_{\{m\}\sigma} & U_{mm''m'm'''}n^{\sigma}_{mm'}n^{\bar{\sigma}}_{m''m'''} \\ & + \sum_{\{m\}\sigma}(U_{mm''m'm'''} - U_{mm''m'''m'})n^{\sigma}_{mm'}n^{\sigma}_{m''m'''}, \end{aligned} \tag{2.67}$$

where $U_{mm''m'''m'}$ is defined as

$$U_{mm''m'm'''} = \langle m, m''|V_{\mathrm{ee}}|m', m'''\rangle \tag{2.68}$$

and V_{ee} is the screened Coulomb potential. Liechtenstein et al. [205] combined

this term with the fully localised limit double counting term given by Eq. 2.65 to create a rotationally invariant DFT+U functional,

$$E_{\mathrm{u}}^{\mathrm{Liechtenstein}} = \frac{1}{2}\sum_{\{m\}\sigma}(U_{mm''m'm'''} - U_{mm''m'''m'})n^{\sigma}_{mm'}n^{\sigma}_{m''m'''}, \tag{2.69}$$
$$+ \frac{1}{2}\sum_{\{m\}\sigma} U_{mm''m'm'''}n^{\sigma}_{mm'}n^{\bar{\sigma}}_{m''m'''} - \frac{U}{2}N(N-1) + \sum_{\sigma}\frac{J}{2}N^{\sigma}(N^{\sigma}-1).$$

Dudarev et al. [183] later developed a rotationally invariant DFT+U functional using only the orbital independent U and J parameters. Combining Anisimov et al.'s interaction term of Eq. 2.50 with Czyżyk et al.'s fully localised limit double counting correction of Eq. 2.65, Dudarev et al. arrived at the DFT+U functional,

$$E_{\mathrm{u}} = \frac{U-J}{2}\sum_{m\sigma} n^{\sigma}_{mm} - n^{\sigma}_{mm}n^{\sigma}_{mm}. \tag{2.70}$$

However, this functional is not rotationally invariant. Dudarev et al. [183] proposed that this functional should be replaced by the following expression,

$$E_{\mathrm{u}}^{\mathrm{Dudarev}} = \frac{U-J}{2}\sum_{mm'\sigma}(n^{\sigma}_{mm'}\delta_{mm'} - n^{\sigma}_{mm'}n^{\sigma}_{m'm}). \tag{2.71}$$

In the case of diagonal occupancy matrices, Eq. 2.70 and Eq. 2.71 are equal. Crucially Eq. 2.71 can also be written in terms of the trace over the product of spin resolved occupancy matrices

$$E_{\mathrm{u}}^{\mathrm{Dudarev}} = \frac{U-J}{2}\sum_{\sigma}\mathrm{Tr}[\mathbf{n}^{\sigma}] - \mathrm{Tr}[\mathbf{n}^{\sigma}\mathbf{n}^{\sigma}] \tag{2.72}$$

and so unlike Eq. 2.70, Eq. 2.71 is invariant under unitary transformations of the orbitals.

The methods of Dudarev [183] and Liechtenstein [205] represent the most widely used DFT+U type functionals in the literature. Despite their widespread deployment, precious few studies have compared the performance of these two corrective functionals. The few studies that do exist show that in many cases similar performance can be achieved using either Dudarev [183] or Liechtenstein's [205] functional, as demonstrated for example in the prediction of enthalpy differences in iron based spin crossover materials [206] or the lattice parameter and bandgap of ThO_2 [207]. Similarly, both DFT+U functionals

have been shown to exhibit problems of meta-stability [208–210], i.e., where the DFT+U functional converges to a local minimum.

However, there will of course exist systems where the presence of independent U and J interaction parameters becomes advantageous over the single effective interaction parameter $U_{\text{eff}} = U - J$ of Dudarev's functional. Bousquet et al. [211] for example, has shown that the correct prediction of spin canting angles and magnetocrystalline anisotropy energies in lithium transition metal orthophosphates and transition metal difluorites necessitates separate treatment of the Hubbard U and exchange interaction J. In exceptional cases, such as iron based pnictides [212], the exchange interaction J may dominate over the Hubbard U interaction, such systems would also likely benefit from the two independent parameter approach of Liechtenstein et al. [205].

2.13 A Hybrid Double Counting Scheme

Petukhov et al. [213] proposed using a linear interpolation between the around mean field and fully localised limit double counting schemes. The authors use a parameter α, $0 \leq \alpha \leq 1$, to interpolate between the two double counting schemes. In the fully localised limit, where $\alpha = 1$, Dudarev et al.'s functional is used. This functional as given in Eqs. 2.71 & 2.72 can also be written in the form,

$$E_{\text{u}}^{\text{Dudarev}} = -\frac{U-J}{2}\Bigg(\sum_{\sigma m m'} n^{\sigma}_{mm'} n^{\sigma}_{m'm} - \sum_{\sigma} n^{\sigma}(2l+1)\Bigg). \tag{2.73}$$

For the $\alpha = 0$ limit, Petukhov et al. develop a novel DFT+U functional with an around mean field double counting scheme. The authors propose treating the first term of Eq. as the interaction term,

$$E_{\text{int}} = -\frac{U-J}{2}\sum_{\sigma m m'} n^{\sigma}_{mm'} n^{\sigma}_{m'm}. \tag{2.74}$$

The raw L(S)DA should yield the correct solution in the limit of uniform spin resolved orbital occupancies so as before, the around mean field DFT+U functional can be found by replacing the $n^{\sigma}_{mm'}$ elements with $n^{\sigma}_{mm'} - n^{\sigma}\delta_{mm'}$ so

that

$$E_{\mathrm{u}}^{\mathrm{Petukhov-AMF}} = -\frac{U-J}{2}\sum_{\sigma mm'}(n^{\sigma}_{mm'} - n^{\sigma}\delta_{mm'})(n^{\sigma}_{m'm} - n^{\sigma}\delta_{m'm})$$
$$= -\frac{U-J}{2}\Bigg(\sum_{\sigma mm'} n^{\sigma}_{mm'}n^{\sigma}_{m'm} - \sum_{\sigma}(n^{\sigma})^2(2l+1)\Bigg). \quad (2.75)$$

To interpolate between these two limits Petukhov et al. [213] proposed the double counting correction term,

$$E_{\mathrm{dc}} = -\frac{U-J}{2}\sum_{\sigma}(1-\alpha)(2l+1)(n^{\sigma})^2 - \frac{U-J}{2}\sum_{\sigma}\alpha(2l+1)n^{\sigma}. \quad (2.76)$$

Combining the interaction and double counting terms of Eqs. 2.74 & 2.76, Petukhov et al. [213] proposed the following functional with a hybrid double counting scheme,

$$E_{\mathrm{u}}^{\mathrm{Petukhov-hybrid}} = -\frac{U-J}{2}\sum_{\sigma mm'} n^{\sigma}_{mm'}n^{\sigma}_{m'm} + \frac{U-J}{2}\sum_{\sigma}(1-\alpha)(2l+1)(n^{\sigma})^2$$
$$+ \frac{U-J}{2}\sum_{\sigma}\alpha(2l+1)n^{\sigma}. \quad (2.77)$$

They proposed setting the value of the parameter α such that the DFT+U functional of Eq. 2.77 corrects only the potential, i.e., offers no correction to the total energy. To satisfy this constraint α is defined as,

$$\alpha = \frac{\sum_{\sigma mm'} n^{\sigma}_{mm'}n^{\sigma}_{m'm} - \sum_{\sigma}(n^{\sigma})^2(2l+1)}{(2l+1)\sum_{\sigma} n^{\sigma}(1-n^{\sigma})}. \quad (2.78)$$

2.14 Extended DFT+U Functionals

2.14.1 DFT+U+J

Himmetoglu et al. [214] developed an extended DFT+U functional, commonly referred to as the DFT+U+J functional. They proposed that the full Hartree-Fock interaction term of Eq. 2.67 is dominated by the two-orbital Coulomb and exchange terms with interaction parameters of the form $U_{mm'mm'}$ and $U_{mm'm'm}$, respectively. Replacing these interaction parameters with their atomic averages,

$$U = \frac{1}{(2l+1)^2}\sum_{mm'}\langle m, m'|V_{\mathrm{ee}}|m, m'\rangle \quad (2.79)$$

and

$$J = \frac{1}{(2l+1)^2} \sum_{mm'} \langle m, m' | V_{\mathrm{ee}} | m', m \rangle \,, \tag{2.80}$$

Himmetoglu et al. [214] arrived at the interaction term

$$\begin{aligned} E_{\mathrm{int}} =& \frac{U}{2} \sum_{mm'\sigma} \left(n^{\sigma}_{mm} n^{\sigma}_{m'm'} + n^{\sigma}_{mm} n^{\bar{\sigma}}_{m'm'} - n^{\sigma}_{mm'} n^{\sigma}_{m'm} \right) \\ &+ \frac{J}{2} \sum_{mm'\sigma} \left(n^{\sigma}_{mm'} n^{\sigma}_{m'm} + n^{\sigma}_{mm'} n^{\bar{\sigma}}_{m'm} - n^{\sigma}_{mm} n^{\sigma}_{m'm'} \right) . \end{aligned} \tag{2.81}$$

This interaction term can also be written in the form

$$\begin{aligned} E_{\mathrm{int}} =& \frac{U}{2} \sum_{\sigma} \mathrm{Tr}[\mathbf{n}^{\sigma}]^2 + \mathrm{Tr}[\mathbf{n}^{\sigma}]\mathrm{Tr}[\mathbf{n}^{\bar{\sigma}}] - \mathrm{Tr}[\mathbf{n}^{\sigma}\mathbf{n}^{\sigma}] \\ &+ \frac{J}{2} \sum_{\sigma} \mathrm{Tr}[\mathbf{n}^{\sigma}\mathbf{n}^{\sigma}] + \mathrm{Tr}[\mathbf{n}^{\sigma}\mathbf{n}^{\bar{\sigma}}] - \mathrm{Tr}[\mathbf{n}^{\sigma}]^2 . \end{aligned} \tag{2.82}$$

Analogous to Dudarev's functional of Eq. 2.72, this interaction term is invariant under unitary transformations of the orbitals. Himmetoglu et al. choose to apply a fully localised limit double counting scheme. Using the orbital representation that diagonalizes the occupation matrix and recalling that in the fully localised limit the orbital occupations (the diagonal elements of the occupation matrix) are equal to zero or one, one can readily show that in the fully localised limit the interaction term of Eq. 2.81 becomes

$$E_{\mathrm{dc}} = \frac{U}{2} N(N-1) - \frac{J}{2} \sum_{\sigma} N^{\sigma}(N^{\sigma} - 1) + J N^{\sigma_{\mathrm{min}}} . \tag{2.83}$$

Combining the interaction and double counting terms of Eq. 2.81 and Eq. 2.83, Himmetoglu et al. proposed the following DFT+U+J functional,

$$\begin{aligned} E_{\mathrm{u}}^{\mathrm{Himmetoglu}} =& \frac{U-J}{2} \sum_{\sigma mm'} (n^{\sigma}_{mm'} \delta_{mm'} - n^{\sigma}_{mm'} n^{\sigma}_{m'm}) \\ &+ \frac{J}{2} \sum_{\sigma mm'} n^{\sigma}_{mm'} n^{\bar{\sigma}}_{m'm} - J N^{\sigma_{\mathrm{min}}} . \end{aligned} \tag{2.84}$$

The final term on the right-hand-side of Eq. 2.84 is referred to as the minority spin term and is sometimes omitted in practical calculations to aid numerical convergence. Despite being derived by very distinct techniques, Eq. 2.84 bears a remarkable resemblance to Dudarev's functional of Eq. 2.71 but also contains

an unlike spin interaction term.

2.14.2 DFT+U+$U_{\uparrow\downarrow}$

Instead of using the Hartree-Fock interaction term of Eq. 2.81, Shishkin et al. used the Hubbard-like interaction term of Eq. 2.50 and applied the same arguments as Himmetoglu et al. in deriving their double counting correction term to arrive at the following expression,

$$E_{\mathrm{u}} = \frac{U-J}{2}\sum_{\sigma mm'}(n^{\sigma}_{mm'}\delta_{mm'} - n^{\sigma}_{mm'}n^{\sigma}_{m'm}) + \frac{U}{2}\sum_{\sigma mm'} n^{\sigma}_{mm'}n^{\bar{\sigma}}_{m'm} - UN^{\sigma_{\min}}. \quad (2.85)$$

Finally, Shishkin et al. [215] choose to denote the like-spin interaction $(U-J)$ simply by U and the unlike-spin interaction U by $U_{\uparrow\downarrow}$,

$$E^{\mathrm{Shishkin}}_{\mathrm{u}} = \frac{U}{2}\sum_{\sigma mm'}(n^{\sigma}_{mm'}\delta_{mm'} - n^{\sigma}_{mm'}n^{\sigma}_{m'm}) + \frac{U_{\uparrow\downarrow}}{2}\sum_{\sigma mm'} n^{\sigma}_{mm'}n^{\bar{\sigma}}_{m'm} - U_{\uparrow\downarrow}N^{\sigma_{\min}}. \quad (2.86)$$

Shishkin et al.'s functional is equiavlent to Himmetoglu et al.'s DFT+U+J except that the unlike-spin interaction is of Coulomb type rather than exchange. Shishkin et al. proposed evaluating [216] the unlike-spin Hubbard U parameter,

$$U_{\uparrow\downarrow} = -U\frac{\sum_{\sigma}\mathrm{Tr}\left[\mathbf{n}_{\sigma}\mathbf{n}_{\bar{\sigma}}\right]}{\sum_{\sigma}\mathrm{Tr}\left[\mathbf{n}_{\sigma}\mathbf{n}_{\sigma}\right]}, \quad (2.87)$$

yielding 0 and $-U$ at the fully spin polarized and non-spin polarized limits.

2.14.3 Judiciously Modified DFT

Bajaj et al. [109,110] proposed that the like-spin interaction term of the DFT+U+J functional can help mitigate static correlation error, in the same spirit that Dudarev's functional acts as a corrector for many-electron self-interaction error. They assert that the standard DFT+U+J functional of Himmetoglu et al. [214] can be used to enforce the flat plane condition in s-valence species when the s-subshell is less than half filled ($N < 1$). Bajaj et al. argue that the like-spin interaction term should be modified for cases when $N > 1$ as the term increases with increased filling of the subshell. Upon assessing several functional forms, Bajaj et al. [109, 110] arrived at the following modified DFT+U+J functional which they refer to as judiciously modified DFT (jmDFT),

$$E_{\mathrm{u}}^{\mathrm{Bajaj}} = \begin{cases} \frac{U-J}{2}\sum_{\sigma}\mathrm{Tr}[\mathbf{n}^{\sigma}(1-\mathbf{n}^{\sigma})] + \frac{J}{2}\sum_{\sigma}\mathrm{Tr}[\mathbf{n}^{\sigma}\mathbf{n}^{\bar{\sigma}}], & N \leq 1, \\ \frac{U-J}{2}\sum_{\sigma}\mathrm{Tr}[\mathbf{n}^{\sigma}(1-\mathbf{n}^{\sigma})] + \frac{J}{2}\sum_{\sigma}\mathrm{Tr}[(\mathbf{n}^{\sigma}-1)(\mathbf{n}^{\bar{\sigma}}-1)], & N > 1. \end{cases} \quad (2.88)$$

Bajaj et al. successfully employed their functional to correct for energetic errors in finite atomic and molecular test systems at fractional values of electron count and magnetization. However, it is worth emphasizing that these promising results were achieved using a bespoke method of evaluating the U and J parameters. The performance of this corrective functional when applied using standard approaches of evaluating U and J remains to be assessed.

2.14.4 DFT+U+V

Campo et al. [217] proposed using an extended DFT+U functional typically referred to as the DFT+U + V method, to treat both on-site and inter-site interactions. Accounting for both on-site and inter-site interactions, Campo et al. [217] started with the Hartree-Fock interaction energy,

$$\begin{aligned} E_{\mathrm{int}} =& \frac{1}{2}\sum_{\{I\}\{m\}\sigma} U^{I\,I''\,I'\,I'''}_{mm''m'm'''} n^{\sigma}_{mm'} n^{\bar{\sigma}}_{m''m'''} \\ &+ \frac{1}{2}\sum_{\{I\}\{m\}\sigma} (U^{I\,I''\,I'\,I'''}_{mm''m'm'''} - U^{I\,I''\,I'''\,I'}_{mm''m'''m'}) n^{\sigma}_{mm'} n^{\sigma}_{m''m'''}, \end{aligned} \quad (2.89)$$

where the interaction matrix elements

$$U^{I\,I''\,I'\,I'''}_{mm''m'm'''} = \langle \phi^{I}_{m}, \phi^{I''}_{m''} | V_{\mathrm{ee}} | \phi^{I'}_{m'}, \phi^{I'''}_{m'''} \rangle \,, \quad (2.90)$$

have both site and orbital indices and the occupancy matrix elements

$$n^{\sigma II'}_{mm'} = \langle \phi^{I}_{m} | \hat{\rho}^{\sigma} | \phi^{I'}_{m'} \rangle \,. \quad (2.91)$$

Campo et al. neglected all but the two-orbital Coulomb terms with interaction parameters of the form $U^{II'II'}_{mm'mm'}$ and replaced these parameters with orbital averages

$$V^{II'} = \frac{1}{(2l_I+1)(2l_{I'}+1)} \sum_{ij} \langle \phi_i^I, \phi_{i'}^{I'} | V_{\text{ee}} | \phi_i^I, \phi_{i'}^{I'} \rangle \,. \tag{2.92}$$

They arrived at the interaction energy expression

$$E_{\text{int}} = \sum_{II'} \frac{V^{II'}}{2} n^I n^{I'} - \sum_{II'\sigma mm'} \frac{V^{II'}}{2} n^{\sigma II'}_{mm'} n^{\sigma I'I}_{m'm}. \tag{2.93}$$

The interaction energy expression of Eq. 2.93 can also be written in terms of the trace over the product of occupancy matrices

$$E_{\text{int}} = \sum_{II'\sigma\sigma'} \frac{V^{II'}}{2} \text{Tr}\left[\mathbf{n}^{I\sigma}\right] \text{Tr}\left[\mathbf{n}^{I'\sigma'}\right] - \sum_{II'\sigma} \frac{V^{II'}}{2} \text{Tr}\left[\mathbf{n}^{\sigma II'} \mathbf{n}^{\sigma I'I}\right], \tag{2.94}$$

and so is invariant under unitary transformations of the orbitals. Campo et al. proposed that in the fully localised limit, the off-diagonal terms $\text{Tr}\left[\mathbf{n}^{\sigma II'} \mathbf{n}^{\sigma I'I}\right]$, where $I \neq I'$, are equal to zero. The on-diagonal terms $\text{Tr}\left[\mathbf{n}^{\sigma II} \mathbf{n}^{\sigma II}\right]$ are equal to $\text{Tr}\left[\mathbf{n}^{\sigma II}\right]$ as discussed in the derivation of Himmetoglu et al.'s DFT+U+J functional. The fully localised limit double counting correction is

$$E_{\text{dc}} = \sum_{II'} \frac{V^{II'}}{2} n^I n^{I'} - \sum_{I} \frac{V^{II}}{2} n^I. \tag{2.95}$$

Subtracting the double counting term of Eq. 2.95 from the interaction term of Eq. 2.93, Campo et al. arrived at the DFT+U functional,

$$E_{\text{u}}^{\text{Campo}} = \sum_{II'\sigma mm'} \frac{V^{II'}}{2} n^{\sigma II'}_{mm'} \delta_{mm'} \delta_{II'} - \frac{V^{II'}}{2} n^{\sigma II'}_{mm'} n^{\sigma I'I}_{m'm}. \tag{2.96}$$

The inclusion of inter-site V interactions can act as a counter balance to the arguably excessive electronic localization of the standard Dudarev functional. The extended DFT+U+V functional has been shown to be particularly adept at treating systems with strong hybridization of atomic orbitals on neighboring sites such as bulk-Si [217], MnO_2 [218] and phospho-olivine cathode materials [219].

2.14.5 DFT+U Functionals for Non-collinear Systems

Dudarev et al. developed a DFT+U functional to treat non-collinear magnetic systems [220]. Starting with the on-site interaction operator used for cubic harmonic p-orbitals,

$$\hat{H} = \frac{1}{2}\left(U - \frac{J}{2}\right)\left(\hat{N}^2 - \hat{N}\right) - \frac{J}{4}\left(\hat{\mathbf{M}}^2 - 3\hat{N}\right) + \frac{J}{2}\sum_{mm'\sigma\sigma'} \hat{c}^\dagger_{m\sigma}\hat{c}^\dagger_{m\sigma'}\hat{c}_{m'\sigma'}\hat{c}_{m'\sigma}. \quad (2.97)$$

The operators $\hat{c}^\dagger_{m\sigma}$ and $\hat{c}_{m\sigma}$ are the orbital m, spin-σ creation and annihilation operators while the total subspace electron count and magnetic moment vector operators,

$$\hat{N} = \sum_{m\sigma} \hat{c}^\dagger_{m\sigma}\hat{c}_{m\sigma}, \qquad \& \qquad \hat{\mathbf{M}} = \sum_{m\sigma\sigma'} \hat{c}^\dagger_{m\sigma}\boldsymbol{\sigma}_{\sigma\sigma'}\hat{c}_{m\sigma'}, \quad (2.98)$$

and $\boldsymbol{\sigma}_{\sigma\sigma'}$ are the Pauli matrices. Focusing solely on terms in the Hamiltonian composed of two creation and two annihilation operators acting on the same electronic state, i.e., terms of the form $\hat{n}_{m\sigma}\hat{n}_{m\sigma}$, Dudarev et al. argue that with approximate DFT functionals such terms contribute an energy proportional to $n^2_{m\sigma}$, when they should contribute an energy proportional to $n_{m\sigma}$. In this case, the terms with a J prefactor cancel to yield the DFT+U functional,

$$E_{\mathrm{u}} = \frac{U}{2}\sum_{\sigma m}\left(n^\sigma_{mm} - n^\sigma_{mm}n^\sigma_{mm}\right). \quad (2.99)$$

Dudarev et al. [220] propose modifying this functional, using the same technique applied to Eq. 2.70 so that the functional is invariant with the respect to the choice of orbitals and spin quantization axis,

$$E^{\mathrm{Dudarev-NC}}_{\mathrm{u}} = \frac{U}{2}\sum_{\sigma\sigma' mm'}\left(n^{\sigma\sigma'}_{mm'}\delta_{mm'}\delta_{\sigma\sigma'} - n^{\sigma\sigma'}_{mm'}n^{\sigma'\sigma}_{m'm}\right), \quad (2.100)$$

where the occupancy matrix elements

$$n^{\sigma\sigma'}_{mm'} = \langle\phi^\sigma_m|\hat{\rho}|\phi^{\sigma'}_{m'}\rangle. \quad (2.101)$$

Interestingly, in the case of collinear spin systems, this functional reduces to Dudarev's standard functional of Eq. 2.71 except with an effective parameter $U_{\mathrm{eff}} = U$ as opposed to $U - J$.

2.15 Evaluating Hubbard Corrective Parameters

Choosing a suitable value for the Hubbard U and Hund's J parameter is of central importance to the practical application of the DFT+U method. The Hubbard U parameter is often chosen via empirical tuning to a material property of interest, such as bandgaps, crystallographic structures [221] or oxidation energies [222]. However, this comes at the expense of DFT+U's predictive power, as in this case the method can only be applied to a material with reliable experimental reference data. Furthermore, discrepancies between a DFT+U prediction and an experimental result is never solely due to the chosen value of the Hubbard U parameter. When empirically tuning to a reference bandgap value, discrepancies can arise for example due to zero point vibrational motion, crystalline defects and exciton binding energies to name but a few. To avoid the shortcomings of this empirical tuning technique, a number of techniques for evaluating the Hubbard corrective parameters have been devised including the constrained DFT method [198, 223–228], the constrained random phase approximation [229–235], the Unrestricted Hartree Fock method [236, 237], density functional perturbation theory [238, 239] as well as the self-consistent field [202, 240, 241] and minimum tracking [242–245] linear response techniques.

In the simple Hubbard model, the Hubbard U parameter is defined [246] as the energy cost of moving am electron from one atomic site to another when both sites were initially equally occupied,

$$U = E[N+1] + E[N-1] - 2E[N]. \tag{2.102}$$

Within the DFT+U scheme, the subspace occupancy N, is a continuous variable. Therefore, in the constrained DFT method, it is assumed that adding or removing a single electron from the subspace is a sufficiently small perturbation [224] for the finite difference expression of Eq. 2.102 to be replaced by,

$$U = \frac{\partial^2 E}{\partial N^2}. \tag{2.103}$$

A series of constrained DFT calculations [223] can then be performed for a

series of chosen values of the subspace occupancy N_{target},

$$E\left[N_{\text{target}}\right] = \min\left[E_{\text{tot}}[\rho(\mathbf{r})] + \lambda\left(N - N_{\text{target}}\right)\right], \tag{2.104}$$

where λ is a Lagrange multiplier. The Hubbard U parameter can then be evaluated as the curvature of $E\left[N_{\text{target}}\right]$ [228]. Alternatively, via application of the Slater transition-state rule, one can evaluate the Hubbard U parameter from the 3d eigenvalue differences [198, 225–227],

$$U = \epsilon_{3d\uparrow}\left[\frac{N_0}{2} + \frac{1}{2}; \frac{N_0}{2}\right] - \epsilon_{3d\uparrow}\left[\frac{N_0}{2} + \frac{1}{2}; \frac{N_0}{2} - 1\right], \tag{2.105}$$

where the first and second arguments of the $3d$ eigenvalue are the spin resolved subspace occupancies. For simplicity, we have assumed that the atomic subspace is of 3d character and N_0 is the bare DFT subspace occupancy. In practical calculations with the constrained DFT method, the 3d occupancy at the other transition metal sites in the subspace are typically kept fixed as the occupancy at the atomic site of interest is varied. The constrained DFT method was a considerable intellectual leap forward, but was ultimately found to significantly overestimate the value of the Hubbard U parameter [225].

2.16 Self Consistent Field Linear Response

As an alternative to the constrained DFT method, the self consistent field linear response technique was developed by Pickett at al. [202] as well as Cococcioni and de Gironcoli [240]. Cococcioni attributed the success of Dudarev's DFT+U functional to its ability to enforce the piecewise linearity condition on localised orbitals. Recalling that Dudarev's functional is invariant under unitary transformations of the orbitals, one has the freedom to choose the orbital representation that diagonalises the subspace occupancy matrix, yielding a set of spin resolved occupancies (eigenvalues) denoted as $\{\lambda_i^\sigma\}$. In this orbital representation Dudarev's functional can be expressed as,

$$E_u^{\text{Dudarev}} = \frac{U_{\text{eff}}}{2}\sum_{i,\sigma}\lambda_i^\sigma(1 - \lambda_i^\sigma). \tag{2.106}$$

If U_{eff} is set equal to the spurious curvature in the total energy with respect to orbital occupancy, Dudarev's functional will enforce a piecewise linearity condition on each localised orbital.

One should however note that the piecewise linearity condition of Perdew et al. [1] applies only to variations in the total energy with respect to total electron count not localised orbital occupancy. However, standard XC approximations are known to violate the piecewise linearity condition with respect to total electron count, yielding a spurious curvature in the total energy. Therefore, it is reasonable to assume that some *but not all* of the curvature in the total energy with respect to localised orbital occupancy is also spurious and should be removed. Cococcioni and de Gironcoli [240] argue that the erroneuous curvature is given by the difference between the curvature of the total energy E with respect to orbital occupancy and the curvature of the bandstructure total energy E_{KS} with respect to orbital occupancy,

$$U = \frac{\partial^2 E}{\partial N^2} - \frac{\partial^2 E_{\text{KS}}}{\partial N^2} \tag{2.107}$$

Eq. 2.107 can furthermore be recast in terms of first order derivatives of the corresponding Lagrange multipliers,

$$U = -\frac{\partial \alpha}{\partial N} + \frac{\partial \alpha^{\text{KS}}}{\partial N}. \tag{2.108}$$

As opposed to running cumbersome constrained DFT calculations, Cococcioni and de Gironcoli apply a Legendre transform so that the set of Lagrange multipliers, $\{\alpha\}$ and $\{\alpha^{\text{KS}}\}$ become the independent variables. The expression for the total energy becomes

$$E = \min \left\{ E[\rho(\mathbf{r})] + \sum_I \alpha_I N_I \right\}, \tag{2.109}$$

and the bandstructure total energy

$$E_{\text{KS}} = \min \left\{ E_{\text{KS}}[\rho(\mathbf{r})] + \sum_I \alpha_I^{\text{KS}} N_I \right\}. \tag{2.110}$$

Through this Legendre transform, the Lagrange multipliers can be simply viewed as the strength of the potential shift applied to the I^{th} atomic subspace and the

two derivatives of interest can be identified as,

$$\frac{\partial n_I}{\partial \alpha_J} = \chi_{IJ} \qquad \text{and} \qquad \frac{\partial n_I}{\partial \alpha_J^{\mathrm{KS}}} = \chi^0_{IJ}, \tag{2.111}$$

where χ_{IJ} and χ^0_{IJ} are the interacting and non-interacting density response functions of the system with respect to the perturbations α_I and α_I^{KS}. Finally, the Hubbard U parameter can be expressed as,

$$U = \left(\chi_0^{-1} - \chi^{-1}\right)_{II}. \tag{2.112}$$

Within this scheme, the inter-site V_{IJ} interaction parameter for use in the DFT+U+V functional [217] can be evaluated as

$$V_{IJ} = \left(\chi_0^{-1} - \chi^{-1}\right)_{IJ}. \tag{2.113}$$

So far we have considered only non-spin polarised perturbations, i.e., where a perturbation of the same strength is applied to both spin channels. If instead we consider the response of the spin σ subspace occupancy to a spin σ' perturbation, then χ and χ_0 become 2×2 response matrices and χ_0 is diagonal. For notational ease, the interaction matrix is defined as

$$f = \chi_0^{-1} - \chi^{-1}. \tag{2.114}$$

The simple Hubbard U and Hund's J parameters [241] can then defined as

$$U_{\mathrm{simple}} = \frac{1}{4}\left(f^{\uparrow\uparrow} + f^{\uparrow\downarrow} + f^{\downarrow\uparrow} + f^{\downarrow\downarrow}\right) \;\&\; J_{\mathrm{simple}} = -\frac{1}{4}\left(f^{\uparrow\uparrow} - f^{\uparrow\downarrow} - f^{\downarrow\uparrow} + f^{\downarrow\downarrow}\right). \tag{2.115}$$

2.17 Minimum Tracking Linear Response

The self-consistent field linear response method has proven to be an extremely popular technique for evaluating the Hubbard U parameter. However, numerical problems can arise in the evaluation of χ_0, it being evaluated following the first iteration of the self-consistent field cycle. Furthermore, the need to evaluate χ_0 limits the technique to self-consistent field based DFT codes at the exclusion of direct minimisation based codes [242].

To avoid using the non-interacting response matrix χ_0, Moynihan et al. [243] and later Linscott et al. [242] developed the minimum tracking linear response method. Within their technique, the Hubbbard U parameter is defined using the subspace projected Hartree Exchange Correlation (Hxc) potential,

$$U = \frac{1}{2}\frac{dv^{\uparrow}_{\mathrm{Hxc}} + dv^{\downarrow}_{\mathrm{Hxc}}}{d(n^{\uparrow} + n^{\downarrow})} \approx \frac{1}{2}\frac{f^{\uparrow\uparrow}\delta n^{\uparrow} + f^{\uparrow\downarrow}\delta n^{\downarrow} + f^{\downarrow\uparrow}\delta n^{\uparrow} + f^{\downarrow\downarrow}\delta n^{\downarrow}}{\delta(n^{\uparrow} + n^{\downarrow})}, \tag{2.116}$$

where $f^{\sigma\sigma'}$ is the projected, subspace averaged, spin-resolved Hxc kernel,

$$f^{\sigma\sigma'} = \frac{\partial}{\partial n^{\sigma'}}\left(\mathrm{Tr}\left[\hat{P}\right]^{-1}\mathrm{Tr}\left[\hat{P}\hat{v}^{\sigma}_{\mathrm{Hxc}}\right]\right)_{n^{\bar{\sigma}'}}. \tag{2.117}$$

Eq. 2.116 can be further approximated using the simple 2×2 method as given in Eq. 2.115, which emulates the partial derivative of the spin averaged v_{Hxc} with respect to subspace occupancy keeping the subspace magnetization fixed. Alternatively, one can approximate Eq. 2.116 using the scaled 2×2 method, which emulates the total derivative of the spin averaged v_{Hxc} with respect to subspace occupancy. Analogous expressions for the Hund's J parameter within the minimum tracking linear response formalism have also been developed,

$$J = -\frac{1}{2}\frac{dv^{\uparrow}_{\mathrm{Hxc}} - dv^{\downarrow}_{\mathrm{Hxc}}}{d(n^{\uparrow} - n^{\downarrow})}. \tag{2.118}$$

2.18 Koopmans-Compliant Functionals

It is worth mentioning that Koopmans-Compliant (KC) functionals [247–250] offer an alternative to the DFT+U method. Like DFT+U functionals, KC functionals are a category of corrective functional used to supplement (semi-)local XC approximations. The piecewise linearity condition with respect to electron count, or equivalently, the piecewise linearity condition with respect to frontier orbital occupation, is used to motivate the form of this corrective functional. KC functionals enforce linearity of the total energy with respect to spin resolved orbital occupancy,

$$E_{\mathrm{KC}} = E_{\mathrm{DFT}} + \sum_{i\sigma}\alpha_{i\sigma}\Pi^{\mathrm{u}}_{i\sigma}. \tag{2.119}$$

Interestingly, this corrective term is applied to every spin resolved orbital of the system as opposed to simply the frontier orbital for which the exact condition rigorously applies. Within the frozen orbital approximation, the unscreened Koopmans correction $\{\Pi^{\mathrm{u}}_{i\sigma}\}$ replaces the non-linearity of the underlying (semi-)local XC functional with a term that is linear with respect to orbital occupancy,

$$\Pi^{\mathrm{u}}_{i\sigma}(f_{i\sigma}) = -\int_0^{f_{i\sigma}} \langle\phi_{i\sigma}|\hat{H}_{KS}(s)|\phi_{i\sigma}\rangle + f_{i\sigma}\eta_{i\sigma}. \tag{2.120}$$

Here $\hat{H}_{KS}(s)$ is the approximate KS Hamiltonian where orbital $\phi_{i\sigma}$ has occupation s. A number of methods have been devised for determining the slope of the linear term $\eta_{i\sigma}$, including the Koopmans integral method and the Koopmans integral Perdew Zunger self-interaction corrected method. Of course in practice, the orbitals relax with respect to occupancy so that the unscreened Koopmans correction $\{\Pi^{\mathrm{u}}_{i\sigma}\}$ will not suffice to enforce linearity, such orbital relaxation effects are accounted for in Eq. 2.119 through the orbital dependent screening parameters $\{\alpha_{i\sigma}\}$, which also need to be evaluated. Through rigorous bench-marking, KC functionals have been shown to significantly improve both the predicted bandgaps and ionization potentials compared to the underlying (semi-)local XC approximations [251–253].

2.19 Pseudopotentials

In practical DFT calculations the Coulombic potentials of the nuclei are replaced by pseudopotentials [254–256] to avoid explicit treatment of the core electronic states. These core states are strongly localised on the atomic sites and almost inert to the chemical environment. Furthermore, if all KS states were treated explicitly, the orthogonality constraint would necessitate rapid spatial oscillations within the core region of the valence states, requiring a prohibitively large basis set. Finally, the large energies associated with these core electronic states necessitates the inclusion of special relativistic effects which can be readily incorporated within the pseudpotential as opposed to explicitly accounting for such effects within the DFT calculation proper. A number of alternative pseudopotential schemes exist including Norm Conserving Pseudopotentials [257], Ultrasoft Pseudopotentials [258] and the Projector Augmented Wave Method [259, 260]. Norm Conserving Pseudopotentials (NCPPs) have

been employed in almost all DFT calculations reported in this thesis.

The NCPP for each angular momentum channel l, has been specifically designed so that the norm of the all electron valence orbital of the isolated atom in a given reference configuration, evaluated using a specified XC functional, is equal to the norm of the corresponding pseudized orbital,

$$\int_0^{r_c^l} r^2 dr |\psi_{nl}^{\mathrm{ae}}(r)|^2 = \int_0^{r_c^l} r^2 dr |\psi_{nl}^{\mathrm{ps}}(r)|^2, \tag{2.121}$$

within a specified cutoff radius r_c^l. Furthermore, the NCPP is designed so that beyond this angular momentum dependent cutoff radius r_c^l, the pseudoized and all electron orbitals are equal,

$$\psi_{nl}^{\mathrm{ps}}(r) = \psi_{nl}^{\mathrm{ae}}(r) \quad \forall \quad r \geq r_c^l. \tag{2.122}$$

The orbital eigenvalue is determined by its asymptotic decay and so the equality specified by Eq. 2.122 ensures that pseudo and all electron eigenvalues will be equal for the reference atomic configuration. Within the valence region, the screened pseudopotential and the all electron Kohn Sham potential must equal to ensure the equaltiy of Eq. 2.122. In the core region, the pseudopotential is chosen so that the pseudo-orbitals are smooth and nodeless. A number of algorithms have been devised to determine a suitable NCPP for the core region [261–263]. The Rappe-Rabe-Kaxiras-Joannopoulos (RRKJ) algorithm [263] was used for all NCPP construction in this thesis. For the reference atomic configuration, the RRKJ algorithm constructs the radial component of the core region of the pseudo-orbital from a sum of Bessel functions $j_l(q_i, r)$ with wavevectors q_i,

$$\psi_{nl}^{\mathrm{ps}}(r) = \sum_{i=1}^{4} \alpha_i j_l(q_i, r) + \sum_{i=1}^{N} \beta_i j_l(q_i, r). \tag{2.123}$$

The wavevectors of the first four Bessel functions are chosen so that their logarithmic derivatives match that of the all electron wavefunction at r_c^l, while the wavevectors of the remaining Bessel functions are chosen to have a node at r_c^l. The coefficients are selected to satisfy the normalisation equality of Eq. 2.121 and to make the pseudo-orbitals continuous, with two continuous derivatives at r_c^l. Furthermore, in order to aid convergence of solid-state calculations with

respect to basis set size, the coefficients $\{\beta_i\}$ are chosen to minimise the kinetic energy beyond a set cutoff value q_c.

The angular momentum dependence necessitates a pseudopotential that, in spherical co-oordinates, can be regarded as nonlocal in θ and ϕ, but local in r,

$$v_{\text{pseudo}}(r) = v_{\text{local}}(r) + \sum_{lm} |Y_{lm}\rangle \left(v_l(r) - v_{\text{local}}(r)\right) \langle Y_{lm}| \,, \tag{2.124}$$

where $\{Y_{lm}\}$ are the spherical harmonics. However, to improve computational efficiency the NCPPs are typically converted in a fully non-local form via the Kleinman-Bylander procedure [264] by replacing the spherical harmonics with the atomic pseudo-orbitals,

$$v_{\text{pseudo}}(r) = v_{\text{local}}(r) + \sum_{lm} \frac{\left(v_l(r) - v_{\text{local}}(r)\right) |\psi^{\text{ps}}_{nlm}\rangle \langle \psi^{\text{ps}}_{nlm}| \left(v_l(r) - v_{\text{local}}(r)\right)}{\langle \psi^{\text{ps}}_{nlm}| \left(v_l(r) - v_{\text{local}}(r)\right) |\psi^{\text{ps}}_{nlm}\rangle}. \tag{2.125}$$

2.20 DFT Codes

A wide variety of different DFT code packages have been developed, many of which have garnered a large, active community of users and developers. The total number of Google Scholar 'Hits' associated with each DFT code package [265–291] is presented in Fig. 2.1. The bar chart shows that VASP [265] is by a considerable margin, the most widely used DFT code package, followed by CASTEP [266] and Quantum Espresso [267]. The CRYSTAL [292] and Gaussian [293] codes were omitted from the bar chart due to homonymic technical terms that frequently arise in DFT papers.

All DFT calculations in this thesis were performed using the Order-N Electronic Total Energy Package or ONETEP for short [281, 294–296]. ONETEP achieves linear scaling by truncating the first-order non-interacting reduced density matrix,

$$\rho(\mathbf{r}, \mathbf{r}') = \sum_i f_i \psi_i(\mathbf{r}) \psi_i^*(\mathbf{r}') \tag{2.126}$$

for large values of $|\mathbf{r} - \mathbf{r}'|$, which is known to decay exponentially for insulators at 0 K and metals at finite temperature [297, 298]. To readily implement this truncation, the KS orbital are expressed in a basis of localised orbitals, namely

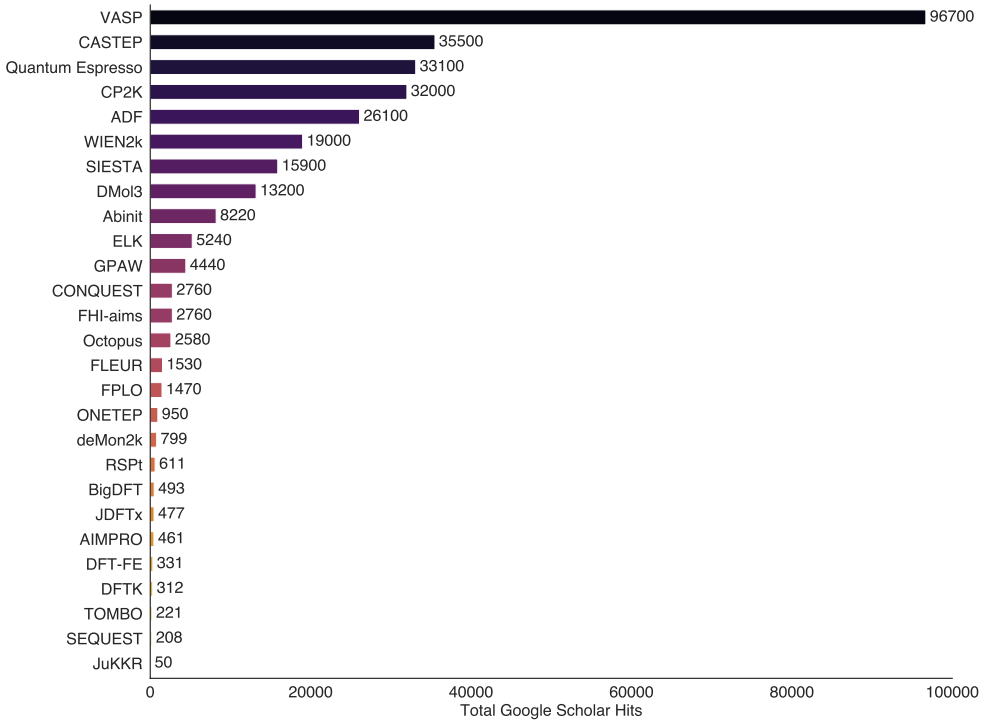

Figure 2.1: The bar chart presents the number of Google Scholar hits for each DFT code package [265–291]. The search was conducted on 23/8/2024 by searching the name of the code package in conjunction with the acronym DFT.

Non-orthogonal Generalized Wannier Functions (NGWFs),

$$\psi_i(\mathbf{r}) = \sum_\alpha \phi_\alpha(\mathbf{r}) M_i^\alpha. \tag{2.127}$$

The first-order non-interacting reduced density matrix $\rho(\mathbf{r}, \mathbf{r}')$, can in turn be expressed in the basis of NGWFs via the density Kernel $\mathbf{K}$,

$$\rho(\mathbf{r}, \mathbf{r}') = \sum_{\alpha\beta} \phi_\alpha(\mathbf{r}) K^{\alpha\beta} \phi_\beta(\mathbf{r}') \quad \text{where} \quad K^{\alpha\beta} = \sum_i M_i^\alpha f_i M_i^{*\beta}. \tag{2.128}$$

However, conventional DFT codes with localised basis sets must be supplemented with extended atomic basis functions in order to properly converge most practical calculations. To avoid including such extended basis functions without compromising on the method's accuracy, the ONETEP code optimises both the density kernel $\mathbf{K}$ and the set of NGWFS, $\{\phi_\alpha\}$. The NGWFs are described in a basis of periodic sinc (psinc) functions, which are unitary transformations of plane waves.

2.21 Martyna-Tuckerman Correction

Many DFT codes such as ONETEP, Quantum Espresso and VASP have been designed to simulate solid-state systems through the use of periodic boundary conditions. This presents a problem when using these codes to model finite systems such as atoms and molecules. In such cases the finite system is typically positioned in a simulation cell with a significant portion of vacuum as padding in all three spatial directions. However, the long range nature of the Hartree potential and the local portion of the pseudopotential necessitate the application of a correction term to avoid use of an unnecessarily large simulation cell. In this thesis, the Martyna-Tuckerman correction scheme [299] is employed for all DFT caculations of finite systems. Within this correction scheme, the Coulomb potential is decomposed into a short and long range contribution through the use of a range separation parameter α,

$$\phi(\mathbf{r}) = \frac{1}{|\mathbf{r}|} = \frac{\mathrm{erf}(\alpha|\mathbf{r}|)}{|\mathbf{r}|} + \frac{\mathrm{erfc}(\alpha|\mathbf{r}|)}{|\mathbf{r}|} = \phi_{\mathrm{long}}(\mathbf{r}) + \phi_{\mathrm{short}}(\mathbf{r}). \tag{2.129}$$

The average classical potential energy can be expressed as

$$\langle\phi\rangle = \frac{1}{2}\int\int d\mathbf{r}d\mathbf{r}'\phi(\mathbf{r}-\mathbf{r}')\rho(\mathbf{r})\rho(\mathbf{r}'). \tag{2.130}$$

If the potential $\phi(\mathbf{r})$ is defined to have the periodicity of the domain (known as the first image form), Eq. 2.130 can be re-expressed as

$$\langle\phi\rangle = \frac{1}{2V}\sum_{\hat{\mathbf{g}}} |\bar{\rho}(\mathbf{g})|^2\bar{\phi}(-\mathbf{g}), \tag{2.131}$$

where $\bar{\rho}(\mathbf{g})$ and $\bar{\phi}(\mathbf{g})$ are the Fourier series representation of the density and the potential and V is the volume of the simulation cell. In the case of the infinitely replicated periodic system, the same expression for $\langle\phi\rangle$ holds except the Fourier series representation of $\bar{\phi}(\mathbf{g})$ is replaced by the Fourier transform $\widetilde{\phi}(\mathbf{g})$. It is assumed that simulation cell is sufficiently large that the difference between $\widetilde{\phi}_{\mathrm{short}}(\mathbf{g})$ and $\bar{\phi}_{\mathrm{short}}(\mathbf{g})$ is negligible. The corresponding difference in the case of the long range components defines the screening function,

$$\hat{\phi}_{\mathrm{screen}}(\mathbf{g}) = \bar{\phi}_{\mathrm{long}}(\mathbf{g}) - \widetilde{\phi}_{\mathrm{long}}(\mathbf{g}), \tag{2.132}$$

so called because it screens the interaction of the system with an infinite array of periodic images. It is this screening function which needs to be evaluated during runtime. The screening potential can then be incorporated within the Hartree and Local pseudopotential energy terms in order to approximate their corresponding values for the truly isolated finite system. The Hartree term

$$E_{\mathrm{H}} = \frac{1}{V} \sum_{\substack{\hat{\mathbf{g}} \\ \mathbf{g} \neq 0}} \rho(-\mathbf{g}) \rho(\mathbf{g}) \left(\frac{4\pi}{\mathbf{g}^2} + \hat{\phi}_{\mathrm{screen}}(\mathbf{g}) \right) + \frac{1}{V} \hat{\phi}_{\mathrm{screen}}(0) \rho(0). \tag{2.133}$$

The corresponding local pseudopotential energy term,

$$\begin{aligned} E_{\mathrm{Loc}} =& \frac{1}{V} \sum_{\substack{\hat{\mathbf{g}} \\ \mathbf{g} \neq 0}} \sum_{I} \rho^*(\mathbf{g}) \exp\left(-i\mathbf{g}\mathbf{R}_I\right) \left(\widetilde{V}_{\mathrm{loc},I}(\mathbf{g}) - q_I \hat{\phi}_{\mathrm{screen}}(\mathbf{g}) \right) \\ &+ \frac{1}{V} \sum_{I} \rho(0) \left(\widetilde{V}^{(0)}_{\mathrm{loc},I} - q_I \hat{\phi}_{\mathrm{screen}}(0) \right), \end{aligned} \tag{2.134}$$

where $\widetilde{V}^{(0)}_{\mathrm{loc},I}$ is the non-singular part of the local pseudopotential at $\mathbf{g} = 0$ and the summation runs over all atomic site I, which each have a specified charge q_I and position $\mathbf{R}_I$. In Martyna & Tuckerman's seminal work, they found that setting $\alpha L \geq 7$, where L is the length of the shortest side of the simulation cell, yields total energies in close agreement to those of the truly isolated finite system so long as $L > 4R$, where R is the minimum radius of a sphere beyond which the density of the finite system is negligible.

Chapter 3

The Convexity Condition

The work in this chapter has been published as a Communication in the Journal of Chemical Physics (J. Chem. Phys. 159, 211102 (2023)). The work is jointly authored with my collaborator Edward Linscott and my supervisor David O'Regan. For this research project, I devised the proof of the convexity condition and wrote the first draft of the manuscript. The text shown in this chapter is the fully polished version of the manuscript including revision and editing by David and Edward as well as improvements made on the foot of peer review.

In this chapter the total energy of a finite electronic system is proven to always be convex with respect to electron count, i.e.,

$$2E_v[N_0] \leq E_v[N_0 - 1] + E_v[N_0 + 1] \quad N_0, \in \mathbb{N}^0. \tag{3.1}$$

This condition has been known empirically to be true for many decades [101], yet a rigorous proof has been lacking to date [132, 300]. Indeed, to quote Parr and Yang in Ref. [301], "*For atoms and molecules, no counterexample is known ... although a first-principles proof has never been given*".

The purpose of this chapter is to provide a mathematical proof of the convexity condition within DFT. Proving the convexity condition is of particular interest because this condition was assumed to be true in the proof of the piecewise linearity condition with respect to electron count by Perdew et al. [1]. The piecewise linearity condition with respect to electron count N states that the total energy of a finite electronic system at non-integer values of electron count is a linear interpolation of the total energies of the system at neighbouring

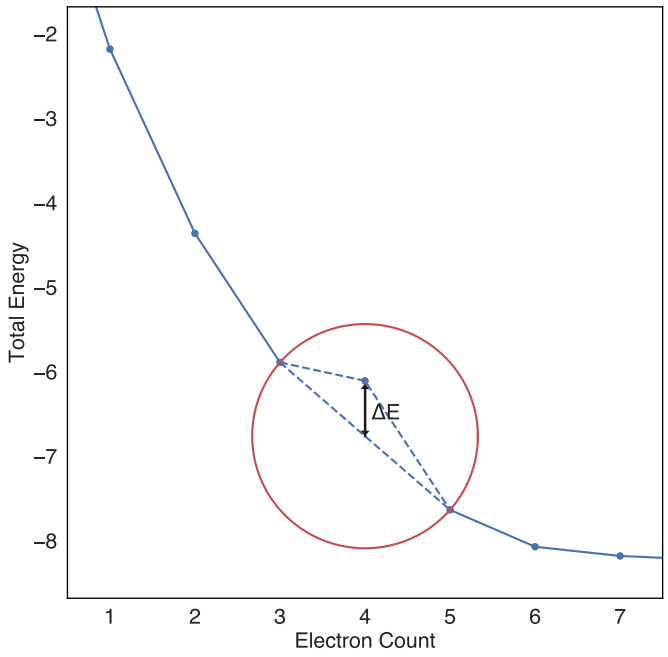

Figure 3.1: The $E_v[N]$ curve of a system which violates the convexity condition at $N = 4$. As a result of violating the convexity condition, the piecewise linearity condition of Perdew et al. [1] cannot be applied to the interval $3 < N < 5$, which is outlined by the red circle. The amount by which the system violates convexity can be quantified by the energy difference $\Delta E = 2E_v[4] - E_v[3] - E_v[5] > 0$. Two reasonable possible options for the ground state total energy curve within the interval $3 < N < 5$ are indicated by the blue dashed lines.

integer values of N,

$$E_v[N_0 + \omega] = (1 - \omega)E_v[N_0] + \omega E_v[N_0 + 1], \qquad 0 \leq \omega \leq 1, \qquad N_0 \in \mathbb{N}^0. \tag{3.2}$$

In addition to its fundamental interest in conceptual DFT [302–304], it is worth emphasizing that the piecewise linearity condition is violated by standard local and semi-local XC approximations resulting in what's known as many electron self-interaction error [107, 108, 119–121], which is linked to the severe underestimation of the band-gap by standard XC functionals. Numerous methods in electronic structure theory have been devised with the express aim of correcting for this error [91, 109, 113, 247]. Proving the convexity condition, will thus position both the piecewise-linearity condition and the corrective

functional approaches derived therefrom, on a firmer theoretical footing. In particular, it is worth noting that the piecewise linearity condition has been employed in the derivation of Hubbard-type corrective functionals [109, 200], an approach which will also be pursued in Chapters 5 & 6 of this thesis, where new DFT+U-type functionals are derived.

Fig 3.1 presents an illustrative example of an system which violates convexity at an electron count of $N_0 = 4$. As a result of violating the convexity condition, the piecewise linearity condition of Perdew et al. [1] cannot be applied in the interval $3 < N_0 < 5$ (as indicated by the red circle) and as such the total energy of a system with fractional value of electron count in this region remains undefined. Proving that within DFT, the convexity condition will always be satisfied would remove this ambiguity and ensure that for all electronic systems across all values of electron count, the $E_v[N]$ curve is properly defined.

Developing mathematical proofs within DFT is particularly challenging in part because there exists numerous inequivalent formulations of DFT, for example the original Hohenberg-Kohn formulation of DFT [33] does not apply to systems with degenerate ground states but this shortcoming can be remedied through use of the Levy constrained search formulation of DFT [41]. The proof of the convexity condition presented in this chapter specifically applies to formulations of DFT that satisfy three minimal requirements, namely that it is (1) exact for all $v-$representable densities, (2) size-consistent, and (3) translationally invariant.

3.1 Method of Proof

For the purposes of this study, we define the ground-state energy of the N electron system with external potential $v(\mathbf{r})$,

$$E_v[N] = \min_{\rho \to \int \rho(\mathbf{r}) d\mathbf{r} = N} E_v[\rho(\mathbf{r})]. \tag{3.3}$$

Yang et al. [92] have shown that in the zero-temperature grand canonical ensemble formulation of DFT, defined for an arbitrary, possibly fractional number of electrons, the total energy must obey the convexity condition (see also Gál et al. [103]). Ayers et al. [44] have shown that this condition is also satisfied in the Fock space constrained search formulation of DFT. In this chapter,

we use the infinite-separation-limit technique [92] to extend the work of Yang, Ayers et al. and show that any formulation of DFT that is (1) exact for all $v-$representable densities, (2) size-consistent, and (3) translationally invariant must obey the convexity condition. We anticipate, but do not assume, that the exact functional should satisfy conditions (1) to (3) in any DFT formulation where the ground state is generally accessible. While there are known DFT formulations in which the ground state is not always accessible, indicating that convexity does not hold in such cases, this proof nonetheless confirms a stringent constraint on the exact exchange-correlation functional. We also provide sufficient conditions for convexity in approximate DFT, which could aid in the development of density-functional approximations.

3.2 Illustrative Example

We claim that all formulations of DFT that satisfy conditions (1) to (3) must obey the convexity condition. In order to show this, suppose that there exists some N_0-electron finite system with external potential $v(\mathbf{r})$, which breaks the convexity condition. Then we have

$$2E_v[N_0] > E_v[N_0 - 1] + E_v[N_0 + 1]. \tag{3.4}$$

In order to proceed, we employ the infinite-separation-limit technique [92, 93] and consider the external potential $v'(\mathbf{r})$, which is composed of two copies of the same external potential $v(\mathbf{r})$, infinitely separated in space, such that

$$v'(\mathbf{r}) = \sum_{l=1}^{2} v_{\mathbf{R}_l}(\mathbf{r}). \tag{3.5}$$

In this illustrative example (only), we assume that the $2N_0$-electron ground-state wavefunction Ψ_1 of the system, with external potential $v'(\mathbf{r})$, is the anti-symmetric product of $\Phi_{N_0-1}(\mathbf{R}_1)$ and $\Phi_{N_0+1}(\mathbf{R}_2)$, where $\Phi_{N_0-1}(\mathbf{R}_1)$ and $\Phi_{N_0+1}(\mathbf{R}_2)$ are the ground-state wavefunctions of the $N_0 - 1$- and $N_0 + 1$-electron systems in the external potential $v(\mathbf{r})$. Specifically, we write

$$\Psi_1 = \hat{A}\Big(\Phi_{N_0-1}(\mathbf{R}_1)\Phi_{N_0+1}(\mathbf{R}_2)\Big). \tag{3.6}$$

Eq. 3.6 is an assumption as one cannot rule out the possibility that the true ground-state wavefunction is for example, the anti-symmetric product of $\Phi_{N_0-2}(\mathbf{R}_1)$ and $\Phi_{N_0+2}(\mathbf{R}_2)$. In the complete proof, this assumption is not invoked because the site electron counts of the wavefunctions $\Phi(\mathbf{R}_l)$ are not specified. We will first show that the convexity condition cannot be violated in this simple case, after which a full proof of the convexity condition will be given.

One may construct the wavefunction Ψ_2 by reversing the position vectors $\mathbf{R_1}$ and $\mathbf{R_2}$,

$$\Psi_2 = \hat{A}\Big(\Phi_{N_0-1}(\mathbf{R}_2)\Phi_{N_0+1}(\mathbf{R}_1)\Big). \tag{3.7}$$

The averaged wavefunction defined by

$$\Psi_{\text{avg}} = \frac{1}{\sqrt{2}}[\Psi_1 + \Psi_2] \tag{3.8}$$

will be degenerate with Ψ_1 and Ψ_2 and its corresponding density will be given by

$$\rho(\mathbf{r}) = \sum_{l=1}^{2} \frac{1}{2}\rho_l(\mathbf{r}; N_0 - 1) + \frac{1}{2}\rho_l(\mathbf{r}; N_0 + 1), \tag{3.9}$$

where $\rho_l(\mathbf{r}; N_0 \pm 1)$ is the ground-state electron density of site l with an electron count $N_0 \pm 1$. To deduce an expression for the total energy of the system with electron density $\rho(\mathbf{r})$, we make three assumptions about the nature of the total energy functional that were previously discussed, namely that it is (1) exact for all $v-$representable densities, (2) size-consistent, and (3) translationally invariant. For the purposes of the proof, these three assumptions are treated as axioms.

Given that Ψ_1 of Eq. 3.6 is a ground-state wavefunction of the system, we know that $\rho(\mathbf{r})$ of Eq. 3.9 is a ground-state density for the system with external potential $v'(\mathbf{r})$ and is thus $v-$representable. From assumption 1 it follows that the total energy functional is exact for the electron density $\rho(\mathbf{r})$. Its total energy should be equal to that of Ψ_1, which is simply the sum of the ground-state energies of two infinitely separated sites with electron counts $N_0 \pm 1$,

$$E_{v'}[\rho(\mathbf{r})] = E_{v_{\mathbf{R}_l}}[N_0 - 1] + E_{v_{\mathbf{R}_l}}[N_0 + 1]. \tag{3.10}$$

Here, $E_v[N]$ is the ground-state energy of the N electron system with external

potential $v(\mathbf{r})$,

$$E_v[N] = \min_{\rho \to \int \rho(\mathbf{r}) d\mathbf{r} = N} E_v[\rho(\mathbf{r})]. \tag{3.11}$$

From assumption 2, the total energy functional should be size-consistent, whereby

$$E_{v'}[\rho(\mathbf{r})] = \sum_{l=1}^{2} E_{v_{\mathbf{R}_l}}\left[\frac{1}{2}\rho_l(\mathbf{r}; N_0 - 1) + \frac{1}{2}\rho_l(\mathbf{r}; N_0 + 1)\right]. \tag{3.12}$$

Eq. 3.12 can be simplified by application of the translational invariance assumption to give

$$E_{v'}[\rho(\mathbf{r})] = 2E_{v_{\mathbf{R}_l}}\left[\frac{1}{2}\rho_l(\mathbf{r}; N_0 - 1) + \frac{1}{2}\rho_l(\mathbf{r}; N_0 + 1)\right], \tag{3.13}$$

where the site electron count is

$$N = \frac{1}{2}(N_0 - 1) + \frac{1}{2}(N_0 + 1) = N_0. \tag{3.14}$$

Eq. 3.13 enforces an upper bound on the total energy of the N_0 electron system in external potential $v_{\mathbf{R}_l}(\mathbf{r})$, namely

$$E_{v'}[\rho(\mathbf{r})] \geq 2E_{v_{\mathbf{R}_l}}[N_0]. \tag{3.15}$$

Equality in Eq. 3.15 is achieved if there exists no wavefunction with a lower total energy per site, for any external potential composed of more than two copies of $v(\mathbf{r})$ that are infinitely separated. Combining Eqs. 3.10 and 3.15 and suppressing the site index label $\mathbf{R}_l$, we find that

$$2E_v[N_0] \leq E_v[N_0 - 1] + E_v[N_0 + 1]. \tag{3.16}$$

This is in direct contradiction to our original assumption in Eq. 3.4. We now proceed to give a complete proof by contradiction of the convexity condition in the general case.

3.3 Complete Proof

Suppose there exists a sequence of consecutive integer values of electron count in the range $(N_0,\, N_0 + z_1)$ that break the convexity condition

$$2E_v[N_0 + z_2] > E_v[N_0 + z_2 - 1] + E_v[N_0 + z_2 + 1], \tag{3.17}$$

where N_0, z_1 and $z_2 \in \mathbb{N}^0$ and z_2 satisfies $0 < z_2 < z_1$. One may construct an external potential $v'(\mathbf{r})$ that is composed of q copies of the same external potential $v(\mathbf{r})$, infinitely separated in space, per

$$v'(\mathbf{r}) = \sum_{l=1}^{q} v_{\mathbf{R}_l}(\mathbf{r}). \tag{3.18}$$

The ground-state of the $q(N_0+z_2)$ electron system with external potential $v'(\mathbf{r})$ will be composed of q_1 sites with electron count N_0-z_3 and q_2 sites with electron count N_0+z_4, where $0 \leq z_3 \leq N_0$, $z_1 \leq z_4$ and q_1, q_2, z_3 and $z_4 \in \mathbb{N}^0$. The value of q_2 is constrained such that

$$q = q_1 + q_2 \tag{3.19}$$

and the value of q_1 is constrained so that the total electron count satisfies

$$q(N_0 + z_2) = q_1(N_0 - z_3) + (q - q_1)(N_0 + z_4). \tag{3.20}$$

This leaves only two free variables, z_3 and z_4. The exact values of z_3 and z_4 are those that minimize the total energy of the $q(N_0 + z_2)$ electron system. In constructing the external potential $v'(\mathbf{r})$, the total number of sites q is chosen so that the ground-state energy per site is minimized.

One possible ground-state is for the first q_1 sites to have an electron count of $N_0 - z_3$ and wave function $\Phi_{N_0-z_3}$, while the remaining $q - q_1$ sites have an electron count $N_0 + z_4$ and wave function $\Phi_{N_0+z_4}$. The ground-state wave function of the total system is then given by

$$\Psi_1 = \hat{A}\Big[\Big(\prod_{i=1}^{q_1}\Phi_{N_0-z_3}(\mathbf{R}_i)\Big)\Big(\prod_{j=q_1+1}^{q}\Phi_{N_0+z_4}(\mathbf{R}_j)\Big)\Big]. \tag{3.21}$$

Swapping position vectors $\mathbf{R}_i$ and $\mathbf{R}_j$ will result in a degenerate ground-state wavefunction. Analogously to Eq. 3.8, one may construct the averaged wave-

function Ψ_{avg} from a linear combination of the ground-state wavefunctions of the form given by Eq. 3.21. The electron density of Ψ_{avg} is

$$\rho(\mathbf{r}) = \sum_{l=1}^{q} \frac{q_1}{q} \rho_l(\mathbf{r}; N_0 - z_3) + \frac{q_2}{q} \rho_l(\mathbf{r}; N_0 + z_4), \tag{3.22}$$

Application of the same three assumptions about the nature of the total energy functional, namely that it is (1) exact for all $v-$representable densities, (2) size-consistent, and (3) translationally invariant results in the total energy, of site l with an electron count $N_0 + z_2$, given by

$$E_{v_{\mathbf{R}_l}}[N_0 + z_2] = \frac{q_1}{q} E_{v_{\mathbf{R}_l}}[N_0 - z_3] + \frac{q_2}{q} E_{v_{\mathbf{R}_l}}[N_0 + z_4]. \tag{3.23}$$

Eq. 3.23 can be simplified, using Eq. 3.19 and Eq. 3.20, to eliminate q_1 and q_2, to wit

$$E_v[N_0 + z_2] = \frac{z_4 - z_2}{z_3 + z_4} E_v[N_0 - z_3] + \frac{z_3 + z_2}{z_3 + z_4} E_v[N_0 + z_4], \tag{3.24}$$

where the site index label $\mathbf{R}_l$ has been suppressed for clarity. This expression for the total energy will hold for all integer values of electron count in the range $[N_0 - z_3, N_0 + z_4]$. Noting that the more restricted interval $[N_0, N_0 + z_1] \subseteq [N_0 - z_3, N_0 + z_4]$, from Eq. 3.24 it follows that, for all integer values of z_2 in the range $0 < z_2 < z_1$, we have

$$2E_v[N_0 + z_2] = E_v[N_0 + z_2 - 1] + E_v[N_0 + z_2 + 1]. \tag{3.25}$$

Comparing Eq. 3.17 with Eq. 3.25 we arrive at a contradiction. Therefore, the convexity condition as given by Eq. 3.1 must hold for all finite electronic systems.

3.4 Extension to 1-RDM Functional Theory

The complete proof of the convexity condition of DFT is also valid for any formulation of one-body reduced density matrix (1-RDM) functional theory that is (1) exact for all $v-$representable 1-RDMs, (2) size-consistent, and (3) translationally invariant. In this case, the electron density in Eq. 3.22 must be

substituted for the 1-RDM of Ψ_{avg},

$$\gamma(\mathbf{x},\mathbf{x}') = \sum_{l=1}^{q} \frac{q_1}{q}\gamma_l(\mathbf{x},\mathbf{x}';N_0 - z_3) + \frac{q_2}{q}\gamma_l(\mathbf{x},\mathbf{x}';N_0 + z_4), \tag{3.26}$$

where $\mathbf{x}$ and $\mathbf{x}'$ are combined space-spin coordinates and $\gamma_l(\mathbf{x},\mathbf{x}';N)$ is the ground-state 1-RDM of site l with electron count N. All other equations in the complete proof remain unchanged.

3.5 Extension to Approximate Functionals

Approximate density functionals will typically not be exact for all v-representable densities (condition 1), however it is possible to substitute this condition with two weaker conditions. An approximate density functional that satisfies (1b) the constancy condition [92, 94, 305–307], (1c) the density-size-consistency condition, (2) the functional-size-consistency condition, and (3) the translational invariance condition, will also obey the convexity condition.

The constancy condition (1b) states that given a set of g-fold degenerate, possibly symmetry-broken ground-state densities $\{\rho_i(\mathbf{r})\}$ of a system with external potential $v(\mathbf{r})$, the total energy functional satisfies

$$E_v\left[\sum_{i=1}^{g} C_i\rho_i(\mathbf{r})\right] = E_v[\rho_i(\mathbf{r})], \quad \forall \quad 0 \leq C_i \leq 1, \quad \sum_{i=1}^{g} C_i = 1. \tag{3.27}$$

We note that the vast majority of existing DFAs do not satisfy this condition [94], which yields strong constraints on the exact density functional [308, 309].

The functional-size-consistency condition (2) and translational invariance condition (3) are the same two conditions used in the general proof above. To avoid confusion with the density-size-consistency condition, we emphasize that the functional-size-consistency condition states that for any system with external potential $v'(\mathbf{r})$ composed of q infinitely separated site external potentials $v_{\mathbf{R}_l}(\mathbf{r})$, as given in Eq. 3.18, with total electron density $\rho(\mathbf{r})$ and site electron density $\rho_l(\mathbf{r})$, the total energy functional may be written as

$$E_v[\rho(\mathbf{r})] = \sum_{l=1}^{q} E_{v_{\mathbf{R}_l}}[\rho_l(\mathbf{r})]. \tag{3.28}$$

The density-size-consistency condition (1c), however, states that for any system with external potential $v'(\mathbf{r})$ of the form given in Eq. 3.18, there exists a ground-state electron density $\rho^0(\mathbf{r})$ that is composed of a linear combination of isolated site electron densities $\rho_l^0(\mathbf{r}; N_l)$, possibly of varying site electron count N_l, so that

$$\rho^0(\mathbf{r}) = \sum_{l=1}^{q} \rho_l^0(\mathbf{r}; N_l), \tag{3.29}$$

were $\rho_l^0(\mathbf{r}; N_l)$ is a ground-state density of the system with external potential $v_{\mathbf{R}_l}(\mathbf{r})$ and integer electron count N_l.

To prove that an approximate functional that satisfies conditions (1b,1c,2,3) will also obey the convexity condition, we follow the same arguments as outlined from Eqs. 3.17 to 3.20 in the complete proof. From the two size consistency conditions (1c,2), there will exist a symmetry-broken ground-state density of the system $\rho_1(\mathbf{r})$ with external potential $v'(\mathbf{r})$, where the first q_1 sites have an electron count of $N_0 - z_3$ and the remaining $q - q_1$ sites have an electron count $N_0 + z_4$, namely

$$\rho_1(\mathbf{r}) = \sum_{l=1}^{q_1} \rho_l(\mathbf{r}; N_0 - z_3) + \sum_{l=q_1+1}^{q} \rho_l(\mathbf{r}; N_0 + z_4). \tag{3.30}$$

Swapping the electron densities $\rho_l(\mathbf{r}; N_0 - z_3)$ and $\rho_l(\mathbf{r}; N_0 + z_4)$ at any two sites results in a degenerate ground-state electron density. From the constancy condition, one may construct the averaged electron density $\rho(\mathbf{r})$ from a linear combination of the ground-state electron densities of the form given by Eq. 3.30,

$$\rho(\mathbf{r}) = \sum_{l=1}^{q} \frac{q_1}{q} \rho_l(\mathbf{r}; N_0 - z_3) + \frac{q_2}{q} \rho_l(\mathbf{r}; N_0 + z_4), \tag{3.31}$$

which is equivalent to the electron density of Eq. 3.22 in the complete proof above.

From the functional-size-consistency condition and translational invariance condition it follows that

$$E_{v'}[\rho_1(\mathbf{r})] = q_1 E_{v_{\mathbf{R}_l}}[N_0 - z_3] + q_2 E_{v_{\mathbf{R}_l}}[N_0 + z_4]. \tag{3.32}$$

Using these same two conditions (2,3) and recalling that the total number of sites q was chosen so that the total ground-state energy per site was minimized,

it follows that

$$E_{v'}[\rho(\mathbf{r})] = qE_{v_{\mathbf{R}_l}}[N_0 + z_2]. \tag{3.33}$$

Invoking the constancy condition once again, $E_{v'}[\rho_1(\mathbf{r})]$ must be equal to $E_{v'}[\rho(\mathbf{r})]$, and hence

$$E_{v_{\mathbf{R}_l}}[N_0 + z_2] = \frac{q_1}{q}E_{v_{\mathbf{R}_l}}[N_0 - z_3] + \frac{q_2}{q}E_{v_{\mathbf{R}_l}}[N_0 + z_4]. \tag{3.34}$$

An analogous proof by contradiction thus follows as per the complete proof. Thus, any approximate functional that satisfies the weaker conditions (1b,1c,2,3) must also obey the convexity condition. We emphasize that the ground-state total energy and densities given by Eqs 3.27 to 3.34 need not be exact.

3.6 Inaccessible N_0-electron pure-states

This proof highlights an unusual characteristic of ground-state formulations of DFT that satisfy conditions (1) to (3): the convexity condition is *always* satisfied for such formulations of DFT irrespective of whether the pure-state convexity condition is satisfied or not. If there exists any system whose lowest energy N_0-electron pure-state $|\Psi_{N_0}\rangle$ does not satisfy the pure-state convexity condition

$$2E_v[\Psi_{N_0}] \leq E_v[\Psi_{N_0-1}] + E_v[\Psi_{N_0+1}], \tag{3.35}$$

then the total energy and electron density associated with $|\Psi_{N_0}\rangle$ is inaccessible to such formulations of ground-state DFT. These formulations of DFT will instead yield a non-pure-state ground-state density for the N_0-electron system. Assuming that the pure-state convexity condition is satisfied for the $N_0 \pm 1$-electron systems, this density will be equal to the site electron density of a pure-state $2N_0$ electron system with two identical sites infinitely separated in space. Based on the arguments presented in the complete proof, these formulations of DFT have a well-defined total energy for such densities. The DFT ground-state total energy for the N_0-electron system will be equal to the average of the

ground-state total energies of the $N_0 - 1$ and $N_0 + 1$-electron systems

$$\begin{aligned} E_v[N_0] =& \frac{1}{2}E_v[N_0 - 1] + \frac{1}{2}E_v[N_0 + 1] \\ =& \frac{1}{2}E_v[\Psi_{N_0-1}] + \frac{1}{2}E_v[\Psi_{N_0+1}] \neq E_v[\Psi_{N_0}], \end{aligned} \tag{3.36}$$

assuming that the pure $N_0 \pm 1$ electron states $|\Psi_{N_0\pm1}\rangle$ satisfy the pure-state convexity condition. Specifically, such formulations of DFT will predict a ground-state density of the N_0-electron system given by

$$\begin{aligned} \rho_{N_0}(\mathbf{r}) &= \frac{1}{2}\rho_{N_0-1}(\mathbf{r}) + \frac{1}{2}\rho_{N_0+1}(\mathbf{r}) \\ &= \frac{1}{2}\langle\Psi_{N_0-1}|\hat{\rho}_{N_0-1}|\Psi_{N_0-1}\rangle + \frac{1}{2}\langle\Psi_{N_0+1}|\hat{\rho}_{N_0+1}|\Psi_{N_0+1}\rangle , \end{aligned} \tag{3.37}$$

where $\hat{\rho}_{N_0\pm1}$ is the $N_0 \pm 1$ electron density operator.

It is worth emphasizing [101] that no experiment has ever found an electronic system that violates the inequality of Eq. 3.35. The pure-state convexity condition of Eq. 3.35 remains an open area of research in its own right. In particular, Gonis et al [310–312] propose a proof of the $E_v[\Psi_{N_0}]$ convexity condition through a description of mixed-states as pure-states in augmented Hilbert spaces. Examples have been found of model systems that violate the pure-state convexity condition of Eq. 3.35 when the $1/|\mathbf{r}|$ inter-electron Coulombic potential is replaced by an alternative potential. In particular, Lieb [42] has identified a specific two-electron system with a hard core inter-electron potential that violates the pure-state convexity condition. If it is possible to construct a density-functional for the hard core inter-electron potential that satisfies conditions (1) to (3), such a density-functional will, for this specific two-electron example, yield a ground-state energy and density equal to the average of the one and three electron pure-states as detailed in Eqs. 3.36 & 3.37.

3.7 Concluding Remarks

In this chapter, the convexity condition of the total energy of a finite electronic system with respect to electron count, within density-functional theory, is derived from using the infinite-separation-limit technique based on three minimal, conditions, with sufficient conditions adapted also for approximate DFT. For

the reasons discussed, this does not imply that the total energy is always convex at the ground-state for all DFT formulations, and counterexamples can be found (for example) in pure-state DFT. Our result nonetheless confirms a stringent constraint on the exact exchange-correlation functional. This proof also lifts an outstanding assumption in the proof of the piecewise linearity condition with respect to electron count, which will be employed in Chapters 6 and 7 to derive a new DFT+U-type functional.

Chapter 4

The Tilted-Plane Condition

The work in this chapter has been published in Physical Review Letters (Phys. Rev. Lett. 133, 026404 (2024)). The work is jointly authored with my collaborator Edward Linscott and my supervisor David O'Regan. For this research project, I devised the proof of each of the exact conditions, I ran the DFT calculations and generated the plots for all the figures with the exception of Fig. 4.5, the DFT calculations for this particular figure were completed by Edward. I also wrote the first draft of the manuscript. The text shown in this chapter is the fully polished version of the manuscript including revision and editing by David and Edward as well as improvements made on the foot of peer review.

In this chapter the shape of the total energy surface $E_v[N, M]$ is rigorously defined for all values of electron count N and magnetization M. Rigorously defining the shape of this total energy surface is of central importance to the advancement of electronic structure theory as many modern methods have, and continue to be developed, based on the shape of this total energy surface, such as DFT+U-type functionals [109, 110], the Localized orbital scaling correction method [112, 313, 314], Koopmans' Compliant Functionals [247–250] and Optimally Tuned Range Separated Hybrids [91, 116, 315] to name but a few. To date, much attention has been given to the flat plane condition [92, 96], but crucially this exact condition defines the shape of the total energy surface only for a limited range in values of magnetization. This shortcoming is highlighted in Fig. 4.1 which presents the total energy surface of the beryllium atom based

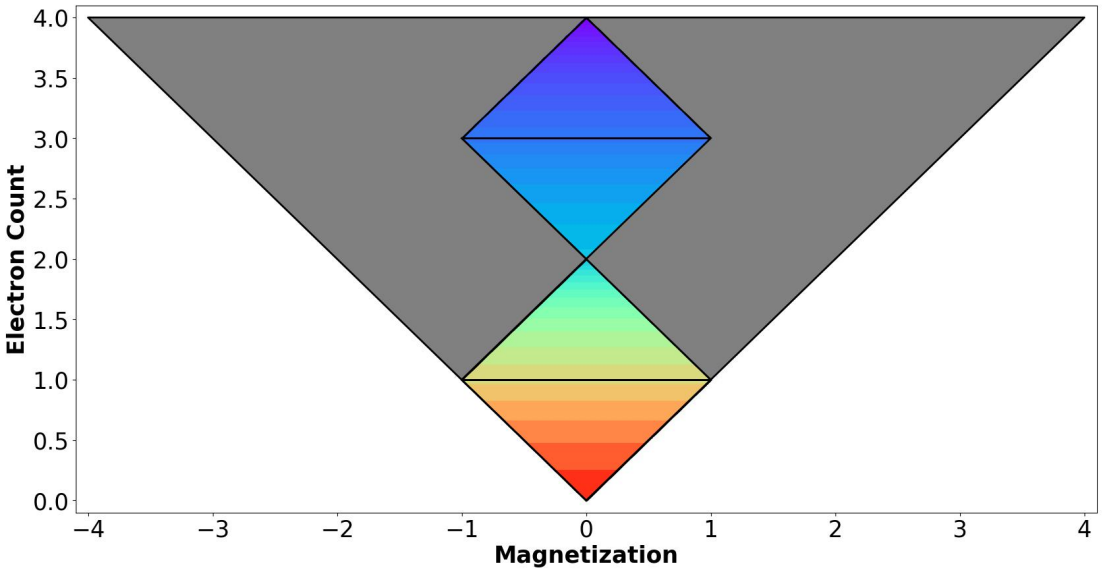

Figure 4.1: The total energy surface of the beryllium atom based on experimental NIST reference data [316]. From the flat plane condition it is known that the total energy surface of the beryllium atom is composed of four triangular shaped planes each of which is outlined in black. Across each plane, the total energy varies linearly with respect to electron count N, derivative discontinuities in the total energy will occur at integer values of N. A large portion of the total energy surface cannot be defined by the flat plane condition and as such has been highlighted in grey in the diagram.

on the flat plane condition. The regions highlighted in grey represent physically allowed values of N and M over which the flat plane condition does not apply. The work presented in this chapter aims to "fill in the blanks" and provide a complete description of this total energy surface. Knowledge of this complete total energy surface will then be employed in later chapters of this thesis to derive a new class of DFT+U-type functionals. It is also anticipated that this generalization of the flat plane condition will aid the development of other advanced electronic structure methods.

To be more specific, in this chapter we first consider the shape of the total energy surface with respect to magnetization (keeping the total electron count fixed.) The piecewise linearity condition on the total energy with respect to the total magnetization of finite quantum systems is derived, using a method of proof in DFT known as the infinite-separation-limit technique. This piecewise linearity condition generalizes the well-known constancy condition, as specified by Eq. 2.35 in the background theory section. The magnetic analog of the DFT

Koopmans' theorem is also derived which relates the slope of these piecewise linear segments to the frontier Kohn Sham eigenvalues. Moving to fractional values of both N and M, the tilted plane condition is derived, lifting certain assumptions in previous works. This generalization of the flat plane condition of Eq. 2.36, characterizes the total energy surface of a finite system for all values of electron count N and magnetization M. Rigorously defining the total energy surface for all values of N and M will be crucial for chapters 5 & 6, as the differing behaviours between the exact and approximate (semi-)local total energy functionals at non-integer values of N and M will be used to motivate the form of the DFT+U-type functionals derived therein.

4.1 Limitations of the Constancy Condition

As a reminder, the constancy condition with respect to magnetization M [92, 94], states that the total ground state energy of a system with electron count N_0 and magnetization M satisfies, for any magnetization $|M| \leq M_0$,

$$E_v(N_0, M) = E_v(N_0, M_0) = E_v(N_0, -M_0). \tag{4.1}$$

Here, $M_0 \in \mathbb{N}^0$ is the maximum magnetization of the lowest-energy state for a given integer electron count $N_0 \in \mathbb{N}^0$. $E_v(N, M)$ denotes the ground state energy of the system with specified electron count N and magnetization M, noting that these are independent parameters in DFT, subject to $|M| \leq N$. Here, and in what follows, it is supposed that no ambient field coupling to spin is present.

Combining the piecewise linearity condition with respect to electron count of Eq. 2.33 and the constancy condition [92, 95–103, 106] yields the flat plane condition

$$E_v(N, M) = (1 - \omega)E_v(N_0, M_0) + \omega E_v(N_0 + 1, M_1) \tag{4.2}$$

for $|M| \leq M_0 + \omega(M_1 - M_0)$, where $N = N_0 + \omega$ and $M_1 \in \mathbb{N}^0$ is the maximum magnetization of the lowest-energy state for the $N_0 + 1$ electron system.

It has long been recognised in the literature that the constancy condition with respect to magnetisation and the accompanying flat-plane condition apply only to the aforementioned limited interval of magnetization states. In pre-

vious works to generalize this, X. Yang et al. [101] proposed the existence of two types of flat planes, for example, and Gál and Geerlings [103] proposed a piecewise linearity condition for magnetization by invoking a zero-temperature grand canonical ensemble.

In this chapter, we rigorously classify the $E_v[N, M]$ surface for all values of magnetization M, as opposed to the limited interval $|M| \leq M_0 + \omega(M_1 - M_0)$, across all formulations of DFT that satisfy three minimum requirements. These are that the total energy functional is (a) exact for all v-representable spin-densities, (b) size-consistent, which is connected to the idea of near-sightedness, and (c) translationally invariant. We derive a piecewise linearity condition with respect to magnetisation (Thm. 1) and an accompanying, general 'tilted plane' condition (Thm. 2). A tilted plane may have a non-zero partial derivative with respect to both N and M, while a flat plane (as defined by Eq. 2.36) can only have a non-zero partial derivative with respect to N. In certain cases only, the tilted plane simplifies to the well-known flat plane. Thm. 2 classifies the $E_v[N, M]$ curve for all values of magnetisation M. Higher-energy magnetisation states are the subject of inherent interest and intense research. For example, the lowest energy triplet state plays a crucial role in phosphorescence [317,318], thermally activated delayed fluorescence [319,320] and singlet fission [321,322]. Within spin-DFT, such higher energy magnetization states are accessible, as one may compute the lowest energy state of each symmetry [39].

4.2 Linearity Condition for Magnetisation

Theorem 1. *The $E_v[N_0, M]$ curve is piecewise linear with respect to magnetization.*

4.2.1 Complete Proof

The structure of the $E_v(N_0, M)$ curve (where $N_0 \in \mathbb{N}$) can be elucidated by employing the technique, developed in W. Yang et al. [92], of constructing a system with external potential $v(\mathbf{r})$ that is composed of q copies of the same finite system with external potential $v_{\mathbf{R}_l}(\mathbf{r})$, with all copies being infinitely separated in space. The duplication of the system, at infinite separation, is a theoretical device used to consider its possible fractional charge and spin, without resorting

to an ensemble treatment. The proof proceeds by analysing the overall system of duplicates, however it is the individual finite sub-system (which may be strongly multi-reference in character) with which we are ultimately concerned. We have that

$$v(\mathbf{r}) = \sum_{l=1}^{q} v_{\mathbf{R}_l}(\mathbf{r}). \tag{4.3}$$

The total electron count is denoted by qN_0, where $N_0 \in \mathbb{N}$. It follows from the convexity condition that, at the infinite separation limit, N_0 electrons will localize on each of the q sites. For brevity, we will not repeat the electron count constraint $|M| \leq N_0 \in \mathbb{N}_0$, but note that it holds throughout Thm. 1 and Cor. 1.1. The total magnetization of the system is denoted by qM, where q and $qM \in \mathbb{Z}$. Typically, $M \notin \mathbb{Z}$ but $M \in \mathbb{Q}$ (which is supposed to be sufficiently dense in $\mathbb{R}$ for present purposes). The system has a set of degenerate ground state wave functions. At least one of these degenerate wave functions will be the antisymmetrized product of ground state wave functions at each site [92, 93]. This follows because in the infinite separation limit, each site cannot interact with its neighbours and, thus, minimizing the energy of the total system is equivalent to separately minimizing the energy associated with each site subject to the constraint that the total magnetisation and electron count is equal to qM and qN_0 respectively. This antisymmetrized product of ground state site wavefunctions will be composed of p sites with a magnetization M_i, and $q-p$ sites with a magnetization M_j, where

$$\begin{aligned} &qM = pM_i + (q-p)M_j, \quad p, q \in \mathbb{N}^0, \\ &p \leq q, \quad M_i, M_j \in \mathbb{Z}, \quad \text{and} \quad M_i \leq M \leq M_j. \end{aligned} \tag{4.4}$$

One such ground state wavefunction will have the first p sites with magnetization M_i and wave function Φ_{M_i}, and the remaining $q-p$ sites with magnetization M_j and wave function Φ_{M_j}. The ground state wave function of the total system is

$$\begin{aligned} \Psi_1 = \hat{A}\,(&\Phi_{M_i}(\mathbf{R}_1)\cdots\Phi_{M_i}(\mathbf{R}_p) \\ &\Phi_{M_j}(\mathbf{R}_{p+1})\cdots\Phi_{M_j}(\mathbf{R}_q)\big)\,. \end{aligned} \tag{4.5}$$

It is important to note that the ground state wave function of Eq. 4.5 holds regardless of whether each finite sub-system can be well-described by a single-

determinant wave function or not.

For fixed values of the external parameters N_0 and M, the total number of sites q is chosen, together with the minimum M_i and maximum M_j, such that the total energy per site is minimized while satisfying the constraints of Eq. 4.4. Often one finds $M_i = M_j - 2$, but not always. For example, in the nitrogen atom $M_i = -3$ and $M_j = +3$ for $-3 < M < +3$. The minimum M_i and maximum M_j values which minimize the total energy per site, while satisfying the constraint of Eq. 4.4, are determined by the following three conditions.

1. The site magnetizations M_i and M_j must satisfy

$$M_i \leq M \leq M_j \quad M_i, M_j \in \mathbb{Z}. \tag{4.6}$$

2. For any values of site magnetization $M_h, M_k \in \mathbb{Z}$ where $M_i \notin \{M_h, M_k\}$, the ground-state energy of the system with magnetization M_i must satisfy

$$\begin{aligned} &E_{v_{\mathbf{R}_l}}(M_i) < c_h E_{v_{\mathbf{R}_l}}(M_h) + c_k E_{v_{\mathbf{R}_l}}(M_k), \\ &M_i = c_h M_h + c_k M_k, \quad c_h, c_k \geq 0 \ \ \& \ \ c_h + c_k = 1. \end{aligned} \tag{4.7}$$

   The equivalent condition for M_j must also be true.

3. For any integer value of site magnetization M' in the range $M_i \leq M' \leq M_j$, the ground-state energy must satisfy

$$\begin{aligned} &E_{v_{\mathbf{R}_l}}(M') \geq c_i E_{v_{\mathbf{R}_l}}(M_i) + c_j E_{v_{\mathbf{R}_l}}(M_j), \\ &M' = c_i M_i + c_j M_j, \quad c_i, c_j \geq 0 \ \ \& \ \ c_i + c_j = 1. \end{aligned} \tag{4.8}$$

   Thus, the same values of M_i and M_j will satisfy these criteria for all values of the external parameter M that satisfy Eq. 4.6.

Exchanging the magnetizations M_i and M_j at any two sites results in a degenerate ground state wave function. Therefore, the average of all such wave functions Ψ_{avg} is also a ground state wave function of the system. The ground state spin σ density of Ψ_{avg} is given by

$$\rho^{\sigma}(\mathbf{r}) = \sum_{l=1}^{q} \frac{p}{q} \rho_l^{\sigma}(\mathbf{r}; M_i) + \frac{q-p}{q} \rho_l^{\sigma}(\mathbf{r}; M_j), \tag{4.9}$$

where $\rho_l^\sigma(\mathbf{r}; M_i)$ is the spin σ spin density of site l with a magnetization of M_i. In this case, each of the p (and separately $q-p$) sites have identical spin-resolved densities. We empahsize that Eq. 4.9 is one of the degenerate ground state spin σ densities of the system with total magnetization qM, where q is the number of sites and M is limited to the interval $M_i \leq M \leq M_j$.

To deduce the piecewise linearity condition for magnetization, we make three reasonable assertions about the nature of the total energy functional, namely that it is (a) exact for all v-representable spin-densities, (b) size-consistent, and (c) translationally invariant. We expect that the exact functional satisfies these in all DFT formulations where the ground state is generally accessible.

From (a), the total energy function should be exact for the spin resolved density of Eq. 4.9, so that

$$E_v[\rho^\sigma] = pE_{v_{\mathbf{R}_l}}(M_i) + (q-p)E_{v_{\mathbf{R}_l}}(M_j). \tag{4.10}$$

From (b), the total energy functional should be size-consistent, whereupon

$$E_v(\rho^\sigma) = \sum_{l=1}^{q} E_{v_{\mathbf{R}_l}}\left(\frac{p}{q}\,\rho_l^\sigma(M_i) + \frac{q-p}{q}\,\rho_l^\sigma(M_j)\right). \tag{4.11}$$

Eq. 4.11 can be simplified by application of (c), translational invariance, following which

$$E_v[\rho^\sigma] = qE_{v_{\mathbf{R}_l}}\left[\frac{p}{q}\,\rho_l^\sigma(M_i) + \frac{q-p}{q}\,\rho_l^\sigma(M_j)\right]. \tag{4.12}$$

From Eqs. 4.10 and 4.12, the total energy of the isolated site l with magnetization M_l is given by

$$E_{v_{\mathbf{R}_l}}(N_0, M_l) = \frac{p}{q}E_{v_{\mathbf{R}_l}}(N_0, M_i) + \frac{q-p}{q}E_{v_{\mathbf{R}_l}}(N_0, M_j), \tag{4.13}$$

where the site magnetization is given by

$$M_l = \frac{p}{q}M_i + \frac{q-p}{q}M_j = M. \tag{4.14}$$

An equivalent argument will hold for any value of M in the range $M_i \leq M \leq M_j$. Making the change of variable $\omega = p/q$ and relabelling the site potential

$v_{\mathbf{R}_l}(\mathbf{r})$ simply as $v(\mathbf{r})$, we may succinctly state that

$$\begin{aligned} &E_v(N_0, M) = \omega E_v(N_0, M_i) + (1-\omega) E_v(N_0, M_j), \\ &M = \omega M_i + (1-\omega) M_j, \quad M_i, M_j \in \mathbb{Z} \;\; \& \;\; 0 \leq \omega \leq 1. \end{aligned} \tag{4.15}$$

Therefore, a spin density functional $E_v[\rho^{\uparrow}(\mathbf{r}), \rho^{\downarrow}(\mathbf{r})]$ satisfying the three aforementioned conditions obeys a piecewise linearity condition with respect to magnetization, as opposed to simply a constancy condition.

We note that Gál and Geerlings [103] arrived at a similar piecewise linearity condition for magnetization by invoking a zero-temperature grand canonical ensemble.

4.2.2 Magnetic Piecewise Linearity Error

Approximate total energy functionals E_v^{aprx} typically do not obey the piecewise linearity condition with respect to magnetization. We may refer to the intrinsic deviation of E_v^{aprx} from the piecewise linear $E_v(N_0, M)$ curve, between the (often inexact) energies at integer magnetization, as magnetic piecewise linearity error (MPLE),

$$\begin{aligned} E^{\text{MPLE}}(N_0, M) = E_v^{\text{aprx}}(N_0, M) \\ - \left[\omega E_v^{\text{aprx}}(N_0, M_i) + (1-\omega) E_v^{\text{aprx}}(N_0, M_j)\right]. \end{aligned} \tag{4.16}$$

Here the electron count is a constant integer value N_0 and M, M_i, M_j and ω are given by equation 4.15. Fig. 4.2 shows the $E^{\text{MPLE}}(M)$ for the neutral helium atom.

MPLE differs from static correlation error (SCE) [94, 307], which is defined as the spurious difference in total energy, due to the use of an approximate XC functional, between states that should be degenerate. MPLE instead is an error in the total energy of non-integer magnetization states, irrespective of whether such a state should be degenerate with one with integer magnetization. It would not be so, typically, in tilted-plane regions, or in a finite external magnetic field. Conversely, not all SCE can be described as MPLE, because SCE may refer to spurious energy differences between states of the same magnetization. An example of an SCE that is not an MPLE is the energy error that may arise in the description of the spherically symmetric boron atom [94].

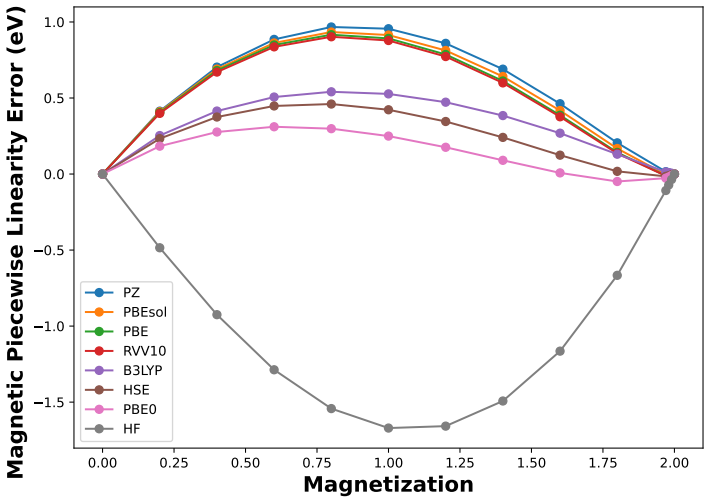

Figure 4.2: The magnetic piecewise linearity error (MPLE) for the neutral Helium atom exhibited by a variety of local [73], semi-local [60, 76], hybrid [75, 85, 86, 89] and van der Waals corrected [323] XC functionals, as well as Hartree-Fock (HF). As defined in Eq. 4.16, the MPLE for each approximate functional vanishes at certain integer values of spin-magnetization. MLPE exhibits a substantial cubic component for all functionals shown. It approximately vanishes near full magnetization (but not elsewhere) for the hybrid functionals, reflecting the negative sign of MPLE for HF in this test system and hence cancellation of error [324]

The DFT calculations on the helium atom, as presented also in Fig. 4.2, were performed using the pw.x code of the Quantum Espresso package [325]. Kinetic-energy cutoffs of 75 Ry and 300 Ry were set for the Kohn Sham wavefunctions and charge density, respectively. Martyna-Tuckerman periodic boundary corrections [299] were applied, along with a Gaussian occupancy smearing of 0.02 Ry. Davidson diagonalization was employed with Broyden charge density mixing, a mixing factor of 0.7, and a convergence threshold of 5×10^{-9} Ry. The helium atom was positioned in the centre of a $20 \times 20 \times 20$ Å^3 cell, with Γ-point only reciprocal space sampling. The Optimized Norm-Conserving Vanderbilt helium pseudopotential [326] from the SG15 collection was used, which is available at www.quantum-simulation.org. In the case of Hartree-Fock, B3LYP, HSE and PBE0, the fully magnetized ($M = 2$) helium calculations would not converge. In this case, the total energy at $M = 2$ was evaluated by linear extrapolation of the total energies from the $M = 1.97$, 1.98 & 1.99 calculations.

4.3 Koopmans' Theorem for Magnetisation

Corollary 1.1. *The partial derivative of the $E_v[N_0, M]$ curve with respect to magnetization M is equal to half the difference between the spin-dependent frontier KS eigenvalues ϵ_f^σ, whenever the partial derivative exists,*

$$\left(\frac{\partial E_v}{\partial M}\right)_N = \frac{1}{2}\left[\epsilon_{\mathrm{f}}^{\uparrow} - \epsilon_{\mathrm{f}}^{\downarrow}\right]. \tag{4.17}$$

The magnetic analogue of the DFT Koopmans' theorem can be derived by simple application of the chain rule in conjunction with the well studied (spin resolved) DFT Koopmans' theorem. This dispenses with the need to invoke total single particle energies or grand canonical ensembles used in previous proofs [103, 327] of this theorem. The partial derivative of the total energy with respect to magnetization may be expressed in terms of the spin resolved electron counts

$$\left(\frac{\partial E_v}{\partial M}\right)_N = \sum_\sigma \left(\frac{\partial E_v}{\partial N^\sigma}\right)_{N^{\bar{\sigma}}} \left(\frac{\partial N^\sigma}{\partial M}\right)_N, \tag{4.18}$$

whenever the necessary partial derivatives exist. The right and left partial derivatives of E_v with respect to N^σ are given, respectively, by

$$\begin{aligned} \lim_{\delta\to 0^+} \left(\frac{\partial E_v}{\partial N^\sigma}\right)\Big|_{N_0^\sigma+\delta} &= \epsilon^\sigma_{\mathrm{LUKS}} + \Delta_{\mathrm{xc}}^{N^\sigma} \text{ and} \\ \lim_{\delta\to 0^-} \left(\frac{\partial E_v}{\partial N^\sigma}\right)\Big|_{N_0^\sigma+\delta} &= \epsilon^\sigma_{\mathrm{HOKS}}, \end{aligned} \tag{4.19}$$

where $\epsilon^\sigma_{\mathrm{HOKS}}$ is the highest occupied spin-σ KS eigenvalue and $\epsilon^\sigma_{\mathrm{LUKS}}$ is the lowest unoccupied spin-σ KS eigenvalue. $\Delta_{\mathrm{xc}}^{N^\sigma}$ is the explicit derivative discontinuity of the exact XC functional through its explicit dependence on N^σ. Eq. 4.19 is the spin resolved analogue of Eqs. 2.43 & 2.44. For further details, see Refs. [95, 142, 328–330].

The right and left partial derivatives of the total energy with respect to magnetization of a system with no fractional KS orbital occupations is thus

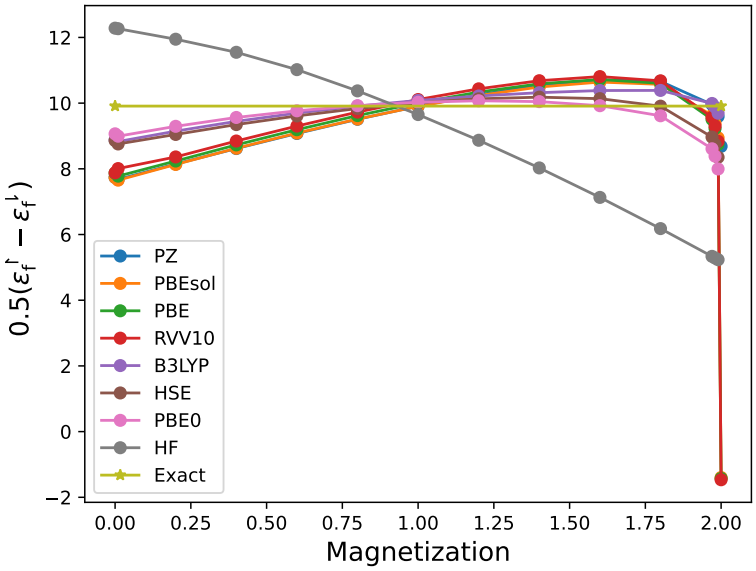

Figure 4.3: Half the difference of the fractionally occupied KS eigenvalues for the He atom, plotted as a function of magnetization M , a variety of local [73], semi-local [60, 76], hybrid [75, 85, 86, 89] and van der Waals corrected XC functionals [323], as well as Hartree-Fock (HF). The exact constant line, based on experimental NIST reference data [316], is also displayed. The lack of a derivative discontinuity within certain XC approximations can result in very large deviations from the magnetic analogue of Koopmans' theorem at certain integer values of M, as is the case shown here for the PBEsol, PBE and RVV10 functionals at $M = 2.0$. As discussed in section 4.2.2, the hybrid functionals as well as Hartree-Fock were evaluated at $M = 1.97$, 1.98 & 1.99 but not at $M = 2.0$.

given by

$$\lim_{M\to M_0^+}\left(\frac{\partial E_v}{\partial M}\right)_N = \frac{1}{2}\left[\epsilon^{\uparrow}_{\mathrm{LUKS}} - \epsilon^{\downarrow}_{\mathrm{HOKS}} + \Delta_{\mathrm{xc}}^{N^{\uparrow}}\right] \quad \text{and}$$
$$\lim_{M\to M_0^-}\left(\frac{\partial E_v}{\partial M}\right)_N = \frac{1}{2}\left[\epsilon^{\uparrow}_{\mathrm{HOKS}} - \epsilon^{\downarrow}_{\mathrm{LUKS}} - \Delta_{\mathrm{xc}}^{N^{\downarrow}}\right], \tag{4.20}$$

since the partial derivative of N^σ with respect to M is equal to one half. For systems with one fractionally occupied spin up frontier KS orbital of eigenvalue $\epsilon^{\uparrow}_{\mathrm{f}}$, and one fractionally occupied spin down one of eigenvalue $\epsilon^{\downarrow}_{\mathrm{f}}$, the expression given by Eq. 4.20 simplifies to

$$\left(\frac{\partial E_v}{\partial M}\right)_N = \frac{1}{2}\left[\epsilon^{\uparrow}_{\mathrm{f}} - \epsilon^{\downarrow}_{\mathrm{f}}\right]. \tag{4.21}$$

Typical XC functionals will break this exact condition. In Fig. 4.3 the slope of the $E_v[N_0, M]$ curve for the Helium atom, as evaluated from the PBE KS eigenvalues, is plotted as a function of magnetization. Use of the exact XC functional would result in a perfect step function.

4.4 The Tilted Plane Condition

Theorem 2. *The $E_v[N, M]$ surface obeys the tilted plane condition described by Eq. 4.24.*

Analysis of the $E_v[N_0, M]$ curve may be extended to include states with not only fractional magnetization M but also fractional electron count N. Again, one may construct an external potential given by Eq. 4.3, in this case typically both N and $M \notin \mathbb{Z}$, but the total system electron count and magnetization, qN and $qM \in \mathbb{Z}$. The ground state of this system will be composed of qc_i sites with electron count N_i and magnetization M_i, where i ranges from 1 to V_{count} with:

$$\sum_{i=1}^{V_{\text{count}}} c_i = 1, \quad 0 \leq c_i \leq 1, \quad N_i,\ M_i,\ qc_i \in \mathbb{Z}. \tag{4.22}$$

The values of c_i, N_i and M_i are constrained so that

$$N = \sum_{i=1}^{V_{\text{count}}} c_i N_i \quad \text{and} \quad M = \sum_{i=1}^{V_{\text{count}}} c_i M_i. \tag{4.23}$$

Following an analogous derivation to that outlined in Thm. 1, one finds that, for $N, M \notin \mathbb{Z}$,

$$E_v[N, M] = \sum_{i=1}^{V_{\text{count}}} c_i E_v[N_i, M_i]. \tag{4.24}$$

Vertices in the energy landscape will occur at the specified integer values of electron count N_i and magnetization M_i. V_{count} is the number of vertices associated with a particular plane, typically equal to 3 or 4, however higher numbers of vertices are possible in very rare circumstances. For example, let us assume that the maximum magnetization of the lowest energy state of the $N-1$, N and $N+1$ electron systems are given by M, $M+1$, and M, respectively, where $M \geq 1$. It is assumed that the convexity condition is satisfied for the

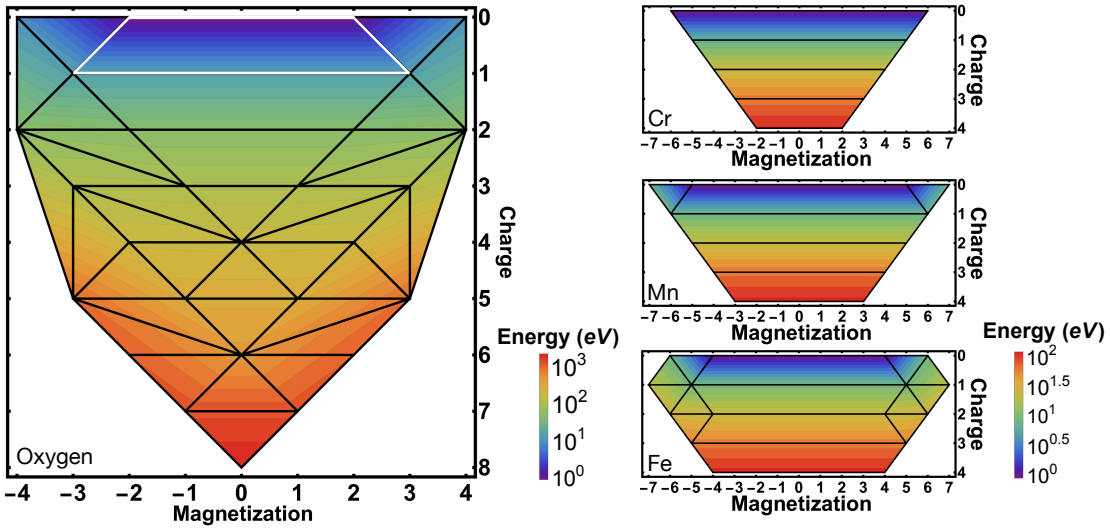

Figure 4.4: The projection of the $E_v[N, M]$ surface of the oxygen, chromium, manganese and iron atoms onto the $N - M$ plane. The $E_v[N, M]$ curves are composed of a series of three- and four-sided planes with vertices at integer values of N and M. (The vertical axis is labelled in terms of the total atomic charge as opposed to total electron count.) The total energy varies linearly across each plane. Each plane is outlined in black. Energy contour lines are plotted at intervals of $10^{0.1x}$eV. For each atom, the total energy values are based on available experimental NIST reference data [316] and are given relative to the ground state total energy of the neutral atom in its lowest energy magnetization state, which is set to 1 eV for visualization purposes. Orbital and nuclear moments are not included. The $E_v[N, M]$ surface of the oxygen atom for charged states between +5 and +6 is composed of a series of five triangular shaped planes, four of which can neither be classed as a type 1 or a type 2 flat plane of X. Yang et al. [101]. Note that planes at the edges are omitted due to absence of experimental reference data. If any additional experimental reference data points not currently included are found to be low enough in energy, they could also affect the shape of the outlying, high-magnetization $E_v[N, M]$ surfaces shown here.

$N-1$, N and $N+1$ electron systems. In the special case where

$$\frac{E_v[N, M+1] - E_v[N-1, M]}{N-(N-1)} = \frac{E_v[N+1, M] - E_v[N, M+1]}{(N+1)-N}, \tag{4.25}$$

the plane in question will have an hexagonal shape (stretched in the magnetization direction whenever $M > 1$). Such a plane would require the summation in Eq. 14 to be extended over six vertices

$$E_v[N, M] = \sum_{i=1}^{6} c_i E_v[N_i, M_i]. \tag{4.26}$$

Higher numbers of vertices will occur when there is a fortuitous equality of certain energy derivatives. Eq. 4.25 specifies the energy derivative equality for this particular example. It is worth noting that Eq. 4.25 simplifies to

$$2E_v[N, M+1] = E_v[N-1, M] + E_v[N+1, M], \tag{4.27}$$

however this simplification will not occur in all cases of high vertex count. To simplify discussion from hereon, we restrict $V_{\text{count}} = 4$, however, the method used to generate Fig. 4.4 includes no restriction on V_{count}.

In cases where the electron counts of the four states at the vertices satisfy $N_1 = N_2 = N_3 - 1 = N_4 - 1$ and the magnetizations $M_1 = -M_2$, $M_3 = -M_4$, with $E_v[N_i, M_i] = \min_M\{E_v[N_i, M]\}$, Eq. 4.24 simplifies to the flat-plane condition as outlined in Eq. 2.36. X. Yang et al. [101] and Cuevas-Saavedra et al. [102] report the existence of two types of flat plane structures. These types are special cases (non-exhaustive ones; see Fig. 4.4 for an exception) of the more general condition outlined by Eq. 4.24, specifically when $c_4 = 0$. Generally, restricting c_4 to be zero prohibits the correct flat plane structure of systems, e.g., the oxygen atom for $7 \leq N \leq 8$ and $|M| \leq 10-N$, as highlighted in white in Fig. 4.4. The correct energy expression for this energy surface, may be written as

$$\begin{aligned} E_v[N, M] =& c_1 E_v[8, 2] + c_2 E_v[8, -2] + c_3 E_v[7, 3] + c_4 E_v[7, -3] \\ =& \frac{(N-7)(10-N+M)}{2(10-N)} E_v[8, 2] + \frac{(N-7)(10-N-M)}{2(10-N)} E_v[8, -2] \\ &+ \frac{(8-N)(10-N+M)}{2(10-N)} E_v[7, 3] + \frac{(8-N)(10-N-M)}{2(10-N)} E_v[7, -3], \end{aligned} \tag{4.28}$$

for all $7 \leq N \leq 8$ and $|M| \leq 10 - N$. The flat plane described by Eq. 4.28 is highlighted in white in Fig. 4.4.

Despite $E_v[8,2] = E_v[8,-2]$ and $E_v[7,3] = E_v[7,-3]$ for the oxygen atom, reduction of Eq. 4.28 to the sum of two terms with coefficients c_1' and c_2' would wrongly give

$$M \neq \sum_{i=1}^{2} c_i' M_i. \tag{4.29}$$

A number of other interesting observations can be made from Fig. 4.4. If we look, for example, at the 5+ oxygen anion, we can read from the graph that the energy is minimized at $M = 1$ (the spin-doublet configuration $1s^2 2s^1$), with a piecewise constant segment for $|M| \leq 1$, while the next lowest magnetization state is $M = 3$ (the spin-quartet configuration $1s^1 2s^1 ({}^3S) 2p^1$), with piecewise linear (not piecewise constant) segments connecting these for $1 \leq |M| \leq 3$.

It is also worth noting that the neutral chromium atom violates the Madelung rule, with a ground state electron configuration of $[Ar]3d^5 4s^1$. This can been seen in the central uppermost plane of the $E_v[N,M]$ surface for Cr, which extends from -6 to $+6$ at zero charge as opposed to -4 to $+4$, which would be the case if the configuration followed the Madelung rule ($[Ar]3d^4 4s^2$).

The black lines within the $E_v[N,M]$ surfaces of Fig. 4.4, correspond to values of N & M where derivative discontinuities in the total energy occur. As shown in the $E_v[N,M]$ surface of the oxygen atom, these derivative discontinuities do not solely occur at integer values of N & M, or at integer values of the spin up and spin down electron counts ($N^{\uparrow}$ and $N^{\downarrow}$). For example, there is a line segment stretching from the point $(0,6)$ to the point $(3,5)$. This line represents a 'seam' on which, in this case, both of the partial derivatives change. Thus, there is a derivative discontinuity in the total energy for all values of total charge $C = 8 - N$ (8 being the atomic number of oxygen) and total magnetization M on this line segment. The equation of the line segment is $C = -\frac{1}{3}M + 6$, and so derivative discontinuies occur, e.g., at $M = 1.5$ and $C = 5.5$ as well as at the integer magnetization $M = 2$ and $C = 5\frac{1}{3}$. This discontinuity (for varying N at constant M) has a magnitude of approximately 10.2 eV.

This example also provides that a derivative discontinuity may be encountered while one spin occupancy alone is varied, at possibly non-integer values. Recall that the spin-indexed occupancies are given by $N^{\uparrow} = (N + M)/2$ and $N^{\downarrow} = (N - M)/2$. We may consider traversing from point $(2,6)$ (which corre-

sponds to $N^{\uparrow} = 2$ and $N^{\downarrow} = 0$) to point $(1, 5)$ (which corresponds to $N^{\uparrow} = 2$ and $N^{\downarrow} = 1$). A derivative discontinuity is encountered at half-integer filling $N^{\downarrow} = 0.5$, which is at the aforementioned point $(1.5, 5.5)$, half-way along the line segment. It is worth noting that there appears to be no possible absent NIST spectroscopic data in the region in question that might correspond to higher-energy spin states, the existance of which might otherwise change the fracturing of the $E_v[N, M]$ landscape and affect this prediction.

Gál and Geerlings [103] reported the existence of a tilted plane energy surface but their energy expressions also have the $c_4 = 0$ restriction, meaning that (N_i, M_i) values in their energy expression will not always represent vertices in the energy landscape. The same is true for Chan's $E_v[N, M]$ energy expression [95]. To the best of our knowledge, a lifting of the $c_4 = 0$ restriction of the generalized flat plane condition has only been discussed to date in the unpublished Ref. [106]. If we assume that (N_i, M_i) values represent vertices in the energy landscape, the $c_4 = 0$ restriction allows for triangular shaped planes but neglects planes of other shapes, such as isosceles trapezoids, which occur in the oxygen atom (Fig. 4.4).

A consequence worthy of future investigation is the appearance of derivative discontinuities both at non-integer values of total electron count N, and of spin-electron count $\frac{1}{2}(N \pm M)$, as seen, e.g., in the oxygen atom between charge states 5+ and 6+ with $1 \leq M \leq 2$ (Fig. 4.4). Knowledge of the occurrence of a tilted plane energy surface has already been applied to correct the PBE total energy of dissociated triplet H_5^+ in Ref. [331].

It is instructive to apply our analysis on the helium energy surface at fractional values of N and M. The $E_v[N, M]$ surface for the helium atom with electron count in the range $1 \leq N \leq 2$ and magnetization $M \geq 2 - N$ is given by

$$E_v[N, M] = (2 - N)E_v[1, 1] + \frac{N - M}{2}E_v[2, 0] + \frac{M + N - 2}{2}E_v[2, 2]. \quad (4.30)$$

This plane will have a non-zero partial derivative with respect to magnetization and thus has a 'tilted plane' shape as opposed to a simple 'flat plane' shape. Approximate XC functionals typically do not obey the tilted plane condition. For example, Fig. 4.5 displays the energy of the helium atom when using the PBE XC functional, with respect to the exact tilted plane outlined in Eq. 4.30.

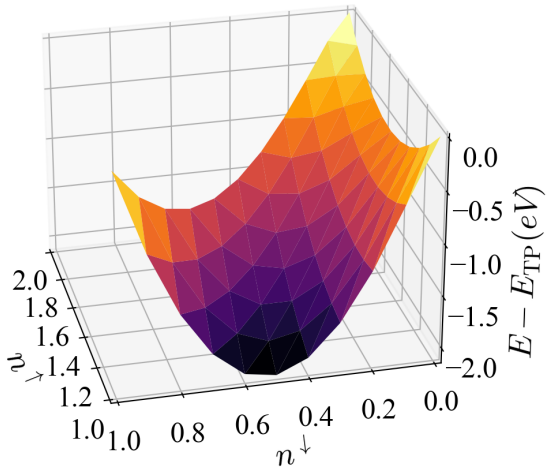

Figure 4.5: A plot of the deviation of the total energy using the PBE XC functional from the tilted plane condition for the Helium atomic system with spin up and spin down electron counts in the range $1 \leq n^{\uparrow} \leq 2$ and $0 \leq n^{\downarrow} \leq 1$, assuming the PBE total energy is exact at integer values of $n^{\uparrow}$ and $n^{\downarrow}$.

4.5 Energy Surface of Transition Metal Systems

The projection of the $E_v[N, M]$ surface onto the $N - M$ plane for the strongly correlated CrMo, VCr and VMo transition metal hetero-dimers are presented in Fig 4.6. In particular, please note that the $E_v[N, M]$ surfaces are composed of a series of three and four sided planes with vertices at integer values of N and M, as is the case with the oxygen, chromium, manganese and iron atoms. The total energy varies linearly across each plane but, for ease of visualization, each plane is colored based on the average of the energies at the vertices. The total energy values for the strongly correlated CrMo, VCr and VMo transition metal hetero-dimers are based on CASSCF/CASPT2 reference calculations on vertical excitations from Ref. [332]. This study classified the ground state of each dimer, in both the neutral and anionic state, as having a pronounced multi-reference character, as well as an effective bond order indicative of a quintuple bond.

For each system, the total energy values are relative to the ground state total energy of the neutral dimer in its lowest energy magnetization state. Note that only a subset of the full $E_v[N, M]$ surface is presented for these systems, this is due to the limited data available. If any additional reference data points not

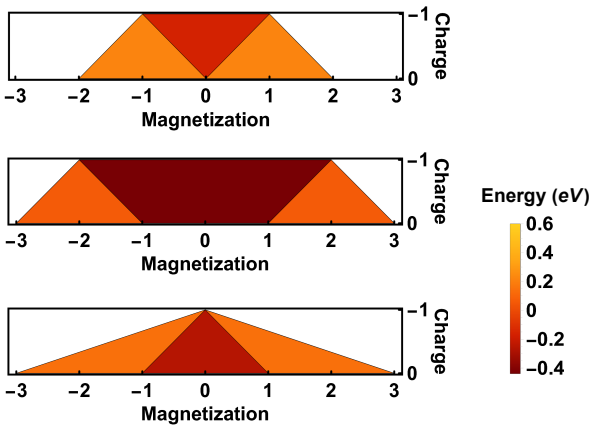

Figure 4.6: The projection of the $E_v[N, M]$ surface onto the $N-M$ plane for the CrMo (A), VCr (B) and VMo (C) hetero-dimers based on CASSCF/CASPT2 reference calculations for vertical charge and spin excitations [332]. The y-axis is labelled in terms of total charge as opposed to total electron count.

currently included are found to be low enough in energy, they could also affect the shape of the $E_v[N, M]$ surfaces shown here.

The energies of localized electronic states within a solid material also obey the tilted plane condition in the limit where the subspace-bath interaction energy varies linearly with spin resolved occupancy. This of course includes the case where the subspace-bath interaction becomes negligible. Fig. 4.7 displays sample tilted plane structures for a d-orbital subspace in the subspace-bath linear interaction limit under octahedral, tetrahedral, and square-planar crystal field splittings. The total energy of the electronic states with integer spin-resolved orbital occupancies were approximated using the model

$$E^{\text{mod}} = \sum_i \epsilon_i n_i + U \sum_i n_i^{\uparrow} n_i^{\downarrow} + \frac{V}{2} \sum_{i \neq j} n_i n_j, \tag{4.31}$$

where U and V are the intra-orbital and inter-orbital interaction parameters, respectively. The values ϵ_i and n_i^{σ} are the energy level and spin-σ electron count, respectively, of orbital i. For each crystal field splitting, and hence degeneracy pattern, a wide variety of possible tilted pane structures exist. Total-energy approximations defined for non-integer spin-occupancies arise in a wide variety of DFT-related methods, e.g., in DFT+U type XC-corrections and in machine learning proxies for total-energy components. These and perhaps next-generation XC approximations, as we approach exactitude, could beneficially (recalling Fig. 4.7) (a) change expressions discretely between different tilted-

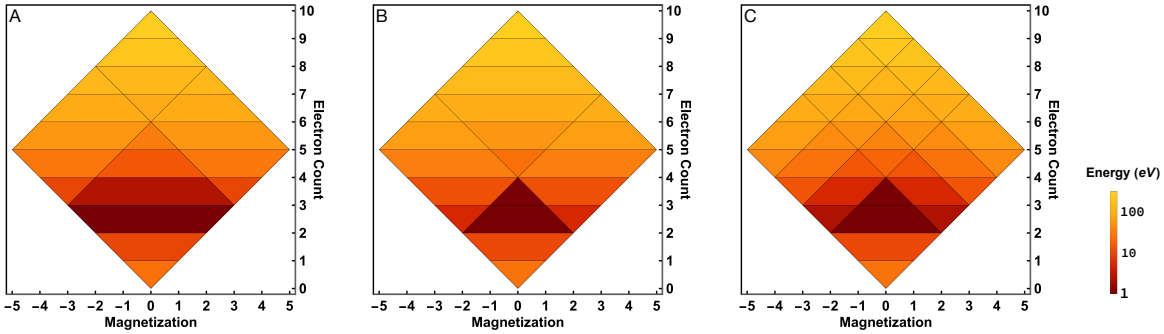

Figure 4.7: Sample tilted plane structures for a d-orbital subspace in the subspace-bath linear interaction limit, under octahedral (A), tetrahedral (B) and square-planar (C) crystal field splittings. In the model energy (see Eq. 4.31), parameters were chosen to show a sample of the the rich coordination-dependence of flat plane shapes. The interaction parameters U and V were set at 11 eV and 10 eV, respectively, and the orbital energy levels were chosen so that $\sum_i \epsilon_i = -80$ eV. The set of orbital energy levels $\{-24, -24, -24, -4, -4\}$, $\{-25, -25, -10, -10, -10\}$ and $\{-25, -25, -18, -10, -2\}$, in eV, were used for the octahedral, tetrahedral and square-planar crystal fields, respectively. The total energy varies linearly across each plane but, for ease of visualization, each plane is colored based on the average of the energies at the vertices. In each example, the energies are reported relative to the plane with lowest average energy, whose energy was set to 1eV to allow a logarithmic color scale.

plane segments, and (b) change in the manner of that change, depending on symmetry-imposed degeneracy patterns.

4.6 Concluding Remarks

In this chapter, the piecewise linearity condition with respect to magnetization and the tilted plane condition were derived from first principles using the infinite-separation-limit technique, and the magnetic analogue of the DFT Koopmans' theorem was derived from the chain rule. These exact conditions have been derived for all formulations of DFT that are exact for all v-representable spin-densities, size-consistent, and translationally invariant. It is important to note that these exact conditions apply only to the lowest $E_v[N, M]$ energy surface. By performing a constrained search over states of a specified spin multiplicity [39], it is possible to access other quantum states within DFT that are not located on this energy surface, for example, the lowest energy singlet state of a system with a triplet ground state.

We have found that many standard density functional approximations violate these exact conditions. These three exact quantum mechanical conditions may aid in the development of post-DFT methods and functional approximations, machine learning and alchemical approaches in both condensed matter physics and quantum chemistry, and error-correction techniques involving total energies in quantum science. We find that in order to approach the exact limit, energy functionals of occupancies must necessarily take different forms depending on symmetry-imposed degeneracies.

Chapter 5

The BLOR Functional

The work in this chapter has been published as a letter in Physical Review B (Phys. Rev. B 107, L121115 (2023)). The work is jointly authored with my collaborator Edward Linscott and my supervisor David O'Regan. For this research project, I derived the BLOR functional and ran all the DFT calculations where the corrective functional was tested and compared against other DFT+U-type functionals using stretched molecules. Edward independently derived the symmetric BLOR functional and ran the DFT calculations on the fractional helium atom (as presented in Fig. 5.1) and also produced Fig. 5.2. I wrote the first draft of the manuscript. The text shown in this chapter is the fully polished version of the manuscript including revision and editing by David and Edward as well as improvements made on the foot of peer review.

In this chapter a new DFT+U type corrective functional is derived from first principles to enforce the flat plane condition on each orbital of a localized subspace. By invoking this exact condition, which defines the total energy $E_v[N, M]$ surface at fractional values of N and M, we dispense with the need to invoke the Hubbard model and a double counting correction scheme. Small, stretched, s-block molecular test systems are used to compare the functional form against conventional DFT+U-type functionals. Promisingly, the newly derived functional yields extremely low relative energetic errors by comparison.

5.1 Conventional DFT+U Functionals

Current XC approximations such as the Local Spin Density Approximations, (LSDAs) [69,71–74], Generalized Gradient Approximations (GGAs) [60,65,75–

77], meta-GGAs [61, 81–84] and hybrid functionals [85, 86] are all known to fail in cases where the electronic system contains one or more isolated, localized subsystems. Noting this failure, Anisimov et al. [198] proposed supplementing local density approximations with an additional electronic interaction term inspired by the Hubbard model [333],

$$E_{\text{int}} = \frac{U}{2} \sum_{mm'\sigma} n_{m\sigma} n_{m'\bar{\sigma}} + \frac{U-J}{2} \sum_{\substack{mm'\sigma \\ m \neq m'}} n_{m\sigma} n_{m'\sigma}, \tag{5.1}$$

which explicitly depends on the spin resolved occupancy $n_{m\sigma}$ of each orbital m in the localized subspace. U and J refer to the Hubbard U and Hund's J interaction parameters which need to be chosen or preferably evaluated [202, 229, 236–238, 240–242], in advance. The inter-electron interactions of Eq. 5.1 however, are already accounted for to a less favourable extent by the original XC functional that the Hubbard-like interaction term is designed to supplement. This necessitates the use of a double counting correction scheme. The inter-electron interaction and double counting scheme together form a DFT+U-type functional [109, 110, 183, 198, 200–205, 213–215, 217, 220, 331, 334, 335]. Over the past three decades numerous double counting correction schemes have been developed including the spin polarized and non-spin polarized analogues of the around mean field [198, 201] and fully localized limit [200, 201] double counting schemes. In practical applications, the predicted physical and chemical properties of a material can strongly depend on the choice of double counting scheme [336, 337]. Despite this strong dependency, DFT+U-type functionals enjoy widespread application, most notably in high throughput material screening [338–341], which can require thousands of DFT+U-type calculations to be executed.

Developing a DFT+U-type functional that yields reliable total energies and bandgaps is thus of crucial importance. Improved understanding in recent years of exact conditions that apply to the atomic limit has given the opportunity to design DFT+U that encode those, without adding complexity, rather than invoking approximate double-counting corrections [331]. Meanwhile, incorporation from the field of quantum chemistry of the use of test systems for which exact total energies, or at least exact total-energy differences, are available, enables the stringent determination of the viable class of functional forms of a given complexity level [109, 110, 331]. Departing entirely from the Hubbard

model and hence circumventing the introduction of a double-counting correction, in this work a DFT+U-type functional is developed whose form is entirely based upon exact conditions in DFT. Specifically, we focus on the regime in which the DFT+U subspaces are relatively weakly interacting with the remainder of the system, so that they harbor the exact flat-plane (or more generally tilted-plane) condition, and where their deviations from that condition, many-body self-interaction error (SIE) and many-body static-correlation error (SCE), are treated in a subspace-averaged fashion in the usual pragmatic, cost-effective manner of DFT+U.

5.2 Two-Electron Flat Plane Condition

The flat plane condition and its generalisation - the tilted plane condition, have already been discussed in detail in chapter 4. Specifically in the case of an isolated system with two or fewer electrons, the energy surface with respect to electron count N and magnetisation M, will typically be composed of two flat planes which meet with a derivative discontinuity along the $N_{\text{tot}} = 1$ line

$$E_v[N,M] = \begin{cases} \frac{1}{2}(N+M)E_v[1,1] + \frac{1}{2}(N-M)E_v[1,-1], & N \leq 1, \\ \frac{1}{2}(2-N+M)E_v[1,1] & \\ \quad + \frac{1}{2}(2-N-M)E_v[1,-1] + (N-1)E_v[2,0], & N > 1. \end{cases} \tag{5.2}$$

This structure is classified as a 'Type 1' flat plane by Yang et al. [101] and is also be referred to as the "diamond" for brevity. Conventional Density Functional Approximations (DFAs) typically violate the flat plane condition. This is shown in in Fig. 5.1, where the deviation of total energy evaluated using the PBE approximation of the helium atom/ion, from the exact flat plane condition is plotted as a function of spin resolved occupancy. This deviation from the flat plane condition is largely quadratic in character. As mentioned in section 2.6, the spurious curvature in the total energy with respect to electron count and magnetisation is referred to as many electron self interaction error and static correlation error respectively. Despite conventional DFAs poor performance at non-integer values of N and M, often the total electronic energies at the vertices

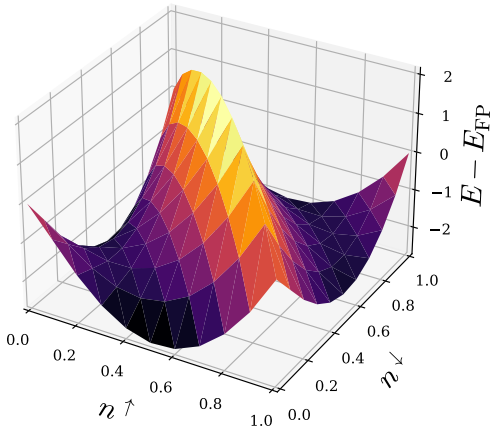

Figure 5.1: Deviation of the total energy E of the He atom/ion for different values of spin up ($n^{\uparrow}$) and spin down ($n^{\downarrow}$) occupancy using the PBE exchange-correlation functional [60]. The PBE total energy is assumed to be exact at integer values of $n^{\uparrow}$ and $n^{\downarrow}$ for the He species. The exact energy from the flat plane condition is denoted as E_{FP}.

of the exact energy surface, which occur at some but not all integer values of N and M, are well-approximated by currently available DFAs.

=

5.3 Localized MSIE

For a system of N_{atom} isolated atomic sites with a total of N_{tot} electrons, a piecewise linearity condition with respect to electron count should occur separately at each atomic site where $N_{\mathrm{atom}}, N_{\mathrm{tot}} \in \mathbb{N}$ but $N_{\mathrm{tot}}/N_{\mathrm{atom}} \notin \mathbb{N}$. The total energy of the system with $N_{\mathrm{tot}}/N_{\mathrm{atom}}$ electrons at each atomic site should be equal in energy to the system with k sites with $N+1$ electrons and $N_{\mathrm{atom}} - k$ sites with N electrons, where $k < N_{\mathrm{atom}}$, $N_{\mathrm{tot}} = NN_{\mathrm{atom}} + k$ and $N = \lfloor N_{\mathrm{tot}}/N_{\mathrm{atom}} \rfloor$, where $\lfloor \cdot \rfloor$ is the floor function (the integer part). However, current DFAs yield incorrect energies for systems with fractional occupancies at the atomic sites [126]. These errors in the total energy will occur even at integer values of global electron count N_{tot}. If one also accounts for magnetization, the energy of each isolated localized state should obey the tilted plane condition [305] in the limit where the interaction between the localized state and the bath (the rest of the electronic system) is negligible, or more generally, when the subspace-bath

interaction energy varies linearly with spin resolved subspace occupancy. Standard XC functionals however, will exhibit spurious curvature in the energy of each isolated, localized state. We refer to these energy errors as localized many electron self interaction errors and localized static correlation errors [185, 331] to distinguish them from their global analogues [1].

Assuming localized-MSIE is predominantly quadratic in nature (as has been reported for global-MSIE [125]), the localized-MSIE at an atomic site can be alleviated with an energetic correction of the form:

$$E_{\mathrm{u}} = \frac{U_{\mathrm{eff}}}{2}\Big[(N - N_0) - (N - N_0)^2\Big], \tag{5.3}$$

where N is the local occupancy at the atomic site, $\lfloor N \rfloor = N_0$, and U_{eff} is a corrective parameter.

DFT+U functionals [183,198,200,205] have often been employed as a correction to localized-MSIE. Much like Eq. 5.3, DFT+U-like functionals comprise of linear and quadratic occupancy-dependent energy corrections. For example, Dudarev et al.'s 1998 Hubbard corrective functional [183] can be written as:

$$E_{\mathrm{u}}^{\mathrm{Dudarev}} = \frac{U_{\mathrm{eff}}}{2}\sum_{\sigma m} n_{mm}^{I\sigma} - (n_{mm}^{I\sigma})^2. \tag{5.4}$$

Unlike Eq. 5.3, here the corrections are given in terms of subspace occupancy matrix elements:

$$n_{mm'}^{I\sigma} = \langle \phi_m^I | \hat{\rho}^\sigma | \phi_{m'}^I \rangle \,, \tag{5.5}$$

where $\hat{\rho}^\sigma$ is the spin-σ Kohn-Sham density operator and $\{\phi_m\}$ are the set of atomically localized orbitals at atom I (the atomic site index is often suppressed for clarity). Eq. 5.4 is written in the basis of localized orbitals that diagonalize this subspace occupancy matrix. In the case where (a) the fractional occupancy at the atomic site is limited to the s-spin channel of one orbital ϕ_m, i.e., $n_{mm}^s = N - N_0$, and (b) all other orbitals $\phi_{m'}$ are fully occupied or unoccupied, Dudarev's 1998 functional provides a perfect correction for localized-MSIE.

Despite DFT+U's success in alleviating localized-MSIE in this limiting case, here we stress two points. Firstly, the DFT+U method was originally derived from the Hubbard model and it is merely fortuitous that it acts as a correc-

[1] The term local could also be used here, but in the DFT context it seems preferable to reserve 'local' to describe variables that depend explicitly upon a single spatial argument.

tion to localized-MSIE. Secondly, the DFT+U method does not correct static correlation error, and will therefore not satisfy the localized flat plane condition.

5.4 Desired Properties of BLOR

In this chapter, a new DFT+U type functional is derived, disregarding entirely its connection with the Hubbard model and instead motivating its form entirely on the local analogue of the flat plane condition. Such a functional should, for a single orbital subspace, satisfy four key conditions, namely that it should:

1. be a continuous function of the subspace electron count N and subspace magnetisation M.

2. yield no correction at integer values of N and M. This is desirable because (semi-)local functionals are expected to yield accurate total energies in this case.

3. have a constant curvature of $-U^\sigma$ with respect to n^σ. This is desirable because (semi-)local functionals are expected to have a spurious curvature with respect to n^σ, due to their deviation from the local-flat plane condition.

4. have a constant curvature of J with respect to M. This is desirable because (semi-)local functionals are expected to have a spurious curvature with respect to M, again due to their deviation from the local-flat plane condition.

The functional which satisfies these four key conditions is BLOR, given for each site by

$$E_{\mathrm{BLOR}} = \begin{cases} \dfrac{U^\uparrow + U^\downarrow}{4}\mathrm{Tr}[\hat{N} - \hat{N}^2] \\ +\dfrac{J}{2}\mathrm{Tr}[\hat{M}^2 - \hat{N}^2] + \dfrac{U^\uparrow - U^\downarrow}{4}\mathrm{Tr}[\hat{M} - \hat{N}\hat{M}], & \mathrm{Tr}[\hat{N}] \leq \mathrm{Tr}[\hat{P}], \\ \\ \dfrac{U^\uparrow + U^\downarrow}{4}\mathrm{Tr}[(\hat{N} - \hat{P}) - (\hat{N} - \hat{P})^2] \\ +\dfrac{J}{2}\mathrm{Tr}[\hat{M}^2 - (\hat{N} - 2\hat{P})^2] + \dfrac{U^\uparrow - U^\downarrow}{4}\mathrm{Tr}[\hat{M} - \hat{N}\hat{M}], & \mathrm{Tr}[\hat{N}] > \mathrm{Tr}[\hat{P}]. \end{cases} \tag{5.6}$$

Here, $\hat{P}$ is the subspace projection operator: $\hat{P} = \sum_m |\phi_m\rangle \langle\phi_m|$. The subspace occupancy and magnetisation operators can be expressed in terms of the spin resolved subspace occupancy operators: $\hat{N} = \hat{n}^{\uparrow} + \hat{n}^{\downarrow}$ and $\hat{M} = \hat{n}^{\uparrow} - \hat{n}^{\downarrow}$, where $\hat{n}^{\sigma} = \hat{P}\hat{\rho}^{\sigma}\hat{P}$. The magnitude of the correction is controlled by three scalars: $U^{\uparrow}$, $U^{\downarrow}$, and J, which correspond respectively to the curvature with respect to $n^{\uparrow}$, $n^{\downarrow}$, and M. The lower and upper versions of the functional have a similar form (the lower version of BLOR is the case where $\mathrm{Tr}[\hat{N}] \leq \mathrm{Tr}[\hat{P}]$).

5.5 Uniqueness of BLOR

One can show that for a single orbital subspace, BLOR is *the unique functional* that satisfies conditions (1)-(4). To do so, we start with the general expression for the corrective functional,

$$E_{\mathrm{u}} = a_0 + a_1 N + a_2 N^2 + a_3 M + a_4 M^2 + a_5 NM, \tag{5.7}$$

where $\{a_i\}$ are co-efficients yet to be determined and it is assumed that we have a single orbital subspace. The co-efficients of any higher order terms must be equal to zero in order for

$$\left(\frac{\partial^2 E_{\mathrm{u}}}{\partial M^2}\right)_N = J \;\; \& \;\; \left(\frac{\partial^2 E_{\mathrm{u}}}{\partial (n^{\sigma})^2}\right)_{n^{-\sigma}} = -U^{\sigma}, \tag{5.8}$$

everywhere in the diamond. In order for $E_{\mathrm{u}}[N, M]$ to satisfy condition 2 in the lower half plane, we have that

$$\begin{aligned} &E_{\mathrm{u}}[0, 0] = a_0 = 0, \\ &E_{\mathrm{u}}[1, 1] = a_0 + a_1 + a_2 + a_3 + a_4 + a_5 = 0, \\ &E_{\mathrm{u}}[1, -1] = a_0 + a_1 + a_2 - a_3 + a_4 - a_5 = 0. \end{aligned} \tag{5.9}$$

From condition 3, we know that E_{u} should have a curvature of J with respect to M,

$$\left(\frac{\partial^2 E_{\mathrm{u}}}{\partial M^2}\right)_N = 2a_4 = J. \tag{5.10}$$

One can re-express Eq. 5.7 in terms of $n^{\uparrow}$ and $n^{\downarrow}$ to facilitate partial differentiation with respect to n^{σ}. From condition 4, we then have that:

$$\begin{aligned}\left(\frac{\partial^2 E_{\mathrm{u}}}{\partial (n^{\uparrow})^2}\right)_{n^{\downarrow}} &= 2a_2 + 2a_4 + 2a_5 = -U^{\uparrow} \\ \left(\frac{\partial^2 E_{\mathrm{u}}}{\partial (n^{\uparrow})^2}\right)_{n^{\downarrow}} &= 2a_2 + 2a_4 - 2a_5 = -U^{\downarrow}. \end{aligned} \tag{5.11}$$

Solving the simultaneous equations and substituting back into Eq. 5.7 yields the expression for the BLOR functional for a single orbital subspace in the lower half-plane.

Repeating this procedure for the upper-half plane, we start again with the general expression for the corrective functional (E_{u}) as given by Eq. 5.7. Condition (2) in this case yields

$$\begin{aligned} E_{\mathrm{u}}[1,1] &= a_0 + a_1 + a_2 + a_3 + a_4 + a_5 = 0, \\ E_{\mathrm{u}}[1,-1] &= a_0 + a_1 + a_2 - a_3 + a_4 - a_5 = 0, \\ E_{\mathrm{u}}[2,0] &= a_0 + 2a_1 + 4a_2 = 0. \end{aligned} \tag{5.12}$$

Conditions (3) and (4) again in this case yield:

$$\begin{aligned}\left(\frac{\partial^2 E_{\mathrm{u}}}{\partial M^2}\right)_{N} &= 2a_4 = J, \\ \left(\frac{\partial^2 E_{\mathrm{u}}}{\partial (n^{\uparrow})^2}\right)_{n^{\downarrow}} &= 2a_2 + 2a_4 + 2a_5 = -U^{\uparrow}, \\ \left(\frac{\partial^2 E_{\mathrm{u}}}{\partial (n^{\uparrow})^2}\right)_{n^{\downarrow}} &= 2a_2 + 2a_4 - 2a_5 = -U^{\downarrow}. \end{aligned} \tag{5.13}$$

Solving these simultaneous equations and substituting back into Eq. 5.7 yields the expression for the BLOR functional for a single orbital subspace in the upper half-plane.

5.6 Analysis of BLOR Functional

The BLOR functional of Eq. 5.6 is divided into three terms. The first term is referred to as the symmetric-MSIE term because for a single orbital subspace it yields zero correction at integer values of N and yields its maximum correction

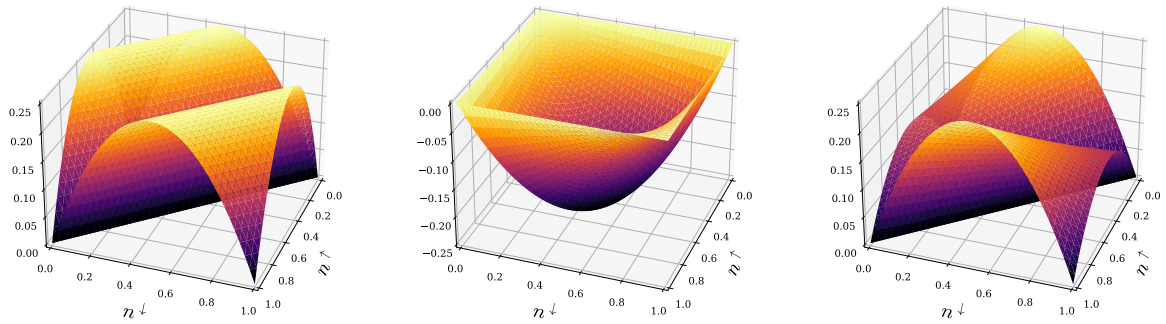

Figure 5.2: The left panel presents the symmetric-MSIE term for an s-orbital subspace as a function of spin up ($n^{\uparrow}$) and spin down ($n^{\downarrow}$) subspace occupancy. The centre panel presents the SCE term as a function of $n^{\uparrow}$ and $n^{\downarrow}$. The right panel presents the sum of the symmetric-MSIE and asymmetric-MSIE terms as a function of $n^{\uparrow}$ and $n^{\downarrow}$.

at $N = \frac{1}{2}, \frac{3}{2}$ as shown in the left panel of Fig. 5.2. The second term is labelled as the SCE-term because, for a single orbital subspace, it yields zero correction when the subspace is maximally spin polarised and yields its maximum correction at $M = 0$, for a given value of N, as shown in the middle panel of Fig. 5.2.

The asymmetric-MSIE term will contribute to E_{BLOR} when an effective magnetic field acts on the subspace. In this case, we cannot assume that the curvatures $U^{\uparrow}$ and $U^{\downarrow}$ are equal in magnitude. This effective magnetic field may be caused by an external magnetic field acting on the isolated atomic site. More notably, in practical calculations the target subspace will not be entirely isolated from its surrounding environment, such as the 3d subspace of face-centered cubic nickel. The 3d atomic subspace will experience an internal exchange-correlation magnetic field from the surrounding nickel atoms and hence we expect that $U^{\uparrow} \neq U^{\downarrow}$ for this site. The difference in magnitude is accounted for in the asymmetric-MSIE term. The combination of the symmetric- and asymmetric-MSIE terms is depicted in the right panel of Fig. 5.2, which unlike the left panel, shows a different curvature along the maximally spin up polarised line compared to the maximally spin down polarised line.

BLOR can also be expressed in terms of subspace occupancy matrix elements,

for each site, as:

$$E_{\mathrm{BLOR}} = \begin{cases} \sum_{\sigma m m'} \left(\frac{U^\sigma}{2} n^\sigma_{mm'} \delta_{mm'} - \frac{U^\sigma}{2} n^\sigma_{mm'} n^\sigma_{m'm} - \frac{U^\sigma + 2J}{2} n^\sigma_{mm'} n^{\bar{\sigma}}_{m'm} \right), & N \leq 2l+1, \\ \sum_{\sigma m m'} \left(\left(U^\sigma + \frac{U^{\bar{\sigma}}}{2} + 2J \right) n^\sigma_{mm'} \delta_{mm'} - \frac{U^\sigma}{2} n^\sigma_{mm'} n^\sigma_{m'm} \right. \\ \qquad \left. - \frac{U^\sigma + 2J}{2} n^\sigma_{mm'} n^{\bar{\sigma}}_{m'm} - \frac{U^\sigma + 2J}{2(2l+1)} \right), & N > 2l+1. \end{cases} \tag{5.14}$$

In both cases, the summation runs over all terms on the right-hand side of Eq 5.14.

BLOR has many similarities with existing functionals. For example, Himmetoglu et al.'s [214] DFT+U+J functional was recently modified by Bajaj et al. [109, 110] to obtain jmDFT, a functional designed to correct for deviations from the global flat plane condition. However, jmDFT fails to satisfy conditions 3 and 4. Meanwhile, setting $U^\sigma = U_{\mathrm{eff}}$, the first two terms of BLOR in the lower-half plane are equal to Dudarev et al.'s 1998 Hubbard functional. Furthermore, for non-spin polarised systems we have that $U^\uparrow = U^\downarrow = U - J$ and the BLOR functional in the lower half plane simplifies to Moynihan et al.'s DFT+U+J method with self consistent formulae for the U and J parameters [342].

5.7 Exact Double Counting Correction Scheme

Our method of deriving BLOR from the flat plane condition bypasses the need to invoke a double counting correction scheme common to most DFT+U functionals. Unlike BLOR, standard DFT+U functionals are given by the difference between a Hubbard like interaction term and a double counting correction term,

$$E_{\mathrm{u}} = E_{\mathrm{int}} - E_{\mathrm{dc}}. \tag{5.15}$$

The double counting correction term must be invoked as the electron-electron interaction has already been accounted for to a less favorable extent by the Hartree Exchange Correlation Energy functional. Starting with the standard

Hubbard like interaction term of Dudarev et al. [183],

$$E_{\text{int}} = \frac{U}{2} \sum_{\sigma m m'} n^{\sigma}_{mm} n^{\bar{\sigma}}_{m'm'} + \frac{U-J}{2} \sum_{\sigma, m \neq m'} n^{\sigma}_{mm} n^{\sigma}_{m'm'}. \tag{5.16}$$

The exact double counting correction term for DFT+U can be reverse engineered from the BLOR functional, approximating $U^{\uparrow} = U^{\downarrow}$,

$$\begin{aligned} E^{\text{exact}}_{\text{dc}} =& \frac{U}{2}\left(N^2 - N\right) - \frac{J}{2}\sum_{\sigma} N^{\sigma} N^{\sigma} + \frac{U+J}{2} \sum_{\sigma m m'} n^{\sigma}_{mm'} n^{\bar{\sigma}}_{m'm} \\ &+ \frac{J}{2} \sum_{\sigma m m'} \left(n^{\sigma}_{mm'} n^{\bar{\sigma}}_{m'm} + n^{\sigma}_{mm'} n^{\sigma}_{m'm} \right) + (U+2J)(N-2l-1)\Theta\{N-2l-1\}, \end{aligned} \tag{5.17}$$

where $\Theta\{N-2l-1\}$ is the Heaviside step function, i.e., a different double-counting correction term is required depending if the subspace is more or less than half-occupied. This exact double counting term can also be expressed as a correction to the standard fully localised limit double counting term,

$$\begin{aligned} E^{\text{exact}}_{\text{dc}} =& E^{\text{FLL}}_{\text{dc}} - \frac{J}{2}N + \frac{U+J}{2} \sum_{\sigma m m'} n^{\sigma}_{mm'} n^{\bar{\sigma}}_{m'm} + \frac{J}{2} \sum_{\sigma m m'} \left(n^{\sigma}_{mm'} n^{\bar{\sigma}}_{m'm} + n^{\sigma}_{mm'} n^{\sigma}_{m'm} \right) \\ &+ (U+2J)(N-2l-1)\Theta\{N-2l-1\}, \end{aligned} \tag{5.18}$$

where

$$E^{\text{FLL}}_{\text{dc}} = \frac{U}{2}\sum_{\sigma} N^{\sigma} N^{\bar{\sigma}} + \frac{U-J}{2}\sum_{\sigma} N^{\sigma}(N^{\sigma}-1). \tag{5.19}$$

The non-trivial form of this exact double counting correction highlights the inherent difficulty of the double-counting approach to functional construction as well as the potential utility of reverse engineering double counting corrections from exact conditions.

5.8 Evaluating Corrective Parameters for BLOR

Returning to the BLOR functional, an appropriate method must be choosen for evaluating the corrective parameters. Measuring the spurious curvature in the energy with respect to occupancy, while fixing the spin-magnetization, would in principle require cumbersome and often ill-conditioned self-consistent constrained DFT calculations. Instead, one can directly evaluate the corrective parameters U and J based on first-order partial derivatives of the spin-resolved,

subspace averaged Hartree and exchange-correlation (Hxc) potential,

$$v^{\sigma}_{Hxc} = \mathrm{Tr}\left[\hat{P}\ \frac{\delta E^{\mathrm{total}}_{\mathrm{Hxc}}}{\delta\hat{\rho}^{\sigma}}\right] \Big/ \mathrm{Tr}[\hat{P}], \tag{5.20}$$

where $E^{\mathrm{total}}_{\mathrm{Hxc}}$ is the total Hxc energy of the system and $\hat{P}$ is the subspace projection operator. Using v^{σ}_{Hxc}, we can define the spin-resolved subspace Hxc interaction

$$f^{\sigma\sigma'} = \left.\frac{\partial v^{\sigma}_{\mathrm{Hxc}}}{\partial n^{\sigma'}}\right|_{n^{\bar{\sigma}'}}, \tag{5.21}$$

where $n^{\sigma'}$ is the spin σ' subspace occupancy. This is known as the minimum-tracking linear response method [242–245]. Within this formalism, the spin resolved Hubbard parameters for BLOR (or mBLOR) can be set as the diagonal elements of the Hxc interaction, namely as

$$U^{\sigma} = f^{\sigma\sigma}. \tag{5.22}$$

The Hund's J parameter is defined as the spurious curvature in the interacting part of the energy with respect to magnetization. Within the minimum-tracking linear response formalism it is normally defined as

$$J = -\frac{1}{2}\frac{dv^{\uparrow}_{\mathrm{Hxc}} - dv^{\downarrow}_{\mathrm{Hxc}}}{d(n^{\uparrow} - n^{\downarrow})}. \tag{5.23}$$

However, this derivative with respect to magnetization should be evaluated at fixed total occupancy. This can be calculated very conveniently using the simple 2×2 method [242], where it is given by

$$J = -\frac{1}{4}(f^{\uparrow\uparrow} - f^{\uparrow\downarrow} - f^{\downarrow\uparrow} + f^{\uparrow\downarrow}). \tag{5.24}$$

Similarly, within the minimum-tracking linear response formalism the spin-independent Hubbard U parameter is usually defined as

$$U = \frac{1}{2}\frac{dv^{\uparrow}_{\mathrm{Hxc}} + dv^{\downarrow}_{\mathrm{Hxc}}}{d(n^{\uparrow} + n^{\downarrow})} \tag{5.25}$$

and, again, there exists an analogous simple 2×2 variant (particularly, but not necessarily only for use with flat-plane condition based functionals),

$$U = \frac{1}{4}(f^{\uparrow\uparrow} + f^{\uparrow\downarrow} + f^{\downarrow\uparrow} + f^{\uparrow\downarrow}). \tag{5.26}$$

5.9 Computational Details

All calculations were completed using the ONETEP (Order-N Electronic Total Energy Package) DFT code [281, 294–296], with the PBE [60] exchange-correlation functional at a high cutoff energy of no lower than 2,300 eV. The stretched molecular test systems were located in a large simulation cell, no smaller than $80 \times 60 \times 60$ a_0^3, with a Martyna-Tuckerman periodic boundary correction cutoff of 7.0 a_0 [299].

For a system with N_σ spin σ KS particles, the occupancy of the lowest N_σ KS particles was set equal to one, and otherwise set equal to zero. The convergence threshold of the root-mean-square gradient of the density kernel and the NGWFs was set at 1×10^{-6} Ha e^{-1} and 1×10^{-7} Ha $a_0^{3/2}$ respectively, and the electronic energy tolerance was set at 1×10^{-6} eV/atom.

Four NGWFs were assigned per atom using the split-valence approach, with 15% of the norm set to be beyond the matching radius r_m. This provides unrestricted variational freedom for each spin-orbital. The NGWF cutoff was set to 14 a_0. A bespoke set of hard, norm-conserving pseudopotentials were made using the OPIUM code [343].

For the non-spin polarised systems (H_2 & Li_2) full spin polarised perturbations were not required because of the spin symmetry of the system, as described in [244]. From a series of α perturbations the slope of $V_{\text{Hxc}}[N]$ can be evaluated. It can be shown that this is equal to twice the value of the Hubbard U parameter (from the simple 2x2 method). Similarly, from a series of beta perturbations, the slope of $[V_{\text{Hxc}}^{\uparrow} - V_{\text{Hxc}}^{\downarrow}][M]$, can be ascertained, where M is the subspace magnetisation. Similarly, it can be shown that the slope of this curve is equal to minus two times the value of the Hund's J parameter (from the simple 2x2 method). Finally, $f^{\uparrow\uparrow}$=U-J, for non-spin-polarised systems.

The non-spin polarised PBE solution for stretched H_2 & Li_2 are at a point of unstable equilibrium in the PBE energy landscape. Applying a perturbation to the atomic subspace can cause the calculation to converge to the lower-energy,

spin-polarised solution. A stabilising potential of the form

$$\hat{v}^{\sigma} = G\hat{n}^{-\sigma} \tag{5.27}$$

was used to stabilise the non-spin-polarised solution. The Hund's J parameter was evaluated at non-zero values of the stabilisation parameter G and extrapolated to $G = 0$. This allows one to evaluate the Hund's J parameter for the non-spin-polarised systems as opposed to the spuriously broken-symmetry spin-polarised system. This technique was also required for the evaluation of the Hubbard U parameter for Li_2.

5.10 Stretched s-block Molecules

In Eqs. 5.6 and 5.14 BLOR is expressed in a generalized from which readily allows its implementation for s, p, d or f valence orbitals. However, in this chapter we explore BLOR's application solely to s-valence species, in which case there is no ambiguity as to whether the localized flat plane condition should be enforced on the localized subspace as a whole or on each localized orbital in the subspace separately. The later of these two options has been used to give BLOR in its current form however, analysis of this choice through benchmarking with p and d valence species will be left to chapter 6.

BLOR was first tested on s-block dimers, (namely H_2, He_2^+, Li_2 and Be_2^+) with large internuclear separation lengths. It is assumed that at these elongated bond lengths the energy of the X_2 dimer is additive:

$$E[X_2] = 2E[X]. \tag{5.28}$$

The subspace occupancies of the atomic species will be located at the vertices of the diamond, hence the bare Perdew-Burke-Ernzerhof approximation [60] (PBE) is expected to be reasonably accurate for $E[X]$. We thus assume that $2E_{PBE}[X]$ yields the exact total energy of our stretched X_2 species. This approximation avoids discrepancies in the total energy from using a pseudopotential. The atomic subspaces of dissociated H_2 and Li_2 are approximately located along the $N = 1$ line of the diamond (the fold) and are thus dominated by localized-SCE. The atomic subspaces of dissociated He_2^+ and Be_2^+ are approximately located along the edges of the diamond and are thus dominated by

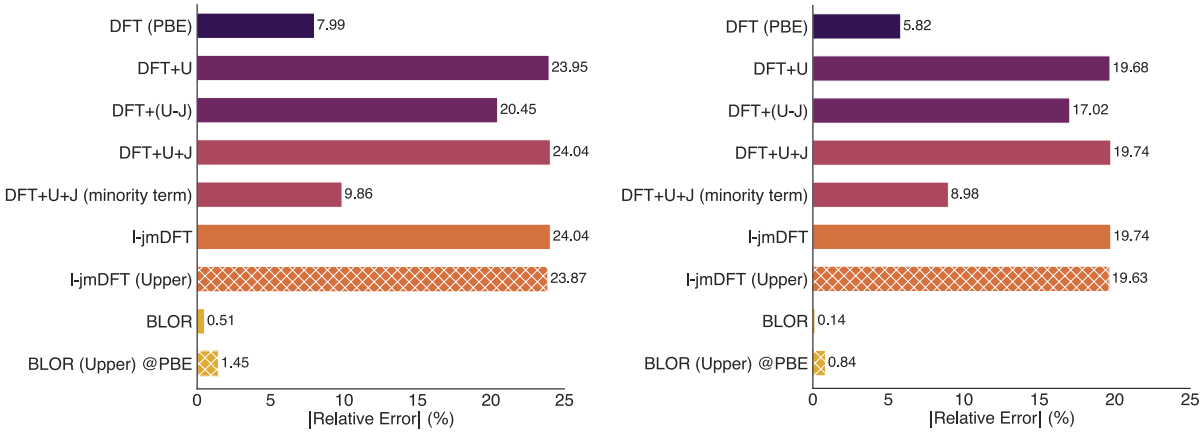

Figure 5.3: Bar chart of the relative errors in the total energies of H_2 and Li_2 at a bond length of 9 and 15 bohr radii respectively using different corrective functionals [60, 109, 110, 183, 214, 220], and symmetry unbroken spin-densities. The raw DFT calculations were performed with the PBE exchange correlation functional [60]. The DFT+U and DFT+$(U-J)$ relative errors were computed using Dudarev et al.'s 1998 functional with the effective Hubbard parameter (U_{eff}) set as U and $U-J$ respectively. Both the lower and upper versions of l-jmDFT and BLOR are included in the bar chart. In the dissociated limit of H_2, each H atom will be singly occupied and hence the lower versions of BLOR and l-jmDFT are the relevant versions for dissociated H_2, despite the computed occupancy due to spillage being greater than one at the large but finite bond length of $9a_0$. The hashing on the bars of the upper versions of BLOR and l-jmDFT indicates the deliberate misapplication of these functionals. The BLOR (Upper) corrective functional was evaluated on the PBE density, as discussed in the main text.

localized-MSIE. These errors will result in the computed $E[X_2] \neq 2E[X]$ for the stretched X_2 species.

Fig. 5.3 presents the relative errors in the total energies for the stretched H_2 and Li_2 molecules using different corrective functionals. Very similar results were obtained for both strecthed, neutral dimers. In the case of the H_2 molecule, PBE yields a significant relative error of 7.99%, however most of the corrective functionals significantly worsen the PBE result, yielding errors up to 24.04%. Use of BLOR in the lower half-plane yields a very low error of 0.510% and 0.14% for the stretched H_2 and Li_2 molecules respectively.

In the bar chart the jmDFT functional form is denoted as l-jmDFT (localised-jmDFT). The jmDFT functional was designed to correct for deviations from the global flat plane condition and was the main inspiration for the development of BLOR, which instead focuses on the localized flat plane condition. In this

work, the jmDFT functional is implemented to correct for deviations from the localized flat plane condition as opposed to the global equivalent. Furthermore, we use the simple 2×2 to compute the U and J parameters for the jmDFT functional, which is not how the functional was intended to be applied. The poor performance of l-jmDFT is thus unsurprising.

Excluding the minority spin term, it is possible to reformulate the DFT+U and DFT+U+J functionals in terms of an MSIE-term: $\mathrm{Tr}[\hat{N} - \hat{N}^2]$ and a SCE-term: $\mathrm{Tr}[\hat{M}^2 - \hat{N}^2]$, with different linear combinations of U and J as prefactors. In the case of stretched H_2, the MSIE-term is negligible because the atomic occupancy is equal to one in the fully dissociated limit. Thus, the failure of the DFT+U and DFT+U+J functionals to predict the correct total energy can be attributed to the incorrect SCE-term prefactor of $-U/4$ in both cases. Indeed, computing the total energy of H_2 at a $9a_0$ bond length with both MSIE and magnetic-term prefactors equal to zero and the correct SCE prefactor of $J/2$ yields a relative error of 0.81%.

Several of the corrective functionals (including BLOR) were found, at least on the basis of analytical non-interacting molecular orbital theory, to yield the incorrect ordering of the KS orbitals upon self-consistent application of the corrective functional. Whenever this occurred, the corrective functional was applied non-self consistently, i.e., the total energy was evaluated on the PBE density, hence we have BLOR@PBE etc. For all corrective functionals where no KS orbital re-ordering occurs, the total energy was evaluated both self-consistently and non-self-consistently and the difference between the two was found to be negligible. This demonstrates that BLOR yields correct total energies but fails to properly correct the KS potential. The corrective potential will be investigated further in chapter 6.

The relative errors in the total energy of the stretched He_2^+ and Be_2^+ molecules are presented in Fig. 5.4. Much smaller relative errors in the total energy occur for these molecules compared to the stretched H_2 and Li_2 systems, however the same trend is observed. Application of standard DFT+U-type functionals are found to significantly worsen the total energies of these systems, while the BLOR functional offers significantly improved total energies compared to the raw DFT(PBE) values. However, for both the He_2^+ and Be_2^+ molecules, the BLOR functional needed to be evaluated non-self consistently at the PBE density. This is because self-consistent application of the BLOR functional

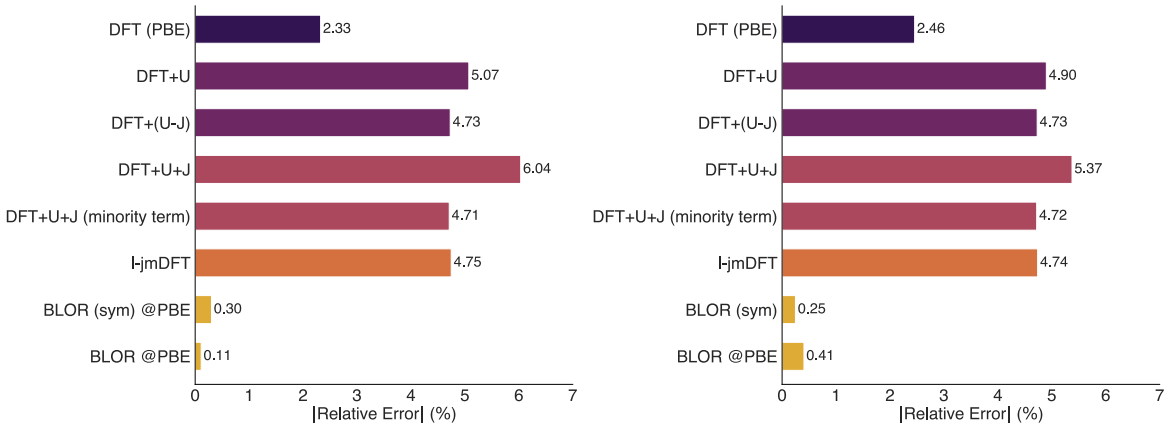

Figure 5.4: Bar chart of the relative errors in the total energies of He_2^+ and Be_2^+ at a bond length of 5 and 10 bohr radii respectively using different corrective functionals [60, 109, 110, 183, 214, 220]. The raw DFT calculations were performed with the PBE exchange correlation functional [60]. The DFT+U and DFT+$(U-J)$ relative errors were computed using Dudarev et al.'s 1998 functional with the effective Hubbard parameter (U_{eff}) set as U and $U-J$ respectively. The label BLOR(sym) refers to the BLOR functional with the spin-resolved Hubbard U parameters evaluated as $U^{\uparrow} = U^{\downarrow} = f^{\downarrow\downarrow}$.

resulted in a spurious re-ordering of the KS orbitals. This suggests that further improvements to the BLOR corrective potential may be required in order to apply this functional self-consistently to material systems at standard bond lengths. Nevertheless, the significantly improved total energies across all four stretched dimers is an extremely promising result.

The BLOR functional was also tested on a dissociated hydrogen ring system, which suffers from both localized-MSIE and localized-SCE (in a system where both localized-MSIE and localized-SCE are present, error cancellation may occur). Specifically, the triplet spin state of the system was considered, which provides a stringent test for the validity of the nascent asymmetric-MSIE correction term. Dissociated triplet H_5^+ is the smallest hydrogen ring system where: (1) the subspaces are not located along the edge or fold of the diamond and (2) the system does not suffer from KS orbital degeneracy problems (where a degenerate pair of KS orbitals is occupied by a single KS particle). For dissociated H_5^+, bare PBE was found to yield a spurious symmetry-broken solution in what should be a 5-fold symmetric spin-density. To stabilise the correct symmetry-unbroken solution, a potential of the form:

$$\hat{v}^{\sigma} = G\hat{n}^{-\sigma} \tag{5.29}$$

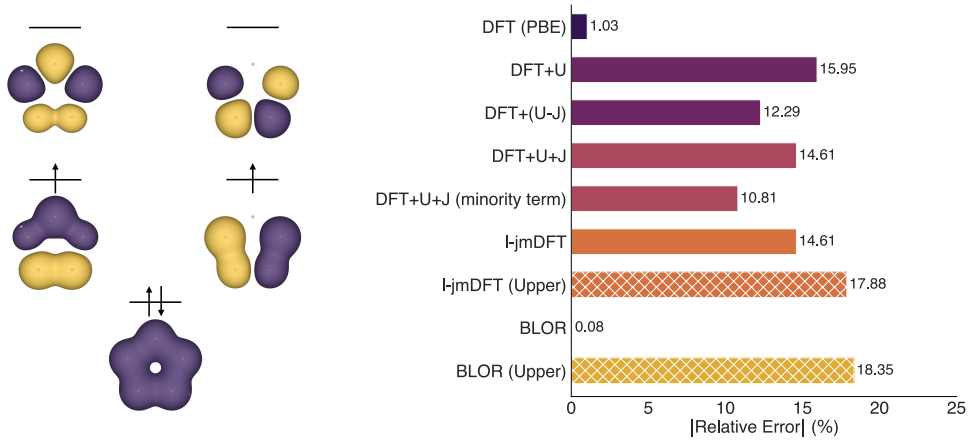

Figure 5.5: The top panel displays the five lowest spin up Kohn Sham orbitals of the dissociated H_5^+ ring at an isosurface value of 0.003 [344]. The bottom planel displays a bar chart of the relative errors in the total energy of dissociated H_5^+ at an internuclear separation of 8 bohr radii using different corrective functionals [60, 109, 110, 183, 214, 220], which have been applied non-self consistently on the extrapolated, symmetry-unbroken PBE spin-density. The atomic subspace occupancy is significantly less than one and will be equal to 0.8 at the dissociated limit, thus the lower versions of BLOR and l-jmDFT are the correct versions for this system.

was applied to the atomic subspaces. The total PBE energy and spin resolved subspace occupancies were then evaluated as functions of G and extrapolated to $G = 0$ to get the correct PBE energy and spin resolved subspace occupancies. These occupancies were then used to obtain the total energy of the H_5^+ system evaluated on the extrapolated, symmetry-unbroken PBE spin-density for different corrective functionals including BLOR.

As shown in Fig. 5.5, bare PBE yields a very low relative error of 1.03% for the dissociated H_5^+ system. Application of any functional is found to worsen the bare PBE result, with the exception of BLOR, which yields a relative error of 0.08%. This extremely low error is investigated further in Fig. 5.6, where the total energy associated with several corrective functionals is decomposed into a symmetric-MSIE term, a SCE term and an asymmetric-MSIE term. All corrective functionals shown yield similar positive energies for the symmetric-MSIE term. However, the corrective functionals all yield large *positive* SCE terms with the exception of BLOR. A positive SCE term leads to a significant overestimation of the total corrective energy.

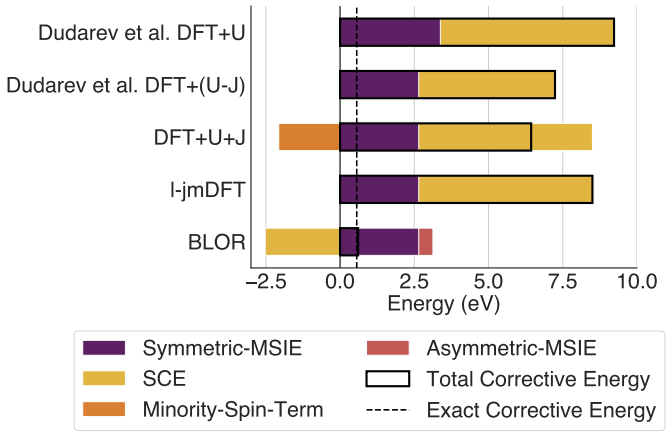

Figure 5.6: The decomposition of the total corrective energy associated with several functionals [109, 110, 183, 214, 220], into a symmetric-MSIE term, a SCE term, a minority-spin term, and an asymmetric-MSIE term. The exact corrective energy is that required to recover the correct dissociated-limit total energy.

5.11 Alternative Methods to Evaluate U & J

In this chapter thus far, the simple 2×2 method, was used to compute the U and J parameters for each corrective functional with the exception of the BLOR functional, where the simple 2×2 $f^{\sigma\sigma'}$ was calculated but spin-dependent U^{σ} were extracted from it. In this section, for completeness, the performance of the various Hubbard type corrective functionals using alternative methods for evaluating the U and J parameters was assessed. Within this section, the total energies for each corrective functional were evaluated non-self consistently using the PBE density. Three different methods were investigated.

5.11.1 Simple 2x2 Method

In this subsection the simple 2×2 method was used to evaluate the corrective parameters for every DFT+U functional, including BLOR. BLOR has spin resolved Hubbard parameters U^{σ} and hence it is necessary to set:

$$U^{\uparrow} = U^{\downarrow} = \frac{1}{4}(f^{\uparrow\uparrow} + f^{\uparrow\downarrow} + f^{\downarrow\uparrow} + f^{\uparrow\downarrow}). \tag{5.30}$$

By setting $U^{\uparrow} = U^{\downarrow}$ the results for BLOR will be equal to BLOR (sym). Evaluating the Hubbard U parameter for BLOR using the simple 2×2 method for He_2^+ (as shown in Fig. 5.7) yields a significant relative error of 4.92%. Evalu-

ating the spin resolved Hubbard parameters, U^{σ}, via this method is thus not a suitable choice for the BLOR functional.

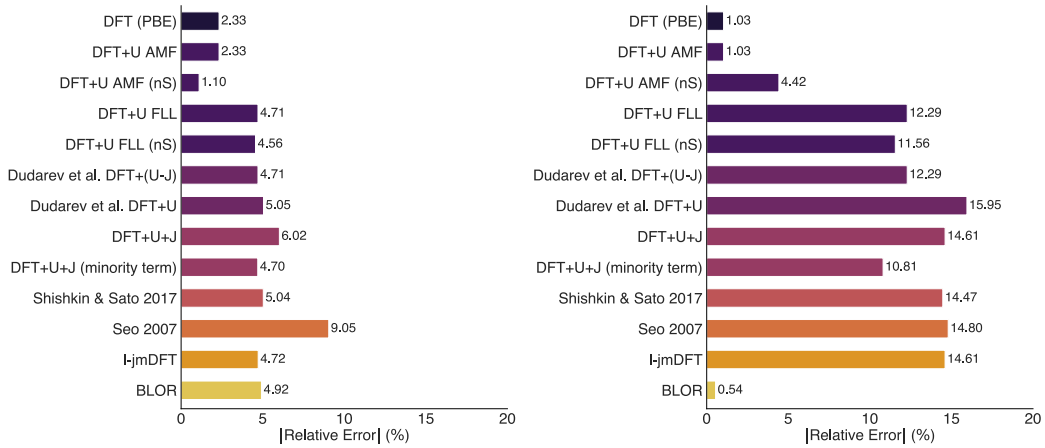

Figure 5.7: Bar chart of the relative errors in the total energies of the stretched He_2^+ and H_5^+ molecules at an internuclear separation of 5 and 8 bohr radii respectively, using different corrective functionals [60,109,110,183,198,200,201, 203,214,220,336,345], which have been applied non-self consistently on the PBE density. The Hubbard U and Hund's J parameter have both been computed by the simple 2x2 method [242,342].

With the exception of the BLOR functional, the results for He_2^+ and H_5^+ in Fig. 5.7 is equivalent to the results given in Figs. 5.4 & 5.5. The minor numerical differences between the He_2^+ bar charts of Figs. 5.7 & 5.4 are due to density self-consistency effects. The total energies in this section have been evaluated at the PBE density while in Fig. 5.4 the total energies were evaluated self-consistently. The density self consistency effects for these dissociated molecular test systems are clearly negligible and will not be considered for the remainder of this subsection.

In Fig. 5.7, DFT+U FLL and DFT+U AMF refer to the original DFT+U functionals with Fully Localised Limit and Around Mean Field double counting schemes of Anisimov et al. [198, 200] and Czyżyk et al. [201]. Spin polarised and non-spin polarised (nS) analogues of the FLL and AMF double counting schemes exist, a detailed discussion of which is given by Ylvisaker et al. [336]. Seo 2007 refers to the DFT+U functional developed by Seo [203], which was discussed in detail in the background theory section. Shishkin & Sato 2017, refers to Shishkin & Sato's variant of the DFT+U + J functional [345].

5.11.2 Simple 2x2 method for J and with U=$f^{\sigma\sigma}$

An alternative scheme for computing the corrective parameters that will be explored in this subsection, is to evaluate the spin-agnostic Hubbard U parameter associated with all other corrective functionals as $f^{\sigma\sigma}$, where σ is the majority spin channel in the lower half plane and the minority spin channel in the upper half plane. Similarly, for the BLOR functional we let $U^{\uparrow} = U^{\downarrow} = f^{\sigma\sigma}$, so that BLOR simplifies to BLOR (sym).

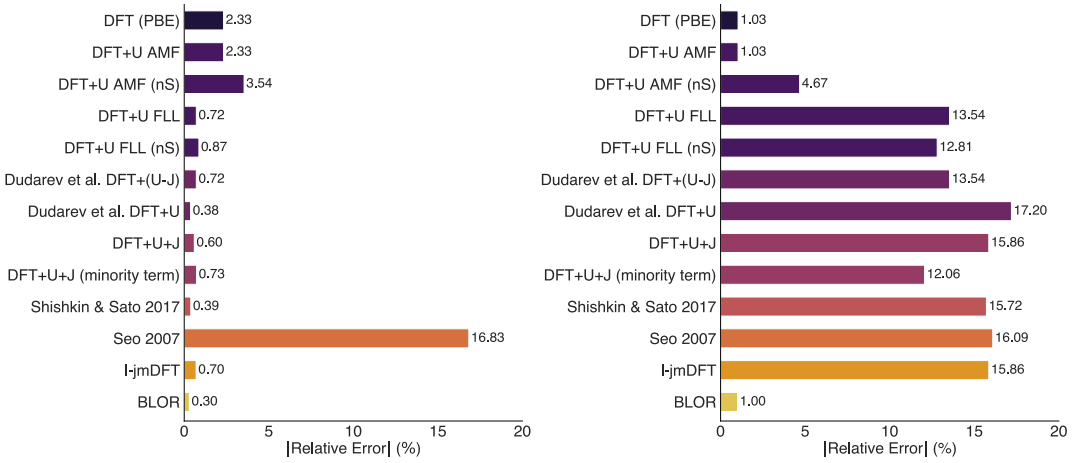

Figure 5.8: Bar chart of the relative errors in the total energies of the stretched He_2^+ and H_5^+ molecules at an internuclear separation of 5 and 8 bohr radii respectively, using different corrective functionals [60, 109, 110, 183, 198, 200, 201, 203, 214, 220, 336, 345], which have been applied non-self consistently on the PBE density. The Hund's J parameter was computed by the simple 2x2 method [242, 342] and the Hubbard U parameter was set as $f^{\sigma\sigma}$, where σ is the majority spin channel in the lower half plane and the minority spin channel in the upper half plane.

Using this prescription, many corrective functionals yield extremely low relative errors for He_2^+ as shown in Fig. 5.8. The atomic subspaces of He_2^+ are approximately located along the edges of the diamond. For an atomic subspace located perfectly along the edge of the diamond, the BLOR functional for a single orbital subspace simplifies to:

$$E_{\text{BLOR}} = \frac{U^{\sigma}}{2}(n^{\sigma} - n^{\sigma}n^{\sigma}), \tag{5.31}$$

where σ is the majority spin channel in the lower half plane and the minority spin channel in the upper half plane. Therefore, if we set the effective Hub-

bard parameter U_{eff} in Dudarev et al.'s functional [183] to $f^{\sigma\sigma}$, it will perfectly emulate the BLOR functional for systems with atomic susbpaces located along the edges of the diamond. Therefore, the extremely low relative error of 0.38% associated with Dudarev et al.'s DFT+U functional is unsurprising.

For systems with atomic susbpaces not located along the edge of the diamond (such as H_5^+), setting $U = f^{\sigma\sigma}$ does not allow Dudarev et al.'s DFT+U functional to perfectly emulate the BLOR functional. The corrective functionals which performed well for He_2^+ using this method for evaluating U and J parameters clearly fail for H_5^+, as shown in Fig. 5.8.

5.11.3 Scaled 2x2 Method

In this subsection the U and J parameters were computed using Linscott et al.'s scaled 2×2 formulae [242]. Unlike the aforementioned simple 2×2 formulae that emulates, e.g. the constraint of N while M is varied to calculate J, scaled 2×2 emulates no such constraint. The scaled 2×2 U is equivalent to the conventional non-spin-resolved formula for U, where M may vary as well as N when the perturbation α is applied. In the case of BLOR both $U^{\uparrow}$ and $U^{\downarrow}$ were set equal to the scaled Hubbard U parameter. With $U^{\uparrow} = U^{\downarrow}$ the results for BLOR will be equal to the results for BLOR (sym).

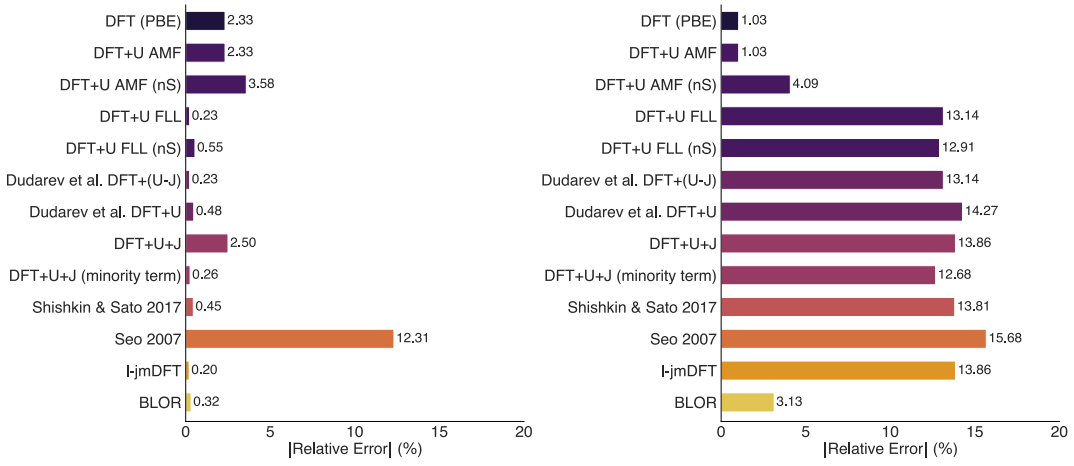

Figure 5.9: Bar chart of the relative errors in the total energies of the stretched He_2^+ and H_5^+ molecules at an internuclear separation of 5 and 8 bohr radii respectively, using different corrective functionals [60,109,110,183,198,200,201, 203,214,220,336,345], which have been applied non-self consistently on the PBE density. The Hubbard U and Hund's J parameter have both been computed by the scaled 2x2 method [242,342].

Many of the corrective functionals perform excellently for He_2^+ as shown in Fig. 5.9. However, the atomic subspaces of He_2^+ is approximately located along the edge of the diamond and hence the system is dominated by local-MSIE. These corrective functionals, which yield low relative errors for He_2^+, perform poorly when significant portions of both local-MSIE and local-SCE are present. This is shown in Fig. 5.9 for H_5^+ where all corrective functionals except BLOR significantly worsen the PBE result. Thus, low relative errors can be achieved only for systems dominated by local-MSIE when the scaled 2×2 method is used to evaluate U and J parameters, with a wide variety of corrective functionals.

As shown in Fig. 5.9, the scaled 2×2 method with the BLOR functional yields a significantly larger relative error for H_5^+ of 3.13% compared to the 0.08% achieved from using the simple 2×2 formula for J and letting $U^\sigma = f^{\sigma\sigma}$.

5.12 Concluding Remarks

In conclusion, our newly derived corrective functional BLOR yielded relative energetic errors below 0.6% across all five dissociated s-block species. This performance was unmatched by any of the other DFT+U type functionals tested. However, the BLOR corrective functional yielded a spurious re-ordering of the KS orbitals for He_2^+ and Be_2^+, a problem which was bypassed for these systems by evaluating the BLOR energy at the PBE density (BLOR@PBE). Most notably, our DFT+U type corrective functional has been derived entirely from first principles and alleviates the need to rely on an ad hoc derivation from the Hubbard model.

Chapter 6

The mBLOR Functional

The work in this chapter has been published as an article in Phys. Rev. B 110, 205150 (2024) [346]. The work is jointly authored with my supervisor David O'Regan. For this research project, I derived the mBLOR functional and ran all the DFT calculations where the corrective functional was tested and compared against other DFT+U-type functionals using stretched molecules. I wrote the first draft of the manuscript. The text shown in this chapter is the fully polished version of the manuscript after revision and editing by David.

In this chapter, the extension of the BLOR functional to address many-body errors (mBLOR) is derived. The mBLOR functional is built to enforce the flat-plane condition on the entire subspace, rather than on each orbital individually. It depends solely on the total subspace occupancy and spin magnetization, bringing consistency with how Hubbard U and Hund J values are typically calculated, and very low complexity. In this way inter-orbital errors are corrected on the same footing as the single-particle ones. Focusing on exact test cases with strong inter-orbital interactions, in this chapter the BLOR and mBLOR functionals are benchmarked against contemporary DFT+U functionals using the total energy extensivity condition on stretched homo-nuclear p-block dimers that represent various self-interaction and static-correlation error regimes, namely singlet N_2 & F_2, non-spin polarized O_2, and doublet Ne_2^+. As mBLOR would not otherwise introduce a band-gap correction in the manner that is a desirable feature of DFT+U, a cost-free technique to reintroduce it automatically by moving the functional's unusual explicit derivative discontinuity into the potential is also developed in this chapter. Its ability to open the band-gap of the stretched neutral homo-nuclear dimers without the aid of

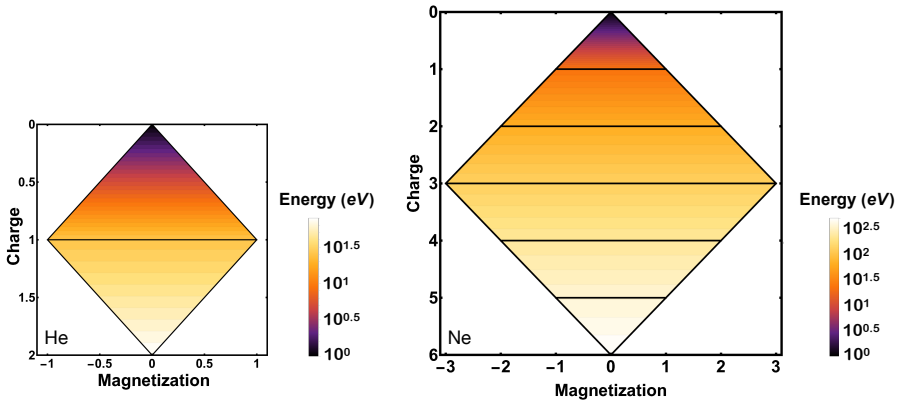

Figure 6.1: The projection of the $E_v[N_{\text{tot}}, M_{\text{tot}}]$ curve of the helium atom (left) and neon atom (right) onto the $N_{\text{tot}} - M_{\text{tot}}$ plane. For simplicity, highly charged and highly magnetized states are omitted. The total energy varies linearly across each plane, which are outlined in black. The total energy values are based on available experimental NIST reference data [316] and are given relative to the lowest energy state of the respective neutral atom which is set to 1 eV. Energy contour lines are plotted at intervals of $10^{0.05x}$ eV. In the BLOR functional [331], the spin-dependent occupancy of each DFT+U subspace spatial orbital can be though of as being separately mapped, conceptually, to its own possibly-tilted helium atom (left) exact energy model. In the introduced mBLOR functional, and taking the example of p-orbital based subspaces, the spin-dependent occupancies of all three subspace spatial orbitals are together mapped to a combined possibly-tilted neon 2p subshell (right) exact energy model.

unphysical spin-symmetry breaking is then investigated.

6.1 Exact Conditions in DFT

In order to enforce the flat plane condition once on a multi-orbital subspace, we must consider the structure of the $E_v[N, M]$ surface when $N \geq 2$. For example, enforcing the flat plane condition on an entire p-orbital subspace as opposed to each orbital separately, would require using a flat plane condition analogous to that of the neon atom. In Fig. 6.1, the exact flat plane condition for the helium and neon atoms are illustrated. As shown in **Fig. 6.1**, the energy surface of the neon atom, excluding high energy magnetization states, will be composed of a series of triangular and isosceles trapezoid shaped planes with derivative discontinuities in the total energy at integer values of electron count.

6.2 Subspace Averaged Hubbard Parameters

The Hubbard U (and Hund's J) parameters are typically evaluated as subspace averaged localized many-body SIE (and SCE) strengths, or subspace averaged interaction strengths of a specfic type, depending on the reader's perspective. For example, as previously discussed in the minimum tracking linear response method, the Hubbard U parameter can be evaluated as

$$U = \frac{1}{4}(f^{\uparrow\uparrow} + f^{\uparrow\downarrow} + f^{\downarrow\uparrow} + f^{\uparrow\downarrow}), \tag{6.1}$$

where $f^{\sigma\sigma'}$ is the spin-resolved subspace Hxc interaction

$$f^{\sigma\sigma'} = \left.\frac{\partial v^{\sigma}_{\mathrm{Hxc}}}{\partial n^{\sigma'}}\right|_{n^{\bar{\sigma}'}} \tag{6.2}$$

and $v^{\sigma}_{\mathrm{Hxc}}$ is the spin resolved, subspace averaged Hxc potential.

Despite this subspace averaging, the U and J parameters are typically employed in orbitally resolved DFT+U-type functionals, such as the original BLOR functional of Eq. 5.6 or Dudarev et al.'s functional [183],

$$E_u = \frac{U - J}{2} \sum_{\sigma m m'} \left(n^{\sigma}_{mm'}\delta_{mm'} - n^{\sigma}_{mm'}n^{\sigma}_{m'm}\right). \tag{6.3}$$

These subspace averaged U and J parameters can in principle be decomposed into orbitally resolved contributions

$$f^{\sigma\sigma'}_{mm'} = \left(\frac{\partial v^{m\sigma}_{\mathrm{Hxc}}}{\partial n_{m'\sigma'}}\right). \tag{6.4}$$

Although we emphasise that this decomposition is not performed in this study. In an atomic subspace of orbital angular momentum quantum number l, for every one on-diagonal intra-orbital term $f^{\sigma\sigma'}_{mm}$ contributing to the subspace averaged U and J parameters there will be $2l$ off-diagonal inter-orbital terms $f^{\sigma\sigma'}_{mm'}$, where $m \neq m'$. Due to the contributions from these inter-orbital terms $f^{\sigma\sigma'}_{mm'}$, it is inconsistent to use such subspace averaged U and J parameters in an orbitally resolved DFT+ U-type functional. This approximation will tend to ascribe all the measured many-body localized SIE and SCE to the inter-orbital (single-particle) terms, likely over-correcting them, while neglecting the numer-

ous inter-orbital corrective terms. How great an issue this is in practice is likely dependent on the system under study and the choice of subspace projection. It seems likely to be more problematic, for the accuracy of the total energy, when there are more than one significantly partially occupied subspace spin-orbitals. This inconsistency can, of course, be resolved by following the long-known route of evaluating orbitally resolved corrective parameters [202, 313, 347, 348] or alternatively, one could develop a non-orbitally resolved DFT+U-type functional designed to mitigate errors or account for on-site interactions associated with the subspace as a whole as opposed to each orbital separately. It is the later of these two options which we choose to pursue in this study. Unlike the orbitally resolved parameter approach, this one does not present challenges in maintaining a functional form that is invariant under unitary transformations of the orbitals. In principle, this latter approach could be applied to subspaces that are not orbital based at all, which might be helpful for example in orbital-free DFT.

6.3 mBLOR in the spin-symmetric case

We are now ready to derive the generalization of the BLOR functional to address many-body SIE and SCE, termed mBLOR for brevity. For simplicity, we will first consider the simpler case of a spin symmetric system whose total subspace energy satisfies

$$E[N, M] = E[N, -M]. \tag{6.5}$$

Here, N and M are the total subspace electron count and subspace spin-magnetization (note here that magnetization is measured in units of electrons, following convenient convention in DFT, not units of $\hbar$), respectively,

$$N = \sum_{\sigma m} n^{\sigma}_{mm} \quad \& \quad M = \sum_{m} (n^{\uparrow}_{mm} - n^{\downarrow}_{mm}). \tag{6.6}$$

This spin-symmetric special case simplifies matters considerably because the spurious curvature in the total subspace energy of an approximate XC functional with respect to spin up subspace occupancy $n^{\uparrow}$ is then equal to the spurious curvature in the total subspace energy with respect to spin down subspace occupancy $n^{\downarrow}$. Furthermore, if $[N, M]$ is a vertex in the energy landscape, then $[N, -M]$ is a degenerate vertex in the energy landscape.

Focusing on the lowest energy magnetization states, and assuming no structure to the weak interaction with the bath for the subspace, the $E[N, M]$ surface is as shown in Fig. 6.1 (for the cases of single s or p-valence subspaces, the d and f cases being straightforward generalizations) assuming two criteria are satisfied.

(a) The total energy of the subspace is strictly convex with respect to electron count, so that

$$2E[N] < E[N-1] + E[N+1]. \tag{6.7}$$

(b) Hund's First Rule is satisfied, i.e., each orbital of the subspace is occupied singly first with electrons of parallel spin, before any double occupation occurs.

As shown in Fig. 6.1, the $E[N, M]$ surface in this case is composed of a series of flat planes, which meet with derivative discontinuities at integer values of electron count. The $E[N, M]$ surface in Fig. 6.1, displays a large number of vertices. In general we expect the approximate XC functional, that BLOR is designed to supplement, to yield accurate total energies for atomic systems whenever N and M are located at vertices in the energy landscape. It is important to note that an analogous $E[N, M]$ surface to Fig. 6.1 will also occur for d and f valence-atoms if criteria (a)-(b) are satisfied.

In order to enforce the tilted plane condition once a subspace that satisfies criteria (a)-(b), the corrective functional must satisfy four key conditions. It must:

1. Be a continuous function of the subspace electron count N and magnetization M.

2. Yield no correction at the vertices in the $E_v[N, M]$ landscape. This is desirable because approximate functionals are expected to yield accurate total energies in this case.

3. Have a constant curvature of $-U$ with respect to N. This is desirable because approximate functionals are expected to have a spurious curvature of U with respect to N due to their deviation from the tilted plane condition, and this should be subtracted off.

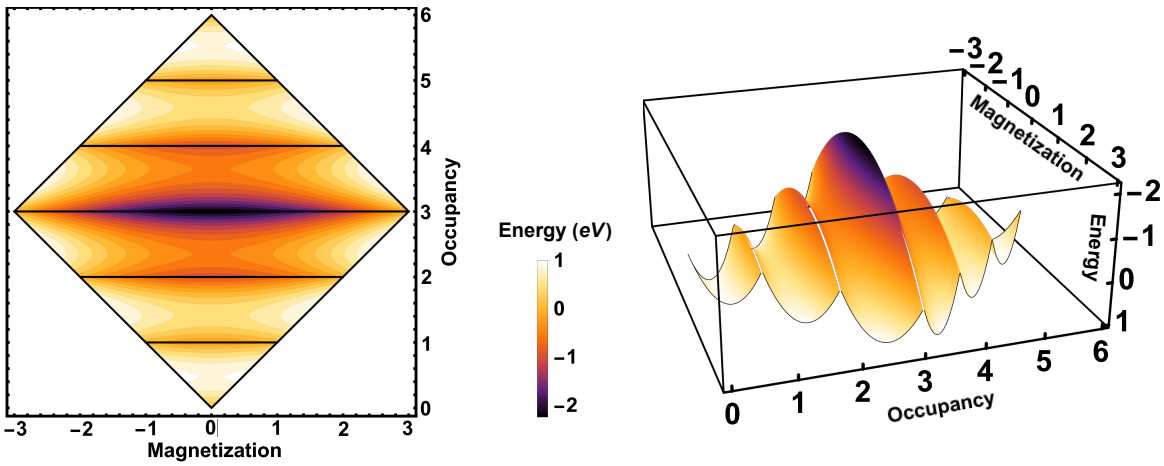

Figure 6.2: Plot of the total corrective energy of the spin-symmetric mBLOR functional of Eq. 6.8 for a p-orbital subspace with Hubbard corrective parameters $U^{\uparrow} = U^{\downarrow} = 8$ eV and $J = 0.5$ eV. In the left-hand image energy contour lines are plotted at intervals of 0.2 eV. In the right hand image a side-on view of the same mBLOR total corrective energy surface is presented.

4. Have a constant curvature of J with respect to M. This is desirable because approximate functionals are expected to have a spurious curvature of $-J$ with respect to M (the minus is due to long-standing convention for defining J), and and this should be subtracted off.

The spin-symmetric version of the mBLOR functional is the mathematically unique functional that satisfies these four conditions for a subspace that meets criteria (a)-(b), and it may be written separately for each subspace as

$$E_{\mathrm{mBLOR}} = \begin{cases} \dfrac{U}{2}\left[(N-N_0)-(N-N_0)^2\right] + \dfrac{J}{2}\left[M^2 - N^2\right], & N \leq \mathrm{Tr}[\hat{P}], \\ \dfrac{U}{2}\left[(N-N_0)-(N-N_0)^2\right] + \dfrac{J}{2}\left[M^2 - (N-2\mathrm{Tr}[\hat{P}])^2\right], & N > \mathrm{Tr}[\hat{P}]. \end{cases} \tag{6.8}$$

In Eq. 6.8 N_0 is defined as $\lfloor N \rfloor$, where $\lfloor \cdot \rfloor$ is the floor function (the integer part). The first term on the right hand side of Eq. 6.8 is the many-electron self interaction error term. It mitigates the localized analogue of MSIE by removing a quadratic term in N of curvature U and replacing it with a linear term. As expected, the MSIE term offers no correction to the total energy for systems with integer subspace occupancy. The second term on the right hand side of

Eq. 6.8 is the static correlation error correction term, which offers no energy correction for a maximally spin polarized subspace and reaches its maximum energy correction at $M = 0$. The SCE term takes a different form depending on whether the subspace is more or less than half occupied, this is a consequence of satisfying Hund's First Rule. We refer to these two forms as the 'early' and 'late' versions of the mBLOR functional, which should be used when $N \leq \mathrm{Tr}[\hat{P}]$, and $N > \mathrm{Tr}[\hat{P}]$, respectively. Beyond half occupancy, the maximum magnetization, i.e., the value of M for which the SCE term vanishes, decreases with increasing N as the orbitals of the subspace are now being filled by a second electron of the opposite spin.

In passing, we note that in addition to its primary application of treating localized spin-symmetric subspaces, the mBLOR functional of Eq. 6.8 can also be used mitigate approximate XC functional's deviation from the *global* flat plane condition. In this case N and M of Eq. 6.8 would be replaced by the total electron count and magnetization of the finite electronic system of interest.

6.4 Computational details

All calculations were performed using the ONETEP (Order-N Electronic Total Energy Package) DFT code [281, 294–296]. The ONETEP code constructs the Kohn-Sham density matrix $\rho(\mathbf{r}, \mathbf{r}')$ from a set of Non-orthogonal Generalized Wannier Functions (NGWFs) $\{\phi_\alpha\}$,

$$\rho(\mathbf{r}, \mathbf{r}') = \sum_{\alpha,\beta} \phi_\alpha(\mathbf{r}) K^{\alpha\beta} \phi_\beta(\mathbf{r}'), \tag{6.9}$$

where $K^{\alpha\beta}$ is the density kernel. The total energy of the system is minimized by optimizing both $K^{\alpha\beta}$ and $\{\phi_\alpha\}$.

All calculations were completed using the PBE [60] exchange-correlation functional at a high cutoff energy of no lower than 1,500 eV. The dissociated molecular test systems were located in a large simulation cell, no smaller than $70 \times 60 \times 60\ a_0^3$, with a Martyna-Tuckerman periodic boundary correction cutoff of 7.0 a_0 [299].

For a system with N_σ spin σ KS particles, the occupancy of the lowest N_σ KS particles was set equal to one, and otherwise set equal to zero. The convergence threshold of the root-mean-square gradient of the density kernel

and the NGWFs was set at 1×10^{-6}Ha e^{-1} and 1×10^{-7}Ha $a_0^{3/2}$, respectively, and the electronic energy tolerance was set at 1×10^{-6} eV/atom.

Seven NGWFs were assigned per atom using the split-valence approach for p orbitals, in which case 15% of the norm set to be beyond the matching radius r_m. The NGWF cutoff was set to 14 a_0. A bespoke set of norm-conserving pseudopotentials with very small cut off radii were made using the OPIUM code [343]. It is important to emphasise that the corrective parameters as well as the subspace occupancies depend strongly on the choice of subspace projection operator $\hat{P}$. For our purposes we use the atomic orbitals generated using the Pseudoatomic Solver in ONETEP with our bespoke norm-conserving pseudopotentials, specifically the pseudoatomic p-orbitals generated in a neutral non-spin-polarized atomic reference state within the PBE approximation. In the limit of large interatomic separation lengths, the atomic orbitals become an ideal choice for the subspace projection operator, particularly when using PBE atomic reference energies as part of the energy extensivity diagnostic. Thus, by testing the Hubbard functionals on molecular species at large interatomic separation lengths, any resulting errors in the total energies can be attributed to failures in the underlying DFT+U-type functional as opposed to failures in the subspace projection scheme.

In the case of the stretched singlet N_2, F_2 and spin-polarized O_2 molecules the raw PBE calculation converged to a spurious spin symmetry broken solution. This results in spin resolved PBE densities that differ qualitatively from the true ground state spin resolved densities of the molecule. This necessitates the evaluation of the Hubbard corrective parameters self-consistently as the spin resolved densities will change appreciably upon application of a Hubbard type corrective functional.

In the case of the stretched F_2 molecule a series of linear response perturbative calculations were used to evaluate the Hubbard corrective parameters (U_{out} and J_{out}) with Dudarev's DFT+U functional applied to stabilise the spin symmetry unbroken ground state. The corrective parameters U_{out} and J_{out} were evaluated at a range of values of U_{in} between -18 eV and -22 eV, where U_{in} is the input value of the Hubbard U parameter used in Dudarev's DFT+U functional to stabilise the spin symmetry unbroken ground state. The self-consistent Hubbard U and Hund's J corrective parameters were found by linearly extrapolating the values of U_{out} and J_{out} back to $U_{\text{in}} = 0$ eV. The same procedure was

also implemented for the stretched N_2 and O_2 molecules. However, for these systems the DFT+U+J functional without the minority spin term was used to stabilise the symmetry unbroken ground state, with the effective Hubbard U_{in} parameter set equal in magnitude to the Hund's J_{in} parameter. U_{out} and J_{out} were evaluated at a range of values of U_{in} between -8 eV and -12 eV in the case of the N_2 molecule and between -21 eV and -24 eV in the case of the O_2 molecule.

Despite the author's best efforts, no suitable range in values of U_{in} were found for the O_2 molecule in its spin polarized state that sufficiently stabilized the symmetry unbroken solution to allow linear extrapolation of $U_{\text{out}}(U_{\text{in}})$ back to $U_{\text{in}} = 0$ eV. As a result, the calculations on the O_2 molecule were performed in its non-spin polarized state as a suitable range in values of U_{in} could be found for this system. It was worth noting that the spin polarized and non-spin polarized states of the O_2 molecule should be degenerate in energy as they represent the $m_s = 1$ and $m_s = 0$ values of the molecule in its triplet ground state. In many regards the non-spin polarized state of the stretched O_2 molecule poses a significantly more challenging test case for the mBLOR functional as unlike the spin polarized state, the non-spin polarized state will be located at the point of maximum localized-SCE and being a neutral homonuclear molecule at large separation lengths, their will be negligible localized-MSIE present. The values of the Hubbard corrective parameters for each stretched molecular species is reported in table 6.1.

6.5 Spin-Symmetric Molecular Test Systems

We tested the spin-symmetric mBLOR corrective functional of Eq. 6.8 on three spin-symmetric homo-nuclear dimers at large inter-nuclear separation lengths, namely N_2, F_2 and (simulating its non-spin polarized triplet ground state) O_2. For these stretched, neutral homo-nuclear dimers, an approximately integer number of electrons localizes on each atomic site. An ambiguity therefore arises as to which integer value to use for N_0 in the mBLOR functional. Following the precedent set in the study of the stretched s-block dimers [331], we choose to set $N_0 = 2$, 3 and 4 for the stretched N_2, O_2 and F_2 molecules, respectively,

	$U^{\uparrow}$	$U^{\downarrow}$	U_{simple}	J_{simple}	Magnetistion	Separation Length
H_2	6.783	6.783	8.689	1.905	0.0	9.0
He_2^+	-37.961	13.729	-13.837	-1.721	1.0	5.0
Li_2	7.507	7.507	9.251	1.743	0.0	15.0
Be_2^+	-11.881	3.988	-4.238	-0.291	1.0	10.0
H_5^+	9.827	4.536	9.154	1.972	2.0	8.0
N_2	7.450	7.450	8.189	0.740	0.0	7.0
O_2	8.156	8.156	9.037	0.881	0.0	6.0
F_2	10.471	10.471	11.429	0.958	0.0	6.0
Ne_2^+	-43.872	12.855	-17.384	-1.875	1.0	5.0

Table 6.1: The Hubbard and Hund corrective parameters (eV) for the stretched dimers, evaluated using the minimum tracking linear response methodology. The total magnetization M (unitless electron count) and inter-nuclear separation length in bohr radii (a_0) is also reported for each molecular species. For completeness and comparison, we also report the values of the first-principles corrective parameters for the stretched s-block species that were evaluated for testing the BLOR corrective functional [331].

so that the MSIE term in the mBLOR functional is equal to zero when the subspace occupancy is equal to that of the neutral atom and 'plus one' cation. This choice in values of N_0 results in the 'early' ($N \leq \text{Tr}[\hat{\text{P}}]$) version of the mBLOR functional being applied to the stretched N_2 system and the 'late' ($N > \text{Tr}[\hat{\text{P}}]$) version of the mBLOR functional being applied to the stretched O_2 and F_2 systems. The corresponding versions of the BLOR functional is applied to the stretched N_2 molecule and to the stretched O_2 and F_2 molecules. In the case of the O_2 molecule, to avoid converging to a broken-symmetry spin-polarized ground state, the occupancy of the two frontier spin up and spin down KS orbitals were permitted, as necessary, to be degenerate with occupancy 0.5. At large inter-nuclear separation lengths, a close to integer number of electrons will localise on each atomic site, therefore these systems will suffer from negligible localized-MSIE. Being non-spin polarized molecules, the magnetization at each of the atomic sites will be equal to zero, thus for a given value of N, these systems are located at the point of maximum localized SCE. Assuming a positive in-situ measured value value of J, as indeed transpires to be the case, the raw uncorrected PBE functional will thus overestimate the total energies of these stretched X_2 systems.

At the dissociated limit the total energy of the X_2 molecule, the energy

extensivity condition holds, namely

$$E[\mathrm{X}_2] = 2E[\mathrm{X}]. \tag{6.10}$$

However, due to localized MSIE and localized SCE, the total energy of the X_2 molecule at large inter-nuclear separation lengths will not be equal to twice the energy of the X atom when evaluated using an approximate XC functional. The difference between these two quantities is thus an intrinsic error associated with the approximate XC functional. By contrast, the raw PBE total energy of the isolated X atom will not suffer from localized MSIE or localized SCE as the system will be located at a vertex of the $E[N, M]$ energy surface by virtue of it being in the lowest energy magnetization state of the atom for a given integer value of electron count. Twice the PBE total energy of the X atom, can thus be used as our reference value. Ideally, application of a Hubbard-type corrective functional to the stretched X_2 system should mitigate this intrinsic energy error. The following bar charts present the energy error associated with each DFT+U-type functional, giving what are close to ideal application conditions (i.e., near the atomic limit). We define this energy error here as the energy difference between the stretched X_2 molecule evaluated with a given DFT(PBE)+U-type functional compared to twice the PBE total energy of the X atom. Using Eq. 6.10 to define the exact total energy provides cancellation errors in the total energy due to the use of (very carefully designed) pseudo-potentials.

The energy results are presented in Figs. 6.3-6.5 for the stretched non-spin polarized N_2, O_2 and F_2 molecules, respectively. The DFT+U and DFT+$(U-J)$ relative errors were computed using Dudarev et al.'s 1998 functional with the effective Hubbard parameter (U_{eff}) set as U and $U-J$, respectively. DFT+U+J and DFT+U+J (minority term) refers to the Hubbard corrective functional of Himmetoglu et al. [214] excluding and including the minority spin term, respectively. The localized-jmDFT (l-jmDFT) functional refers to the localized subspace application corrective functional of Bajaj et al. [109,110], in which the use of different functional forms for different flat-plane tiles was pioneered. It applied in this work using U and J parameters evaluated via the simple 2×2 method, which is not how the functional was originally intended to be applied.

Uncorrected approximate DFT, using the PBE approximation, yielded errors in the total energy as high as 232 mHa. Application of Dudarev's 1998 DFT+U

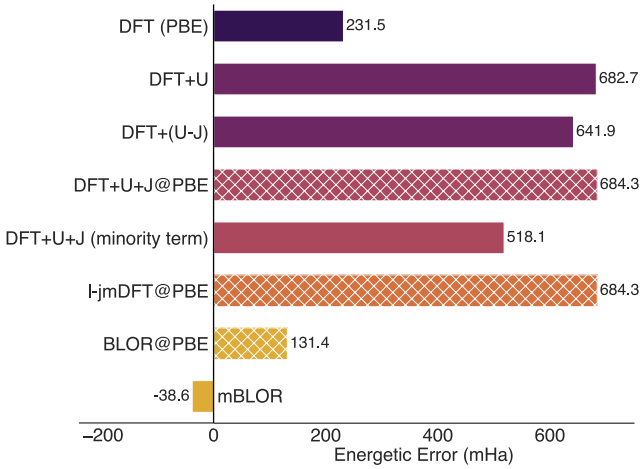

Figure 6.3: Bar chart of the errors in the total energy of singlet N_2 at an inter-nuclear separation length of $7a_0$ using different corrective functionals [109,110,183,214,331]. The hasing on the DFT+U+J, l-jmDFT and BLOR bars is used to indicate that these functionals were evaluated non-self consistently using the PBE density, as self-consistent application of these functionals (in a non-spin polarized DFT calculation), results in a symmetry broken ground state charge density. To avoid spurious spin-symmetry breaking, all other corrective functionals were evaluated self-consistently via a non-spin polarized DFT calculation. The raw DFT calculations were performed with the PBE functional [60]. The U and J parameters were evaluated using the simple 2×2 method [242] and U^σ was computed via Eq. 5.22.

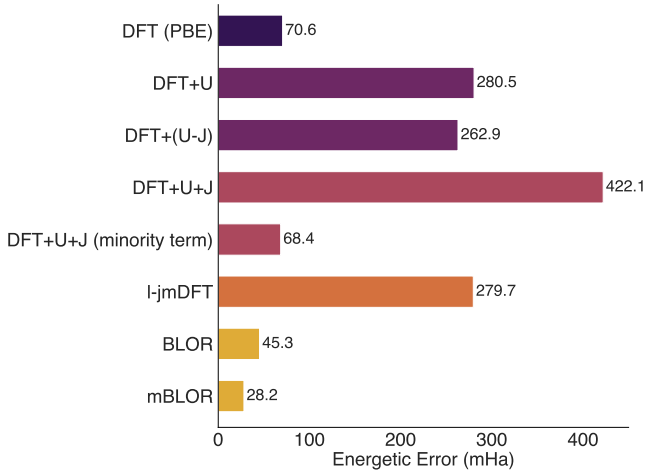

Figure 6.4: Bar chart of the errors in the total energy of singlet F_2 at an internuclear separation length of $6a_0$ using different corrective functionals [109, 110, 183, 214, 331]. With the exception of the raw DFT(PBE) functional, all total energy errors have been evaluated self-consistently via a non-spin polarized DFT calculation to avoid spurious spin-symmetry breaking. The symmetry unbroken DFT(PBE) calculation failed to converge. The energy error for the DFT(PBE) functional has been evaluated by extrapolating the DFT+U_{in} total energy (for a series of values of U_{in}), back to $U_{\text{in}} = 0$. The U and J parameters were evaluated using the simple 2×2 method [242] and U^{σ} was computed via Eq. 5.22.

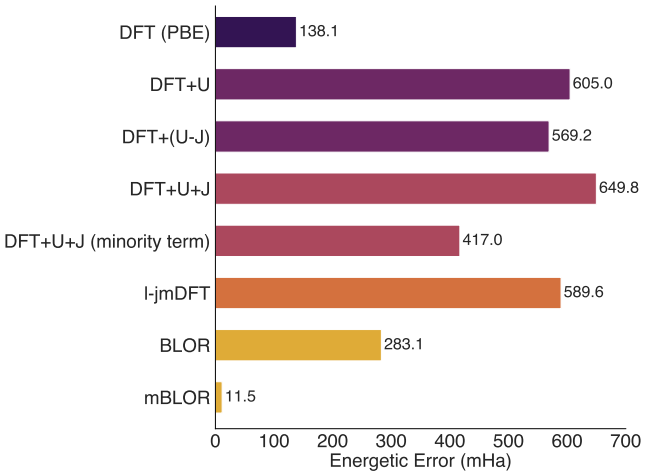

Figure 6.5: Bar chart of the errors in the total energy of non-spin polarized O_2 at an inter-nuclear separation length of $6a_0$ using different corrective functionals [109, 110, 183, 214, 331]. To simulate the non-spin polarized O_2 molecule, the spin up and spin down occupancies of the doubly degenerate KS orbitals at the fermi level were all set equal to 0.5. The raw DFT calculations were performed with the PBE functional [60]. The U and J parameters were evaluated using the simple '2×2' method [242] and U^{σ} was computed via Eq. 5.22. The ground state PBE total energy and spin resolved subspace occupancies were evaluated by linearly extrapolating the results from the O_2 calculations with a DFT+U+J-type stabilising potential back to $U_{\text{in}} = J_{\text{in}} = 0$, see Appendix II for further details. Self-consistent application of the corrective functionals via non-spin polarized DFT calculations results in symmetry broken ground state charge densities, and so for this system the corrective functionals have been evaluated non-self consistently using the extrapolated PBE density.

corrective functional significantly worsened these total energies yielding errors as high as 682 mHa. This result suggests that Dudarev's DFT+U functional, the most widely used Hubbard corrective functional in the literature, does not yield reliable total energies. By comparison, our newly developed mBLOR functional significantly improved the raw DFT total energies, with relative errors below 39 mHa across all three test systems.

The original BLOR functional of Eq. 5.6 improved the total energies over raw DFT (PBE) in some cases but notably worsens the total energy compared to raw DFT for the non-spin polarized O_2 molecule, yielding an energy error of 283 mHa. The success of the mBLOR functional over the original BLOR functional suggests that inter-orbital interactions cannot be neglected in the development of DFT+U-type functionals that yield reliable total energies, although there may of course prove to be cases where BLOR outperforms mBLOR. The present

bar charts show that only the mBLOR DFT+U functional reduces the error in the raw DFT total energies across all three test systems.

6.6 mBLOR in the spin-asymmetric case

We are now ready to expand on our previous arguments and derive the mBLOR functional which can be applied to either spin polarized or non-spin polarized systems. The functional can also be used to enforce the global tilted plane condition on finite electronic systems that are in an external Zeeman field, or just when treated with spin-symmetry-broken approximate DFT. To derive this corrective functional we can no longer assume that the spurious curvature in the total subspace energy of an approximate XC functional with respect to spin up subspace occupancy $n^{\uparrow}$, is equal to the spurious curvature in the total subspace energy with respect to spin down subspace occupancy $n^{\downarrow}$. We denote these curvatures simply as $U^{\uparrow}$ and $U^{\downarrow}$, respectively. Now that $U^{\uparrow} \neq U^{\downarrow}$, the isosceles trapezoid shaped planes in the $E[N, M]$ energy surface of Fig. 6.1 will, in the simplest case, fracture into two triangular shaped planes. The breaking of this spin symmetry may be thought of as being due to an effective magnetic field $B_{\mathrm{xc}}(\mathbf{r})$, acting on the subspace and due to the surrounding spin polarized material environment. This effective magnetic field is due to the differing spin resolved exchange-correlation potentials,

$$B_{\mathrm{xc}}(\mathbf{r}) = \frac{1}{2}\left(v_{\mathrm{xc}}^{\uparrow}(\mathbf{r}) - v_{\mathrm{xc}}^{\downarrow}(\mathbf{r})\right), \tag{6.11}$$

in atomic units. A large variety of different $E[N, M]$ surfaces can arise due to this fracturing. In this study we consider only the simplest case, where each isosceles trapezoid shaped plane fractures into two triangular shaped planes, as presented in section 6.7. This fracturing pattern will occur if the subspace satisfies the following three criteria.

(a) The total energy of the subspace obeys the strong convexity condition with respect to electron count N,

$$2E[N, -|M_j|] < E[N-1, M_i] + E[N+1, M_k], \tag{6.12}$$

where M_i, M_j, and M_j are the lowest energy magnetization states of the

subspace with integer occupancies $N-1$, N and $N+1$.

(b) The subspace-bath interaction energy varies linearly with spin-resolved occupancy.

(c) Vertices in the subspace energy surface occur only when $M = \pm M_0$, where M_0 is the maximum magnetization of the subspace for a given integer value of occupancy. There exists $4\mathrm{Tr}[\hat{P}]$ such vertices for a given subspace.

In order to enforce the localized tilted plane condition once on an entire multi-orbital subspace that meets criteria (a)-(c), the mBLOR functional is designed to satisfy four key conditions. It must:

1. Be a continuous function of the subspace electron count N and subspace magnetization M.

2. Yield no correction at the $4\mathrm{Tr}[\hat{P}]$ vertices. This is desirable because reasonable approximate functionals are expected to yield accurate total energies in this case.

3. Have a constant curvature of $-U^\sigma$ with respect to n^σ. This is desirable because approximate functionals are expected to have a spurious curvature of U^σ with respect to n^σ due to their deviation from the localized flat plane condition, and this should be subtracted off.

4. Have a constant curvature of J with respect to M. This is desirable because approximate functionals are expected to have a spurious curvature of $-J$ with respect to M (the minus is due to long-standing convention for defining J), and again this should be subtracted off.

The mBLOR functional is the mathematically unique functional that satisfies these four key conditions, given for each site by

$$E_{\mathrm{mBLOR}} = \begin{cases} \dfrac{U^\uparrow + U^\downarrow}{4}\left[(N-N_0)-(N-N_0)^2\right] & \\ \quad + \dfrac{J}{2}\left[M^2 - N^2\right] + \dfrac{U^\uparrow - U^\downarrow}{4} F^{\mathrm{early}}_{\mathrm{AMSIE}}[N,M], & N \leq \mathrm{Tr}[\hat{P}], \\ & \\ \dfrac{U^\uparrow + U^\downarrow}{4}\left[(N-N_0)-(N-N_0)^2\right] & \\ \quad + \dfrac{J}{2}\left[M^2 - (N - 2\mathrm{Tr}[\hat{P}])^2\right] + \dfrac{U^\uparrow - U^\downarrow}{4} F^{\mathrm{late}}_{\mathrm{AMSIE}}[N,M], & N > \mathrm{Tr}[\hat{P}], \end{cases} \tag{6.13}$$

which generates the corresponding terms in the spin-dependent potential

$$\hat{v}^{\sigma}_{\mathrm{mBLOR}} = \begin{cases} \dfrac{U^{\uparrow}+U^{\downarrow}}{4}\left[1-2\left(N-N_0\right)\right]\hat{P} & \\ \quad -2JN^{\bar{\sigma}}\hat{P} + \dfrac{U^{\uparrow}-U^{\downarrow}}{4}\hat{v}^{\sigma\,\mathrm{early}}_{\mathrm{AMSIE}}[N,M], & N \leq \mathrm{Tr}[\hat{P}], \\ & \\ \dfrac{U^{\uparrow}+U^{\downarrow}}{4}\left[1-2\left(N-N_0\right)\right]\hat{P} & \\ \quad -2J\left[N^{\bar{\sigma}}-\mathrm{Tr}[\hat{P}]\right]\hat{P} + \dfrac{U^{\uparrow}-U^{\downarrow}}{4}\hat{v}^{\sigma\,\mathrm{late}}_{\mathrm{AMSIE}}[N,M], & N > \mathrm{Tr}[\hat{P}], \end{cases} \tag{6.14}$$

Here, $N^{\bar{\sigma}}$ is the subspaces occupancy for the opposite spin channel to that indexed by σ. The unitless quantity $F_{\mathrm{AMSIE}}\left[N,M\right]$ is here termed the asymmetric-many electron self interaction error function and $\hat{v}^{\sigma}_{\mathrm{AMSIE}}[N,M]$ is the correspondingly generated spin σ Asymmetric-MSIE potential operator. These are defined in section 6.7. The $F_{\mathrm{AMSIE}}\left[N,M\right]$ function arises whenever $U^{\uparrow} \neq U^{\downarrow}$. In such cases, a spin-symmetric and spin-asymmetric term is needed to properly mitigate the localized many electron self interaction error. The asymmetric-MSIE term has already been studied for s-valence systems by Burgess et al. [331] and its inclusion was found to be necessary for yielding accurate total energies for the stretched triplet H_5^+ ring system. The eight different forms of the asymmetric-MSIE function are presented in section 6.7 along with the corresponding Asymmetric-MSIE potential operators.

It is worth emphasising that for non-spin polarized systems the mBLOR functional of Eq. 6.13 simplifies to the spin symmetric functional of Eq. 6.8. Furthermore, in the case of single orbital subspaces, Eq. 6.13 is equivalent to the original BLOR functional, which unlike standard DFT+U functionals has been shown to yield accurate total energies for dissociated s-valence molecules, namely H_2, He_2^+, Li_2, Be_2^+ and triplet H_5^+.

It is worth mentioning that the implementation of the mBLOR functional does not require substantial modifications to an existing simplified rotationally invariant DFT+U code. Terms in the energy that ordinarily look like $\mathrm{Tr}[\hat{\mathrm{n}}^{\sigma}\hat{\mathrm{n}}^{\sigma'}]$ are converted to the form $\mathrm{Tr}[\hat{\mathrm{n}}^{\sigma}]\mathrm{Tr}[\hat{\mathrm{n}}^{\sigma'}]$, while terms in the potential that ordinarily look like $\hat{n}^{\sigma}$ are converted to the form $N^{\sigma}\hat{P}$. If starting, as we have, with a code equipped with simplified rotationally invariant DFT+U+J

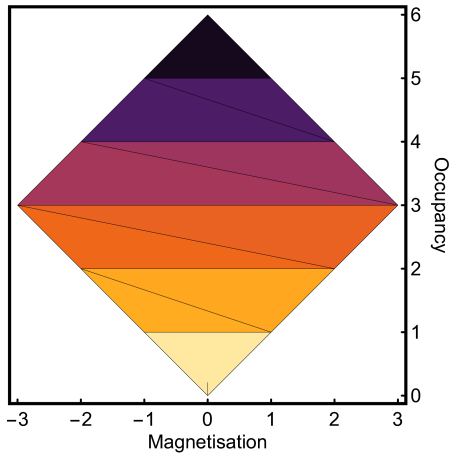

Figure 6.6: The fractured $E_v[N, M]$ energy surface for a p-orbital subspace that satisfies criteria (a)-(c), with $U^{\uparrow} > U^{\downarrow}$. For ease of visualization, each $N_0 \leq N \leq N_0 + 1$ segment is highlighted a different color. A single line of fracture occurs within each $N_0 \leq N \leq N_0 + 1$ segment, with the exception of the $0 \leq N \leq 1$ and $2\mathrm{Tr}[\hat{P}] - 1 \leq N \leq 2\mathrm{Tr}[\hat{P}]$ segments. The mirror image, through the vertical $M = 0$ line, of this fracturing pattern will occur if $U^{\uparrow} < U^{\downarrow}$, while no diagonal fracturing occurs for $U^{\uparrow} = U^{\downarrow}$. Over-simplistically, but perhaps helpfully for visualization of the shown $U^{\uparrow} > U^{\downarrow}$ example, we can envisage the greater discretized energy curvature in the spin-up direction (which points at 45 degrees up-and-right away from the origin) necessitating additional fracturing on along vertex connection lines that are near-perpendicular to that direction.

together which 'α' and 'β' potential shifts (that may of course be put to use other than for perturbation), then the aforementioned, along with the provision for spin-dependent Hubbard U parameters, is all the in-code modification that is strictly needed for mBLOR. The rest can be done by parameter rearrangement externally. This is even more so the case for the spin-symmetric approximation to BLOR, which requires no code modification at all with starting point, as discussed in the SM of Ref. [331].

6.7 Asymmetric-MSIE Function

The fracturing pattern for a p-orbital subspace (as an example) that satisfies criteria (a)-(c), as explicated in the derivation of the mBLOR functional is displayed in Fig. 6.6. The Asymmetric-MSIE function $F_{\mathrm{AMSIE}}[N, M]$, is an explicit function of the subspace occupancy and magnetization but it has eight different forms. The following three criteria can be used to determine which

$U^{\uparrow} > U^{\downarrow}$, lower
$F^{\text{early}}_{\text{AMSIE}}[N, M] = N_0 M - NM + (N_0 - N)(1 + N_0)$ $F^{\text{late}}_{\text{AMSIE}}[N, M] = N_0 M - NM + (N_0 - N)(2\text{Tr}[\hat{P}] - N_0 - 1)$
$U^{\uparrow} > U^{\downarrow}$, upper
$F^{\text{early}}_{\text{AMSIE}}[N, M] = M - NM + N_0(N - N_0 - 1) + N_0 M$ $F^{\text{late}}_{\text{AMSIE}}[N, M] = M - NM + (2\text{Tr}[\hat{P}] - N_0)(N - N_0 - 1) + N_0 M$
$U^{\uparrow} < U^{\downarrow}$, lower
$F^{\text{early}}_{\text{AMSIE}}[N, M] = N_0 M - NM + (N - N_0)(1 + N_0)$ $F^{\text{late}}_{\text{AMSIE}}[N, M] = N_0 M - NM + (N - N_0)(2\text{Tr}[\hat{P}] - N_0 - 1)$
$U^{\uparrow} < U^{\downarrow}$, upper
$F^{\text{early}}_{\text{AMSIE}}[N, M] = M - NM + N_0(N_0 + 1 - N) + N_0 M$ $F^{\text{late}}_{\text{AMSIE}}[N, M] = M - NM + (2\text{Tr}[\hat{P}] - N_0)(N_0 + 1 - N) + N_0 M$

Table 6.2: The eight different forms of the Asymmetric-MSIE function, $F_{\text{AMSIE}}[N, M]$.

form of the AMSIE function should be employed for a given subspace.

1. The relative magnitude of $U^{\uparrow}$ and $U^{\downarrow}$. A different version of the AMSIE function should be employed if $U^{\uparrow} > U^{\downarrow}$ or vice-versa.

2. If the subspace occupancy is less than half occupied, i.e., $N \leq \text{Tr}[\hat{P}]$, the 'early' version of the AMSIE function should be employed. If the subspace is more than half occupied, i.e., $N > \text{Tr}[\hat{P}]$, the 'late' version of the AMSIE function is required.

3. The 'upper' or 'lower' version of the AMSIE function should be employed depending whether the point (N, M) on the N-M plane, where N is the subspace occupancy and M the subspace magnetization, is located above or below the line of fracture within a given $N_0 \leq N \leq N_0 + 1$ segment. The 'upper' version should be employed if it is located above the line of fracture and the 'lower' version should be employed if it is located below the line of fracture. No line of fracture occurs in the segment $0 \leq N \leq 1$, in this case the 'upper' version should always be employed, similarly no line of fracture occurs in the segment $2\text{Tr}[\hat{P}] - 1 \leq N \leq 2\text{Tr}[\hat{P}]$ and in this case the 'lower' version should always be employed.

The eight different forms of the $F_{\text{AMSIE}}[N, M]$ function are listed in table 6.2.

$\hat{v}^{\uparrow}_{\text{AMSIE}}$	$\hat{v}^{\downarrow}_{\text{AMSIE}}$
$U^{\uparrow} > U^{\downarrow}$, lower	$U^{\uparrow} > U^{\downarrow}$, lower
$\hat{v}^{\text{early}}_{\text{AMSIE}}[N,M] = -\hat{P} - 2N^{\uparrow}\hat{P}$ $\hat{v}^{\text{late}}_{\text{AMSIE}}[N,M] = (2N_0 + 1 - 2\text{Tr}[\hat{P}])\hat{P} - 2N^{\uparrow}\hat{P}$	$\hat{v}^{\text{early}}_{\text{AMSIE}}[N,M] = (-2N_0 - 1)\hat{P} + 2N^{\downarrow}\hat{P}$ $\hat{v}^{\text{late}}_{\text{AMSIE}}[N,M] = (1 - 2\text{Tr}[\hat{P}])\hat{P} + 2N^{\downarrow}\hat{P}$
$U^{\uparrow} > U^{\downarrow}$, upper	$U^{\uparrow} > U^{\downarrow}$, upper
$\hat{v}^{\text{early}}_{\text{AMSIE}}[N,M] = (1 + 2N_0)\hat{P} - 2N^{\uparrow}\hat{P}$ $\hat{v}^{\text{late}}_{\text{AMSIE}}[N,M] = (1 + 2\text{Tr}[\hat{P}])\hat{P} - 2N^{\uparrow}\hat{P}$	$\hat{v}^{\text{early}}_{\text{AMSIE}}[N,M] = -\hat{P} + 2N^{\downarrow}\hat{P}$ $\hat{v}^{\text{late}}_{\text{AMSIE}}[N,M] = (2\text{Tr}[\hat{P}] - 2N_0 - 1)\hat{P} + 2N^{\downarrow}\hat{P}$
$U^{\uparrow} < U^{\downarrow}$, lower	$U^{\uparrow} < U^{\downarrow}$, lower
$\hat{v}^{\text{early}}_{\text{AMSIE}}[N,M] = (1 + 2N_0)\hat{P} - 2N^{\uparrow}\hat{P}$ $\hat{v}^{\text{late}}_{\text{AMSIE}}[N,M] = (2\text{Tr}[\hat{P}] - 1)\hat{P} - 2N^{\uparrow}\hat{P}$	$\hat{v}^{\text{early}}_{\text{AMSIE}}[N,M] = \hat{P} + 2N^{\downarrow}\hat{P}$ $\hat{v}^{\text{late}}_{\text{AMSIE}}[N,M] = (2\text{Tr}[\hat{P}] - 2N_0 - 1)\hat{P} + 2N^{\downarrow}\hat{P}$
$U^{\uparrow} < U^{\downarrow}$, upper	$U^{\uparrow} < U^{\downarrow}$, upper
$\hat{v}^{\text{early}}_{\text{AMSIE}}[N,M] = \hat{P} - 2N^{\uparrow}\hat{P}$ $\hat{v}^{\text{late}}_{\text{AMSIE}}[N,M] = (1 + 2N_0 - 2\text{Tr}[\hat{P}])\hat{P} - 2N^{\uparrow}\hat{P}$	$\hat{v}^{\text{early}}_{\text{AMSIE}}[N,M] = (-2N_0 - 1)\hat{P} + 2N^{\downarrow}\hat{P}$ $\hat{v}^{\text{late}}_{\text{AMSIE}}[N,M] = (-2\text{Tr}[\hat{P}] - 1)\hat{P} + 2N^{\downarrow}\hat{P}$

Table 6.3: The eight different forms of the spin resolved Asymmetric-MSIE potential operator.

The different forms of the spin up and spin down Asymmetric-MSIE potential operator are listed in table 6.3.

6.8 Spin-Asymmetric Molecular Test

In the case of the singlet N_2, F_2 and non-spin polarized O_2 molecules, the mBLOR functional of Eq. 6.13 simplifies to the spin symmetric mBLOR functional which has been shown to yield energy errors below 39 mHa across these three test systems. The stretched Ne_2^+ molecule was selected as a spin-polarized test system for the mBLOR functional due to its potential for harboring both symmetric and asymmetric SIE in their many-body forms. Unlike the singlet N_2, F_2 and non-spin polarized O_2 molecules, at large inter-nuclear separation lengths a non-integer number of electrons (approximately 5.5 electrons) will localize on each of the two atomic sites and hence the system will suffer from localized-MSIE. The atomic susbpaces of the Ne_2^+ molecule are maximally spin polarized and so the system is expected to suffer from negligible localized-SCE. Mori-Sánchez et al. [126] have shown that standard DFT functionals either yield accurate total energies for the stretched H_2^+ molecule, which is dominated by localized MSIE or accurate total energies for the stretched H_2 molecule, which is dominated by localized SCE, but never accurate total energies for both sys-

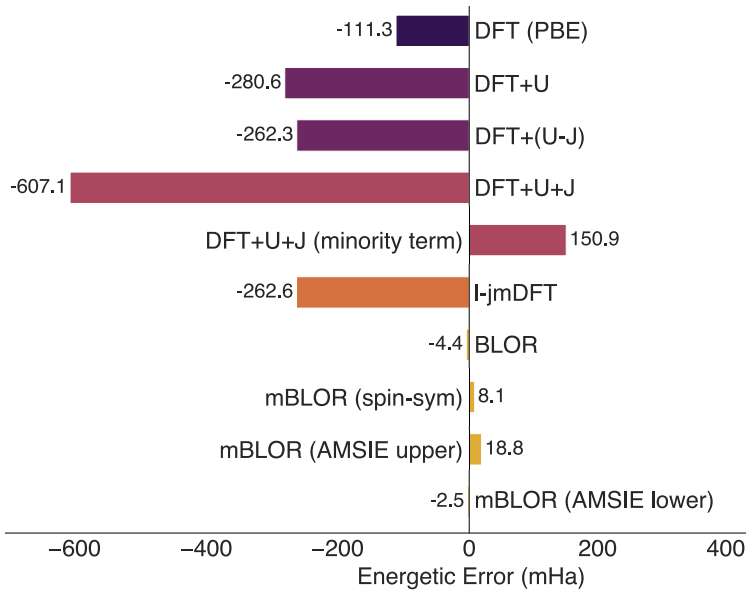

Figure 6.7: Bar chart of the errors in the total energy of the doublet Ne_2^+ molecule at an inter-nuclear separation length of $5a_0$ using different corrective functionals [109, 110, 183, 214, 331]. The raw DFT calculations were performed with the PBE exchange correlation functional [60]. The energy errors for the Hubbard type corrective functionals reported in this bar chart have been evaluated non-self consistently using the PBE density as all self consistent corrective functional calculations failed to converge for this system, with the notable exception of the mBLOR functional.

tems (of course some DFT functionals perform poorly for both). These four molecules at large separation lengths are therefore challenging test cases for any DFT+U-type functional, as in order to yield reliable total energies across all four test systems, the DFT+U functional must be able to mitigate both forms of error.

In the dissociated limit the total energy of a cationic dimer X_2^+ should converge to the sum of the energies of the X atom and cation, in what might be considered the generalized extensivity condition

$$E[X_2^+] = E[X] + E[X^+]. \tag{6.15}$$

As was the case with the non-spin polarized test systems, we use the PBE total energies from the right-hand side of Eq. 6.15 as our reference value, i.e., the sum of the PBE X atom and X^+ cation total energies. The bar chart of the energy errors associated with each DFT+U-type functional are presented in Fig. 6.7.

As shown in the bar chart of Fig. 6.7, the raw PBE functional yeilds an energy

error of 111 mHa and application of other DFT+U-type functionals significantly worsen this total energy, with the exception of BLOR and mBLOR. The optimal mBLOR functional reduces the PBE energy error to only -2.5 mHa, the original BLOR functional also performs exceptionally well for this test system, yielding an energy error of only -4.4 mHa. The success of the original BLOR functional in this particular test system is attributed to the fractional occupancy at the atomic site being limited to a single orbital, with the other two orbitals being almost fully occupied.

When applying the mBLOR functional to spin polarized systems, as was the case for non-spin polarized systems, one must choose between the 'early' and 'late' versions of the mBLOR functional. In the case of the stretched Ne_2^+ molecule, the subspace is significantly more than half occupied ($N \approx 5.5$) and thus the 'late' version of the functional should be applied. For spin polarized systems, one must also choose the correct AMSIE function, of which there are eight. The eight different forms of the AMSIE function are given in section 6.7, along with a practical selection procedure to ensure the correct AMSIE function is chosen for a given subspace. In the case of the stretched Ne_2^+ molecule, the most important step in the AMSIE function selection procedure is choosing between the 'lower' and 'upper' versions of the AMSIE function. Both correctly yield no energy correction when the subspace occupancy is equal to that of the neutral neon atom, i.e., $N = 6$ and $M = 0$, but only the 'lower' version of the AMSIE function yields no energy correction when the spin resolved subspace occupancy is equal to that of the spin polarized neon cation, i.e., $N = 5$ and $M = \pm 1$. The 'lower' version of the AMSIE function is thus the correct version to apply to this molecular system. Unsurprisingly, it yielded the smallest energy error of -2.5 mHa. If one instead choose (incorrectly) to apply the 'upper' version of the AMSIE function, the energy error increases to 18.8 mHa. Alternatively, choosing to omit the AMSIE function and instead apply the spin-symmetric mBLOR functional with $U^{\uparrow} = U^{\downarrow} = f^{\downarrow\downarrow}$, yields an energy error of 8.1 mHa.

The mBLOR functional is thus the only Hubbard type corrective functional that yielded low energy errors across all four test systems. The significantly improved total energies offered by the mBLOR corrective functional may facilitate the reliable prediction of chemical properties of transition metal compounds that have proven particularly challenging for current DFT+U-type functionals,

such as spin-state energies [349, 350], Heisenberg exchange coupling [351] and surface formation energies [352] but this are avenues for future research.

6.9 Potentialised Derivative Discontinuities

The mBLOR functional of Eq. 6.13 will exhibit derivative discontinuities [126, 133, 140–144] at integer values of subspace occupancy due to the functional's explicit dependence on N. Therefore, it is neither a differentiable functional of the electron density or the first-order non-interacting density matrix. The mBLOR functional thus fits into category D of Yang et al.'s [142] functional classification scheme, which is defined as any "*functional of the density or first-order density matrix with explicit discontinuity.*" This derivative discontinuity Δ_{xc}^{N}, will contribute to the quasi-particle bandgap Δ, whenever increasing the global electron count N_{tot} by one, causes the subspace occupancy at any of the atomic sites to increase through an integer value so that $\lfloor N \rfloor = N_0$ also increases by one. This contribution to the quasi-particle bandgap Δ_{xc}^{N}, will not appear in the Kohn-Sham gap Δ_{KS} or the Generalized Kohn-Sham gap Δ_{GKS}, unless something is done. This is unlike the situation in DFT+U functionals such as the Dudarev simplified rotationally-invariant one or even BLOR, as those comprise substantial (on the order of $U - J$) *implicit* derivative discontinuities via their subspace projected density-matrix dependence. An implicit derivative discontinuity may arise in mBLOR due to possibly different subspace projection weightings at the valence (occupied) and conduction (virtual) band edges, and this is expected to be a small effect for most applications of interest. However, substantial *explicit* derivative discontinuities appear in mBLOR, due to both the N_0 terms and to switch between early and late version, and these are rather unusual in the approximate or corrective functional contexts.

Ordinarily, calculating the mBLOR fundamental gap would not be strictly possible only via the single-particle eigenspectrum, because explicit derivative discontinuities do not manifest there, but it would instead require adding a separate contribution to the bandgap post hoc, as in

$$\Delta = \Delta_{\text{GKS}} + \Delta_{\text{xc}}^{N}. \tag{6.16}$$

Even this seems difficult as, opposed to being a constant global derivative dis-

continuity, the derivative discontinuity of the mBLOR functional is a non-local operator in character (non-local in the sense of exhibiting more than one spatial argument) and more generally a sum over sites of those. For a single site, we may write

$$\hat{\Delta}^N_{\mathrm{xc}} = \widetilde{\Delta}_{\mathrm{xc}}\,[N]\,\hat{P}. \tag{6.17}$$

The $\widetilde{\Delta}_{\mathrm{xc}}$ function of Eq. 6.17 itself depends on the subspace occupancy N. For subspaces with $U^{\uparrow} \geq U^{\downarrow}$, we have

$$\widetilde{\Delta}_{\mathrm{xc}} = \begin{cases} U^{\downarrow} - \frac{U^{\uparrow}-U^{\downarrow}}{2} N_0, & N < \mathrm{Tr}[\hat{P}], \\ U^{\uparrow} + 2J\mathrm{Tr}[\hat{P}] - \frac{U^{\uparrow}-U^{\downarrow}}{2}\mathrm{Tr}[\hat{P}], & N = \mathrm{Tr}[\hat{P}], \\ U^{\uparrow} - \frac{U^{\uparrow}-U^{\downarrow}}{2}\left(2\mathrm{Tr}[\hat{P}] - N_0\right), & N > \mathrm{Tr}[\hat{P}], \end{cases} \tag{6.18}$$

where $N_0 = \lfloor N \rfloor \approx N - 1$. For non-spin polarized systems $\widetilde{\Delta}_{\mathrm{xc}} = U^{\sigma} = U - J$, except at half filling. The apparently larger than might expected contribution of $\widetilde{\Delta}_{\mathrm{xc}}$ to the bandgap at subspace half filling ($N = \mathrm{Tr}[\hat{P}]$) is explained in the Bandgap Analysis section.

Accounting for the Δ^N_{xc} contribution to the quasi-particle band-gap post calculation would be a rather disappointing if necesary, given that one of the most prominent and convenient features of conventional DFT+U is that its derivative discontinuity manifests automatically in the Generalized Kohn-Sham bandgap. To solve this and restore the convenient bandgap opening in the GKS eigensystem, we have found that it is possible to 'potentialize' the mBLOR explicit derivative discontinuity, that is to represent is an additional term in the potential. As the derivative discontinuity arises when adding an additional electron to the neutral system, only the conduction band should be affected by this potential. The additional term that achieves a shift of $\widetilde{\Delta}_{\mathrm{xc}}\,[N]$ to the portion of the conduction band that projects onto the localized subspace is

$$\hat{v}^{\sigma}_{\Delta\mathrm{xc}} = \widetilde{\Delta}_{\mathrm{xc}}\,[N]\,(1-\hat{\rho})\hat{P}(1-\hat{\rho}), \tag{6.19}$$

The corresponding energy term may be found, by integration, and it is

$$\begin{aligned} E_{\Delta\mathrm{xc}} =& \frac{1}{2}\widetilde{\Delta}_{\mathrm{xc}}\left[N\right]\mathrm{Tr}\left[\left(\hat{\rho}-\frac{\hat{\rho}^2}{2}\right)\hat{P}\left(1-\hat{\rho}\right)+\left(1-\hat{\rho}\right)\hat{P}\left(\hat{\rho}-\frac{\hat{\rho}^2}{2}\right)\right] \\ =& \frac{1}{2}\widetilde{\Delta}_{\mathrm{xc}}\left[N\right]\mathrm{Tr}\left[\hat{P}\left(2\hat{\rho}-3\hat{\rho}^2+\hat{\rho}^3\right)\right]. \end{aligned} \tag{6.20}$$

This yields a vanishing correction to the total energy under the assumption that $\hat{\rho}=\hat{\rho}^2$, which holds for insulators at zero temperature as well as for molecules with non-degenerate ground states. In practice, we have found as long as the initial guess for the electronic structure exhibts a gap, it is possible to apply the $\hat{v}^{\sigma}_{\Delta\mathrm{xc}}$ self-consistently without adding the vanishing $E_{\Delta\mathrm{xc}}$ to E_{mBLOR} at all, without appreciable loss of convergence performance. Of course, for finite-temperature systems, metals, or degenerate molecules, it would be necessary to add $E_{\Delta\mathrm{xc}}$ to the energy, for consistency.

Interestingly, at subspace half-filling, the jmDFT functional also introduces an explicit derivative discontinuity, as the system is on the cusp of switching between the lower and upper versions of the jmDFT functional. Like the mBLOR functional without the correction term of Eq. 6.20, this explicit derivative discontinuity should be added a posteriori to both the GKS gap and the lowest unoccupied GKS eignevalue to evaluate the jmDFT prediction of the quasiparticle gap and electron affinity. In the idealized case where the valence and conduction band edges perfectly project onto the localized subspace defined by $\hat{P}$, the jmDFT functional introduces an explicit derivative discontinuity of $-J$.

6.10 Bandgap Analysis

To illustrate the corrective nature of the mBLOR functional, we may consider its application to a homo-nuclear spin-polarized system of transition metal atoms at half occupancy, so that each atomic d-orbital subspace is occupied by five spin up electrons and zero spin down electrons. For simplicity assume that the total subspace occupancy is infinitesimally greater than five and $U^{\uparrow}=U^{\downarrow}=U$, so that the late version of the mBLOR functional is applied and the $F^{\mathrm{late}}_{\mathrm{AMSIE}}\left[N,M\right]$ function can be neglected. Furthermore, assume that the highest occupied and lowest unoccupied KS orbitals project perfectly onto the atomic subspace. The spin-up subspace is maximally occupied so that the highest

$\Delta\epsilon_{\mathrm{LUMO}}$	$\Delta\epsilon_{\mathrm{HOMO}}$	$\widetilde{\Delta}_{\mathrm{xc}}[N]$	Δ
$\frac{1}{2}U$	$\frac{1}{2}U + 10J$	$U + 10J$	U

Table 6.4: A summary of the effect of the mBLOR corrective functional on a homo-nuclear spin polarized d-orbital system at half occupancy to first-order perturbation theory. $\Delta\epsilon_{\mathrm{LUMO}}$ and $\Delta\epsilon_{\mathrm{HOMO}}$ denote the shift to the lowest unoccupied and highest occupied GKS eigenvalues excluding the affect of the $\widetilde{\Delta}_{\mathrm{xc}}[N]$ term. The third column presents the gap opening due to the $\widetilde{\Delta}_{\mathrm{xc}}[N]$ term and finally Δ denotes the mBLOR functional's total contribution to the GKS gap.

occupied GKS eigenvalue (ϵ_{HOMO}) is spin-up and the lowest unoccupied GKS eigenvalue (ϵ_{LUMO}) is spin-down.

In this particular example, the subspace is at a vertex in the $E[N, M]$ surface and so, to first-order in perturbation theory, the mBLOR corrective functional offers no correction to the total energy. If we now turn our attention to the potential. Excluding the $\widetilde{\Delta}_{\mathrm{xc}}[N]$ term, application of the mBLOR corrective functional will, to first order perturbation theory, shift the highest occupied GKS eigenvalue by

$$\Delta\epsilon_{\mathrm{HOMOS}} = \frac{U}{2} + 10J, \tag{6.21}$$

and shift the lowest unoccupied GKS eigenvalue by

$$\Delta\epsilon_{\mathrm{LUMO}} = \frac{U}{2}. \tag{6.22}$$

This results in a closing of the GKS gap by $10J$, a very surprising result at first. However, the incorporation $\widetilde{\Delta}_{\mathrm{xc}}[N]$ term will counteract this affect precisely, by opening the gap by order $U + 10J$, resulting in an effective gap opening of U. These results are summarized in Table 6.4.

While further testing will be needed, based on the systems tested here, the mBLOR functional may offers improved bandgaps over other DFT+U-type functionals. In the case of the stretched N_2 and F_2 molecules, the mBLOR functional is found to be the only known DFT+U functional to open the bandgap appreciabily. In these systems an approximately integer number of electrons localizes on each atomic site, so we employ the derivative discontinuity correction term when applying the mBLOR functional. In the stretched N_2 system the subspace occupancy is approximately equal to 3.0 and so we let $\widetilde{\Delta}_{\mathrm{xc}}[N] = U^{\uparrow} + 6J$ and in the stretched F_2 system the subspace occupancy is

approximately equal to 5.0 and so we let $\widetilde{\Delta}_{\mathrm{xc}}[N] = U^{\uparrow}$, where we recall that $U^{\uparrow} = U^{\downarrow}$ in these spin symmetric systems. The raw DFT calculation at the PBE level yields a gap of only 0.06 eV and 0.28 eV, respectively. Application of other DFT+U-type functionals including Dudarev's 1998 Hubbard functional and the original BLOR functional fail to improve the poor PBE result. In contrast, the mBLOR functional opens the gap to 11.92 eV and 9.42 eV, respectively. These bandgaps are still smaller than the anticipated values of 14.60 and 14.02 eV, but this represents an improvement by over one-order of magnitude compared to all other DFT+U functionals tested here. The anticipated values are based on the assumption that the fundamental bandgap of the stretched N_2 and F_2 molecules are at the dissociated limit, in which case the gap will be equal to that of the isolated nitrogen or fluorine atom, respectively. These results are presented in Fig 6.8.

The failure of Dudarev's functional to improve the bandgap prediction for the stretched, symmetry unbroken N_2 and F_2 molecules compared to raw DFT is not a result unique to these two molecules, in fact Dudarev's functional will fail to open the bandgap of any symmetry unbroken, stretched, neutral, homonuclear dimer. This can be readily explained using the stretched H_2 molecule. At these large inter-nuclear separation lengths, the highest occupied and lowest unoccupied KS orbitals can be approximated as a linear combination of the hydrogenic atomic orbitals centred at the atomic sites 1 and 2,

$$|\psi_{\mathrm{KS}}\rangle = \frac{1}{\sqrt{2}}\left(|\psi_1\rangle \pm |\psi_2\rangle\right), \tag{6.23}$$

and the spin resolved KS density operator is

$$\hat{\rho}^{\sigma} = \frac{1}{2}\left(|\psi_1\rangle\langle\psi_1| + |\psi_1\rangle\langle\psi_2| + |\psi_2\rangle\langle\psi_1| + |\psi_2\rangle\langle\psi_2|\right). \tag{6.24}$$

Dudarev's functional contributes an additional term to the KS potential,

$$\hat{v}_{\mathrm{u}} = \frac{U_{\mathrm{eff}}}{2}\left(\sum_I \hat{P}_I - 2\hat{P}_I\hat{\rho}^{\sigma}\hat{P}_I\right), \tag{6.25}$$

where the summation runs over the two atomic sites and $\hat{P}_I$ is the atomic projection operator centred at site I, which in the case of an s-valence system,

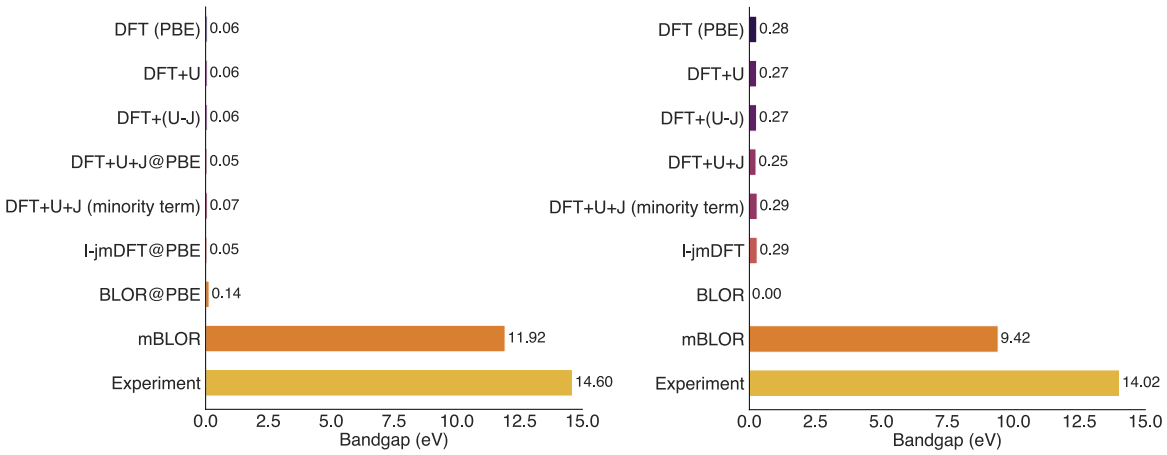

Figure 6.8: Bar chart of the predicted bandgaps of the stretched singlet N_2 and F_2 molecules at an inter-nuclear separation length of $7a_0$ and $6a_0$, respectively, using different corrective functionals [109,110,183,214,331]. The PBE exchange correlation functional [60] was employed through out. With the exception of the mBLOR functional, all bandgap predictions needed to be evaluated via non-spin polarized DFT calculations to avoid spurious spin symmetry breaking. For the N_2 molecule, the DFT+U+J, l-jmDFT and BLOR functionals were evaluated non-self consistently using the PBE density, as self-consistent application of these functionals (in a non-spin polarized DFT calculation), results in a symmetry broken ground state charge density. For the F_2 molecule, the symmetry unbroken DFT(PBE) calculation failed to converge and so the bandgap for the DFT(PBE) functional has been evaluated by extrapolating the DFT+U_{in} bandgap (for a series of values of U_{in}), back to $U_{\text{in}} = 0$. The reference experimental bandgaps for the stretched N_2 and F_2 molecules were assumed to be equal to their respective bandgaps at the dissociated limit and as such were evaluated as the difference between the reference atomic ionization potential [316] and atomic electron affinity [353] of the respective elements. One should note that the reference value for the electron affinity of the nitrogen atom is negative at -0.07 eV.

will be composed of a single atomic orbital

$$\hat{P}_I = |\psi_I\rangle \langle\psi_I| \,. \tag{6.26}$$

To first order perturbation theory, Dudarev's DFT+U correction to the highest occupied KS eigenvalue,

$$\langle\psi_{\text{HOKS}}|\hat{v}_{\text{u}}|\psi_{\text{HOKS}}\rangle = \frac{U_{\text{eff}}}{2} \sum_{IK} \frac{1}{\sqrt{2}} \langle\psi_I| \left(\sum_J \hat{P}_J - 2\hat{P}_J \hat{\rho}^\sigma \hat{P}_J \right) \frac{1}{\sqrt{2}} |\psi_K\rangle \,, \tag{6.27}$$

which through use of Eqs 6.24 & 6.26 one can readily show is equal to zero assuming the H_2 molecule is sufficiently stretched so that $\langle\psi_I|\psi_J\rangle \approx 0$, when $I \neq J$. Therefore, to first order perturbation theory, Dudarev's functional will offer no correction to the highest occupied KS eigenvalue, the same is true for the lowest unoccupied KS eigenvalue and thus Dudarev's functional cannot be used to open the KS gap of the stretched H_2 molecule. The same argument can also be applied to any symmetry unbroken, stretched, neutral, homo-nuclear p-block and d-block dimer (we exclude van der Waals molecules in this discussion), assuming the KS orbitals are quasi-degenerate at the raw DFT level and can be approximated as an equally weighted linear combination of one p/d orbital centred on each atomic site. To further highlight the failure of conventional DFT+U functional to improve the bandgap of such systems without spurious symmetry breaking, we also present the bandgap of the symmetry unbroken stretched H_2 molecule in Fig 6.9. By comparison, the mBLOR functional yields a bandgap of 10.67 eV, in close but not perfect agreement with the anticipated value of 12.84 eV.

For the stretched Ne_2^+ molecule, a non-integer number of electrons localizes on each atomic site ($N \approx 5.5$) and so in this case no derivative discontinuity correction will be applied with the mBLOR functional. The fundamental bandgap of the Ne_2^+ molecule is equal to the difference in magnitude of the ionization potential and electron affinity,

$$\Delta = \left(E[\mathrm{Ne}_2^+] - E[\mathrm{Ne}_2^{+2}]\right) - \left(E[\mathrm{Ne}_2] - E[\mathrm{Ne}_2^+]\right). \tag{6.28}$$

In the dissociated limit, each total energy term in Eq 6.28 simplifies to the sum of two isolated neon atom/ion energies,

$$\Delta = \left(E[\mathrm{Ne}] + E[\mathrm{Ne}^+] - 2E[\mathrm{Ne}^+]\right) - \left(2E[\mathrm{Ne}] - E[\mathrm{Ne}] - E[\mathrm{Ne}^+]\right) = 0. \tag{6.29}$$

Therefore the anticipated value of the bandgap of the stretched Ne_2^+ is 0 eV, assuming the fundamental bandgap of the Ne_2^+ molecule at $5a_0$ is at the dissociated limit. The raw DFT calculation at the PBE level yields a bandgap of 0.327 eV and similarly, the mBLOR functional yields a gap of 0.359 eV. These small residual gaps can be attributed to the Ne_2^+ molecule not completely reaching its dissociated limit at this inter-nuclear separation length.

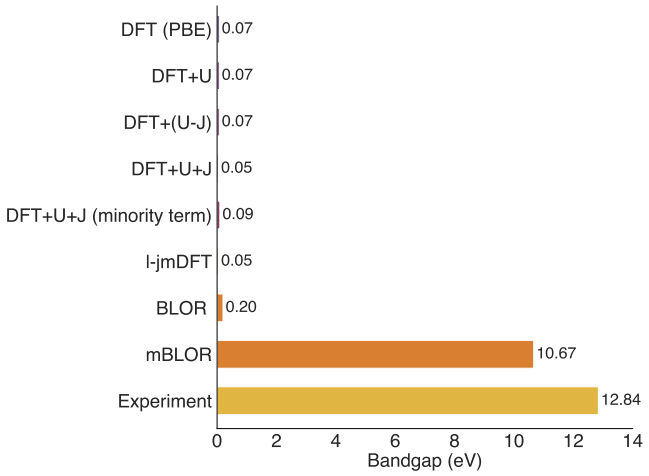

Figure 6.9: Bar chart of the predicted bandgaps of the stretched singlet H_2 molecule at an inter-nuclear separation length of $9a_0$ using different corrective functionals [109, 110, 183, 214, 331]. The raw DFT calculations were performed with the PBE exchange correlation functional [60]. The DFT+ U and DFT+$(U - J)$ relative errors were computed using Dudarev et al.'s 1998 functional with the effective Hubbard parameter (U_{eff}) set as U and $U - J$, respectively. The reference experimental bandgap for the stretched H_2 molecule was assumed to be equal to its respective bandgap at the dissociated limit and as such was evaluated as the difference between the reference atomic ionization potential [316] and atomic electron affinity [353]. All bandgap predictions were evaluated via spin-polarized DFT calculations, for this system all corrective functionals preserved spin symmetry.

6.11 Concluding Remarks

In this chapter a double-counting approximation free DFT+U-type corrective functional named mBLOR has been derived from first principles to enforce the tilted plane condition on localized, multi-orbital subspaces. This corrective functional is designed to depend only on the total subspace occupancy and magnetization, so that the many-body (inter-orbital including) self-interaction (symmetric and asymmetric) and static correlation errors are addressed in a very cost-effective and easy to implement way. This approach ensures consistency between how subspace-resolved errors are measured, via the Hubbard and Hund parameters, and how they are corrected. The formalism is readily applicable to orbital-free DFT, ensemble DFT, or many other types of electronic structure theory. The mBLOR functional was benchmarked against a variety of other DFT+U-type functionals using stretched, homo-nuclear, p-block

dimers and was the only corrective functional that consistently yielded significantly improved total energies, in this idealized and hence stringent limit for such functionals, when compared to the raw DFT (PBE) values. The mBLOR functional was also the only DFT+U functional that opened the bandgap of the stretched, spin-symmetric N_2 and F_2 molecules, as well as H_2, when its explicit derivative discontinuity is 'potentialized', a technique that may prove useful in other contexts. Much further study will be needed to understand how the mBLOR (and its progenitor BLOR) functionals perform in applied simulation, both for total-energy and GKS eigenspectrum based properties. Its effect on the potential, in particular, appears to typically be greater in general than from its BLOR or DFT+U counterparts, due to the inclusion of inter-orbital contributions, and this warrants exploration. Yet the present results are most encouraging, and in general our findings highlight the diagnostic potential of using exact results that hold for idealized yet physical test systems, as well as the promising route of building expedient correctors for approximate DFT using exact conditions such as the tilted-plane condition.

Chapter 7

Transition Metal Oxides

In testing and bench-marking the BLOR functional and its many body generalisation thus far, we have relied on small, stretched homo-nuclear s and p block molecules. These represent ideal initial test systems for our newly derived DFT+U-type functionals in part due to their low computational cost. In the large atomic separation length limit, the atomic orbitals become an ideal choice for the projection operator $\hat{P}$ and an exact value for the total energy of these systems is known based on the assumption of additivity. Furthermore, these stretched homo-nuclear molecules represent some of the most strongly correlated systems on a per electron basis. The significantly improved total energies offered by the BLOR and mBLOR functionals offer strong numerical evidence that the BLOR and mBLOR corrective energy functionals are a vast improvement over standard DFT+U-type functionals. However, the same conclusions cannot be drawn for the corresponding BLOR and mBLOR corrective potentials. This is because the inclusion of any DFT+U-type corrective potential will have little to no affect on the density and KS orbitals at these large separation lengths. Indeed, this is clearly demonstrated in chapter 5, where the relative errors in the total energies evaluated at the PBE density in Fig. 5.7 are almost identical to the relative errors in the self-consistently evaluated total energies as reported in Figs. 5.4 & 5.5. Thus, these stretched homo-nuclear molecules represent stringent tests for the corrective energy functional but not the potential, i.e., thus far we have demonstrated BLOR and mBLOR's ability to mitigate functional driven errors but not density driven errors [354–356]. To properly investigate the performance of the BLOR and mBLOR corrective potentials we must apply these corrective functionals to materials systems in the

	U_{simple}	U_{scaled}	J_{simple}	J_{scaled}
Mn	8.38	5.37	0.51	0.49
O	10.92	10.92	1.03	1.03

Table 7.1: The Hubbard corrective parameters in eV, as evaluated by Linscott et al. [242] for the manganese and oxygen sites in MnO using the minimum tracking linear response method.

bonding regime, i.e., at standard inter-atomic separation lengths.

We choose to apply the mBLOR functional to 3d-transition metal oxides, in particular MnO. This system has been selected as 3d-transition metal oxides are the archetypal systems for applying DFT+U-type corrective functionals. Indeed, Anisimov et al. [198] and Dudarev et al. [183] appealed to this class of materials systems in developing and testing their original corrective functionals. The highly localised 3d states make these systems extremely challenging to model using solely a local or semi-local XC functional. In particular MnO has been selected from the relatively large class of 3d transition metal oxides thanks to the highly accurate Diffusion Monte Carlo benchmark results that have recently been completed for this system [19, 20, 357] at great computational expense. Furthermore, U and J corrective parameters have already been evaluated by Linscott et al. [242], using the minimum tracking linear response method.

7.1 Computational Details

The U and J parameters for MnO are readily available from a previous study by Linscott et al. [242] and for completeness are reported in Table 7.1. A large $33.6 \times 33.6 \times 33.6$ a_0^3 simulation cell containing 512 atoms was used to avoid the perturbed atom from interacting with its periodic replica and also to achieve effective k-point sampling using ONETEP. The PBE XC functional was employed with a kinetic energy cutoff of 1,030 eV. The convergence threshold of the root-mean-square gradient of the NGWFs was set at 2×10^{-6} Ha$a_0^{3/2}$ and the electronic energy tolerance was set at 3.675×10^{-6} Ha/atom. 10 NGWFs were employed per manganese atom and 4 NGWFs were employed per oxygen atom, all with an 11 a_0 cutoff. The ensemble DFT algorithm was enabled with a small smearing width of 3.675×10^{-5} Ha. Experimental lattice geometries were used

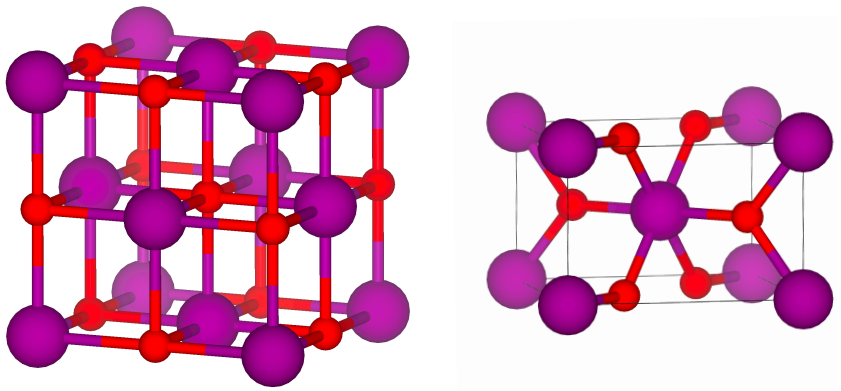

Figure 7.1: Units cells of rocksalt MnO and tetragonal rutile-type MnO_2 with manganese and oxygen atoms colored purple and red respectively, plotted using the VESTA [344] software.

for the rocksalt MnO [358]. The MnO structure has an anti-ferromagnetically ordered ground states at the bare DFT(PBE) level.

7.2 Flat Plane Switching

Self-consistent application of the mBLOR functional to MnO suffered from convergence issues primarily due to the MSIE-term in the mBLOR corrective potential. Assuming that $U^{\uparrow} = U^{\downarrow} = U$, the MSIE-term in the corrective potential takes the form,

$$\hat{v}_{\text{MSIE}} = \frac{U}{2}\left(1 - 2N + 2N_0\right)\hat{P}. \tag{7.1}$$

For any value of $N > N_0 + \frac{1}{2}$, this term in the corrective potential will be negative and will thus promote an increase in subspace occupancy. If the integer value of N_0 is selected at the start of the calculation based on $\lfloor N_{\text{DFT}} \rfloor$, where N_{DFT} is the subspace occupancy at the bare DFT level, a positive feedback loop can readily ensue, spuriously driving the subspace to full occupancy. Similarly, if the initial value of $N < N_0 + \frac{1}{2}$, an analogous feedback loop can readily ensue with the subspace spuriously driven to zero occupancy. In many electronic systems of interest, the Hund's J parameter can often be one order of magnitude smaller than the Hubbard U parameter and as such, the MSIE-term in the mBLOR corrective potential will often dominate over the SCE-term, which will exacerbate this convergence issue.

Although, it is yet to be tested, it is expected that if the value of N_0 was instead allowed to change dynamically over the course of the calculation so that N_0 always remains equal to $\lfloor N \rfloor$, a similar convergence issue is expected to occur, with the value of N_0 oscillating between two consecutive integer values, thus preventing the calculation from converging. We coin this convergence issue, 'flat plane switching' as it is caused by the subspace switching between planes on the subspace $E[N, M]$ energy surface over the course of the calculation, thus requiring different values of N_0.

In order to ameliorate this convergence issue, an additional term must be added to the corrective functional. However, this additional term should minimally affect the total energy and bandgap. Assuming that the total subspace occupancy changes minimally upon application of the mBLOR corrective functional, an additional energy term that depends on the difference between the subspace occupancy N^I and the subspace occupancy at the bare DFT level N^I_{DFT} will yield a negligible contribution to the total energy. Thus, the additional energy term will take the form,

$$E^{\mathrm{add}} = C \sum_I (N^I - N^I_{\mathrm{DFT}}), \tag{7.2}$$

where C is a constant yet to be determined and the summation runs over all atomic sites I. The corresponding term in the corrective potential,

$$v^{\mathrm{add}} = C \sum_I \hat{P}_I, \tag{7.3}$$

will yield the same bandgap prediction as the standard mBLOR functional from chapter 6, assuming that the conduction and valence bands both perfectly project onto the subspace projection operator $\hat{P}_I$. In order to counteract the relatively large strength of the MSIE-term in the corrective potential and thus hopefully avoid the spurious feedback loop discussed earlier, we set the constant C to minus the average value, across all atomic sites, of this MSIE term based on the bare DFT subspace occupancy,

$$C = -\frac{1}{N_{\mathrm{sites}}} \sum_I \frac{U^I}{2} \left(1 - 2N^I_{\mathrm{DFT}} + 2N^I_0\right). \tag{7.4}$$

Promisingly, inclusion of this additional term within the mBLOR corrective

potential allowed the MnO calculation to converge, while the corresponding energy term of Eq. 7.2, offered a negligible contribution to the total energy of 0.02 eV per formula unit. With the convergence issue resolved at least for the MnO system of interest, we are now in a position to evaluate the total energies and bandgaps of manganese oxide and compare the results to other values in the literature.

7.3 MnO Energy of Cohesion

In order to asses the reliability of the energies evaluated using the mBLOR corrective functional for transition metal oxides, we use mBLOR to compute the energy of cohesion of MnO. The energy of cohesion is defined as the energy required to separate a solid into its constituent atoms,

$$E_{\text{cohesion}}[\text{MnO}] = E_{\text{bulk}}[\text{MnO}] - E_{\text{atom}}[\text{Mn}] - E_{\text{atom}}[\text{O}], \tag{7.5}$$

where $E_{\text{bulk}}[\text{MnO}]$ is the total energy per formula unit of solid state MnO and $E_{\text{atom}}[\text{Mn}]$ & $E_{\text{atom}}[\text{O}]$ are the reference atom energies. In this study, the energy of cohesion of MnO has been evaluated using the bare DFT(PBE), DFT+U and mBLOR functionals, where DFT+U refers to the standard DFT+U functional of Dudarev et al. [183] with effective Hubbard U parameter $U_{\text{eff}} = U$ applied to both the Mn and O atomic sites. The mBLOR corrective functional has also been applied to both the Mn and O atomic sites including the derivative discontinuity correction term of Eq. 6.19 and the stabilisation term of Eq. 7.3. The subspace occupancy at the bare DFT(PBE) level (N^I_{DFT}) is equal to 5.645 and 5.600 at the manganese and oxygen sites respectively, thus in both cases the value of N_0 was set at 5.0 for application of the mBLOR functional. Based on these values of N^I_{DFT}, the stabilisation constant C was evaluated through the use of Eq. 7.4, as 0.848 eV. At both atomic sites, $\text{Tr}[\hat{N}] > \text{Tr}[\hat{P}]$ and thus in both cases the late version of the mBLOR corrective functional was applied. Furthermore, at both atomic sites $\widetilde{\Delta}_{\text{xc}} = U^{\uparrow} = U_{\text{scaled}} - J_{\text{scaled}}$.

The value of the U and J parameters for MnO are available from the study by Linscott et al. [242]. However, no values are reported for $U^{\uparrow}$ and $U^{\downarrow}$ and hence these will need to be approximated. In the case of a non-spin polarised

system,

$$U^{\uparrow} = U^{\downarrow} = U_{\text{simple}} - J_{\text{simple}} = U_{\text{scaled}} - J_{\text{scaled}}, \tag{7.6}$$

which thus offers two possible approximations for the spin resolved Hubbard U parameters using either the simple 2×2 or the scaled 2×2 U and J values. In the case of a fully spin polarised system, of the three corrective parameters used in the mBLOR functional ($U^{\uparrow}$, $U^{\downarrow}$ and J), the value of the mBLOR energy correction will, to first-order perturbation theory, depend only on the value of U^{σ}, where σ is the majority spin channel for subspaces at less than half occupancy and the minority spin channel for subspaces at more than half occupancy.

Unlike U_{simple} and J_{simple}, the scaled corrective parameters are defined through the use of rescaling factors λ_U and λ_J,

$$U_{\text{scaled}} = \frac{\lambda_U(f^{\uparrow\uparrow} + f^{\downarrow\uparrow}) + f^{\uparrow\downarrow} + f^{\downarrow\downarrow}}{2\lambda_U + 2} \quad \& \quad J_{\text{scaled}} = \frac{\lambda_J(f^{\uparrow\uparrow} - f^{\downarrow\uparrow}) + f^{\uparrow\downarrow} - f^{\downarrow\downarrow}}{2 - 2\lambda_J}. \tag{7.7}$$

In the idealised case of a fully spin polarised subspace at less than half occupancy, where the minority spin bands of the system are extremely far from the majority spin valence and conduction band edges, $\lambda_U, \lambda_J \to \infty$. This will ensure that $U_{\text{scaled}} - J_{\text{scaled}} \approx U^{\uparrow}$, which for this system is the spin-resolved Hubbard U parameter of importance to the mBLOR energy expression. An analogous argument holds for subspaces at more than half occupancy so that $U_{\text{scaled}} - J_{\text{scaled}} \approx U^{\downarrow}$, which again in this case is the spin-resolved Hubbard U parameter of importance to the mBLOR energy expression. Therefore, $U^{\uparrow} = U^{\downarrow} = U_{\text{scaled}} - J_{\text{scaled}}$ is a suitable approximation in both the non-spin polarised and fully spin polarised limits and is the option chosen for applying the mBLOR functional to MnO. This approximation also allows the asymmetric-MSIE term of the mBLOR functional to be neglected. For consistency, we also used the scaled 2×2 value of the Hund's J parameters as opposed to the simple 2×2 values, however as shown in table 7.1, the difference between these two options is negligible.

In Fig. 7.2, we present the energy of cohesion of MnO evaluated using a variety of methods. As shown in Fig. 7.2 the bare DFT(PBE) functional already yields an energy of cohesion for MnO in close agreement with the Diffusion Monte Carlo reference value [20]. This makes the energy of cohesion of MnO

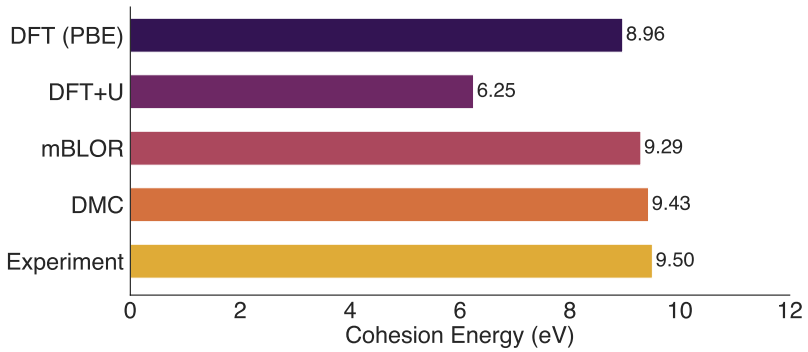

Figure 7.2: Energy of cohesion of MnO per formula unit, evaluated using the bare DFT(PBE), DFT+U and mBLOR functionals. Reference Diffusion Monte Carlo (DMC) [20] and experimental values [365] are also given.

an extremely challenging test case for any DFT+U-type functional, as any error in the corrective functional will likely worsen the predicted value for the energy of cohesion. Indeed, as shown in Fig. 7.2 application of Dudarev's DFT+U functional (using the scaled Hubbard U parameter) significantly worsens the predicted energy of cohesion compared to the bare DFT(PBE) value. By contrast, the mBLOR corrective functional yields a energy of cohesion of 9.29 eV, in close agreement to the Diffusion Monte Carlo reference value [20] of 9.43 eV. Thus for the MnO system, the mBLOR corrective functional offers an improved energy of cohesion over the already satisfactory bare DFT(PBE) value. If this promising energetic result for the mBLOR corrective functional is repeated across other transition metal oxide systems, this novel DFT+U functional could offer a reliable yet computationally inexpensive technique of evaluating a suite of physical and chemical properties of transition metal oxide systems that depend on the total energy, such as redox potentials in Li-ion battery cathodes [345,359,360], surface formation energies for photo-catalysts [352, 361, 362] and crystallographic structures of high T_c superconductors in their normal state [363, 364].

7.4 MnO Fundamental Bandgap

In Fig. 7.3 the bandgap of MnO as evaluated using DFT(PBE), DFT+U and the mBLOR functionals is presented. Reference DMC [20] and experimental [366] values are also reported. The reported DMC value is a prediction of the fundamental (quasi-particle) bandgap for the system, which was evaluated through the use of charged simulation cells. The reference experimental value

is a measure of the optical bandgap, which thus includes exciton binding effects. Standard KS and GKS calculations evaluate the fundamental bandgap as opposed to the opical gap. However, the small difference between the experimental and DMC value of 0.08 eV suggest that exciton binding effects are small for this system. The bare DFT calculation using the PBE [60] approximation significantly underestimates the bandgap of the system yielding a value of only 1.35 eV. This underestimation was expected, the bandgap problem of local and semi-local XC functionals has already been well documented in the literature and has been discussed at length in the background theory section of this thesis. Application of Dudarev's DFT+U corrective functional significantly improves on the bare DFT result yielding a value of 4.34 eV, albeit this is slightly larger than the reference DMC and experimental values. Resolving the bandgap problem of (semi-)local XC functionals in transition metal oxide systems at low computational cost is one of the hallmarks of the DFT+U method which is clearly corroborated by this result.

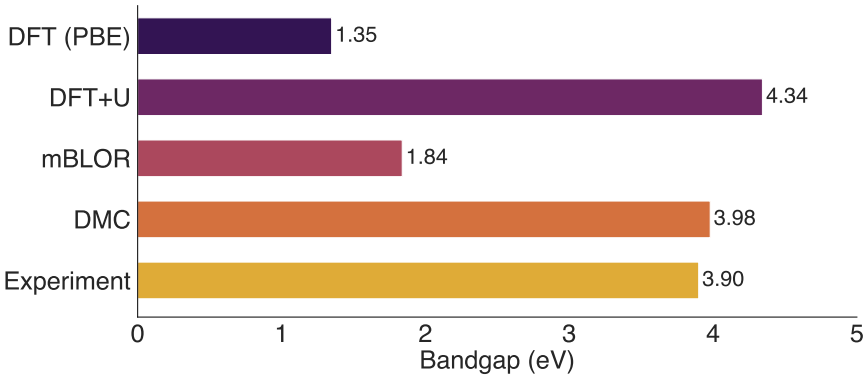

Figure 7.3: Bandgap of MnO evaluated using the bare DFT(PBE), DFT+U and mBLOR functionals. Reference Diffusion Monte Carlo (DMC) [20] and experimental values [366] are also given.

Unfortunately, the mBLOR corrective functional with the derivative discontinuity correction term of Eq. 6.19, fails to sufficiently open the bandgap of the MnO system. The predicted bandgap of 1.84 eV is less than half the value of the reference DMC result and only 0.49 eV larger than the bare DFT(PBE) bandgap. The failure of the mBLOR functional to sufficiently open the bandgap of the MnO system can be readily understood through the Projected Density of States (PDOS) plots in Fig. 7.4.

In the PDOS plot at the bare DFT(PBE) level, the valence and conduction

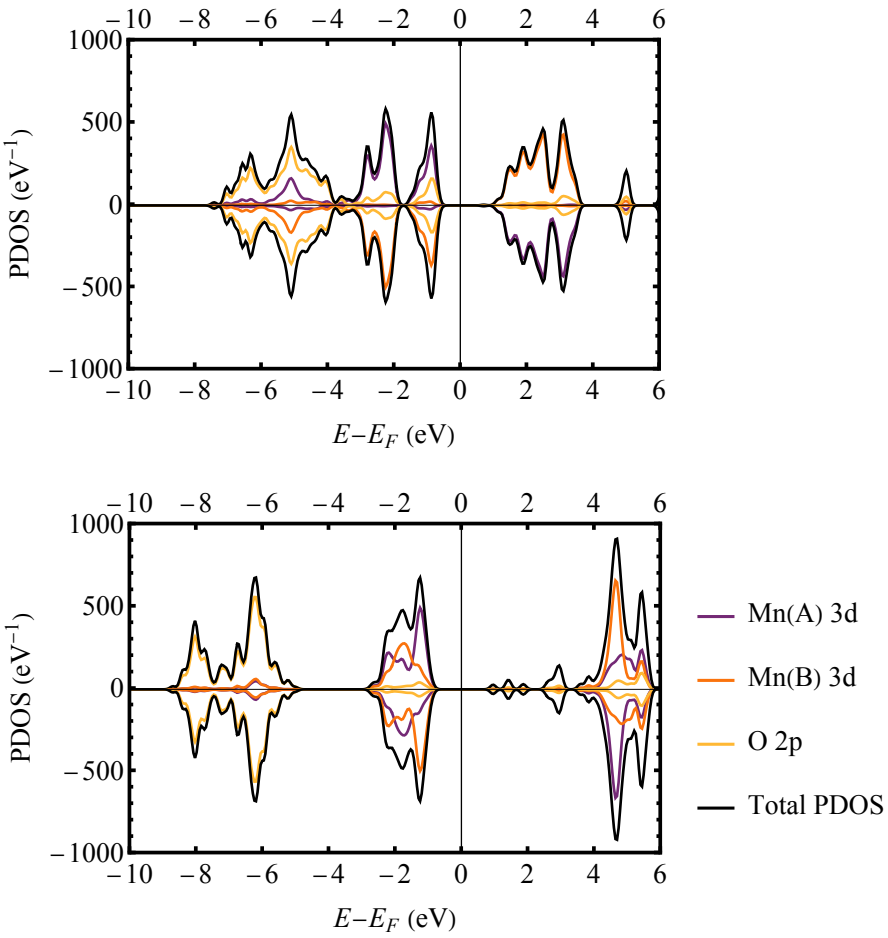

Figure 7.4: The Projected Density of States (PDOS) of MnO at the bare DFT(PBE) level (top) and with application of the mBLOR corrective functional (bottom). The majority spin up and majority spin down manganese atoms are labelled Mn(A) and Mn(B) respectively. As is convention, the projected spin up and projected spin down density of states are taken as positive and negative.

band edges are primarily of Mn-3d character, thus suggesting that the MnO system is a Mott-Hubbard type insulator. Promisingly, the mBLOR corrective functional opens the gap between these bands of Mn-3d character, yielding a d-d transition energy of approximately 4 eV, in close agreement to the experimental and DMC bandgaps. However, application of the mBLOR functional changes the character of the conduction band edge. The conduction band edge, is now predominantly Mn-4s and O-2p in character, while the valence band edge remains predominantly Mn-3d in character. It is this energy difference between the conduction band edge of unexpected atomic character and valence edge, i.e. the bandgap, which remains low at 1.84 eV. A possible solution to this problem

worthy of further research is the application of the mBLOR corrective functional to the Mn-4s states in addition to the Mn-3d and O-2p states. However, this will require evaluation of U and J parameters for the Mn-4s states and modification of the ONETEP code in order to apply the DFT+U method to multiple angular momentum channels on the same atomic site.

7.5 Concluding Remarks

This preliminary test of the mBLOR corrective functional on a transition metal oxide system yields some quite promising results for both the cohesive energy and the d-d transition energy, however a number of unanswered questions remain. Can application of the mBLOR functional to the Mn-4s states yield a bandgap for the MnO system in agreement with the d-d transition energy and DMC reference values? Does the stabilisation term of Eq. 7.3 resolve the flat plane switching convergence issue across a broad class of materials or is MnO an outlier? Does our current corrective functional yield cohesive energy values in close agreement with DMC and experimental reference results for all transition metal oxide systems or again is MnO an exception? These questions are subject to ongoing research as we attempt to develop a DFT+U functional that broadly improves on the current state of the art. Designing a corrective functional that yields excellent energies of cohesion while also resolving the bandgap problem of (semi-)local XC functionals will be key to the method's wide scale adoption.

Chapter 8

Discussion and Conclusion

For the benefit of both the examiners and other interested readers, I have gone to significant lengths to write this thesis in a comprehensive but also succinct manner. I hope that it will stand as a testament to my great enthusiasm for electronic structure theory, which I have developed over the course of my PhD studies. Furthermore, I sincerely hope that the research work expounded in this thesis will act as a catalyst for future theoretical and computational developments in the field. In the following two sections I will finally present a synopsis of the work completed in this thesis as well as a brief discussion of the vast number of avenues for future research. I hope you have enjoyed looking at this thesis as much as I have enjoyed completing the work.

8.1 Synopsis

We began our discussion in chapter two by introducing the numerous non-equivalent formulations of Density Functional Theory as well as the practical realization of these theories via the Thomas Fermi and Kohn Sham methods. We highlighted several approaches for approximating the exchange correlation functional, which is necessary for all practical Kohn Sham calculations. However, we emphasised that standard local and semi-local exchange correlation approximations suffer from many electron self interaction error, static correlation error and the bandgap problem. We introduced the DFT+U method as a technique to treat some of the aforementioned pervasive issues of (semi-)local XC functionals. A detailed overview of the DFT+U functionals that have been developed over the last thirty years is then given and methods of evaluating

the Hubbard corrective parameters for use in practical DFT+U calculations is also presented.

In chapter three the convexity condition is derived using the infinite-separation limit technique. This long assumed but never before proven exact condition of the exact exchange correlation functional lifts a standing assumption in the proof of the piecewise linearity condition with respect to electron count, another exact condition which is widely employed in DFT, including to motivate the mathematical form of Hubbard type corrective functionals.

In chapter four the piecewise linearity condition for magnetization is derived using the infinite separation limit technique. The piecewise linearity conditions with respect to electron count and magnetization are then combined and generalized to give the tilted plane condition. We also found that many standard density functional approximations violate these exact conditions.

In chapter five we derived a new DFT+U-type functional, which is uniquely defined to enforce the flat plane condition on each orbital of a localized subspace. The new corrective functional is shown to yield promising energetic results for the stretched s-block, homo-nuclear molecules. By contrast, we showed that standard DFT+U-type functionals significantly worsen the bare DFT(PBE) total energies for the same systems.

In chapter six, the many-body generalisation of the BLOR functional, known as mBLOR was derived. It is the unique functional that enforces the flat plane condition once on an entire multi-orbital subspace. We showed that the mBLOR functional significantly improved the bare DFT(PBE) total energies for the stretched p-block, homo-nuclear dimers, while standard DFT+U functionals yielded large eneregtic errors for the same systems. Unlike standard DFT+U functionals, mBLOR is defined piecewise with respect to subspace occupancy N, which results in explicit derivative discontinuities with respect to N. A derivative discontinuity correction term was added to the mBLOR functional to incorporate this contribution to the fundamental bandgap explicitly within the Generalized Kohn Sham gap. We found that the derivative discontinuity corrected mBLOR functional is the only DFT+U functional to open the bandgap of the stretched, spin symmetry unbroken, homo-nuclear dimers.

Finally, in chapter seven, we tested the mBLOR functional on solid-state manganese oxide. The mBLOR functional yielded an energy of cohesion in close agreement with the reference Diffusion Monte Carlo and experimental

values. However, the mBLOR functional yielded a severe underestimation of the MnO bandgap, due to the change in atomic character of the conduction band edge. Treatment of the Mn-4s states in the hope of yielding a bandgap in agreement with the current d-d transition energy remains a topic for future research.

8.2 Future Work

The research work completed in this thesis has opened many avenues for future work. In chapter four, the exact total energy surface as a function of particle count N and magnetization M was rigorously derived. However, Gunnarsson and Lundqvist [39] in their seminal work, extended Density Functional Theory beyond ground state total energies and showed that within DFT, one can find the lowest possible energy of a system for every symmetry. In the case of an isolated atom, in the absence of spin-orbit coupling, its electronic state can be specified by the complete set of commuting observables $|S, M_S, L, M_L\rangle$, where S & L are the spin and orbital quantum numbers and M_S & M_L are their respective z-axis components. Excluding M_S, which is simply half the value of the magnetization M, the $E_v[N, S, M_S, L, M_L]$ surface within co-linear spin DFT has yet to be fully explored. In the case of the $E_v[N, S, M_S, L, M_L]$ surface, a generalized analogue of the tilted plane condition may exist, which standard density functional approximations are highly unlikely to satisfy. Correcting for such errors within localized subspaces will require a generalization of the BLOR and mBLOR corrective functionals as well as the development of new methods for computing the corresponding corrective parameters.

A further avenue for future research is the development and testing of the mBLOR functional in systems with strong crystal and ligand field splittings. In such cases, enforcing the flat plane condition of the isolated atom may not be the ideal choice due to the large energy level splitting between d-orbitals, which would be degenerate in the case of an isolated atom. Indeed in Fig. 4.7 of Chapter 4, we showed that the $E[N, M]$ surface of a low spin d-orbital subspace can exhibit a variety of crystal field dependent structures, many of which are significantly different to that of the truly isolated atom. This suggests that it may be necessary to develop state and structure dependent analogues of the mBLOR functional. Indeed, in the case of a low-spin d-orbital system with

an octahedral or tetrahedral field, the flat plane $E[N, M]$ energy surfaces from Fig. 4.7 suggest that the SCE term of the mBLOR functional should take the form,

$$E^{\mathrm{SCE}}_{\mathrm{mBLOR}}[N, M, D] = \begin{cases} \frac{J}{2}\left(M^2 - N^2\right), & N \leq D, \\ \frac{J}{2}\left(M^2 - (N-2D)^2\right), & D < N \leq D + 2l + 1, \\ \frac{J}{2}\left(M^2 - (N-2(2l+1))^2\right), & \mathrm{D} + 2l + 1 < N, \end{cases} \tag{8.1}$$

where D is the degeneracy of the subset of d-orbitals of lower energy, which is specified by the Mulliken symbol of the respective irreducible representation of the point group. By contrast, the symmetric-MSIE term, where we approximate that $U^{\uparrow} = U^{\downarrow} = U$, will remain unchanged as

$$E^{\mathrm{MSIE}}_{\mathrm{mBLOR}}[N, M] = \frac{U}{2}\left((N - N_0) - (N - N_0)^2\right). \tag{8.2}$$

The modified SCE term ensures that the mBLOR functional offers zero energetic correction at the vertices of the $E[N, M]$ energy surface for a low spin d-orbital subspace in an octahedral or tetrahedral field, the location of which differ from those in a spherical crystal field. Interestingly, this modified mBLOR functional will result in a smaller energetic contribution from the SCE term for all subspaces where $D < N \leq D + 2l + 1$. For low spin systems, the corresponding SCE term from the standard mBLOR functional will yield a particularly large energetic contribution for values of subspace occupancy within this range. Whether such a state and structure dependent version of the mBLOR functional can yield improved results is certainly worth investigating.

In the short-term however, attention must be given to further preliminary testing of the standard mBLOR functional on transition metal oxides, in particular the treatment of 4s states in MnO as well as the testing of this corrective functional on other transition metal oxide systems of interest, with MnO_2 and $LiMnO_2$ being the primary initial targets. Additional terms and improvements to the mBLOR functional may need to be made in order to avoid the flat plane switching convergence issue and to further improve the bandgap predictions.

Upon completion of the these preliminary tests, in the longer term the mBLOR functional will need wide scale testing using a large and diverse set of transition metal compounds. A wide variety of material properties such as

bandgaps, cohesive energies, magnetic moments, lattice constants, bulk moduli, formation energies, polymorph energy differences, ground state magnetic orderings and molecular spin state splittings will need to be evaluated using the mBLOR functional and compared to reference values. The relative scarcity of reliable bench-marking data for solid state systems compared to the well developed molecular bench-marking databases will complicate matters. Where necessary, Diffusion Monte Carlo reference data may need to be generated for the specific purpose of bench-marking the newly derived DFT+U functional.

If upon completion of the rigorous bench-marking, the DFT+U functional's results show close agreement to DMC and experimental reference data, the utility of the mBLOR functional could be showcased through the prediction of strongly correlated transition metal compounds with technologically important applications, including lithium and sodium ion battery cathodes, inorganic solid state electrolytes, high-temperature superconducting oxides in their normal state, heterogenous catalysts for hydrogen production and exotic magnetic materials as well as scientifically important metallo-enzymes and proteins. For these more targeted systems, additional properties of particular importance such as ion insertion energies, defect formation energies, phase diagrams, reaction barrier heights and surface formation and adsorption energies could be evaluated depending of course on which properties of the compound are of particular interest.

Chapter 9

Appendices

9.1 Alternative Derivation of BLOR

To derive the corrective functional, we first consider a single orbital embedded within a material, which can be occupied by up to two electrons of opposite spin. We use the same definition of U^σ and J as given by Eqs. 9.1 and 9.2 in the main text, where the spin resolved HUbbard U parameter us given as:

$$U^\sigma = \frac{1}{2}\left(\frac{\partial^2 E_{\mathrm{Hxc}}^{\mathrm{approx}}}{\partial (n^\sigma)^2}\right)_{n^{-\sigma}}, \tag{9.1}$$

and Hund's J parameter is given as:

$$J = -\frac{1}{2}\left(\frac{\partial^2 E_{\mathrm{Hxc}}^{\mathrm{approx}}}{\partial (M)^2}\right)_{N}, \tag{9.2}$$

where n^σ, N and M are the spin-resolved subspace occupancy, the subspace electron count and the subspace magnetisation, respectively. For the purposes of this work we assume that U^σ and J are subspace specific constants and leave considerations of higher order partial derivatives to future studies.

Using these definitions, we can now derive the correction $[E_u(n^\uparrow = 1, n^\downarrow)]$ to the Hartree-exchange-correlation energy along the maximally spin up polarised line (along the edge of the diamond), in the upper half plane. The exact Hartree-exchange-correlation energy $E_{\mathrm{Hxc}}^{\mathrm{exact}}(n^\uparrow, n^\downarrow)$ should follow a linear curve along the maximally spin polarised line:

$$E_{\mathrm{Hxc}}^{\mathrm{exact}}(n^\uparrow = 1, n^\downarrow) = [E_{\mathrm{Hxc}}^{\mathrm{exact}}(1,1)]n^\downarrow. \tag{9.3}$$

Meanwhile, the approximate Hxc energy will follow a quadratic curve along the maximally spin polarised line. It will have curvature $-U^{\downarrow}$ and its endpoints will be equal to $E_{\text{Hxc}}^{\text{approx}}(1,0)$ and $E_{\text{Hxc}}^{\text{approx}}(1,1)$, so that the approximate Hxc curve is given as:

$$E_{\text{Hxc}}^{\text{approx}} = \left[E_{\text{Hxc}}^{\text{approx}}(1,1) - E_{\text{Hxc}}^{\text{approx}}(1,0) - \frac{U^{\downarrow}}{2}\right] n^{\downarrow} + \frac{U^{\downarrow}}{2}(n^{\downarrow})^2 + E_{\text{Hxc}}^{\text{approx}}(1,0). \tag{9.4}$$

Now, assuming that $E_{\text{Hxc}}^{\text{approx}}$ yields a close to exact result at certain integer $n^{\uparrow}$ & $n^{\downarrow}$ occupancies, we can approximate that:

$$E_{\text{Hxc}}^{\text{exact}}(1,1) - E_{\text{Hxc}}^{\text{approx}}(1,1) \approx 0. \tag{9.5}$$

Similarly, at $n^{\uparrow} = 1, n^{\downarrow} = 0$ we can approximate that:

$$E_{\text{Hxc}}^{\text{approx}}(1,0) \approx E_{\text{Hxc}}^{\text{exact}}(1,0) = 0. \tag{9.6}$$

Hence, the correction to E_{Hxc} along the maximally spin polarised line becomes:

$$E_u(n^{\uparrow} = 1, n^{\downarrow}) = E_{\text{Hxc}}^{\text{exact}} - E_{\text{Hxc}}^{\text{approx}} = \frac{U^{\downarrow}}{2}\left[n^{\downarrow} - (n^{\downarrow})^2\right]. \tag{9.7}$$

Along the maximally spin polarised line in the upper half plane, $n^{\uparrow} = 1$ and $n^{\downarrow} = N - 1$, where N is the total subspace occupancy. Hence, we may re-write that:

$$E_u(n^{\uparrow} = 1, n^{\downarrow}) = \frac{U^{\downarrow}}{2}\left[(N-1) - (N-1)^2\right]. \tag{9.8}$$

We now wish to find an expression for $E_u(n^{\uparrow}, n^{\downarrow})$ at an arbitrary point in the upper half plane. To evaluate this we can define $\Delta_m(n^{\uparrow}, n^{\downarrow})$ as:

$$\Delta_m(n^{\uparrow}, n^{\downarrow}) = E_u(n^{\uparrow}, n^{\downarrow}) - E_u(1, n^{\uparrow} + n^{\downarrow} - 1). \tag{9.9}$$

Here Δ_m is the change in the energetic correction upon moving at constant total occupancy from the point $(1, N-1)$ to the point $(n^{\uparrow}, n^{\downarrow})$, where $N = n^{\uparrow} + n^{\downarrow}$. The exact Hxc energy should be constant as one varies M keeping N fixed, at this stage of our analysis. However, $E_{\text{Hxc}}^{\text{approx}}$ will exhibit a spurious curvature of

$-J$. Unlike Eq. 9.8, there will be no linear term in this case due to the spin symmetry of the system. Hence, the change in the energetic correction is given by:

$$\Delta_m = \frac{J}{2}M^2 - \frac{J}{2}M_{\max}^2, \tag{9.10}$$

where $M_{\max}$ is the subspace magnetisation along the maximally spin polarised line in the upper half-plane, $M_{\max} = 2 - N$. The constant $\frac{J}{2}M_{\max}^2$ term ensures that $\Delta_m = 0$ along the maximally spin polarised line, where SCE vanishes. Therefore Eq. 9.10 becomes:

$$\Delta_m = \frac{J}{2}\Big[M^2 - (N-2)^2\Big]. \tag{9.11}$$

We may choose to make the further approximation that $U^{\uparrow} = U^{\downarrow} = U$, in which case we denote the total corrective energy as E_u^{sym}. Noting that analogous expressions hold for the corrective functional in the lower half plane, the total corrective functional for a two-electron subspace is given by:

$$E_u^{\text{sym}} = \begin{cases} \dfrac{U}{2}[N - N^2] & + \quad \dfrac{J}{2}[M^2 - N^2], & N \leq 1. \\ \dfrac{U}{2}[(N-1) - (N-1)^2] & + \quad \dfrac{J}{2}[M^2 - (N-2)^2], & N > 1. \end{cases} \tag{9.12}$$

The previously derived functional assumes that the interaction between the localized electrons and the surrounding environment can be approximated by an effective electric field. However, an effective magnetic field may also be acting on the subspace embedded in the material environment. In this case, the state with one spin up electron is no longer degenerate to the state with one spin down electron. The constancy condition with respect to magnetisation becomes a linearity condition:

$$E[N, M] = \omega E[N, M_i] + (1 - \omega)E[N, M_j], \tag{9.13}$$

where the magnetisation M is given by:

$$M = \omega M_i + (1 - \omega)M_j, \quad M_i, M_j \in \mathbb{Z} \quad \& \quad 0 \leq \omega \leq 1. \tag{9.14}$$

The piecewise linearity condition with respect to magnetisation has consequences for the derivation of the corrective functional. In such cases one cer-

tainly cannot assume that $U^{\uparrow} = U^{\downarrow}$. The corrective functional along the maximally spin up polarised line in the upper half plane is still given by Eq. 9.8. Meanwhile, the corrective functional along the maximally spin down polarised line, in the upper-half plane, is given by:

$$E_u(n^{\uparrow}, n^{\downarrow} = 1) = \frac{U^{\uparrow}}{2}\Big[(N-1) - (N-1)^2\Big]. \tag{9.15}$$

Due to the presence of the magnetic field, the spin symmetry of the system is broken, and $E[N, M = N-1] \neq E[N, M = 1-N]$. Hence, Δ_m in this case will have a linear term in M. The linear term in M ensures that Δ_m continues to give zero contribution to E_u along the maximally spin-down polarised line, while it gives a non-zero contribution along the maximally spin-up polarised line so that the total corrective functional reduces to Eq. 9.8 when $n^{\uparrow} = 1$. Hence, in the presence of an effective magnetic field, Eq. 9.11 becomes:

$$\Delta_m = \frac{J}{2}\Big[M^2 - (N-2)^2\Big] + \frac{U^{\downarrow} - U^{\uparrow}}{2}\Big[(N-1) - (N-1)^2\Big] \cdot \frac{1}{2}\Big(1 + \frac{M}{2-N}\Big). \tag{9.16}$$

Ultimately, the BLOR functional for a single-orbital subspace is given by the sum of Eqs. 9.15 and 9.16, which after some rearrangement gives:

$$E^{\text{single}}_{\text{BLOR}} = \begin{cases} \dfrac{U^{\uparrow} + U^{\downarrow}}{4}\text{Tr}[N - N^2] \\ \quad + \dfrac{J}{2}\text{Tr}[M^2 - N^2] + \dfrac{U^{\uparrow} - U^{\downarrow}}{4}\text{Tr}[M - NM], & \text{Tr}[\hat{N}] \leq \text{Tr}[\hat{P}], \\ \\ \dfrac{U^{\uparrow} + U^{\downarrow}}{4}\text{Tr}[(N-1) - (N-1)^2] \\ \quad + \dfrac{J}{2}\text{Tr}[M^2 - (N-2)^2] + \dfrac{U^{\uparrow} - U^{\downarrow}}{4}\text{Tr}[M - NM], & \text{Tr}[\hat{N}] > \text{Tr}[\hat{P}]. \end{cases} \tag{9.17}$$

We now wish to extend this technique to multi-orbital subspaces such as the five d-orbitals at a transition metal site. The naïve approach would be to separately apply the corrective functional given by Eq. 9.17 to each orbital with electron count N_i and magnetisation M_i. Assuming the occupancy of each orbital does

not exceed one, the corrective functional would take the following form:

$$E_{\mathrm{BLOR}}^{\mathrm{naive}} = \sum_i \frac{U_i^{\uparrow} + U_i^{\downarrow}}{4}\left[N_i - N_i^2\right] + \frac{J_i}{2}\left[M_i^2 - N_i^2\right] + \frac{U_i^{\uparrow} - U_i^{\downarrow}}{4}\left[M_i - N_i M_i\right]. \quad (9.18)$$

However, such a corrective functional would not be rotationally invariant, or more generally invariant under unitary transformations among the basis orbitals. To counteract this problem, we firstly assume that the deviation of each orbital from the flat plane condition can be treated using a subspace-averaged corrective parameters. Secondly, we assume that the spin up and spin down subspace occupancy matrices have the same eigenbasis. We can then let the orbitals be equal to the eigenvectors of the susbspace occupancy matrix. This allows us to express the multi-orbital corrective functional in a rotationally invariant form as:

$$E_{\mathrm{BLOR}} = \begin{cases} \dfrac{U^{\uparrow} + U^{\downarrow}}{4}\mathrm{Tr}[\hat{N} - \hat{N}^2] & \\ \quad + \dfrac{J}{2}\mathrm{Tr}[\hat{M}^2 - \hat{N}^2] + \dfrac{U^{\uparrow} - U^{\downarrow}}{4}\mathrm{Tr}[\hat{M} - \hat{N}\hat{M}], & \mathrm{Tr}[\hat{N}] \leq \mathrm{Tr}[\hat{P}], \\ & \\ \dfrac{U^{\uparrow} + U^{\downarrow}}{4}\mathrm{Tr}[(\hat{N} - \hat{P}) - (\hat{N} - \hat{P})^2] & \\ \quad + \dfrac{J}{2}\mathrm{Tr}[\hat{M}^2 - (\hat{N} - 2\hat{P})^2] + \dfrac{U^{\uparrow} - U^{\downarrow}}{4}\mathrm{Tr}[\hat{M} - \hat{N}\hat{M}], & \mathrm{Tr}[\hat{N}] > \mathrm{Tr}[\hat{P}]. \end{cases} \quad (9.19)$$

Here $\hat{P}$ is the subspace projection operator. To maintain rotational invariance, the above corrective functional has implicitly assumed that Hund's First Rule applies to the multi-orbital subspace. There are of course some multi-orbital subspaces for which Hund's First Rule does not apply, such as in certain low-spin transition metal complexes. A modified BLOR type corrective functional will be required for such systems.

9.2 Sample ONETEP Input File

```
#------------------------------------------------------------
#---------------------- INPUT FILE --------------------------
#------------------------------------------------------------
task : singlepoint
output_detail : verbose
psinc_spacing : 0.2793650794 0.2666666667 0.2666666667
xc_functional : PBE
edft : T
edft_smearing_width : 0.0
write_converged_dk_ngwfs : T
write_denskern : T
write_tightbox_ngwfs : T
read_denskern : F
read_tightbox_ngwfs : F
lnv_threshold_orig : 1.0e-6
lnv_cg_max_step : 10.0
maxit_lnv : 20
minit_lnv : 1
lnv_check_trial_steps : T
kernel_update : T
ngwf_threshold_orig : 1.0e-7
ngwf_cg_max_step : 100.0
maxit_ngwf_cg : 100
delta_e_conv : F
elec_energy_tol : 1.0e-6 eV
maxit_pen : 0
maxit_palser_mano : -1
maxit_kernel_fix : 0
kerfix : 1
occ_mix : 0.5
maxit_hotelling : 0
charge : 1
spin : 1.0
dos_smear : 0.10 eV
pbc_correction_cutoff : 7.0
timings_level : 1
spin_polarized : T
turn_off_hartree : F
hubbard_unify_sites : F
hubbard_calculating_U : T
hubbard_ngwf_spin_threshold : 1.0e-20
print_qc : F
cube_format : F
grd_format : F
write_density_plot : F
lumo_dens_plot : -1
homo_dens_plot : -1
lumo_plot : -1
homo_plot : -1
check_atoms : F
```

```
write_ngwf_plot : F
write_initial_radial_ngwfs : T
do_properties : T
polarisation_calculate : F
ngwf_analysis : F
write_forces : T
popn_calculate : T
threads_max : 14
threads_num_fftboxes : 14
threads_per_cellfft : 14

%block species_ngwf_plot
Be1
Be2
%endblock species_ngwf_plot

%block species
bohr
Be1 Be 4 2 14.0
Be2 Be 4 2 14.0
%endblock species

%block species_atomic_set
Be1 “SOLVE conf=2s2: 0.15"
Be2 “SOLVE conf=2s2: 0.15"
%endblock species_atomic_set

%block species_pot
Be1 be.recpot
Be2 be.recpot
%endblock species_pot

%block species_ldos_groups
Be1
Be2
%endblock species_ldos_groups

%block lattice_cart
bohr
88.0 0.00 0.00
0.00 60.0 0.00
0.00 0.00 60.0
%endblock lattice_cart

%block hubbard
Be1 0 0.00 0.00 0.00 -0.25 0.00 0.0
Be2 0 0.00 0.00 0.00 -0.25 0.00 0.0
%endblock hubbard

%block positions_abs
bohr
Be1 39.0 30.0 30.0
```

```
Be2 49.0 30.0 30.0
%endblock positions_abs

#------------------------------------------------------------
#------------------ END INPUT FILE ------------------------
#------------------------------------------------------------
```

9.3 Sample Quantum Espresso Input File

```
&CONTROL
calculation = 'scf'
restart_mode = 'from_scratch'
outdir = './TMP'
prefix = 'helium'
pseudo_dir = '/projects/pi-oregan/HPC_20_01119/Andrew_Burgess/fractional_helium/pseudo'
/

&SYSTEM
ibrav = 0
nat = 1
ntyp = 1
nbnd = 2
tot_charge = 0.0
tot_magnetization = 0.8
ecutwfc = 75.0
ecutrho = 300.0
occupations = 'smearing'
degauss = 0.02
smearing = 'gauss'
nspin = 2
input_dft = 'pbe0'
assume_isolated = 'm-t'
starting_magnetization(1) = 0.0
/

&ELECTRONS
conv_thr = 5e-09
mixing_mode = 'plain'
mixing_beta = 0.7
diagonalization = 'david'
/ &IONS
/
&CELL
/

ATOMIC_SPECIES
He 4.002602 He_ONCV_PBE-1.0.upf

K_POINTS gamma

CELL_PARAMETERS angstrom
20.00000000000000 0.00000000000000 0.00000000000000
0.00000000000000 20.00000000000000 0.00000000000000
0.00000000000000 0.00000000000000 20.00000000000000

ATOMIC_POSITIONS angstrom

He 10.0000000000 10.0000000000 10.0000000000
```

9.4 Evaluation of Hubbard Parameters

9.4.1 Stretched H_2

Figs. 9.1 & 9.2 display the linear response curves for the H_2 molecule at 9 bohr radii. The $\beta-$type perturbations used to evaluate the Hund's J parameter (see Eq. 9.21), caused the system to converge to a lower-energy, spin-polarised system. The Hund's J parameter was thus evaluated with a stabilising potential (see Eq. 5.29). Fig. 9.3 displays the plot of the Hund's J parameter at different stabilising potential strengths G. Application of an $\alpha-$type perturbation (see Eq. 9.21), did not cause the system to converge to a spin-polarised state and hence the Hubbard U parameter could be evaluated at $G = 0$ eV. No extrapolation of the Hubbard U parameter was thus required.

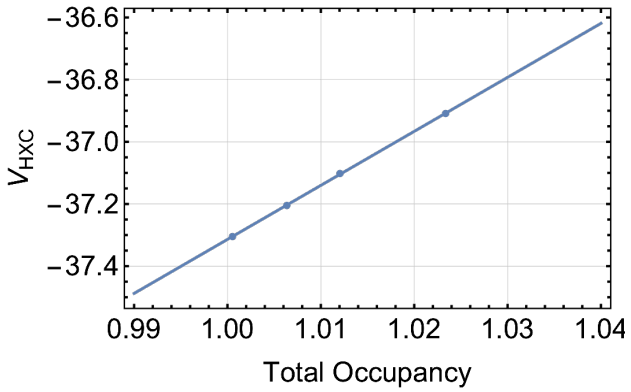

Figure 9.1: Linear response curve of V_{Hxc} versus total occupancy for the H_2 molecule at 9 bohr radii . The slope of the best-fit line is used to compute the Hubbard U parameter. One of the perturbative calculations failed to converge, hence four instead of five data points are displayed.

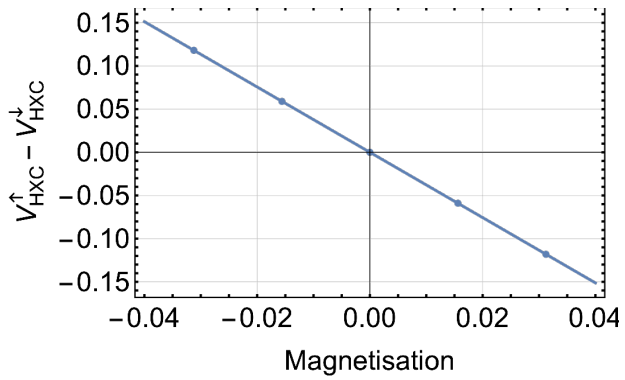

Figure 9.2: Linear response curve of $V^{\uparrow}_{\mathrm{Hxc}} - V^{\downarrow}_{\mathrm{Hxc}}$ versus subspace magnetisation for the H_2 molecule at $9a_0$ with a stabilising potential of $G = -10$ eV. The slope of the best-fit line is used to compute the Hund's J parameter at $G = -10$ eV.

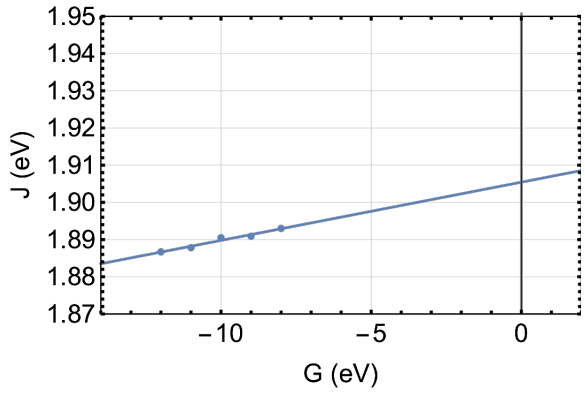

Figure 9.3: Plot of the Hund's J parameter versus the stabilising potential parameter G. Extrapolation of the best-fit line to $G = 0$ eV, yields the Hund's J parameter for use in the corrective functionals.

9.4.2 Stretched H_5^+

Figs. 9.4, 9.5, 9.6 & 9.7 display the linear response curves for the triplet H_5^+ system at 8 bohr radii. All perturbations had to be applied using a stabilising potential of strength G (see Eq. 5.29). The corrective parameters were computed at several values of G and the best-fit line was extrapolated to $G = 0$ eV. The plot of the spin agnostic Hubbard U parameter versus the stabilising potential strength G is shown in Fig. 9.8. Similarly, Fig. 9.9 displays the plot of the Hund's J parameter versus the stabilising potential strength G.

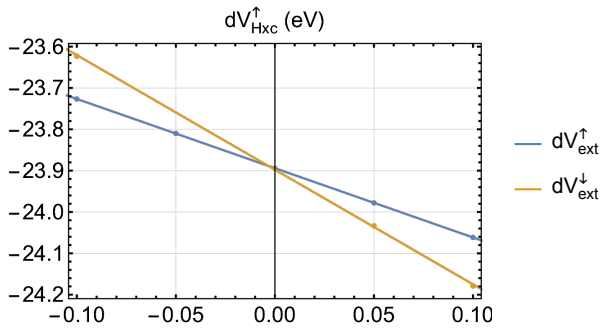

Figure 9.4: Linear response graph of the variation in $V^{\uparrow}_{\mathrm{Hxc}}$ with respect to spin up and spin down perturbations for H_5^+ at 8 bohr radii with a stabilising potential of $G = -14$ eV (see Eq.14).

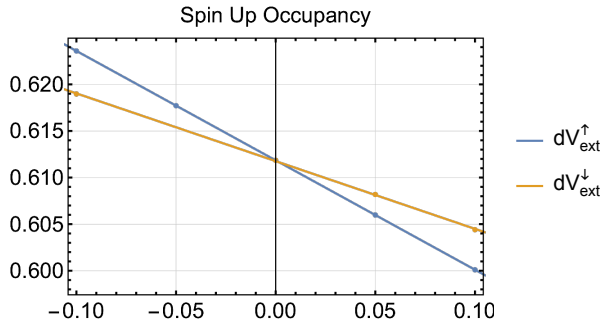

Figure 9.5: Linear response graph of the variation in the spin up subspace occupancy with respect to spin up and spin down perturbations for H_5^+ at 8 bohr radii with a stabilising potential of $G = -14$ eV (see Eq. 14).

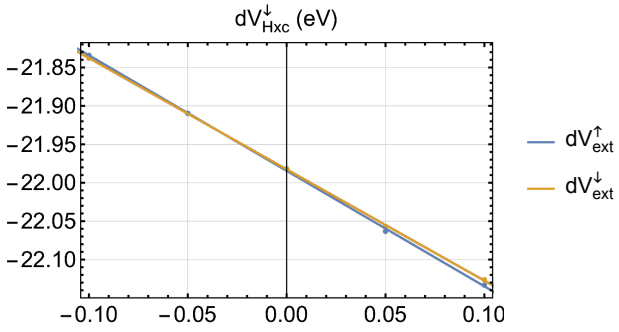

Figure 9.6: Linear response graph of the variation in $V^{\downarrow}_{\mathrm{Hxc}}$ with respect to spin up and spin down perturbations for H_5^+ at 8 bohr radii with a stabilising potential of $G = -14$ eV (see Eq. 14).

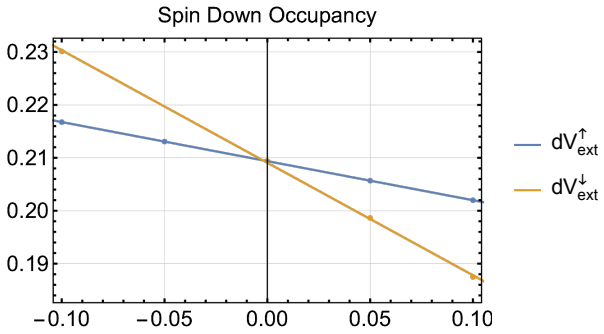

Figure 9.7: Linear response graph of the variation in the spin down subspace occupancy with respect to spin up and spin down perturbations for H_5^+ at 8 bohr radii with a stabilising potential of $G = -14$ eV (see Eq. 14).

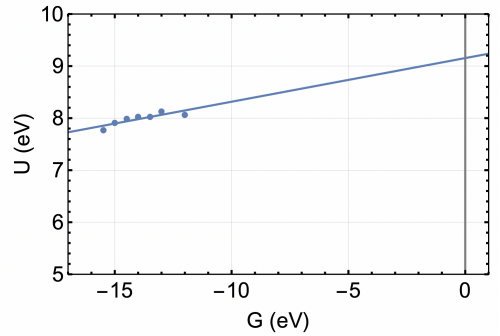

Figure 9.8: Plot of the Hubbard U parameter versus the stabilising potential parameter G (see Eq. 14). Extrapolation of the best-fit line to $G = 0$ eV, yields the Hubbard U parameter for use in the corrective functionals.

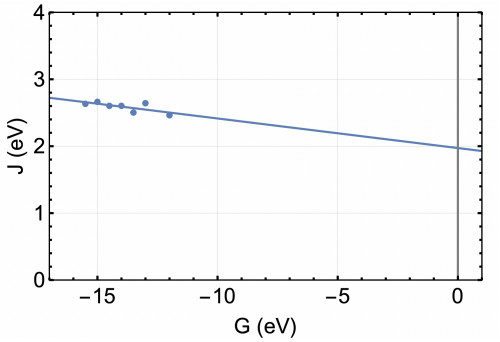

Figure 9.9: Plot of the Hund's J parameter versus the stabilising potential parameter G (see Eq. 14). Extrapolation of the best-fit line to $G = 0$ eV, yields the Hund's J parameter for use in the corrective functionals.

9.4.3 Stretched N_2

In order to evaluate the Hubbard U and Hund's J parameter for the stretched N_2 molecule a stabilising potential,

$$\hat{v}^{\sigma} = \frac{G}{2}\left(1 - 2\hat{n}^{\sigma} + 2\hat{n}^{\bar{\sigma}}\right) \tag{9.20}$$

was applied in conjunction with the α and β type perturbations used to compute the Hubbard U and Hund's J parameters respectively. The U and J parameters were thus evaluated at a series of different stabilising potential strengths G and the results were extrapolated back to $G = 0$ eV. Sample linear response curves used for the evaluating the Hubbard U and Hund's J parameters at a non-zero value of G are shown in Figs. 9.10 & 9.11. The plot of the Hubbard U parameter versus the stabilising potential strength G is shown in Fig. 9.12 and finally, Fig. 9.13 displays the plot of the Hund's J parameter versus the stabilising potential strength G.

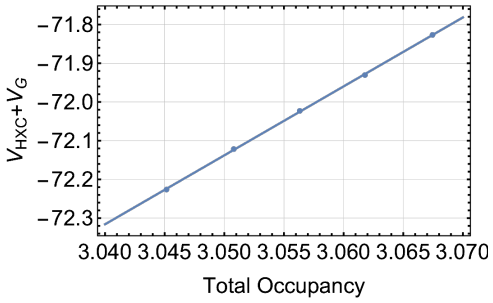

Figure 9.10: Linear response curve of $V_{\mathrm{HXC}} + V_{\mathrm{G}}$ versus subspace occupancy for the N_2 molecule at 7 bohr radii with a stabilising potential of $G = -10$ eV. V_{G} refers to the subspace averaged stabilisation potential. The slope of the best-fit line is used to compute the Hubbard U parameter at $G = -10$ eV.

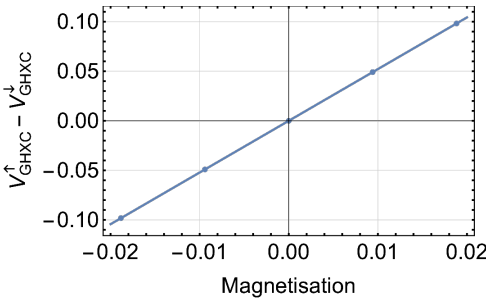

Figure 9.11: Linear response curve of $V^{\uparrow}_{\mathrm{GHXC}} - V^{\downarrow}_{\mathrm{GHXC}}$ versus subspace magnetisation for the N_2 molecule at 7 bohr radii with a stabilising potential of $G = -10$ eV. $V^{\sigma}_{\mathrm{GHXC}}$ refers to the spin-resolved, subspace averaged Hartree Exchange Correlation potential including the stabilisation potential. The slope of the best-fit line is used to compute the Hund's J parameter at $G = -10$ eV.

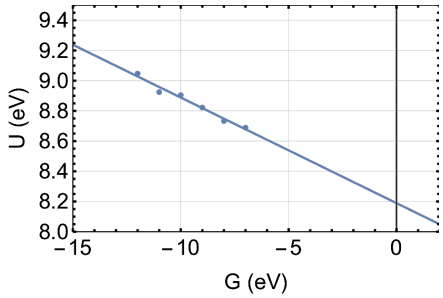

Figure 9.12: Plot of the Hubbard U parameter versus the stabilising potential parameter G. Extrapolation of the best-fit line to $G = 0$ eV, yields the Hund's J parameter for use in the corrective functionals.

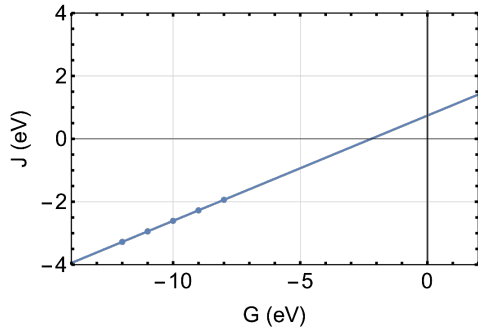

Figure 9.13: Plot of the Hund's J parameter versus the stabilising potential parameter G. Extrapolation of the best-fit line to $G = 0$ eV, yields the Hund's J parameter for use in the corrective functionals.

9.5 Application of Corrective Functionals

Suppose that we are using any one of several DFT codes with the following DFT+U functional E_{u} available:

$$\begin{aligned} E_{\mathrm{u}} =& \frac{U_{\mathrm{input}} - J_{\mathrm{input}}}{2} \sum_{\sigma mm'} \left[n^{\sigma}_{mm'} \delta_{mm'} - n^{\sigma}_{mm'} n^{\sigma}_{m'm} \right] + \frac{J_{\mathrm{input}}}{2} \sum_{\sigma mm'} n^{\sigma}_{mm'} n^{\bar{\sigma}}_{m'm} \\ &+ \alpha_{\mathrm{input}} \sum_{\sigma mm'} n^{\sigma}_{mm'} \delta_{mm'} + \beta_{\mathrm{input}} \sum_{mm'} \left[n^{\uparrow}_{mm'} \delta_{mm'} - n^{\downarrow}_{mm'} \delta_{mm'} \right] + C(2l+1), \end{aligned} \tag{9.21}$$

where C is a constant, l is the subspace orbital angular momentum quantum number and α & β are free parameters, typically used to apply perturbations to the subspace. Careful choice of the value of U_{input}, J_{input}, α_{input}, and β_{input} specified in the DFT input file allows one to use the DFT code to simulate the corrective functionals listed in the proceeding table. The constant C may be added by hand afterwards, for each site. The proceeding table specifies the required input parameters for spin polarised systems. Please note that the BLOR corrective functional also requires separate U parameters for the two spin channels.

Hubbard Functional	U_{input}	J_{input}	α_{input}	β_{input}	C
DFT+U+J ($U_{\text{eff}} = U$) NSCF	$U + J$	J	0	0	0
DFT+U+J ($U_{\text{eff}} = U$) SCF	$-2J$	$-U - J$	0	0	0
DFT+U+J no minority spin term	U	J	0	0	0
DFT+U+J with minority spin term	U	J	$-J/2$	$J/2$	0
DFT+J ($U_{\text{eff}} = 0$)	$-2J$	$-2J$	0	0	0
Shishkin & Sato (2017)	$U + J$	J	$-J/2$	$J/2$	0
Shishkin & Sato (2019)	$U + U_{\uparrow\downarrow}$	$U_{\uparrow\downarrow}$	$-U_{\uparrow\downarrow}/2$	$U_{\uparrow\downarrow}/2$	0
Dudarev et al. (1998)	$U - J$	0	0	0	0
Dudarev et al. (2019)	U	0	0	0	0
Bajaj, Kulik et al. (lower)	U	J	0	0	0
Bajaj, Kulik et al. (upper)	U	J'	$-J'$	0	J
BLOR (sym) (lower)	$-2J$	$-U - 2J$	0	0	0
BLOR (sym) (upper)	$-2J$	$-U - 2J$	$U + 2J$	0	$(-U - 2J)$
BLOR (lower)	$U^{\sigma}_{input} = U^{\sigma} - \frac{1}{2}(U^{\uparrow} + U^{\downarrow} + 4J)$	$-\frac{1}{2}(U^{\uparrow} + U^{\downarrow} + 4J)$	0	0	0
BLOR (upper)	$U^{\sigma}_{input} = U^{\sigma} - \frac{1}{2}(U^{\uparrow} + U^{\downarrow} + 4J)$	$-\frac{1}{2}(U^{\uparrow} + U^{\downarrow} + 4J)$	$\frac{1}{2}(U^{\uparrow} + U^{\downarrow} + 4J)$	0	$-\frac{1}{2}(U^{\uparrow} + U^{\downarrow} + 4.$

Bibliography

[1] J. P. Perdew, R. G. Parr, M. Levy, and J. L. Balduz, "Density-Functional Theory for Fractional Particle Number: Derivative Discontinuities of the Energy," *Phys. Rev. Lett.*, vol. 49, pp. 1691–1694, Dec. 1982.

[2] M. Born and R. Oppenheimer, "Zur Quantentheorie der Molekeln," *Ann. Phys.*, vol. 389, no. 20, pp. 457–484, 1927.

[3] E. Schrödinger, "An Undulatory Theory of the Mechanics of Atoms and Molecules," *Phys. Rev.*, vol. 28, pp. 1049–1070, Dec. 1926.

[4] R. J. Bartlett and M. Musiał, "Coupled-cluster theory in quantum chemistry," *Rev. Mod. Phys.*, vol. 79, pp. 291–352, Feb. 2007.

[5] R. J. Bartlett, "Perspective on Coupled-cluster Theory. The evolution toward simplicity in quantum chemistry," *Phys. Chem. Chem. Phys.*, vol. 26, no. 10, pp. 8013–8037, 2024.

[6] I. Y. Zhang and A. Grüneis, "Coupled Cluster Theory in Materials Science," *Front. Mater.*, vol. 6, June 2019.

[7] J. J. Eriksen, "The Shape of Full Configuration Interaction to Come," *J. Phys. Chem. Lett.*, vol. 12, pp. 418–432, Jan. 2021.

[8] C. David Sherrill and H. F. Schaefer, "The Configuration Interaction Method: Advances in Highly Correlated Approaches," in *Advances in Quantum Chemistry*, vol. 34, pp. 143–269, Academic Press, Jan. 1999.

[9] I. Shavitt, "The history and evolution of configuration interaction," *Mol. Phys.*, vol. 94, pp. 3–17, May 1998.

[10] B. O. Roos, "The Complete Active Space Self-Consistent Field Method and its Applications in Electronic Structure Calculations," in *Advances in Chemical Physics*, pp. 399–445, John Wiley & Sons, Ltd, 1987.

[11] J. Olsen, "The CASSCF method: A perspective and commentary," *Int. J. Quantum Chem.*, vol. 111, no. 13, pp. 3267–3272, 2011.

[12] V. Veryazov, P. Å. Malmqvist, and B. O. Roos, "How to select active space for multiconfigurational quantum chemistry?," *Int. J. Quantum Chem.*, vol. 111, no. 13, pp. 3329–3338, 2011.

[13] J. McClain, Q. Sun, G. K.-L. Chan, and T. C. Berkelbach, "Gaussian-Based Coupled-Cluster Theory for the Ground-State and Band Structure of Solids," *J. Chem. Theory Comput.*, vol. 13, pp. 1209–1218, Mar. 2017.

[14] T. Gruber, K. Liao, T. Tsatsoulis, F. Hummel, and A. Grüneis, "Applying the Coupled-Cluster Ansatz to Solids and Surfaces in the Thermodynamic Limit," *Phys. Rev. X*, vol. 8, p. 021043, May 2018.

[15] G. H. Booth, A. Grüneis, G. Kresse, and A. Alavi, "Towards an exact description of electronic wavefunctions in real solids," *Nature*, vol. 493, pp. 365–370, Jan. 2013.

[16] A. F. White, Y. Gao, A. J. Minnich, and G. K.-L. Chan, "A coupled cluster framework for electrons and phonons," *J. Chem. Phys.*, vol. 153, p. 224112, Dec. 2020.

[17] J. Toulouse, R. Assaraf, and C. J. Umrigar, "Chapter Fifteen - Introduction to the Variational and Diffusion Monte Carlo Methods," in *Advances in Quantum Chemistry*, vol. 73 of *Electron Correlation in Molecules – Ab Initio Beyond Gaussian Quantum Chemistry*, pp. 285–314, Academic Press, Jan. 2016.

[18] R. J. Needs, M. D. Towler, N. D. Drummond, and P. L. Ríos, "Continuum variational and diffusion quantum Monte Carlo calculations," *J. Phys.: Condens. Matter*, vol. 22, p. 023201, Dec. 2009.

[19] J. A. Schiller, L. K. Wagner, and E. Ertekin, "Phase stability and properties of manganese oxide polymorphs: Assessment and insights from diffusion Monte Carlo," *Phys. Rev. B*, vol. 92, p. 235209, Dec. 2015.

[20] K. Saritas, J. T. Krogel, P. R. C. Kent, and F. A. Reboredo, "Diffusion Monte Carlo: A pathway towards an accurate theoretical description of manganese oxides," *Phys. Rev. Mater.*, vol. 2, p. 085801, Aug. 2018.

[21] C. Mitra, J. T. Krogel, J. A. Santana, and F. A. Reboredo, "Many-body ab initio diffusion quantum Monte Carlo applied to the strongly correlated oxide NiO," *J. Chem. Phys.*, vol. 143, p. 164710, Oct. 2015.

[22] Y. Luo, A. Benali, L. Shulenburger, J. T. Krogel, O. Heinonen, and P. R. C. Kent, "Phase stability of TiO_2 polymorphs from diffusion Quantum Monte Carlo," *New J. Phys.*, vol. 18, p. 113049, Nov. 2016.

[23] K. Saritas, E. R. Fadel, B. Kozinsky, and J. C. Grossman, "Charge Density and Redox Potential of $LiNiO_2$ Using Ab Initio Diffusion Quantum Monte Carlo," *J. Phys. Chem. C*, vol. 124, pp. 5893–5901, Mar. 2020.

[24] A. Jain, Y. Shin, and K. A. Persson, "Computational predictions of energy materials using density functional theory," *Nat Rev Mater*, vol. 1, pp. 1–13, Jan. 2016.

[25] J. C. Thomas, W. Chen, Y. Xiong, B. A. Barker, J. Zhou, W. Chen, A. Rossi, N. Kelly, Z. Yu, D. Zhou, S. Kumari, E. d. S. Barnard, J. A. Robinson, M. Terrones, A. Schwartzberg, D. F. Ogletree, E. Rotenberg, M. M. Noack, S. Griffin, A. Raja, D. A. Strubbe, G.-M. Rignane se, A. Weber-Bargioni, and G. Hautier, "A substitutional quantum defect in WS_2 discovered by high-throughput computational screening and fabricated by site-selective STM manipulation," *Nat Commun*, vol. 15, p. 3556, Apr. 2024.

[26] D. Wines, K. Choudhary, A. J. Biacchi, K. F. Garrity, and F. Tavazza, "High-Throughput DFT-Based Discovery of Next Generation Two-Dimensional (2D) Superconductors," *Nano Lett.*, vol. 23, pp. 969–978, Feb. 2023.

[27] Y. Zhu, V. W. Yu, and G. Galli, "First-Principles Investigation of Near-Surface Divacancies in Silicon Carbide," *Nano Lett.*, vol. 23, pp. 11453–11460, Dec. 2023.

[28] K. Hoang and M. D. Johannes, "Defect chemistry in layered transition-metal oxides from screened hybrid density functional calculations," *J. Mater. Chem. A*, vol. 2, pp. 5224–5235, Mar. 2014.

[29] S. Carlotto, M. M. Natile, A. Glisenti, and A. Vittadini, "Electronic structure of $SrTi_{1-x}M_xO_{3-\delta}$ (M = Co, Ni, Cu) perovskite-type doped-titanate crystals by DFT and DFT+U calculations," *Chem. Phys. Lett.*, vol. 588, pp. 102–108, Nov. 2013.

[30] A. M. Teale, T. Helgaker, A. Savin, C. Adamo, B. Aradi, A. V. Arbuznikov, P. W. Ayers, E. Jan Baerends, V. Barone, P. Calaminici, E. Cancès, E. A. Carter, P. Kumar Chattaraj, H. Chermette, I. Ciofini, T. Daniel Crawford, F. D. Proft, J. F. Dobson, C. Draxl, T. Frauenheim, E. Fromager, P. Fuentealba, L. Gagliardi, G. Galli, J. Gao, P. Geerlings, N. Gidopoulos, P. M. W. Gill, P. Gori-Giorgi, A. Görling, T. Gould, S. Grimme, O. Gritsenko, H. J. Aagaard Jensen, E. R. Johnson, R. O. Jones, M. Kaupp, A. M. Köster, L. Kronik, A. I. Krylov, S. Kvaal, A. Laestadius, M. Levy, M. Lewin, S. Liu, P.-F. Loos, N. T. Maitra, F. Neese, J. P. Perdew, K. Pernal, P. Pernot, P. Piecuch, E. Rebolini, L. Reining, P. Romaniello, A. Ruzsinszky, D. R. Salahub, M. Scheffler, P. Schwerdtfeger, V. N. Staroverov, J. Sun, E. Tellgren, D. J. Tozer, S. B. Trickey, C. A. Ullrich, A. Vela, G. Vignale, T. A. Wesolowski, X. Xu, and W. Yang, "DFT exchange: Sharing perspectives on the workhorse of quantum chemistry and materials science," *Phys. Chem. Chem. Phys.*, vol. 24, no. 47, pp. 28700–28781, 2022.

[31] L. H. Thomas, "The calculation of atomic fields," *Math. Proc. Camb. Philos. Soc.*, vol. 23, pp. 542–548, Jan. 1927.

[32] E. Fermi, "Un metodo statistico per la determinazione di alcune priopri età dell'atomo," *Rend. Accad. Naz. Lincei*, vol. 6, pp. 602–607, 1927.

[33] P. Hohenberg and W. Kohn, "Inhomogeneous Electron Gas," *Phys. Rev.*, vol. 136, pp. B864–B871, Nov. 1964.

[34] M. Levy, "Electron densities in search of Hamiltonians," *Phys. Rev. A*, vol. 26, pp. 1200–1208, Sept. 1982.

[35] H. Englisch and R. Englisch, "Hohenberg-Kohn theorem and non-v-representable densities," *Phys. Stat. Mech. Its Appl.*, vol. 121, pp. 253–268, Aug. 1983.

[36] A. Gonis, X. G. Zhang, M. Däne, G. M. Stocks, and D. M. Nicholson, "Reformulation of density functional theory for N-representable densities and the resolution of the v-representability problem," *J. Phys. Chem. Solids*, vol. 89, pp. 23–31, Feb. 2016.

[37] P. W. Ayers, "Axiomatic formulations of the Hohenberg-Kohn functional," *Phys. Rev. A*, vol. 73, p. 012513, Jan. 2006.

[38] P. W. Ayers and S. Liu, "Necessary and sufficient conditions for the N-representability of density functionals," *Phys. Rev. A*, vol. 75, p. 022514, Feb. 2007.

[39] O. Gunnarsson and B. I. Lundqvist, "Exchange and correlation in atoms, molecules, and solids by the spin-density-functional formalism," *Phys. Rev. B*, vol. 13, pp. 4274–4298, May 1976.

[40] N. D. Mermin, "Thermal Properties of the Inhomogeneous Electron Gas," *Phys. Rev.*, vol. 137, pp. A1441–A1443, Mar. 1965.

[41] M. Levy, "Universal variational functionals of electron densities, first-order density matrices, and natural spin-orbitals and solution of the v-representability problem," *Proc. Natl. Acad. Sci.*, vol. 76, pp. 6062–6065, Dec. 1979.

[42] E. H. Lieb, "Density functionals for coulomb systems," *Int. J. Quantum Chem.*, vol. 24, no. 3, pp. 243–277, 1983.

[43] S. M. Valone, "A one-to-one mapping between one-particle densities and some N-particle ensembles," *J. Chem. Phys.*, vol. 73, pp. 4653–4655, July 2008.

[44] P. W. Ayers and M. Levy, "Levy Constrained Search in Fock Space: An Alternative Approach to Noninteger Electron Number," *Acta Phys. -Chim. Sin.*, vol. 34, no. 6, pp. 625–630.

[45] P. M. Dirac, "Note on Exchange Phenomena in the Thomas Atom," *Math. Proc. Camb. Philos. Soc.*, vol. 26, pp. 376–385, July 1930.

[46] C. V. Weizsäcker, "Zur theorie der kernmassen," *Z. Für Phys.*, vol. 96.7, pp. 431–458, 1935.

[47] Y. A. Wang and E. A. Carter, "Orbital-Free Kinetic-Energy Density Functional Theory," in *Theoretical Methods in Condensed Phase Chemistry*, pp. 117–184, Dordrecht: Springer Netherlands, 2002.

[48] Q. Xu, C. Ma, W. Mi, Y. Wang, and Y. Ma, "Recent advancements and challenges in orbital-free density functional theory," *WIREs Comput. Mol. Sci.*, vol. 14, no. 3, p. e1724, 2024.

[49] V. V. Karasiev and S. B. Trickey, "Issues and challenges in orbital-free density functional calculations," *Comput. Phys. Commun.*, vol. 183, pp. 2519–2527, Dec. 2012.

[50] W. Mi, K. Luo, S. B. Trickey, and M. Pavanello, "Orbital-Free Density Functional Theory: An Attractive Electronic Structure Method for Large-Scale First-Principles Simulations," *Chem. Rev.*, vol. 123, pp. 12039–12104, Nov. 2023.

[51] Y. A. Wang, N. Govind, and E. A. Carter, "Orbital-free kinetic-energy density functionals with a density-dependent kernel," *Phys. Rev. B*, vol. 60, pp. 16350–16358, Dec. 1999.

[52] L.-W. Wang and M. P. Teter, "Kinetic-energy functional of the electron density," *Phys. Rev. B*, vol. 45, pp. 13196–13220, June 1992.

[53] P. Golub and S. Manzhos, "Kinetic energy densities based on the fourth order gradient expansion: Performance in different classes of materials and improvement via machine learning," *Phys. Chem. Chem. Phys.*, vol. 21, no. 1, pp. 378–395, 2019.

[54] R. Meyer, M. Weichselbaum, and A. W. Hauser, "Machine Learning Approaches toward Orbital-free Density Functional Theory: Simultaneous Training on the Kinetic Energy Density Functional and Its Functional Derivative," *J. Chem. Theory Comput.*, vol. 16, pp. 5685–5694, Sept. 2020.

[55] W. Kohn and L. J. Sham, "Self-Consistent Equations Including Exchange and Correlation Effects," *Phys. Rev.*, vol. 140, pp. A1133–A1138, Nov. 1965.

[56] A. D. Kaplan, M. Levy, and J. P. Perdew, "The predictive power of exact constraints and appropriate norms in density functional theory," *Annu. Rev. Phys. Chem.*, vol. 74, pp. 193–218, 2023.

[57] N. Mardirossian and M. Head-Gordon, "Thirty years of density functional theory in computational chemistry: An overview and extensive assessment of 200 density functionals," *Mol. Phys.*, vol. 115, pp. 2315–2372, Oct. 2017.

[58] R. Peverati and D. G. Truhlar, "Quest for a universal density functional: The accuracy of density functionals across a broad spectrum of databases in chemistry and physics," *Philos. Trans. R. Soc. Math. Phys. Eng. Sci.*, vol. 372, p. 20120476, Mar. 2014.

[59] J. P. Perdew, A. Ruzsinszky, J. Tao, V. N. Staroverov, G. E. Scuseria, and G. I. Csonka, "Prescription for the design and selection of density functional approximations: More constraint satisfaction with fewer fits," *J. Chem. Phys.*, vol. 123, p. 062201, Aug. 2005.

[60] J. P. Perdew, K. Burke, and M. Ernzerhof, "Generalized Gradient Approximation Made Simple," *Phys. Rev. Lett.*, vol. 77, pp. 3865–3868, Oct. 1996.

[61] J. Sun, A. Ruzsinszky, and J. P. Perdew, "Strongly Constrained and Appropriately Normed Semilocal Density Functional," *Phys. Rev. Lett.*, vol. 115, p. 036402, July 2015.

[62] E. H. Lieb and S. Oxford, "Improved lower bound on the indirect Coulomb energy," *Int. J. Quantum Chem.*, vol. 19, pp. 427–439, Mar. 1981.

[63] M. Levy and J. P. Perdew, "Hellmann-Feynman, virial, and scaling requisites for the exact universal density functionals. Shape of the correlation potential and diamagnetic susceptibility for atoms," *Phys. Rev. A*, vol. 32, pp. 2010–2021, Oct. 1985.

[64] M. Levy and J. P. Perdew, "Tight bound and convexity constraint on the exchange-correlation-energy functional in the low-density limit, and

other formal tests of generalized-gradient approximations," *Phys. Rev. B*, vol. 48, pp. 11638–11645, Oct. 1993.

[65] A. D. Becke, "Density-functional exchange-energy approximation with correct asymptotic behavior," *Phys. Rev. A*, vol. 38, pp. 3098–3100, Sept. 1988.

[66] G. G. Spink, R. J. Needs, and N. D. Drummond, "Quantum Monte Carlo study of the three-dimensional spin-polarized homogeneous electron gas," *Phys. Rev. B*, vol. 88, p. 085121, Aug. 2013.

[67] F. H. Zong, C. Lin, and D. M. Ceperley, "Spin polarization of the low-density three-dimensional electron gas," *Phys. Rev. E*, vol. 66, p. 036703, Sept. 2002.

[68] D. M. Ceperley and B. J. Alder, "Ground State of the Electron Gas by a Stochastic Method," *Phys. Rev. Lett.*, vol. 45, pp. 566–569, Aug. 1980.

[69] U. von Barth and L. Hedin, "A local exchange-correlation potential for the spin polarized case. i," *J. Phys. C: Solid State Phys.*, vol. 5, p. 1629, July 1972.

[70] A. K. Rajagopal and J. Callaway, "Inhomogeneous Electron Gas," *Phys. Rev. B*, vol. 7, pp. 1912–1919, Mar. 1973.

[71] S. H. Vosko, L. Wilk, and M. Nusair, "Accurate spin-dependent electron liquid correlation energies for local spin density calculations: A critical analysis," *Can. J. Phys.*, vol. 58, pp. 1200–1211, Aug. 1980.

[72] J. P. Perdew and Y. Wang, "Accurate and simple analytic representation of the electron-gas correlation energy," *Phys. Rev. B*, vol. 45, pp. 13244–13249, June 1992.

[73] J. P. Perdew and A. Zunger, "Self-interaction correction to density-functional approximations for many-electron systems," *Phys. Rev. B*, vol. 23, pp. 5048–5079, May 1981.

[74] M. T. Entwistle, M. J. P. Hodgson, J. Wetherell, B. Longstaff, J. D. Ramsden, and R. W. Godby, "Local density approximations from finite systems," *Phys. Rev. B*, vol. 94, p. 205134, Nov. 2016.

[75] C. Lee, W. Yang, and R. G. Parr, "Development of the Colle-Salvetti correlation-energy formula into a functional of the electron density," *Phys. Rev. B*, vol. 37, pp. 785–789, Jan. 1988.

[76] J. P. Perdew, A. Ruzsinszky, G. I. Csonka, O. A. Vydrov, G. E. Scuseria, L. A. Constantin, X. Zhou, and K. Burke, "Restoring the Density-Gradient Expansion for Exchange in Solids and Surfaces," *Phys. Rev. Lett.*, vol. 100, p. 136406, Apr. 2008.

[77] P. Verma and D. G. Truhlar, "HLE16: A Local Kohn–Sham Gradient Approximation with Good Performance for Semiconductor Band Gaps and Molecular Excitation Energies," *J. Phys. Chem. Lett.*, vol. 8, pp. 380–387, Jan. 2017.

[78] G. Kin-Lic Chan and N. C. Handy, "Optimized Lieb-Oxford bound for the exchange-correlation energy," *Phys. Rev. A*, vol. 59, pp. 3075–3077, Apr. 1999.

[79] M. Lewin, E. H. Lieb, and R. Seiringer, "Improved Lieb–Oxford bound on the indirect and exchange energies," *Lett Math Phys*, vol. 112, p. 92, Sept. 2022.

[80] G. L. Oliver and J. P. Perdew, "Spin-density gradient expansion for the kinetic energy," *Phys. Rev. A*, vol. 20, pp. 397–403, Aug. 1979.

[81] J. M. del Campo, J. L. Gázquez, S. B. Trickey, and A. Vela, "A new meta-GGA exchange functional based on an improved constraint-based GGA," *Chemical Physics Letters*, vol. 543, pp. 179–183, Aug. 2012.

[82] J. Tao, J. P. Perdew, V. N. Staroverov, and G. E. Scuseria, "Climbing the Density Functional Ladder: Nonempirical Meta–Generalized Gradient Approximation Designed for Molecules and Solids," *Phys. Rev. Lett.*, vol. 91, p. 146401, Sept. 2003.

[83] Y. Zhao and D. G. Truhlar, "A new local density functional for main-group thermochemistry, transition metal bonding, thermochemical kinetics, and noncovalent interactions," *J. Chem. Phys.*, vol. 125, p. 194101, Nov. 2006.

[84] Y. Wang, X. Jin, H. S. Yu, D. G. Truhlar, and X. He, "Revised M06-L functional for improved accuracy on chemical reaction barrier heights,

noncovalent interactions, and solid-state physics," *Proc. Natl. Acad. Sci. U.S.A.*, vol. 114, pp. 8487–8492, Aug. 2017.

[85] A. D. Becke, "Density-functional thermochemistry. III. The role of exact exchange," *J. Chem. Phys.*, vol. 98, pp. 5648–5652, Apr. 1993.

[86] J. P. Perdew, M. Ernzerhof, and K. Burke, "Rationale for mixing exact exchange with density functional approximations," *J. Chem. Phys.*, vol. 105, pp. 9982–9985, Dec. 1996.

[87] T. M. Henderson, B. G. Janesko, and G. E. Scuseria, "Range Separation and Local Hybridization in Density Functional Theory," *J. Phys. Chem. A*, vol. 112, pp. 12530–12542, Dec. 2008.

[88] B. Himmetoglu, A. Floris, S. de Gironcoli, and M. Cococcioni, "Hubbard-corrected DFT energy functionals: The LDA+U description of correlated systems," *Int. J. Quantum Chem.*, vol. 114, no. 1, pp. 14–49, 2014.

[89] J. Heyd, G. E. Scuseria, and M. Ernzerhof, "Hybrid functionals based on a screened Coulomb potential," *J. Chem. Phys.*, vol. 118, pp. 8207–8215, May 2003.

[90] S. Grimme, "Semiempirical hybrid density functional with perturbative second-order correlation," *J. Chem. Phys.*, vol. 124, p. 034108, Jan. 2006.

[91] D. Wing, G. Ohad, J. B. Haber, M. R. Filip, S. E. Gant, J. B. Neaton, and L. Kronik, "Band gaps of crystalline solids from Wannier-localization–based optimal tuning of a screened range-separated hybrid functional," *Proc. Natl. Acad. Sci.*, vol. 118, p. e2104556118, Aug. 2021.

[92] W. Yang, Y. Zhang, and P. W. Ayers, "Degenerate Ground States and a Fractional Number of Electrons in Density and Reduced Density Matrix Functional Theory," *Phys. Rev. Lett.*, vol. 84, pp. 5172–5175, May 2000.

[93] P. W. Ayers, "The dependence on and continuity of the energy and other molecular properties with respect to the number of electrons," *J Math Chem*, vol. 43, pp. 285–303, Jan. 2008.

[94] A. J. Cohen, P. Mori-Sánchez, and W. Yang, "Fractional spins and static correlation error in density functional theory," *J. Chem. Phys.*, vol. 129, p. 121104, Sept. 2008.

[95] G. K.-L. Chan, "A fresh look at ensembles: Derivative discontinuities in density functional theory," *J. Chem. Phys.*, vol. 110, pp. 4710–4723, Mar. 1999.

[96] P. Mori-Sánchez, A. J. Cohen, and W. Yang, "Discontinuous Nature of the Exchange-Correlation Functional in Strongly Correlated Systems," *Phys. Rev. Lett.*, vol. 102, p. 066403, Feb. 2009.

[97] J. P. Perdew and E. Sagvolden, "Exact exchange-correlation potentials in spin-density functional theory and their discontinuities at unit electron number," *Can. J. Chem.*, vol. 87, pp. 1268–1272, Oct. 2009.

[98] X. De Vriendt, L. Lemmens, S. De Baerdemacker, P. Bultinck, and G. Acke, "Quantifying Delocalization and Static Correlation Errors by Imposing (Spin)Population Redistributions through Constraints on Atomic Domains," *J. Chem. Theory Comput.*, vol. 17, pp. 6808–6818, Nov. 2021.

[99] X. De Vriendt, D. Van Hende, S. De Baerdemacker, P. Bultinck, and G. Acke, "Uncovering phase transitions that underpin the flat-planes in the tilted Hubbard model using subsystems and entanglement measures," *J. Chem. Phys.*, vol. 156, p. 244115, June 2022.

[100] B. G. Janesko, "Replacing hybrid density functional theory: Motivation and recent advances," *Chem. Soc. Rev.*, vol. 50, no. 15, pp. 8470–8495, 2021.

[101] X. D. Yang, A. H. G. Patel, R. A. Miranda-Quintana, F. Heidar-Zadeh, C. E. González-Espinoza, and P. W. Ayers, "Communication: Two types of flat-planes conditions in density functional theory," *J. Chem. Phys.*, vol. 145, p. 031102, July 2016.

[102] R. Cuevas-Saavedra, D. Chakraborty, S. Rabi, C. Cárdenas, and P. W. Ayers, "Symmetric Nonlocal Weighted Density Approximations from the Exchange-Correlation Hole of the Uniform Electron Gas," *J. Chem. Theory Comput.*, vol. 8, pp. 4081–4093, Nov. 2012.

[103] T. Gál and P. Geerlings, "Energy surface, chemical potentials, Kohn–Sham energies in spin-polarized density functional theory," *J. Chem. Phys.*, vol. 133, p. 144105, Oct. 2010.

[104] Y. Goshen and E. Kraisler, "Ensemble Ground State of a Many-Electron System with Fractional Electron Number and Spin: Piecewise-Linearity and Flat-Plane Condition Generalized," *J. Phys. Chem. Lett.*, vol. 15, pp. 2337–2343, Mar. 2024.

[105] M. Richer, F. Heidar-Zadeh, M. Ríos-Gutiérrez, X. D. Yang, and P. W. Ayers, "Spin-Polarized Conceptual Density Functional Theory from the Convex Hull," *J. Chem. Theory Comput.*, vol. 20, pp. 4616–4628, June 2024.

[106] A. M. Malek and R. Balawender, "Discontinuities of energy derivatives in spin-density functional theory," vol. arXiv:1310.6918, Oct. 2013.

[107] A. Ruzsinszky, J. P. Perdew, G. I. Csonka, O. A. Vydrov, and G. E. Scuseria, "Spurious fractional charge on dissociated atoms: Pervasive and resilient self-interaction error of common density functionals," *J. Chem. Phys.*, vol. 125, p. 194112, Nov. 2006.

[108] P. Mori-Sánchez, A. J. Cohen, and W. Yang, "Many-electron self-interaction error in approximate density functionals," *J. Chem. Phys.*, vol. 125, p. 201102, Nov. 2006.

[109] A. Bajaj, J. P. Janet, and H. J. Kulik, "Communication: Recovering the flat-plane condition in electronic structure theory at semi-local DFT cost," *J. Chem. Phys.*, vol. 147, p. 191101, Nov. 2017.

[110] A. Bajaj, F. Liu, and H. J. Kulik, "Non-empirical, low-cost recovery of exact conditions with model-Hamiltonian inspired expressions in jmDFT," *J. Chem. Phys.*, vol. 150, p. 154115, Apr. 2019.

[111] B. G. Janesko, "Multiconfigurational Correlation at DFT + U cost: On-Site Electron–Electron Interactions Yield a Block-Localized Configuration Interaction Hamiltonian," *J. Phys. Chem. A*, vol. 128, pp. 5077–5087, June 2024.

[112] N. Q. Su, C. Li, and W. Yang, "Describing strong correlation with fractional-spin correction in density functional theory," *Proc. Natl. Acad. Sci.*, vol. 115, pp. 9678–9683, Sept. 2018.

[113] E. Proynov and J. Kong, "Correcting the Charge Delocalization Error of Density Functional Theory," *J. Chem. Theory Comput.*, vol. 17, pp. 4633–4638, Aug. 2021.

[114] J. Kong and E. Proynov, "Density Functional Model for Nondynamic and Strong Correlation," *J. Chem. Theory Comput.*, vol. 12, pp. 133–143, Jan. 2016.

[115] E. R. Johnson and J. Contreras-García, "Communication: A density functional with accurate fractional-charge and fractional-spin behaviour for s-electrons," *J. Chem. Phys.*, vol. 135, p. 081103, Aug. 2011.

[116] G. Prokopiou, M. Hartstein, N. Govind, and L. Kronik, "Optimal Tuning Perspective of Range-Separated Double Hybrid Functionals," *J. Chem. Theory Comput.*, vol. 18, pp. 2331–2340, Apr. 2022.

[117] F. Zhou and V. Ozolins, "A unified treatment of derivative discontinuity, delocalization and static correlation effects in density functional calculations," *arXiv:1710.08973*, Mar. 2018.

[118] H. van Aggelen, Y. Yang, and W. Yang, "Exchange-correlation energy from pairing matrix fluctuation and the particle-particle random-phase approximation," *Phys. Rev. A*, vol. 88, p. 030501, Sept. 2013.

[119] A. J. Cohen, P. Mori-Sánchez, and W. Yang, "Fractional charge perspective on the band gap in density-functional theory," *Phys. Rev. B*, vol. 77, p. 115123, Mar. 2008.

[120] O. A. Vydrov, G. E. Scuseria, and J. P. Perdew, "Tests of functionals for systems with fractional electron number," *J. Chem. Phys.*, vol. 126, p. 154109, Apr. 2007.

[121] A. Ruzsinszky, J. P. Perdew, G. I. Csonka, O. A. Vydrov, and G. E. Scuseria, "Density functionals that are one- and two- are not always many-electron self-interaction-free, as shown for H_2^+, He_2^+, LiH^+, and Ne_2^+," *J. Chem. Phys.*, vol. 126, p. 104102, Mar. 2007.

[122] O. A. Vydrov and G. E. Scuseria, "Effect of the Perdew–Zunger self-interaction correction on the thermochemical performance of approximate density functionals," *J. Chem. Phys.*, vol. 121, pp. 8187–8193, Nov. 2004.

[123] M. R. Pederson, A. Ruzsinszky, and J. P. Perdew, "Communication: Self-interaction correction with unitary invariance in density functional theory," *J. Chem. Phys.*, vol. 140, p. 121103, Mar. 2014.

[124] T. Tsuneda and K. Hirao, "Self-interaction corrections in density functional theory," *J. Chem. Phys.*, vol. 140, p. 18A513, Mar. 2014.

[125] D. Hait and M. Head-Gordon, "Delocalization Errors in Density Functional Theory Are Essentially Quadratic in Fractional Occupation Number," *J. Phys. Chem. Lett.*, vol. 9, pp. 6280–6288, Nov. 2018.

[126] P. Mori-Sánchez and A. J. Cohen, "The derivative discontinuity of the exchange–correlation functional," *Phys. Chem. Chem. Phys.*, vol. 16, no. 28, pp. 14378–14387, 2014.

[127] M. Levy, J. P. Perdew, and V. Sahni, "Exact differential equation for the density and ionization energy of a many-particle system," *Phys. Rev. A*, vol. 30, pp. 2745–2748, Nov. 1984.

[128] C.-O. Almbladh and U. Von Barth, "Exact results for the charge and spin densities, exchange-correlation potentials, and density-functional eigenvalues," *Phys. Rev. B*, vol. 31, pp. 3231–3244, Mar. 1985.

[129] P. Gori-Giorgi, T. Gál, and E. J. Baerends, "Asymptotic behaviour of the electron density and the Kohn–Sham potential in case of a Kohn–Sham HOMO nodal plane," *Mol. Phys.*, vol. 114, pp. 1086–1097, Apr. 2016.

[130] P. Gori-Giorgi and E. J. Baerends, "Asymptotic nodal planes in the electron density and the potential in the effective equation for the square root of the density," *Eur. Phys. J. B*, vol. 91, p. 160, July 2018.

[131] M. E. Casida, "Correlated optimized effective-potential treatment of the derivative discontinuity and of the highest occupied Kohn-Sham eigenvalue: A Janak-type theorem for the optimized effective-potential model," *Phys. Rev. B*, vol. 59, pp. 4694–4698, Feb. 1999.

[132] T. Gould, S. Pittalis, J. Toulouse, E. Kraisler, and L. Kronik, "Asymptotic behavior of the Hartree-exchange and correlation potentials in ensemble density functional theory," *Phys. Chem. Chem. Phys.*, vol. 21, no. 36, pp. 19805–19815, 2019.

[133] E. Kraisler, M. J. P. Hodgson, and E. K. U. Gross, "From Kohn–Sham to Many-Electron Energies via Step Structures in the Exchange-Correlation Potential," *J. Chem. Theory Comput.*, vol. 17, pp. 1390–1407, Mar. 2021.

[134] R. van Leeuwen and E. J. Baerends, "Exchange-correlation potential with correct asymptotic behavior," *Phys. Rev. A*, vol. 49, pp. 2421–2431, Apr. 1994.

[135] L. Kronik and S. Kümmel, "Piecewise linearity, freedom from self-interaction, and a Coulomb asymptotic potential: Three related yet inequivalent properties of the exact density functional," *Phys. Chem. Chem. Phys.*, vol. 22, pp. 16467–16481, July 2020.

[136] J. F. Janak, "Proof that $\frac{\partial E}{\partial n_i} = \epsilon_i$ in density-functional theory," *Phys. Rev. B*, vol. 18, pp. 7165–7168, Dec. 1978.

[137] J. P. Perdew and M. Levy, "Comment on "Significance of the highest occupied Kohn-Sham eigenvalue"," *Phys. Rev. B*, vol. 56, pp. 16021–16028, Dec. 1997.

[138] J. C. Slater and J. H. Wood, "Statistical exchange and the total energy of a crystal," *Int. J. Quantum Chem.*, vol. 5, no. S4, pp. 3–34, 1970.

[139] T. Koopmans, "Über die Zuordnung von Wellenfunktionen und Eigenwerten zu den Einzelnen Elektronen Eines Atoms," *Physica*, vol. 1, pp. 104–113, Jan. 1934.

[140] J. P. Perdew and M. Levy, "Physical Content of the Exact Kohn-Sham Orbital Energies: Band Gaps and Derivative Discontinuities," *Phys. Rev. Lett.*, vol. 51, pp. 1884–1887, Nov. 1983.

[141] L. J. Sham and M. Schlüter, "Density-Functional Theory of the Energy Gap," *Phys. Rev. Lett.*, vol. 51, pp. 1888–1891, Nov. 1983.

[142] W. Yang, A. J. Cohen, and P. Mori-Sánchez, "Derivative discontinuity, bandgap and lowest unoccupied molecular orbital in density functional theory," *J. Chem. Phys.*, vol. 136, p. 204111, May 2012.

[143] T. Gould and J. Toulouse, "Kohn-Sham potentials in exact density-functional theory at noninteger electron numbers," *Phys. Rev. A*, vol. 90, p. 050502(R), Nov. 2014.

[144] F. Cernatic, B. Senjean, V. Robert, and E. Fromager, "Ensemble Density Functional Theory of Neutral and Charged Excitations," *Top. Curr. Chem.*, vol. 380, p. 4, Nov. 2021.

[145] J. P. Perdew, "Density functional theory and the band gap problem," *Int. J. Quantum Chem.*, vol. 28, no. S19, pp. 497–523, 1985.

[146] P. Borlido, T. Aull, A. W. Huran, F. Tran, M. A. L. Marques, and S. Botti, "Large-Scale Benchmark of Exchange–Correlation Functionals for the Determination of Electronic Band Gaps of Solids," *J. Chem. Theory Comput.*, vol. 15, pp. 5069–5079, Sept. 2019.

[147] V. I. Anisimov, F. Aryasetiawan, and A. I. Lichtenstein, "First-principles calculations of the electronic structure and spectra of strongly correlated systems: The LDA+U method," *J. Phys.: Condens. Matter*, vol. 9, p. 767, Jan. 1997.

[148] N. E. Kirchner-Hall, W. Zhao, Y. Xiong, I. Timrov, and I. Dabo, "Extensive Benchmarking of DFT+U Calculations for Predicting Band Gaps," *Appl. Sci.*, vol. 11, p. 2395, Jan. 2021.

[149] W. Yang and Y. Fan, "Orbital Energies Are Chemical Potentials in Ground-State Density Functional Theory and Excited-State ΔSCF Theory," *arXiv:2408.10059*, Aug. 2024.

[150] G. Sai Gautam and E. A. Carter, "Evaluating transition metal oxides within DFT-SCAN and SCAN+U frameworks for solar thermochemical applications," *Phys. Rev. Materials*, vol. 2, p. 095401, Sept. 2018.

[151] N. Artrith, J. A. Garrido Torres, A. Urban, and M. S. Hybertsen, "Data-driven approach to parameterize SCAN+U for an accurate description of 3d transition metal oxide thermochemistry," *Phys. Rev. Mater.*, vol. 6, p. 035003, Mar. 2022.

[152] Y. Crespo and N. Seriani, "Electronic and magnetic properties of α-MnO_2 from ab initio calculations," *Phys. Rev. B*, vol. 88, p. 144428, Oct. 2013.

[153] A. Floris, S. gironcolide Gironcoli, E. K. U. Gross, and M. Cococcioni, "Vibrational properties of MnO and NiO from DFT+U-based density

functional perturbation theory," *Phys. Rev. B*, vol. 84, p. 161102, Oct. 2011.

[154] C. Franchini, R. Podloucky, J. Paier, M. Marsman, and G. Kresse, "Ground-state properties of multivalent manganese oxides: Density functional and hybrid density functional calculations," *Phys. Rev. B*, vol. 75, p. 195128, May 2007.

[155] Z. Hu and H. Metiu, "Choice of U for DFT+U Calculations for Titanium Oxides," *J. Phys. Chem. C*, vol. 115, pp. 5841–5845, Apr. 2011.

[156] A. Kiejna, T. Ossowski, and T. Pabisiak, "Surface properties of the clean and Au/Pd covered Fe_3O_4(111): DFT and DFT+U study," *Phys. Rev. B*, vol. 85, p. 125414, Mar. 2012.

[157] J. S. Lim, D. Saldana-Greco, and A. M. Rappe, "Improved pseudopotential transferability for magnetic and electronic properties of binary manganese oxides from DFT+U+J calculations," *Phys. Rev. B*, vol. 94, p. 165151, Oct. 2016.

[158] O. Y. Long, G. Sai Gautam, and E. A. Carter, "Evaluating optimal U for 3d transition-metal oxides within the SCAN+U framework," *Phys. Rev. Mater.*, vol. 4, p. 045401, Apr. 2020.

[159] A. C. M. Padilha, A. R. Rocha, and G. M. Dalpian, "DFT+U Simulation of the Ti_4O_7 - TiO_2 Interface," *Phys. Rev. Appl.*, vol. 3, p. 024009, Feb. 2015.

[160] C. Rödl, F. Fuchs, J. Furthmüller, and F. Bechstedt, "Quasiparticle band structures of the antiferromagnetic transition-metal oxides MnO, FeO, CoO, and NiO," *Phys. Rev. B*, vol. 79, p. 235114, June 2009.

[161] G. Rollmann, A. Rohrbach, P. Entel, and J. Hafner, "First-principles calculation of the structure and magnetic phases of hematite," *Phys. Rev. B*, vol. 69, p. 165107, Apr. 2004.

[162] N. Tancogne-Dejean, M. A. Sentef, and A. Rubio, "Ultrafast Modification of Hubbard U in a Strongly Correlated Material: *Ab initio* High-Harmonic Generation in NiO," *Phys. Rev. Lett.*, vol. 121, p. 097402, Aug. 2018.

[163] D. A. Tompsett, D. S. Middlemiss, and M. S. Islam, "Importance of anisotropic Coulomb interactions and exchange to the band gap and antiferromagnetism of β-MnO_2 from DFT+U," *Phys. Rev. B*, vol. 86, p. 205126, Nov. 2012.

[164] F. Zhou, M. Cococcioni, C. A. Marianetti, D. Morgan, and G. Ceder, "First-principles prediction of redox potentials in transition-metal compounds with LDA+U," *Phys. Rev. B*, vol. 70, p. 235121, Dec. 2004.

[165] J.-J. Zhou, J. Park, I. Timrov, A. Floris, M. Cococcioni, N. Marzari, and M. Bernardi, "Ab Initio Electron-Phonon Interactions in Correlated Electron Systems," *Phys. Rev. Lett.*, vol. 127, p. 126404, Sept. 2021.

[166] G. Carchini, M. García-Melchor, Z. Łodziana, and N. López, "Understanding and Tuning the Intrinsic Hydrophobicity of Rare-Earth Oxides: A DFT+U Study," *ACS Appl. Mater. Interfaces*, vol. 8, pp. 152–160, Jan. 2016.

[167] C. W. M. Castleton, J. Kullgren, and K. Hermansson, "Tuning LDA+U for electron localization and structure at oxygen vacancies in ceria," *J. Chem Phys.*, vol. 127, p. 244704, Dec. 2007.

[168] J. A. Colón Santana, J. M. An, N. Wu, K. D. Belashchenko, X. Wang, P. Liu, J. Tang, Y. Losovyj, I. N. Yakovkin, and P. A. Dowben, "Effect of gadolinium doping on the electronic band structure of europium oxide," *Phys. Rev. B*, vol. 85, p. 014406, Jan. 2012.

[169] T. Hamada and T. Ohno, "A new constraint DFT technique for self-consistent determination of U values," *J. Phys.: Condens. Matter*, vol. 31, p. 065501, Dec. 2018.

[170] M. Huang and S. Fabris, "CO Adsorption and Oxidation on Ceria Surfaces from DFT+U Calculations," *J. Phys. Chem. C*, vol. 112, pp. 8643–8648, June 2008.

[171] S. Li, Y. Li, M. Bäumer, and L. V. Moskaleva, "Assessment of PBE+U and HSE06 methods and determination of optimal parameter U for the structural and energetic properties of rare earth oxides," *J. Chem. Phys.*, vol. 153, p. 164710, Oct. 2020.

[172] A. H. Reshak, M. Piasecki, S. Auluck, I. V. Kityk, R. Khenata, B. Andriyevsky, C. Cobet, N. Esser, A. Majchrowski, M. Świrkowicz, R. Diduszko, and W. Szyrski, "Effect of U on the Electronic Properties of Neodymium Gallate ($NdGaO_3$): Theoretical and Experimental Studies," *J. Phys. Chem. B*, vol. 113, pp. 15237–15242, Nov. 2009.

[173] Z. Yang, Q. Wang, S. Wei, D. Ma, and Q. Sun, "The Effect of Environment on the Reaction of Water on the Ceria(111) Surface: A DFT+U Study," *J. Phys. Chem. C*, vol. 114, pp. 14891–14899, Sept. 2010.

[174] D. A. Scherlis, M. Cococcioni, P. Sit, and N. Marzari, "Simulation of Heme Using DFT+U: A Step toward Accurate Spin-State Energetics," *J. Phys. Chem. B*, vol. 111, pp. 7384–7391, June 2007.

[175] P. M. Panchmatia, M. E. Ali, B. Sanyal, and P. M. Oppeneer, "Halide Ligated Iron Porphines: A DFT+U and UB3LYP Study," *J. Phys. Chem. A*, vol. 114, pp. 13381–13387, Dec. 2010.

[176] P. M. Panchmatia, B. Sanyal, and P. M. Oppeneer, "GGA+U modeling of structural, electronic, and magnetic properties of iron porphyrin-type molecules," *Chem. Phys.*, vol. 343, pp. 47–60, Jan. 2008.

[177] H. J. Kulik, L. C. Blasiak, N. Marzari, and C. L. Drennan, "First-Principles Study of Non-heme Fe(II) Halogenase SyrB2 Reactivity," *J. Am. Chem. Soc.*, vol. 131, pp. 14426–14433, Oct. 2009.

[178] H. J. Kulik, M. Cococcioni, D. A. Scherlis, and N. Marzari, "Density Functional Theory in Transition-Metal Chemistry: A Self-Consistent Hubbard U Approach," *Phys. Rev. Lett.*, vol. 97, p. 103001, Sept. 2006.

[179] I. E. Brumboiu, S. Haldar, J. Lüder, O. Eriksson, H. C. Herper, B. Brena, and B. Sanyal, "Influence of Electron Correlation on the Electronic Structure and Magnetism of Transition-Metal Phthalocyanines," *J. Chem. Theory Comput.*, vol. 12, pp. 1772–1785, Apr. 2016.

[180] C. Cao, S. Hill, and H.-P. Cheng, "Strongly Correlated Electrons in the $[Ni(hmp)(ROH)X]_4$ Single Molecule Magnet: A DFT+U Study," *Phys. Rev. Lett.*, vol. 100, p. 167206, Apr. 2008.

[181] K. R. Bryenton, A. A. Adeleke, S. G. Dale, and E. R. Johnson, "Delocalization error: The greatest outstanding challenge in density-functional theory," *Wiley Interdiscip. Rev. Comput. Mol. Sci.*, vol. 13, p. e1631, 2023.

[182] P. Mori-Sánchez, A. J. Cohen, and W. Yang, "Localization and Delocalization Errors in Density Functional Theory and Implications for Band-Gap Prediction," *Phys. Rev. Lett.*, vol. 100, p. 146401, Apr. 2008.

[183] S. L. Dudarev, G. A. Botton, S. Y. Savrasov, C. J. Humphreys, and A. P. Sutton, "Electron-energy-loss spectra and the structural stability of nickel oxide: An LSDA+U study," *Phys. Rev. B*, vol. 57, pp. 1505–1509, Jan. 1998.

[184] H. J. Kulik, "Perspective: Treating electron over-delocalization with the DFT+U method," *J. Chem. Phys.*, vol. 142, p. 240901, June 2015.

[185] Q. Zhao, E. I. Ioannidis, and H. J. Kulik, "Global and local curvature in density functional theory," *J. Chem. Phys.*, vol. 145, p. 054109, Aug. 2016.

[186] A. Jain, S. P. Ong, G. Hautier, W. Chen, W. D. Richards, S. Dacek, S. Cholia, D. Gunter, D. Skinner, G. Ceder, and K. A. Persson, "Commentary: The Materials Project: A materials genome approach to accelerating materials innovation," *APL Materials*, vol. 1, p. 011002, July 2013.

[187] M. Esters, C. Oses, S. Divilov, H. Eckert, R. Friedrich, D. Hicks, M. J. Mehl, F. Rose, A. Smolyanyuk, A. Calzolari, X. Campilongo, C. Toher, and S. Curtarolo, "Aflow.org: A web ecosystem of databases, software and tools," *Comput. Mater. Sci.*, vol. 216, p. 111808, Jan. 2023.

[188] S. Kirklin, J. E. Saal, B. Meredig, A. Thompson, J. W. Doak, M. Aykol, S. Rühl, and C. Wolverton, "The Open Quantum Materials Database (OQMD): Assessing the accuracy of DFT formation energies," *npj Comput Mater*, vol. 1, pp. 1–15, Dec. 2015.

[189] X. Deng, L. Wang, X. Dai, and Z. Fang, "Local density approximation combined with Gutzwiller method for correlated electron systems: Formalism and applications," *Phys. Rev. B*, vol. 79, p. 075114, Feb. 2009.

[190] K. M. Ho, J. Schmalian, and C. Z. Wang, "Gutzwiller density functional theory for correlated electron systems," *Phys. Rev. B*, vol. 77, p. 073101, Feb. 2008.

[191] G. Wang, Y. Qian, G. Xu, X. Dai, and Z. Fang, "Gutzwiller Density Functional Studies of FeAs-Based Superconductors: Structure Optimization and Evidence for a Three-Dimensional Fermi Surface," *Phys. Rev. Lett.*, vol. 104, p. 047002, Jan. 2010.

[192] G. Kotliar, S. Y. Savrasov, K. Haule, V. S. Oudovenko, O. Parcollet, and C. A. Marianetti, "Electronic structure calculations with dynamical mean-field theory," *Rev. Mod. Phys.*, vol. 78, pp. 865–951, Aug. 2006.

[193] A. Georges, G. Kotliar, W. Krauth, and M. J. Rozenberg, "Dynamical mean-field theory of strongly correlated fermion systems and the limit of infinite dimensions," *Rev. Mod. Phys.*, vol. 68, pp. 13–125, Jan. 1996.

[194] L. F. Cugliandolo, "Recent Applications of Dynamical Mean-Field Methods," *Annu. Rev. Condens. Matter Phys.*, vol. 15, pp. 177–213, Mar. 2024.

[195] R. Schade, E. Kamil, and P. Blöchl, "Reduced density-matrix functionals from many-particle theory," *Eur. Phys. J. Spec. Top.*, vol. 226, pp. 2677–2692, July 2017.

[196] T. L. Gilbert, "Hohenberg-Kohn theorem for nonlocal external potentials," *Phys. Rev. B*, vol. 12, pp. 2111–2120, Sept. 1975.

[197] S. Kümmel and L. Kronik, "Orbital-dependent density functionals: Theory and applications," *Rev. Mod. Phys.*, vol. 80, pp. 3–60, Jan. 2008.

[198] V. I. Anisimov, J. Zaanen, and O. K. Andersen, "Band theory and Mott insulators: Hubbard U instead of Stoner I," *Phys. Rev. B*, vol. 44, pp. 943–954, July 1991.

[199] K. Terakura, T. Oguchi, A. R. Williams, and J. Kübler, "Band theory of insulating transition-metal monoxides: Band-structure calculations," *Phys. Rev. B*, vol. 30, pp. 4734–4747, Oct. 1984.

[200] V. I. Anisimov, I. V. Solovyev, M. A. Korotin, M. T. Czyżyk, and G. A. Sawatzky, "Density-functional theory and NiO photoemission spectra," *Phys. Rev. B*, vol. 48, pp. 16929–16934, Dec. 1993.

[201] M. T. Czyżyk and G. A. Sawatzky, "Local-density functional and on-site correlations: The electronic structure of La_2CuO_4 and $LaCuO_3$," *Phys. Rev. B*, vol. 49, pp. 14211–14228, May 1994.

[202] W. E. Pickett, S. C. Erwin, and E. C. Ethridge, "Reformulation of the LDA+U method for a local-orbital basis," *Phys. Rev. B*, vol. 58, pp. 1201–1209, July 1998.

[203] D.-K. Seo, "Self-interaction correction in the LDA+U method," *Phys. Rev. B*, vol. 76, p. 033102, July 2007.

[204] I. V. Solovyev, P. H. Dederichs, and V. I. Anisimov, "Corrected atomic limit in the local-density approximation and the electronic structure of d impurities in Rb," *Phys. Rev. B*, vol. 50, pp. 16861–16871, Dec. 1994.

[205] A. I. Liechtenstein, V. I. Anisimov, and J. Zaanen, "Density-functional theory and strong interactions: Orbital ordering in Mott-Hubbard insulators," *Phys. Rev. B*, vol. 52, pp. R5467–R5470, Aug. 1995.

[206] M. Ohlrich and B. J. Powell, "Fast, accurate enthalpy differences in spin crossover crystals from DFT+U," *J. Chem. Phys.*, vol. 153, p. 104107, Sept. 2020.

[207] X. Han and N. Kaltsoyannis, "Computational study of the energy landscape of water on the ThO_2 {111} surface," *J. Nucl. Mater.*, vol. 559, p. 153476, Feb. 2022.

[208] B. Dorado, G. Jomard, M. Freyss, and M. Bertolus, "Stability of oxygen point defects in UO_2 by first-principles DFT+U calculations: Occupation matrix control and Jahn-Teller distortion," *Phys. Rev. B*, vol. 82, p. 035114, July 2010.

[209] B. Dorado, M. Freyss, B. Amadon, M. Bertolus, G. Jomard, and P. Garcia, "Advances in first-principles modelling of point defects in UO_2: f-electron correlations and the issue of local energy minima," *J. Phys.: Condens. Matter*, vol. 25, p. 333201, July 2013.

[210] R. Qiu, "Circumventing the Metastable States within DFT+U through Random Orbital-Dependent Local Perturbation," *J. Chem. Theory Comput.*, Jan. 2025.

[211] E. Bousquet and N. Spaldin, "J dependence in the LSDA+U treatment of noncollinear magnets," *Phys. Rev. B*, vol. 82, p. 220402, Dec. 2010.

[212] H. Nakamura, N. Hayashi, N. Nakai, M. Okumura, and M. Machida, "First-principle electronic structure calculations for magnetic moment in iron-based superconductors: An LSDA+negative U study," *Phys. C: Supercond.*, vol. 469, pp. 908–911, Oct. 2009.

[213] A. G. Petukhov, I. I. Mazin, L. Chioncel, and A. I. Lichtenstein, "Correlated metals and the LDA+U method," *Phys. Rev. B*, vol. 67, p. 153106, Apr. 2003.

[214] B. Himmetoglu, R. M. Wentzcovitch, and M. Cococcioni, "First-principles study of electronic and structural properties of CuO," *Phys. Rev. B*, vol. 84, p. 115108, Sept. 2011.

[215] M. Shishkin and H. Sato, "DFT+U in Dudarev's formulation with corrected interactions between the electrons with opposite spins: The form of Hamiltonian, calculation of forces, and bandgap adjustments," *J. Chem. Phys.*, vol. 151, p. 024102, July 2019.

[216] M. Shishkin and H. Sato, "Evaluation of redox potentials of cathode materials of alkali-ion batteries using extended DFT+U+$U_{\uparrow\downarrow}$ method: The role of interactions between the electrons with opposite spins," *J. Chem. Phys.*, vol. 154, p. 114709, Mar. 2021.

[217] V. L. Campo and M. Cococcioni, "Extended DFT+U+V method with on-site and inter-site electronic interactions," *J. Phys.: Condens. Matter*, vol. 22, p. 055602, Jan. 2010.

[218] R. Mahajan, I. Timrov, N. Marzari, and A. Kashyap, "Importance of intersite Hubbard interactions in β-MnO_2 : A first-principles DFT+U+V study," *Phys. Rev. Materials*, vol. 5, p. 104402, Oct. 2021.

[219] I. Timrov, F. Aquilante, M. Cococcioni, and N. Marzari, "Accurate Electronic Properties and Intercalation Voltages of Olivine-Type Li-Ion Cathode Materials from Extended Hubbard Functionals," *PRX Energy*, vol. 1, p. 033003, Oct. 2022.

[220] S. L. Dudarev, P. Liu, D. A. Andersson, C. R. Stanek, T. Ozaki, and C. Franchini, "Parametrization of LSDA+U for noncollinear magnetic configurations: Multipolar magnetism in UO_2," *Phys. Rev. Materials*, vol. 3, p. 083802, Aug. 2019.

[221] S. M. Griffin, "Origin of correlated isolated flat bands in copper-substituted lead phosphate apatite," vol. arXiv:2307.16892, Aug. 2023.

[222] L. Wang, T. Maxisch, and G. Ceder, "Oxidation energies of transition metal oxides within the GGA+U framework," *Phys. Rev. B*, vol. 73, p. 195107, May 2006.

[223] P. H. Dederichs, S. Blügel, R. Zeller, and H. Akai, "Ground States of Constrained Systems: Application to Cerium Impurities," *Phys. Rev. Lett.*, vol. 53, pp. 2512–2515, Dec. 1984.

[224] I. V. Solovyev and P. H. Dederichs, "*Ab Initio* calculations of Coulomb U parameters for transition-metal impurities," *Phys. Rev. B*, vol. 49, pp. 6736–6740, Mar. 1994.

[225] V. I. Anisimov and O. Gunnarsson, "Density-functional calculation of effective Coulomb inte ractions in metals," *Phys. Rev. B*, vol. 43, pp. 7570–7574, Apr. 1991.

[226] A. K. McMahan, R. M. Martin, and S. Satpathy, "Calculated effective Hamiltonian for La_2CuO_4 and solution in the impurity Anderson approximation," *Phys. Rev. B*, vol. 38, pp. 6650–6666, Oct. 1988.

[227] O. Gunnarsson, O. K. Andersen, O. Jepsen, and J. Zaanen, "Density-functional calculation of the parameters in the Anderson model: Application to Mn in CdTe," *Phys. Rev. B*, vol. 39, pp. 1708–1722, Jan. 1989.

[228] M. S. Hybertsen, M. Schlüter, and N. E. Christense n, "Calculation of Coulomb-interaction parameters for La_2CuO_4 using a constrained-density-functional approach," *Phys. Rev. B*, vol. 39, pp. 9028–9041, May 1989.

[229] M. Springer and F. Aryasetiawan, "Frequency-dependent screened interaction in Ni within the random-phase approximation," *Phys. Rev. B*, vol. 57, pp. 4364–4368, Feb. 1998.

[230] T. Kotani, "Ab initio random-phase-approximation calculation of the frequency-dependent effective interaction between 3d electrons: Ni, Fe, and MnO," *J. Phys.: Condens. Matter*, vol. 12, p. 2413, Mar. 2000.

[231] F. Aryasetiawan, M. Imada, A. Georges, G. Kotliar, S. Biermann, and A. I. Lichtenstein, "Frequency-dependent local interactions and low-energy effective models from electronic structure calculations," *Phys. Rev. B*, vol. 70, p. 195104, Nov. 2004.

[232] F. Aryasetiawan, K. Karlsson, O. Jepsen, and U. Schönberger, "Calculations of Hubbard U from first-principles," *Phys. Rev. B*, vol. 74, p. 125106, Sept. 2006.

[233] E. Şaşıoğlu, C. Friedrich, and S. Blügel, "Effective Coulomb interaction in transition metals from constrained random-phase approximation," *Phys. Rev. B*, vol. 83, p. 121101, Mar. 2011.

[234] L. Vaugier, H. Jiang, and S. Biermann, "Hubbard U and Hund exchange J in transition metal oxides: Screening versus localization trends from constrained random phase approximation," *Phys. Rev. B*, vol. 86, p. 165105, Oct. 2012.

[235] B. Amadon, T. Applencourt, and F. Bruneval, "Screened Coulomb interaction calculations: cRPA implementation and applications to dynamical screening and self-consistency in uranium dioxide and cerium," *Phys. Rev. B*, vol. 89, p. 125110, Mar. 2014.

[236] N. J. Mosey and E. A. Carter, "Ab initio evaluation of Coulomb and exchange parameters for DFT+U calculations," *Phys. Rev. B*, vol. 76, p. 155123, Oct. 2007.

[237] N. J. Mosey, P. Liao, and E. A. Carter, "Rotationally invariant ab initio evaluation of Coulomb and exchange parameters for DFT+U calculations," *J. Chem. Phys.*, vol. 129, p. 014103, July 2008.

[238] I. Timrov, N. Marzari, and M. Cococcioni, "Hubbard parameters from density-functional perturbation theory," *Phys. Rev. B*, vol. 98, p. 085127, Aug. 2018.

[239] I. Timrov, N. Marzari, and M. Cococcioni, "Self-consistent Hubbard parameters from density-functional perturbation theory in the ultrasoft and projector-augmented wave formulations," *Phys. Rev. B*, vol. 103, p. 045141, Jan. 2021.

[240] M. Cococcioni and S. de Gironcoli, "Linear response approach to the calculation of the effective interaction parameters in the LDA+U method," *Phys. Rev. B*, vol. 71, p. 035105, Jan. 2005.

[241] D. S. Lambert and D. D. O'Regan, "Use of DFT+U + J with linear response parameters to predict non-magnetic oxide band gaps with hybrid-functional accuracy," *Phys. Rev. Res.*, vol. 5, p. 013160, Mar. 2023.

[242] E. B. Linscott, D. J. Cole, M. C. Payne, and D. D. O'Regan, "Role of spin in the calculation of Hubbard U and Hund's J parameters from first principles," *Phys. Rev. B*, vol. 98, p. 235157, Dec. 2018.

[243] G. Moynihan, G. Teobaldi, and D. D. O'Regan, "A self-consistent ground-state formulation of the first-principles Hubbard U parameter validated on one-electron self-interaction error," *arXiv:1704.08076*, Apr. 2017.

[244] O. K. Orhan and D. D. O'Regan, "First-principles Hubbard U and Hund's J corrected approximate density functional theory predicts an accurate fundamental gap in rutile and anatase TiO_2," *Phys. Rev. B*, vol. 101, p. 245137, June 2020.

[245] S. Berman, A. Zhussupbekova, J. E. Boschker, J. Schwarzkopf, D. D. O'Regan, I. V. Shvets, and K. Zhussupbekov, "Reconciling the theoretical and experimental electronic structure of NbO_2," *Phys. Rev. B*, vol. 108, p. 155141, Oct. 2023.

[246] C. Herring, *Magnetism: Exchange interactions among itinerant electrons*. Academic Press, 1966.

[247] I. Dabo, A. Ferretti, N. Poilvert, Y. Li, N. Marzari, and M. Cococcioni, "Koopmans' condition for density-functional theory," *Phys. Rev. B*, vol. 82, p. 115121, Sept. 2010.

[248] G. Borghi, A. Ferretti, N. L. Nguyen, I. Dabo, and N. Marzari, "Koopmans-compliant functionals and their performance against reference molecular data," *Phys. Rev. B*, vol. 90, p. 075135, Aug. 2014.

[249] N. Colonna, R. De Gennaro, E. Linscott, and N. Marzari, "Koopmans Spectral Functionals in Periodic Boundary Conditions," *J. Chem. Theory Comput.*, vol. 18, pp. 5435–5448, Sept. 2022.

[250] E. B. Linscott, N. Colonna, R. De Gennaro, N. L. Nguyen, G. Borghi, A. Ferretti, I. Dabo, and N. Marzari, "Koopmans: An Open-Source Package for Accurately and Efficiently Predicting Spectral Properties with Koopmans Functionals," *J. Chem. Theory Comput.*, vol. 19, pp. 7097–7111, Oct. 2023.

[251] N. Colonna, N. L. Nguyen, A. Ferretti, and N. Marzari, "Koopmans-Compliant Functionals and Potentials and Their Application to the GW100 Test Set," *J. Chem. Theory Comput.*, vol. 15, pp. 1905–1914, Mar. 2019.

[252] J. M. almeidade Almeida, N. L. Nguyen, N. Colonna, W. Chen, C. Rodrigues Miranda, A. Pasquarello, and N. Marzari, "Electronic Structure of Water from Koopmans-Compliant Functionals," *J. Chem. Theory Comput.*, vol. 17, pp. 3923–3930, July 2021.

[253] N. L. Nguyen, N. Colonna, A. Ferretti, and N. Marzari, "Koopmans-Compliant Spectral Functionals for Extended Systems," *Phys. Rev. X*, vol. 8, p. 021051, May 2018.

[254] W. E. Pickett, "Pseudopotential methods in condensed matter applications," *Comput. Phys. Rep.*, vol. 9, pp. 115–197, Apr. 1989.

[255] V. Heine, "The Pseudopotential Concept," in *Solid State Physics*, vol. 24, pp. 1–36, Academic Press, Jan. 1970.

[256] K. F. Garrity, J. W. Bennett, K. M. Rabe, and D. Vanderbilt, "Pseudopotentials for high-throughput DFT calculations," *Comput. Mater. Sci.*, vol. 81, pp. 446–452, Jan. 2014.

[257] D. R. Hamann, M. Schlüter, and C. Chiang, "Norm-Conserving Pseudopotentials," *Phys. Rev. Lett.*, vol. 43, pp. 1494–1497, Nov. 1979.

[258] D. Vanderbilt, "Soft self-consistent pseudopotentials in a generalized eigenvalue formalism," *Phys. Rev. B*, vol. 41, pp. 7892–7895, Apr. 1990.

[259] P. E. Blöchl, "Projector augmented-wave method," *Phys. Rev. B*, vol. 50, pp. 17953–17979, Dec. 1994.

[260] G. Kresse and D. Joubert, "From ultrasoft pseudopotentials to the projector augmented-wave method," *Phys. Rev. B*, vol. 59, pp. 1758–1775, Jan. 1999.

[261] G. P. Kerker, "Non-singular atomic pseudopotentials for solid state applications," *J. Phys. C: Solid State Phys.*, vol. 13, p. L189, Mar. 1980.

[262] N. Troullier and J. L. Martins, "Efficient pseudopotentials for plane-wave calculations," *Phys. Rev. B*, vol. 43, pp. 1993–2006, Jan. 1991.

[263] A. M. Rappe, K. M. Rabe, E. Kaxiras, and J. D. Joannopoulos, "Optimized pseudopotentials," *Phys. Rev. B*, vol. 41, pp. 1227–1230, Jan. 1990.

[264] L. Kleinman and D. M. Bylander, "Efficacious Form for Model Pseudopotentials," *Phys. Rev. Lett.*, vol. 48, pp. 1425–1428, May 1982.

[265] G. Kresse and J. Furthmüller, "Efficient iterative schemes for ab initio total-energy calculations using a plane-wave basis set," *Phys. Rev. B*, vol. 54, pp. 11169–11186, Oct. 1996.

[266] S. J. Clark, M. D. Segall, C. J. Pickard, P. J. Hasnip, M. I. J. Probert, K. Refson, and M. C. Payne, "First principles methods using CASTEP," *Z. Für Krist. - Cryst. Mater.*, vol. 220, pp. 567–570, May 2005.

[267] P. Giannozzi, O. Andreussi, T. Brumme, O. Bunau, M. B. Nardelli, M. Calandra, R. Car, C. Cavazzoni, D. Ceresoli, M. Cococcioni, N. Colonna, I. Carnimeo, A. D. Corso, S. de Gironcoli, P. Delugas, R. A. DiStasio, A. Ferretti, A. Floris, G. Fratesi, G. Fugallo, R. Gebauer, U. Gerstmann, F. Giustino, T. Gorni, J. Jia, M. Kawamura, H.-Y. Ko, A. Kokalj, E. Küçükbenli, M. Lazzeri, M. Marsili, N. Marzari, F. Mauri, N. L. Nguyen, H.-V. Nguyen, A. Otero-de-la-Roza, L. Paulatto, S. Poncé, D. Rocca, R. Sabatini, B. Santra, M. Schlipf, A. P. Seitsonen, A. Smogunov, I. Timrov, T. Thonhauser, P. Umari, N. Vast, X. Wu, and

S. Baroni, "Advanced capabilities for materials modelling with Quantum ESPRESSO," *J. Phys.: Condens. Matter*, vol. 29, p. 465901, Oct. 2017.

[268] T. D. Kühne, M. Iannuzzi, M. Del Ben, V. V. Rybkin, P. Seewald, F. Stein, T. Laino, R. Z. Khaliullin, O. Schütt, F. Schiffmann, D. Golze, J. Wilhelm, S. Chulkov, M. H. Bani-Hashemian, V. Weber, U. Borštnik, M. Taillefumier, A. S. Jakobovits, A. Lazzaro, H. Pabst, T. Müller, R. Schade, M. Guidon, S. Andermatt, N. Holmberg, G. K. Schenter, A. Hehn, A. Bussy, F. Belleflamme, G. Tabacchi, A. Glöß, M. Lass, I. Bethune, C. J. Mundy, C. Plessl, M. Watkins, J. VandeVondele, M. Krack, and J. Hutter, "CP2K: An electronic structure and molecular dynamics software package - Quickstep: Efficient and accurate electronic structure calculations," *J. Chem. Phys.*, vol. 152, p. 194103, May 2020.

[269] G. te Velde, F. M. Bickelhaupt, E. J. Baerends, C. Fonseca Guerra, S. J. A. van Gisbergen, J. G. Snijders, and T. Ziegler, "Chemistry with ADF," *J. Comput. Chem.*, vol. 22, no. 9, pp. 931–967, 2001.

[270] P. Blaha, K. Schwarz, G. K. Madsen, D. Kvasnicka, J. Luitz, *et al.*, "wien2k, An augmented plane wave+local orbitals program for calculating crystal properties," vol. 60, no. 1, 2001.

[271] E. Artacho, E. Anglada, O. Diéguez, J. D. Gale, A. García, J. Junquera, R. M. Martin, P. Ordejón, J. M. Pruneda, D. Sánchez-Portal, and J. M. Soler, "The SIESTA method; developments and applicability," *J. Phys.: Condens. Matter*, vol. 20, p. 064208, Jan. 2008.

[272] B. Delley, "From molecules to solids with the DMol3 approach," *J. Chem. Phys.*, vol. 113, pp. 7756–7764, Nov. 2000.

[273] X. Gonze, B. Amadon, P. M. Anglade, J. M. Beuken, F. Bottin, P. Boulanger, F. Bruneval, D. Caliste, R. Caracas, M. Côté, T. Deutsch, L. Genovese, Ph. Ghosez, M. Giantomassi, S. Goedecker, D. R. Hamann, P. Hermet, F. Jollet, G. Jomard, S. Leroux, M. Mancini, S. Mazevet, M. J. T. Oliveira, G. Onida, Y. Pouillon, T. Rangel, G. M. Rignanese, D. Sangalli, R. Shaltaf, M. Torrent, M. J. Verstraete, G. Zerah, and J. W. Zwanziger, "ABINIT: First-principles approach to material and nanosystem properties," *Comput. Phys. Commun.*, vol. 180, pp. 2582–2615, Dec. 2009.

[274] "The Elk Code: See http://elk.sourceforge.net/ for The Elk Code."

[275] J. J. Mortensen, A. H. Larsen, M. Kuisma, A. V. Ivanov, A. Taghizadeh, A. Peterson, A. Haldar, A. O. Dohn, C. Schäfer, E. Ö. Jónsson, E. D. Hermes, F. A. Nilsson, G. Kastlunger, G. Levi, H. Jónsson, H. Häkkinen, J. Fojt, J. Kangsabanik, J. Sødequist, J. Lehtomäki, J. Heske, J. Enkovaara, K. T. Winther, M. Dulak, M. M. Melander, M. Ovesen, M. Louhivuori, M. Walter, M. Gjerding, O. Lopez-Acevedo, P. Erhart, R. Warmbier, R. Würdemann, S. Kaappa, S. Latini, T. M. Boland, T. Bligaard, T. Skovhus, T. Susi, T. Maxson, T. Rossi, X. Chen, Y. L. A. Schmerwitz, J. Schiøtz, T. Olsen, K. W. Jacobsen, and K. S. Thygesen, "GPAW: An open Python package for electronic structure calculations," *J. Chem. Phys.*, vol. 160, p. 092503, Mar. 2024.

[276] A. Nakata, J. S. Baker, S. Y. Mujahed, J. T. L. Poulton, S. Arapan, J. Lin, Z. Raza, S. Yadav, L. Truflandier, T. Miyazaki, and D. R. Bowler, "Large scale and linear scaling DFT with the CONQUEST code," *J. Chem. Phys.*, vol. 152, p. 164112, Apr. 2020.

[277] V. Blum, R. Gehrke, F. Hanke, P. Havu, V. Havu, X. Ren, K. Reuter, and M. Scheffler, "*Ab Initio* molecular simulations with numeric atom-centered orbitals," *Comput. Phys. Commun.*, vol. 180, pp. 2175–2196, Nov. 2009.

[278] N. Tancogne-Dejean, M. J. T. Oliveira, X. Andrade, H. Appel, C. H. Borca, G. Le Breton, F. Buchholz, A. Castro, S. Corni, A. A. Correa, U. De Giovannini, A. Delgado, F. G. Eich, J. Flick, G. Gil, A. Gomez, N. Helbig, H. Hübener, R. Jestädt, J. Jornet-Somoza, A. H. Larsen, I. V. Lebedeva, M. Lüders, M. A. L. Marques, S. T. Ohlmann, S. Pipolo, M. Rampp, C. A. Rozzi, D. A. Strubbe, S. A. Sato, C. Schäfer, I. Theophilou, A. Welden, and A. Rubio, "Octopus, a computational framework for exploring light-driven phenomena and quantum dynamics in extended and finite systems," *J. Chem. Phys.*, vol. 152, p. 124119, Mar. 2020.

[279] "The FLEUR project." `https://www.flapw.de/`.

[280] K. Koepernik and H. Eschrig, "Full-potential nonorthogonal local-orbital minimum-basis band-structure scheme," *Phys. Rev. B*, vol. 59, pp. 1743–1757, Jan. 1999.

[281] J. C. A. Prentice, J. Aarons, J. C. Womack, A. E. A. Allen, L. Andrinopoulos, L. Anton, R. A. Bell, A. Bhandari, G. A. Bramley, R. J. Charlton, R. J. Clements, D. J. Cole, G. Constantinescu, F. Corsetti, S. M.-M. Dubois, K. K. B. Duff, J. M. Escartín, A. Greco, Q. Hill, L. P. Lee, E. Linscott, D. D. O'Regan, M. J. S. Phipps, L. E. Ratcliff, Á. R. Serrano, E. W. Tait, G. Teobaldi, V. Vitale, N. Yeung, T. J. Zuehlsdorff, J. Dziedzic, P. D. Haynes, N. D. M. Hine, A. A. Mostofi, M. C. Payne, and C.-K. Skylaris, "The ONETEP linear-scaling density functional theory program," *J. Chem. Phys.*, vol. 152, p. 174111, May 2020.

[282] G. Geudtner, P. Calaminici, J. Carmona-Espíndola, J. M. del Campo, V. D. Domínguez-Soria, R. F. Moreno, G. U. Gamboa, A. Goursot, A. M. Köster, J. U. Reveles, T. Mineva, J. M. Vásquez-Pérez, A. Vela, B. Zúñinga-Gutierrez, and D. R. Salahub, "deMon2k," *WIREs Comput. Mol. Sci.*, vol. 2, no. 4, pp. 548–555, 2012.

[283] J. M. Wills, M. Alouani, P. Andersson, A. Delin, O. Eriksson, and O. Grechnyev, *Full-Potential Electronic Structure Method: Energy and Force Calculations with Density Functional and Dynamical Mean Field Theory*. Springer Science & Business Media, Dec. 2010.

[284] L. E. Ratcliff, W. Dawson, G. Fisicaro, D. Caliste, S. Mohr, A. Degomme, B. Videau, V. Cristiglio, M. Stella, M. D'Alessandro, S. Goedecker, T. Nakajima, T. Deutsch, and L. Genovese, "Flexibilities of wavelets as a computational basis set for large-scale electronic structure calculations," *J. Chem. Phys.*, vol. 152, no. 19, p. 194110, 2020.

[285] R. Sundararaman, K. Letchworth-Weaver, K. A. Schwarz, D. Gunceler, Y. Ozhabes, and T. A. Arias, "JDFTx: Software for joint density-functional theory," *SoftwareX*, vol. 6, pp. 278–284, Jan. 2017.

[286] P. R. Briddon and M. J. Rayson, "Accurate Kohn–Sham DFT with the speed of tight binding: Current techniques and future directions in materials modelling," *Phys. Status Solidi B*, vol. 248, no. 6, pp. 1309–1318, 2011.

[287] P. Motamarri, S. Das, S. Rudraraju, K. Ghosh, D. Davydov, and V. Gavini, "DFT-FE – A massively parallel adaptive finite-element code

for large-scale density functional theory calculations," *Comput. Phys. Commun.*, vol. 246, p. 106853, Jan. 2020.

[288] M. F. Herbst, A. Levitt, and E. Cancès, "Dftk: A julian approach for simulating electrons in solids," *Proc. JuliaCon Conf.*, vol. 3, p. 69, 2021.

[289] S. Ono, Y. Noguchi, R. Sahara, Y. Kawazoe, and K. Ohno, "TOMBO: All-electron mixed-basis approach to condensed matter physics," *Comput. Phys. Commun.*, vol. 189, pp. 20–30, Apr. 2015.

[290] P. Schulz and R. Muller, "QUantum Electronic STructure (SeqQuest Electronic Structure Code)," *Sandia National Laboratories, Albuquerque (NM)*, 2004.

[291] "The JuKKR code package." `ttps://jukkr.fz-juelich.de`.

[292] R. Dovesi, F. Pascale, B. Civalleri, K. Doll, N. M. Harrison, I. Bush, P. D'Arco, Y. Noël, M. Rérat, P. Carbonnière, M. Causà, S. Salustro, V. Lacivita, B. Kirtman, A. M. Ferrari, F. S. Gentile, J. Baima, M. Ferrero, R. Demichelis, and M. De La Pierre, "The CRYSTAL code, 1976–2020 and beyond, a long story," *J. Chem. Phys.*, vol. 152, p. 204111, May 2020.

[293] M. J. Frisch, G. W. Trucks, H. B. Schlegel, G. E. Scuseria, M. A. Robb, J. R. Cheeseman, G. Scalmani, V. Barone, G. A. Petersson, H. Nakatsuji, X. Li, M. Caricato, A. V. Marenich, J. Bloino, B. G. Janesko, R. Gomperts, B. Mennucci, H. P. Hratchian, J. V. Ortiz, A. F. Izmaylov, J. L. Sonnenberg, D. Williams-Young, F. Ding, F. Lipparini, F. Egidi, J. Goings, B. Peng, A. Petrone, T. Henderson, D. Ranasinghe, V. G. Zakrzewski, J. Gao, N. Rega, G. Zheng, W. Liang, M. Hada, M. Ehara, K. Toyota, R. Fukuda, J. Hasegawa, M. Ishida, T. Nakajima, Y. Honda, O. Kitao, H. Nakai, T. Vreven, K. Throssell, J. A. Montgomery, Jr., J. E. Peralta, F. Ogliaro, M. J. Bearpark, J. J. Heyd, E. N. Brothers, K. N. Kudin, V. N. Staroverov, T. A. Keith, R. Kobayashi, J. Normand, K. Raghavachari, A. P. Rendell, J. C. Burant, S. S. Iyengar, J. Tomasi, M. Cossi, J. M. Millam, M. Klene, C. Adamo, R. Cammi, J. W. Ochterski, R. L. Martin, K. Morokuma, O. Farkas, J. B. Foresman, and D. J. Fox, "Gaussian 16," 2016. Gaussian Inc. Wallingford CT.

[294] C.-K. Skylaris, P. D. Haynes, A. A. Mostofi, and M. C. Payne, "Introducing ONETEP: Linear-scaling density functional simulations on parallel computers," *J. Chem. Phys.*, vol. 122, p. 084119, Feb. 2005.

[295] C.-K. Skylaris, A. A. Mostofi, P. D. Haynes, O. Diéguez, and M. C. Payne, "Nonorthogonal generalized Wannier function pseudopotential plane-wave method," *Phys. Rev. B*, vol. 66, p. 035119, July 2002.

[296] D. D. O'Regan, N. D. M. Hine, M. C. Payne, and A. A. Mostofi, "Linear-scaling DFT+U with full local orbital optimization," *Phys. Rev. B*, vol. 85, p. 085107, Feb. 2012.

[297] E. Prodan and W. Kohn, "Nearsightedness of electronic matter," *Proc. Natl. Acad. Sci.*, vol. 102, pp. 11635–11638, Aug. 2005.

[298] C. Brouder, G. Panati, M. Calandra, C. Mourougane, and N. Marzari, "Exponential Localization of Wannier Functions in Insulators," *Phys. Rev. Lett.*, vol. 98, p. 046402, Jan. 2007.

[299] G. J. Martyna and M. E. Tuckerman, "A reciprocal space based method for treating long range interactions in ab initio and force-field-based calculations in clusters," *J. Chem. Phys.*, vol. 110, pp. 2810–2821, Feb. 1999.

[300] R. M. Dreizler and E. K. U. Gross, *Density Functional Theory: An Approach to the Quantum Many-Body Problem*. Springer Science & Business Media, Dec. 2012.

[301] R. G. Parr and W. Yang, *Density-Functional Theory of Atoms and Molecules*.

[302] P. Geerlings, E. Chamorro, P. K. Chattaraj, F. De Proft, J. L. Gázquez, S. Liu, C. Morell, A. Toro-Labbé, A. Vela, and P. Ayers, "Conceptual density functional theory: Status, prospects, issues," *Theor Chem Acc*, vol. 139, p. 36, Jan. 2020.

[303] W. Yang, A. J. Cohen, F. De Proft, and P. Geerlings, "Analytical evaluation of Fukui functions and real-space linear response function," *J. Chem. Phys.*, vol. 136, p. 144110, Apr. 2012.

[304] D. Peng and W. Yang, "Fukui function and response function for nonlocal and fractional systems," *J. Chem. Phys.*, vol. 138, p. 184108, May 2013.

[305] A. C. Burgess, E. Linscott, and D. D. O'Regan, "Tilted-Plane Structure of the Energy of Finite Quantum Systems," *Phys. Rev. Lett.*, vol. 133, p. 026404, July 2024.

[306] C. R. Jacob and M. Reiher, "Spin in density-functional theory," *Int. J. Quantum Chem.*, vol. 112, no. 23, pp. 3661–3684, 2012.

[307] H. G. A. Burton, C. Marut, T. J. Daas, P. Gori-Giorgi, and P.-F. Loos, "Variations of the Hartree–Fock fractional-spin error for one electron," *J. Chem. Phys.*, vol. 155, p. 054107, Aug. 2021.

[308] M. Levy, J. S. M. Anderson, F. H. Zadeh, and P. W. Ayers, "Kinetic and electron-electron energies for convex sums of ground state densities with degeneracies and fractional electron number," *J. Chem. Phys.*, vol. 140, p. 18A538, May 2014.

[309] P. W. Ayers and M. Levy, "Tight constraints on the exchange-correlation potentials of degenerate states," *J. Chem. Phys.*, vol. 140, p. 18A537, May 2014.

[310] A. Gonis, X. G. Zhang, D. M. Nicholson, and G. M. Stocks, "Energy convexity as a consequence of decoherence and pair-extensive interactions in many-electron systems," *J. Phys. Chem. Solids*, vol. 75, pp. 680–687, May 2014.

[311] A. Gonis, X.-G. Zhang, D. M. Nicholson, and G. M. Stocks, "Antisymmetric wave functions for mixed fermion states and energy convexity," *Phys. Rev. B*, vol. 84, p. 045121, July 2011.

[312] A. Gonis, X.-G. Zhang, D. Nicholson, and G. Stocks, "Self-entanglement and the dissociation of homonuclear diatomic molecules," *Mol. Phys.*, vol. 112, pp. 453–461, Feb. 2014.

[313] C. Li, X. Zheng, N. Q. Su, and W. Yang, "Localized orbital scaling correction for systematic elimination of delocalization error in density functional approximations," *National Science Review*, vol. 5, pp. 203–215, Mar. 2018.

[314] A. Mahler, J. Williams, N. Q. Su, and W. Yang, "Localized orbital scaling correction for periodic systems," *Phys. Rev. B*, vol. 106, p. 035147, July 2022.

[315] S. Refaely-Abramson, R. Baer, and L. Kronik, "Fundamental and excitation gaps in molecules of relevance for organic photovoltaics from an optimally tuned range-separated hybrid functional," *Phys. Rev. B*, vol. 84, p. 075144, Aug. 2011.

[316] A. Kramida, Yu. Ralchenko, J. Reader, and NIST ASD Team. NIST Atomic Spectra Database (ver. 5.10), [Online]. Available: `https://physics.nist.gov/asd` [2023, July 7]. National Institute of Standards and Technology, Gaithersburg, MD., 2022.

[317] X.-K. Ma and Y. Liu, "Supramolecular Purely Organic Room-Temperature Phosphorescence," *Acc. Chem. Res.*, vol. 54, pp. 3403–3414, Sept. 2021.

[318] W. Ye, H. Ma, H. Shi, H. Wang, A. Lv, L. Bian, M. Zhang, C. Ma, K. Ling, M. Gu, Y. Mao, X. Yao, C. Gao, K. Shen, W. Jia, J. Zhi, S. Cai, Z. Song, J. Li, Y. Zhang, S. Lu, K. Liu, C. Dong, Q. Wang, Y. Zhou, W. Yao, Y. Zhang, H. Zhang, Z. Zhang, X. Hang, Z. An, X. Liu, and W. Huang, "Confining isolated chromophores for highly efficient blue phosphorescence," *Nat. Mater.*, vol. 20, pp. 1539–1544, Nov. 2021.

[319] Z. Yang, Z. Mao, Z. Xie, Y. Zhang, S. Liu, J. Zhao, J. Xu, Z. Chi, and M. P. Aldred, "Recent advances in organic thermally activated delayed fluorescence materials," *Chem. Soc. Rev.*, vol. 46, no. 3, pp. 915–1016, 2017.

[320] M. Amy Bryden and E. Zysman-Colman, "Organic thermally activated delayed fluorescence (TADF) compounds used in photocatalysis," *Chem. Soc. Rev.*, vol. 50, no. 13, pp. 7587–7680, 2021.

[321] M. B. Smith and J. Michl, "Singlet Fission," *Chem. Rev.*, vol. 110, pp. 6891–6936, Nov. 2010.

[322] P. J. Budden, L. R. Weiss, M. Müller, N. A. Panjwani, S. Dowland, J. R. Allardice, M. Ganschow, J. Freudenberg, J. Behrends, U. H. F.

Bunz, and R. H. Friend, "Singlet exciton fission in a modified acene with improved stability and high photoluminescence yield," *Nat. Commun.*, vol. 12, p. 1527, Mar. 2021.

[323] R. Sabatini, T. Gorni, and S. de Gironcoli, "Nonlocal van der Waals density functional made simple and efficient," *Phys. Rev. B*, vol. 87, p. 041108, Jan. 2013.

[324] M. Bernardi, "Physical origin of the one-quarter exact exchange in density functional theory," *J. Phys.: Condens. Matter*, vol. 32, p. 385501, June 2020.

[325] P. Giannozzi, S. Baroni, N. Bonini, M. Calandra, R. Car, C. Cavazzoni, D. Ceresoli, G. L. Chiaro tti, M. Cococcioni, I. Dabo, A. D. Corso, S. de Gironcoli, S. Fabris, G. Fratesi, R. p. Gebauer, U. Gerstmann, C. Gougoussis, A. Kokalj, M. Lazzeri, L. Martin-Samos, N. Marzari, F. Mauri, R. M azzarello, S. Paolini, A. Pasquarello, L. Paulatto, C. Sbraccia, S. Scandolo, G. Sclauzero, A. S eitsonen, Ari P. an d Smogunov, P. Umari, and R. M. Wentzcovitch, "QUANTUM ESPRESSO: A modular and open-source software project for quantum simulations of materials," *J. Phys.: Condens. Matter*, vol. 21, p. 395502, Sept. 2009.

[326] D. R. Hamann, "Optimized norm-conserving Vanderbilt pseudopotentials," *Phys. Rev. B*, vol. 88, p. 085117, Aug. 2013.

[327] K. Capelle, G. Vignale, and C. A. Ullrich, "Spin gaps and spin-flip energies in density-functional theory," *Phys. Rev. B*, vol. 81, p. 125114, Mar. 2010.

[328] O. V. Gritsenko and E. J. Baerends, "The analog of Koopmans' theorem in spin-density functional theory," *J. Chem. Phys.*, vol. 117, pp. 9154–9159, Nov. 2002.

[329] O. V. Gritsenko and E. J. Baerends, "The spin-unrestricted molecular Kohn–Sham solution and the analogue of Koopmans's theorem for open-shell molecules," *J. Chem. Phys.*, vol. 120, pp. 8364–8372, Apr. 2004.

[330] T. Gál, P. W. Ayers, F. De Proft, and P. Geerlings, "Nonuniqueness of magnetic fields and energy derivatives in spin-polarized density functional theory," *J. Chem. Phys.*, vol. 131, p. 154114, Oct. 2009.

[331] A. C. Burgess, E. Linscott, and D. D. O'Regan, "DFT+U-type functional derived to explicitly address the flat plane condition," *Phys. Rev. B*, vol. 107, p. L121115, Mar. 2023.

[332] F. Ruipérez, J. M. Ugalde, and I. Infante, "Electronic Structure and Bonding in Heteronuclear Dimers of V, Cr, Mo, and W: A CASSCF/CASPT2 Study," *Inorg. Chem.*, vol. 50, pp. 9219–9229, Oct. 2011.

[333] J. Hubbard, "Electron Correlations in Narrow Energy Bands," *Proc. R. Soc. Lond. Ser. Math. Phys. Sci.*, vol. 276, no. 1365, pp. 238–257, 1963.

[334] F. Flores, D. Soler-Polo, and J. Ortega, "A closed local-orbital unified description of DFT and many-body effects," *J. Phys.: Condens. Matter*, vol. 34, p. 304006, May 2022.

[335] H. Park, A. J. Millis, and C. A. Marianetti, "Density functional versus spin-density functional and the choice of correlated subspace in multivariable effective action theories of electronic structure," *Phys. Rev. B*, vol. 92, p. 035146, July 2015.

[336] E. R. Ylvisaker, W. E. Pickett, and K. Koepernik, "Anisotropy and magnetism in the LSDA+U method," *Phys. Rev. B*, vol. 79, p. 035103, Jan. 2009.

[337] S. Ryee and M. J. Han, "The effect of double counting, spin density, and Hund interaction in the different DFT+U functionals," *Sci Rep*, vol. 8, p. 9559, June 2018.

[338] G. C. Moore, M. K. Horton, E. Linscott, A. M. Ganose, M. Siron, D. D. O'Regan, and K. A. Persson, "High-throughput determination of Hubbard U and Hund J values for transition metal oxides via the linear response formalism," *Phys. Rev. Mater.*, vol. 8, p. 014409, Jan. 2024.

[339] J. W. Bennett, B. G. Hudson, I. K. Metz, D. Liang, S. Spurgeon, Q. Cui, and S. E. Mason, "A systematic determination of Hubbard U using the GBRV ultrasoft pseudopotential set," *Comput. Mater. Sci.*, vol. 170, p. 109137, Dec. 2019.

[340] M. K. Horton, J. H. Montoya, M. Liu, and K. A. Persson, "High-throughput prediction of the ground-state collinear magnetic order of inorganic materials using Density Functional Theory," *npj Comput Mater*, vol. 5, pp. 1–11, June 2019.

[341] V. I. Hegde, C. K. H. Borg, Z. Del Rosario, Y. Kim, M. Hutchinson, E. Antono, J. Ling, P. Saxe, J. E. Saal, and B. Meredig, "Quantifying uncertainty in high-throughput density functional theory: A comparison of AFLOW, Materials Project, and OQMD," *Phys. Rev. Materials*, vol. 7, p. 053805, May 2023.

[342] G. Moynihan, *A Self-Contained Ground-State Approach for the Correction of Self-Interaction Error in Approximate Density-Functional Theory*. Thesis, Trinity College Dublin. School of Physics. Discipline of Physics, 2018.

[343] "OPIUM: The optimized pseudopotential interface unification module." `https://opium.sourceforge.net`.

[344] K. Momma and F. Izumi, "VESTA: A three-dimensional visualization system for electronic and structural analysis," *J Appl Cryst*, vol. 41, pp. 653–658, June 2008.

[345] M. Shishkin and H. Sato, "Challenges in computational evaluation of redox and magnetic properties of Fe-based sulfate cathode materials of Li- and Na-ion batteries," *J. Phys.: Condens. Matter*, vol. 29, p. 215701, Apr. 2017.

[346] A. C. Burgess and D. D. O'Regan, "Flat plane based double-counting free and parameter free many-body DFT+U," *Phys. Rev. B*, vol. 110, p. 205150, Nov. 2024.

[347] E. Macke, I. Timrov, N. Marzari, and L. C. Ciacchi, "Orbital-Resolved DFT+U for Molecules and Solids," *J. Chem. Theory Comput.*, vol. 20, pp. 4824–4843, June 2024.

[348] Y. Mei, Z. Chen, and W. Yang, "Exact Second-Order Corrections and Accurate Quasiparticle Energy Calculations in Density Functional Theory," *J. Phys. Chem. Lett.*, vol. 12, pp. 7236–7244, Aug. 2021.

[349] L. A. Mariano, B. Vlaisavljevich, and R. Poloni, "Biased Spin-State Energetics of Fe(II) Molecular Complexes within Density-Functional Theory and the Linear-Response Hubbard U Correction," *J. Chem. Theory Comput.*, vol. 16, pp. 6755–6762, Nov. 2020.

[350] S. Vela, M. Fumanal, J. Cirera, and J. Ribas-Arino, "Thermal spin crossover in Fe(II) and Fe(III). Accurate spin state energetics at the solid state," *Phys. Chem. Chem. Phys.*, vol. 22, no. 9, pp. 4938–4945, 2020.

[351] L. MacEnulty and D. D. O'Regan, "Optimization strategies developed on NiO for Heisenberg exchange coupling calculations using projector augmented wave based first-principles DFT+U+J," *Phys. Rev. B*, vol. 108, p. 245137, Dec. 2023.

[352] Q. Zhao and H. J. Kulik, "Stable Surfaces That Bind Too Tightly: Can Range-Separated Hybrids or DFT+U Improve Paradoxical Descriptions of Surface Chemistry?," *J. Phys. Chem. Lett.*, vol. 10, pp. 5090–5098, Sept. 2019.

[353] J. C. Rienstra-Kiracofe, G. S. Tschumper, H. F. Schaefer, S. Nandi, and G. B. Ellison, "Atomic and Molecular Electron Affinities: Photoelectron Experiments and Theoretical Computations," *Chem. Rev.*, vol. 102, pp. 231–282, Jan. 2002.

[354] M.-C. Kim, E. Sim, and K. Burke, "Understanding and Reducing Errors in Density Functional Calculations," *Phys. Rev. Lett.*, vol. 111, p. 073003, Aug. 2013.

[355] R. C. R. Pennifold, S. J. Bennie, T. F. Miller, III, and F. R. Manby, "Correcting density-driven errors in projection-based embedding," *J. Chem. Phys.*, vol. 146, p. 084113, Feb. 2017.

[356] Y. Kim, S. Song, E. Sim, and K. Burke, "Halogen and Chalcogen Binding Dominated by Density-Driven Errors," *J. Phys. Chem. Lett.*, vol. 10, pp. 295–301, Jan. 2019.

[357] J.-W. Lee, L. Mitas, and L. K. Wagner, "Quantum Monte Carlo study of MnO solid," *arXiv:cond-mat/0411247*, Nov. 2004.

[358] R. W. G. Wyckoff, "Crystal structures," *2nd ed. (Inter-science Publishers, New York)*, 1963.

[359] T. Mueller, G. Hautier, A. Jain, and G. Ceder, "Evaluation of Tavorite-Structured Cathode Materials for Lithium-Ion Batteries Using High-Throughput Computing," *Chem. Mater.*, vol. 23, pp. 3854–3862, Sept. 2011.

[360] M. Cococcioni and N. Marzari, "Energetics and cathode voltages of LiMPO$_4$ olivines (M=Fe,Mn) from extended Hubbard functionals," *Phys. Rev. Mater.*, vol. 3, p. 033801, Mar. 2019.

[361] X. Torrelles, G. Cabailh, R. Lindsay, O. Bikondoa, J. Roy, J. Zegenhagen, G. Teobaldi, W. A. Hofer, and G. Thornton, "Geometric Structure of TiO$_2$(011)(2×1)," *Phys. Rev. Lett.*, vol. 101, p. 185501, Oct. 2008.

[362] M. Batzill, "Fundamental aspects of surface engineering of transition metal oxide photocatalysts," *Energy Environ. Sci.*, vol. 4, no. 9, pp. 3275–3286, 2011.

[363] E. Been, W.-S. Lee, H. Y. Hwang, Y. Cui, J. Zaanen, T. Devereaux, B. Moritz, and C. Jia, "Electronic Structure Trends Across the Rare-Earth Series in Superconducting Infinite-Layer Nickelates," *Phys. Rev. X*, vol. 11, p. 011050, Mar. 2021.

[364] J. W. Furness, Y. Zhang, C. Lane, I. G. Buda, B. Barbiellini, R. S. Markiewicz, A. u. Bansil, and J. Sun, "An accurate first-principles treatment of doping-dependent electronic structure of high-temperature cuprate superconductors," *Commun Phys*, vol. 1, pp. 1–6, Mar. 2018.

[365] I. Barin, "Thermochemical data of pure substances," 1989.

[366] J. Van Elp, R. H. Potze, H. Eskes, R. Berger, and G. A. Sawatzky, "Electronic structure of MnO," *Phys. Rev. B*, pp. 1530–1537, July 1991.